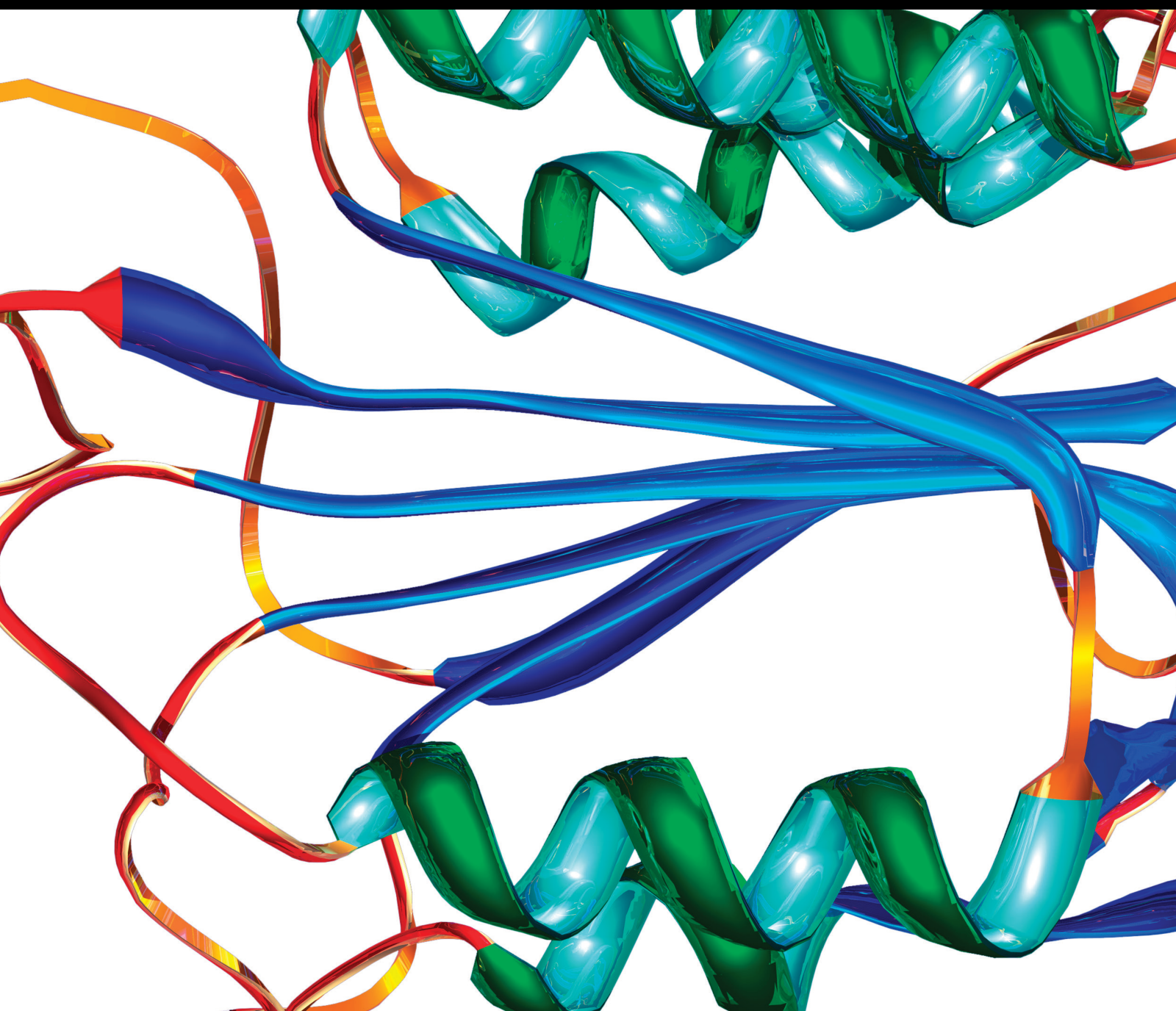


Possible Biomarkers in Malignant and Benign Neurological Disease

Lead Guest Editor: Wen-Jun Tu

Guest Editors: Xianwei Zeng, Baoqiang Guo, and Han-Cheng Qiu





Possible Biomarkers in Malignant and Benign Neurological Disease

Disease Markers

Possible Biomarkers in Malignant and Benign Neurological Disease

Lead Guest Editor: Wen-Jun Tu

Guest Editors: Xianwei Zeng, Baoqiang Guo, and Han-Cheng Qiu




Copyright © 2021 Hindawi Limited. All rights reserved.

This is a special issue published in "Disease Markers." All articles are open access articles distributed under the Creative Commons Attribution License, which permits unrestricted use, distribution, and reproduction in any medium, provided the original work is properly cited.



Chief Editor

Paola Gazzaniga, Italy

Associate Editors

Donald H. Chace , USA
Mariann Harangi, Hungary
Hubertus Himmerich , United Kingdom
Yi-Chia Huang , Taiwan
Giuseppe Murdaca , Italy
Irene Rebelo , Portugal

Academic Editors

Muhammad Abdel Ghafar, Egypt
George Agrogiannis, Greece
Mojgan Alaeddini, Iran
Atif Ali Hashmi , Pakistan
Cornelia Amalinei , Romania
Pasquale Ambrosino , Italy
Paul Ashwood, USA
Faryal Mehwish Awan , Pakistan
Atif Baig , Malaysia
Valeria Barresi , Italy
Lalit Batra , USA
Francesca Belardinilli, Italy
Elisa Belluzzi , Italy
Laura Bergantini , Italy
Sourav Bhattacharya, USA
Anna Birková , Slovakia
Giulia Bivona , Italy
Luisella Bocchio-Chiavetto , Italy
Francesco Paolo Busardó , Italy
Andrea Cabrera-Pastor , Spain
Paolo Cameli , Italy
Chiara Caselli , Italy
Jin Chai, China
Qixing Chen, China
Shaoqiu Chen, USA
Xiangmei Chen, China
Carlo Chiarla , Italy
Marcello Ciaccio , Italy
Luciano Colangelo , Italy
Alexandru Corlateanu, Moldova
Miriana D'Alessandro , Saint Vincent and the Grenadines
Waaqo B. Daddacha, USA
Xi-jian Dai , China
Maria Dalamaga , Greece






Serena Del Turco , Italy
Jiang Du, USA
Xing Du , China
Benoit Dugue , France
Paulina Dumnicka , Poland
Nashwa El-Khazragy , Egypt
Zhe Fan , China
Rudy Foddis, Italy
Serena Fragiotta , Italy
Helge Frieling , Germany
Alain J. Gelibter, Italy
Matteo Giulietti , Italy
Damjan Glavač , Slovenia
Alvaro González , Spain
Rohit Gundamaraju, USA
Emilia Hadziyannis , Greece
Michael Hawkes, Canada
Shih-Ping Hsu , Taiwan
Menghao Huang , USA
Shu-Hong Huang , China
Xuan Huang , China
Ding-Sheng Jiang , China
Esteban Jorge Galarza , Mexico
Mohamed Gomaa Kamel, Japan
Michalis V. Karamouzis, Greece
Muhammad Babar Khawar, Pakistan
Young-Kug Kim , Republic of Korea
Mallikarjuna Korivi , China
Arun Kumar , India
Jinan Li , USA
Peng-fei Li , China
Yiping Li , China
Michael Lichtenauer , Austria
Daniela Ligi, Italy
Hui Liu, China
Jin-Hui Liu, China
Ying Liu , USA
Zhengwen Liu , China
César López-Camarillo, Mexico
Xin Luo , USA
Zhiwen Luo, China
Valentina Magri, Italy
Michele Malaguarnera , Italy
Erminia Manfrin , Italy
Utpender Manne, USA

Alexander G. Mathioudakis, United Kingdom
Andrea Maugeri , Italy
Prasenjit Mitra , India
Ekansh Mittal , USA
Hiroshi Miyamoto , USA
Naoshad Muhammad , USA
Chiara Nicolazzo , Italy
Xing Niu , China
Dong Pan , USA
Dr.Krupakar Parthasarathy, India
Robert Pichler , Austria
Dimitri Poddighe , Kazakhstan
Roberta Rizzo , Italy
Maddalena Ruggieri, Italy
Tamal Sadhukhan, USA
Pier P. Sainaghi , Italy
Cristian Scheau, Romania
Jens-Christian Schewe, Germany
Alexandra Scholze , Denmark
Shabana , Pakistan
Anja Hviid Simonsen , Denmark
Eric A. Singer , USA
Daniele Sola , Italy
Timo Sorsa , Finland
Yaying Sun , China
Mohammad Tarique , USA
Jayaraman Tharmalingam, USA
Sowjanya Thatikonda , USA
Stamatios E. Theocharis , Greece
Tilman Todenhöfer , Germany
Anil Tomar, India
Alok Tripathi, India
Drenka Trivanović , Germany
Natacha Turck , Switzerland
Azizah Ugusman , Malaysia
Shailendra K. Verma, USA
Aristidis S. Veskoukis, Greece
Arianna Vignini, Italy
Jincheng Wang, Japan
Zhongqiu Xie, USA
Yuzhen Xu, China
Zhijie Xu , China
Guan-Jun Yang , China
Yan Yang , USA







Chengwu Zeng , China
Jun Zhang Zhang , USA
Qun Zhang, China
Changli Zhou , USA
Heng Zhou , China
Jian-Guo Zhou, China

Contents

Homocysteine Level and Risk of Hemorrhage in Brain Arteriovenous Malformations

Chaofan Zeng , Fa Lin , Peicong Ge, Dong Zhang , Shuo Wang , and Jizong Zhao 
Research Article (9 pages), Article ID 8862299, Volume 2021 (2021)








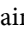


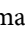


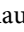
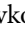
The Genetic and Epigenetic Mechanisms Involved in Irreversible Pulp Neural Inflammation

Xiaoxi Xi , Yihong Ma , Yuzhen Xu , Anthony Chukwunonso Ogbuehi , Xiangqiong Liu , Yupei Deng , Junming Xi , Haitong Pan , Qian Lin , Bo Li , Wanchen Ning , Xiao Jiang , Hanluo Li , Simin Li , and Xianda Hu 
Research Article (26 pages), Article ID 8831948, Volume 2021 (2021)


Differentially Expressed Circular RNA Profile in an Intracranial Aneurysm Group Compared with a Healthy Control Group

Yonggang Ma , Baoqing Zhang , Dong Zhang , Shuo Wang , Maogui Li , and Jizong Zhao 
Research Article (8 pages), Article ID 8889569, Volume 2021 (2021)


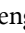

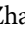
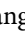
Identification of miRNAs as the Crosstalk in the Interaction between Neural Stem/Progenitor Cells and Endothelial Cells

Xin Wang , Simin Li , Yihong Ma , Yuzhen Xu , Anthony Chukwunonso Ogbuehi , Xianda Hu , Aneesha Acharya , Rainer Haak , Dirk Ziebolz , Gerhard Schmalz , Hanluo Li , Sebastian Gaus , Bernd Lethaus , Vuk Savkovic , and Zhiqiang Su 
Research Article (29 pages), Article ID 6630659, Volume 2020 (2020)



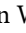
Responsive Expression of MafF to β -Amyloid-Induced Oxidative Stress

Xiaoxuan Wang, Yu Zhang, Xinkun Wan, Chenjia Guo, Jing Cui, Jing Sun, and Liang Li 
Research Article (14 pages), Article ID 8861358, Volume 2020 (2020)


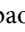
Prognostic Significance of Homocysteine Level on Neurological Outcome in Brain Arteriovenous Malformations

Fa Lin , Chaofan Zeng , Peicong Ge , Dong Zhang, Shuo Wang , and Jizong Zhao 
Research Article (8 pages), Article ID 6661475, Volume 2020 (2020)

FAM225B Is a Prognostic lncRNA for Patients with Recurrent Glioblastoma

Junsheng Li , Qian Zhang, Peicong Ge, Chaofan Zeng , Fa Lin, Wen Wang , and Jizong Zhao 
Research Article (7 pages), Article ID 8888085, Volume 2020 (2020)


Analysis of Long Noncoding RNA ZNF667-AS1 as a Potential Biomarker for Diagnosis and Prognosis of Glioma Patients

Qin Yuan, Chao Gao, Xiao-dong Lai, Liang-yi Chen , and Tian-bao Lai 
Research Article (7 pages), Article ID 8895968, Volume 2020 (2020)

Explicating the Pivotal Pathogenic, Diagnostic, and Therapeutic Biomarker Potentials of Myeloid-Derived Suppressor Cells in Glioblastoma

Seidu A. Richard 
Review Article (13 pages), Article ID 8844313, Volume 2020 (2020)

Elevated Levels of Serum Neurofilament Light Chain Associated with Cognitive Impairment in Vascular Dementia

Weibin Ma, Jingjing Zhang, Jialei Xu , Depeng Feng, Xiaoling Wang, and Fengyu Zhang
Research Article (5 pages), Article ID 6612871, Volume 2020 (2020)


Diagnostic and Prognostic Potentials of Long Noncoding RNA ELF3-AS1 in Glioma Patients

Jun-chi Mei, Ge Yan, and Si-qing Mei 
Research Article (7 pages), Article ID 8871746, Volume 2020 (2020)


Updating a Strategy for Histone Deacetylases and Its Inhibitors in the Potential Treatment of Cerebral Ischemic Stroke

Yuzhen Xu , Qian Wang , Jianxin Chen , Yihong Ma , and Xueyuan Liu 
Review Article (8 pages), Article ID 8820803, Volume 2020 (2020)

Peripheral Blood Occludin Level as a Biomarker for Perioperative Cerebral Edema in Patients with Brain Tumors

Shuhai Shi, Jingli Cheng, Chunyang Zhang, Tao Liang, Yunxin Zhang, Yongxing Sun, Ying Zhao, Weili Li, and Baoguo Wang 
Research Article (9 pages), Article ID 8813535, Volume 2020 (2020)

Association of Serum FAM19A5 with Cognitive Impairment in Vascular Dementia

Juan Li, Shoulin Li, Yihong Song, Wei Zhou, Xiaohao Zhu, Suo Xu, Yihong Ma, and Chunlin Zhu 
Research Article (5 pages), Article ID 8895900, Volume 2020 (2020)

Research Article

Homocysteine Level and Risk of Hemorrhage in Brain Arteriovenous Malformations

Chaofan Zeng ^{1,2,3,4} Fa Lin ^{1,2,3,4} Peicong Ge,^{1,2,3,4} Dong Zhang ^{1,2,3,4}
Shuo Wang ^{1,2,3,4} and Jizong Zhao ^{1,2,3,4,5}

¹Department of Neurosurgery, Beijing Tiantan Hospital, Capital Medical University, No. 119 South Fourth Ring Rd West, Fengtai District, Beijing 100070, China

²China National Clinical Research Center for Neurological Diseases, Beijing 100070, China

³Center of Stroke, Beijing Institute for Brain Disorders, Beijing 100070, China

⁴Beijing Key Laboratory of Translational Medicine for Cerebrovascular Disease, Beijing 100070, China

⁵Savaid Medical School, University of the Chinese Academy of Sciences, Beijing, China

Correspondence should be addressed to Jizong Zhao; zhaojz205@163.com

Received 18 August 2020; Revised 10 September 2020; Accepted 20 March 2021; Published 31 March 2021

Academic Editor: Wen-Jun Tu

Copyright © 2021 Chaofan Zeng et al. This is an open access article distributed under the Creative Commons Attribution License, which permits unrestricted use, distribution, and reproduction in any medium, provided the original work is properly cited.

Objective. We aimed to investigate the risk factors associated with hemorrhage and clarify the relation of homocysteine (Hcy) with brain arteriovenous malformations (bAVMs). **Method.** We retrospectively reviewed bAVM patients from Beijing Tiantan Hospital between January 2019 and December 2019. Clinical and laboratory variables were analyzed in enrolled patients with bAVMs. Potential predictors associated with hemorrhage were evaluated by logistic regression analysis. **Results.** A total of 143 bAVM patients were identified in the study, including 69 unruptured and 74 ruptured cases. Patients with hemorrhage were less likely to have hyperhomocysteinemia ($P = 0.023$). Logistic regression analysis showed that increased maximum diameter of bAVM lesions (odds ratio (OR) 0.634, 95% confidence intervals (CI) 0.479-0.839; $P = 0.001$) and serum Hcy level (OR 0.956, 95% CI 0.920-0.993; $P = 0.021$) were associated with lower risk of hemorrhage in bAVMs. **Conclusion.** The present study provided evidence regarding the association between serum Hcy and hemorrhage in patients with bAVMs. Higher Hcy level was correlated with a lower risk of rupture. Detection of factors for subsequent hemorrhage is necessary to develop therapeutic strategies for bAVMs preferably.

1. Introduction

Brain arteriovenous malformations (bAVMs) are congenital collection of dilated arteries and draining veins without capillary beds, forming high-flow arterial blood shunts directly into the venous system [1, 2]. Intracranial hemorrhage manifests as the most common onset symptom with an annual rupture rate ranged from 2%-4%, which results in a high incidence of neurological morbidity and mortality [3, 4]. Although our understanding of bAVMs has progressed in recent years, causal relationships and the mechanisms by which bAVMs initiation, progression, and rupture remain poorly elusive.

Homocysteine (Hcy) is a nonessential amino acid from the methionine and folate cycle, a metabolic product critical for numerous biochemical processes. Clinically, normal serum level ranges from 5-10 $\mu\text{mol/L}$, and incremental elevation above 15 $\mu\text{mol/L}$ is termed as hyperhomocysteinemia (HHcy) [5]. Previous studies and analyses suggested the atherogenic, thrombogenic, and procoagulant effects of Hcy [6, 7], which overlap the acknowledged pathogenic mechanism of bAVMs [8]. The major mechanisms were summarized as intracranial vascular injuries [9, 10], vascular wall remodeling [11, 12], hemodynamic stress [11], and diameter and hematoma expansion [13, 14]. Elevated serum Hcy is emerging as an independent risk factor for slow-flow occlusive

cardiovascular diseases, neurodegenerative diseases, and ischemic stroke [6, 15]. However, after McEvoy et al. first presented the relationship between Hcy and hemorrhagic stroke [16], its role in hemorrhagic stroke subsequently reported remains controversial [17–19], let alone in bAVMs. Currently, most studies, including meta-analyses, failed to confirm this association [20–22].

To the best of our knowledge, no clinical study with relevant evidence that correlates Hcy with bAVMs has been performed so far. Thus, in the present study, we conducted this untargeted analysis to explore the risk factors associated with initial rupture and to clarify the relation of Hcy with bAVMs.

2. Materials and Methods

2.1. Study Design and Participants. We retrospectively reviewed patients diagnosed with bAVMs at the Department of Neurosurgery, Beijing Tiantan Hospital from January 2019 to December 2019. This study was approved by the Institutional Review Board of our institution. Informed consent was waived considering the retrospective design of the study.

Among 356 patients with cerebral vascular malformations admitted to our hospital between January 2019 and December 2019, 332 patients were diagnosed with bAVMs using magnetic resonance imaging (MRI) or digital subtraction angiography (DSA). Patients were excluded as follows: (1) with malignancies, chronic renal insufficiency, hematological diseases, or hypothyroidism; (2) with inadequate laboratory or DSA data. Finally, 143 patients were included in the study (Figure 1).

2.2. Data Collection. Demographic data, medical and operative history, clinical manifestations, bAVM characteristics, and laboratory results were obtained. Medical history including hypertension, diabetes mellitus, hyperlipidemia, cigarette smoking, and alcohol drinking were obtained. The history of prior treatment included endovascular embolization, radiosurgery, and microsurgery. Initial manifestations were summarized into three categories: hemorrhage, seizure, and neurological dysfunction. bAVM characteristics included size of lesion, eloquent and deep location, venous drainage, and associated aneurysms. The AVM volume was calculated by $(a \times b \times c)/2$ [23], and the Spetzler-Martin (SM) grading scale was evaluated to classify the bAVMs. Two experienced investigators (C.Z. and F.L.) independently reviewed the MRI and DSA images. Neurological status was assessed using the modified Rankin Scale (mRS) score at admission.

Heart rate and blood pressure were also recorded. Body mass index (BMI) was calculated as $\text{weight (kg)}/[\text{height (m)}]^2$. Besides, fast venous blood samples were collected in the morning after admission for all patients. Levels of blood glucose, albumin (ALB), creatinine, uric acid (UA), total cholesterol (TC), triglyceride (TG), high-density lipoprotein cholesterol (HDL-C), low-density lipoprotein cholesterol (LDL-C), apolipoprotein A (ApoA), apolipoprotein B (ApoB), and homocysteine (Hcy) were measured using enzymatic methods. Serum Hcy $\geq 15.0 \mu\text{mol/L}$ was considered as HHcy.

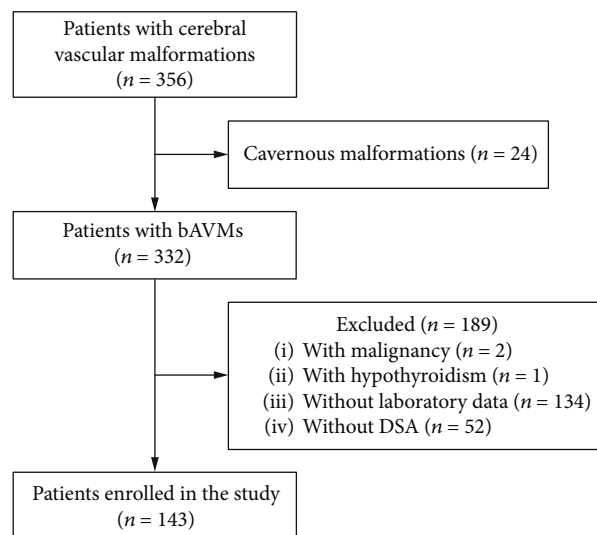


FIGURE 1: Flow diagram of the study participants. bAVMs: brain arteriovenous malformations; DSA: digital subtraction angiography.

2.3. Statistical Analysis. All statistical analyses were performed using SPSS (version 26.0, IBM). The categorical variables were presented as frequencies, and continuous variables were described with mean (standard deviation, SD) or median (interquartile range, IQR). The chi-square test or Fisher exact test was conducted to compare categorical variables between groups. Continuous variables were compared using the two-tailed Student-*t* test or Mann-Whitney *U* test. The association between characteristics and Hcy quartiles was assessed using the Cochran-Armitage test for bivariate variables and Spearman's rank correlation test for continuous variables. Logistic regression analysis was performed to identify the risk factors for hemorrhage of bAVMs. Odds ratios (ORs) were calculated with 95% confidence intervals (CIs). Further exploration of Hcy associated with hemorrhage was conducted by adjusted models. *P* value < 0.05 indicated statistical significance.

3. Results

3.1. Clinical and Laboratory Characteristics of bAVM Patients. Baseline characteristics according to the hemorrhagic manifestation were shown in Table 1. A total of 143 patients with bAVMs were enrolled in the study. Compared with unruptured participants, patients with ruptured bAVMs tended to exhibit poor neurological status (mRS > 2) and less likely presented with seizure ($P < 0.001$ for both). Although the SM grade was found no difference between groups ($P = 0.149$), the average size of bAVMs was smaller in ruptured patients than in those without hemorrhage ($P < 0.001$). In addition, ruptured bAVMs showed lower levels of UA ($P = 0.032$). HHcy was found in 28 (40.6%) unruptured patients and 17 (23.0%) ruptured patients ($P = 0.023$).

3.2. Clinical Characteristics of bAVM Patients according to Hcy Quartiles. Analysis of the clinical characteristics according to Hcy quartiles was summarized in Table 2. A

TABLE 1: Baseline characteristics of bAVM patients.

Variables	Total (n = 143)	Unruptured (n = 69)	Ruptured (n = 74)	P value
Age, y, mean (SD)	29.6 (14.0)	31.0 (13.1)	28.2 (14.6)	0.221
Sex, male (%)	79 (55.2)	37 (53.6)	42 (56.8)	0.706
Medical history (%)				
Hypertension	9 (6.3)	2 (2.9)	7 (9.5)	0.204
Diabetes mellitus	3 (2.1)	1 (1.4)	2 (2.7)	1.000
Hyperlipidemia	1 (0.7)	0 (0)	1 (1.4)	1.000
Cigarette smoking	26 (18.2)	12 (17.4)	14 (18.9)	0.813
Alcohol drinking	16 (11.2)	7 (10.1)	9 (12.2)	0.702
Prior treatments (%)				
Embolization	21 (14.7)	7 (10.1)	14 (18.9)	0.139
Radiosurgery	6 (4.2)	1 (1.4)	5 (6.8)	0.244
Microsurgery	5 (3.5)	2 (2.9)	3 (4.1)	1.000
Primary symptom (%)				
Hemorrhage	74 (51.7)	0 (0)	74 (100.0)	<0.001*
Seizure	30 (21.0)	25 (36.2)	5 (6.8)	<0.001*
Neurological dysfunction	29 (20.3)	15 (21.7)	14 (18.9)	0.675
Admission mRS > 2 (%)	15 (10.5)	1 (1.4)	14 (18.9)	<0.001*
AVM characteristics				
Spetzler-Martin grade (%)				0.149
I-II	81 (56.6)	34 (49.3)	47 (63.5)	
III	42 (29.4)	22 (31.9)	20 (27.0)	
IV-V	20 (14.0)	13 (18.8)	7 (9.5)	
Maximum diameter, cm, median (IQR)	3.4 (2.5-4.6)	3.9 (3.0-5.1)	2.9 (2.3-4.1)	<0.001*
Volume, cm ³ , median (IQR)	8.6 (4.4-25.0)	15.8 (6.2-33.7)	6.0 (3.5-15.3)	<0.001*
Deep location (%)	33 (23.1)	16 (23.2)	17 (23.0)	0.976
Eloquent location (%)	72 (50.3)	34 (49.3)	38 (51.4)	0.804
Deep venous drainage (%)	43 (30.1)	21 (30.4)	22 (29.7)	0.927
Associated aneurysms (%)	21 (14.7)	10 (14.5)	11 (14.9)	0.950
Clinical features, mean (SD)				
Heart rate, bpm	80 (10)	80 (9)	81 (11)	0.405
SBP, mm Hg	120 (15)	120 (13)	120 (17)	1.000
DBP, mm Hg	77 (10)	76 (10)	78 (11)	0.434
BMI, kg/m ²	22.6 (4.4)	23.2 (4.4)	22.0 (4.4)	0.099
Laboratory results, median (IQR)				
Glucose, mmol/L	4.6 (4.3-5.0)	4.6 (4.3-4.8)	4.6 (4.4-5.1)	0.141
Albumin, g/L	43.9 (41.3-46.0)	44.4 (41.6-46.1)	43.5 (41.0-45.9)	0.511
Creatinine, μmol/L	58.6 (46.6-68.5)	59.5 (49.7-70.9)	56.2 (45.2-67.8)	0.109
UA, μmol/L	314.0 (257.7-366.5)	324.5 (280.8-374.8)	294.0 (241.8-357.1)	0.032*
TC, mmol/L	4.3 (3.6-4.8)	4.3 (3.8-4.9)	4.2 (3.5-4.8)	0.468
TG, mmol/L	1.0 (0.7-1.5)	1.1 (0.8-1.6)	0.9 (0.7-1.5)	0.130
HDL-C, mmol/L	1.2 (1.0-1.5)	1.2 (1.0-1.4)	1.2 (1.1-1.5)	0.701
LDL-C, mmol/L	2.6 (2.0-3.2)	2.8 (2.1-3.5)	2.5 (1.9-3.1)	0.080
ApoA, g/L	1.3 (1.1-1.4)	1.3 (1.1-1.4)	1.3 (1.1-1.4)	0.588
ApoB, g/L	0.8 (0.7-1.0)	0.9 (0.7-1.1)	0.8 (0.7-0.9)	0.211
Hcy, μmol/L	12.4 (9.9-16.2)	13.3 (10.4-18.9)	11.7 (9.7-14.6)	0.057
HHcy (%)	45 (31.5)	28 (40.6)	17 (23.0)	0.023*

bAVM: brain arteriovenous malformation; SD: standard deviation; mRS: modified Rankin Scale; IQR: interquartile range; SBP: systolic blood pressure; DBP: diastolic blood pressure; BMI: body mass index; UA: uric acid; TC: total cholesterol; TG: triglyceride; HDL-C: high-density lipoprotein cholesterol; LDL-C: low-density lipoprotein cholesterol; ApoA: apolipoprotein A; ApoB: apolipoprotein B; Hcy: homocysteine; HHcy: hyperhomocysteinemia. *P < 0.05, significant difference.

TABLE 2: Characteristics of bAVM patients according to Hcy quartiles.

Variables	Hcy quartiles ^a , $\mu\text{mol/L}$					<i>P</i> trend
	All (<i>n</i> = 143)	Q1 (<i>n</i> = 36)	Q2 (<i>n</i> = 35)	Q3 (<i>n</i> = 36)	Q4 (<i>n</i> = 36)	
Age, y, mean (SD)	29.6 (14.0)	23.8 (16.0)	30.2 (13.7)	35.4 (12.8)	28.9 (10.9)	0.005*
Sex, male (%)	79 (55.2)	11 (30.6)	17 (48.6)	22 (61.1)	29 (80.6)	<0.001*
Medical history (%)						
Hypertension	9 (6.3)	1 (2.8)	2 (5.7)	4 (11.1)	2 (5.6)	0.448
Diabetes mellitus	3 (2.1)	0 (0)	1 (2.9)	1 (2.8)	1 (2.8)	0.438
Hyperlipidemia	1 (0.7)	0 (0)	0 (0)	1 (2.8)	0 (0)	0.657
Cigarette smoking	26 (18.2)	1 (2.8)	6 (17.1)	10 (27.8)	9 (25.0)	0.007*
Alcohol drinking	16 (11.2)	0 (0)	4 (11.4)	8 (22.2)	4 (11.1)	0.060
Primary symptom (%)						
Hemorrhage	74 (51.7)	21 (58.3)	20 (57.1)	19 (52.8)	14 (38.9)	0.093
Seizure	30 (21.0)	4 (11.1)	6 (17.1)	9 (25.0)	11 (30.6)	0.029*
Neurological dysfunction	29 (20.3)	8 (22.2)	7 (20.0)	8 (22.2)	6 (16.7)	0.629
Admission mRS > 2 (%)	15 (10.5)	9 (25.0)	1 (2.9)	2 (5.6)	3 (8.3)	0.037*
AVM characteristics						
Spetzler-Martin grade (%)						0.660
I-II	81 (56.6)	17 (47.2)	23 (65.7)	20 (55.6)	21 (58.3)	
III	42 (29.4)	13 (36.1)	8 (22.9)	12 (33.3)	9 (25.0)	
IV-V	20 (14.0)	6 (16.7)	4 (11.4)	4 (11.1)	6 (16.7)	
Maximum diameter, cm, median (IQR)	3.4 (2.5-4.6)	4.0 (2.6-4.7)	3.0 (2.5-4.4)	3.0 (2.3-3.9)	3.7 (2.6-5.1)	0.183
Volume, cm^3 , median (IQR)	8.6 (4.4-25.0)	10.9 (5.2-29.7)	7.2 (5.0-19.3)	8.2 (3.2-17.7)	13.9 (4.3-31.8)	0.239
Deep location (%)	33 (23.1)	8 (22.2)	7 (20.0)	8 (22.2)	10 (27.8)	0.549
Eloquent location (%)	72 (50.3)	19 (52.8)	18 (51.4)	19 (52.8)	16 (44.4)	0.526
Diffusive nidus (%)	68 (47.6)	21 (58.3)	17 (48.6)	10 (27.8)	20 (55.6)	0.434
Deep venous drainage (%)	43 (30.1)	12 (33.3)	8 (22.9)	13 (36.1)	10 (27.8)	0.916
Associated aneurysms (%)	21 (14.7)	6 (16.7)	5 (14.3)	6 (16.7)	4 (11.1)	0.588

bAVM: brain arteriovenous malformation; Hcy: homocysteine; SD: standard deviation; mRS: modified Rankin Scale; IQR: interquartile range. * $P < 0.05$, significant difference. ^aSerum levels of Hcy in quartiles: Q1, <10.0 $\mu\text{mol/L}$; Q2, 10.0-12.3 $\mu\text{mol/L}$; Q3, 12.4-16.1 $\mu\text{mol/L}$; and Q4, >16.1 $\mu\text{mol/L}$.

relationship was observed between Hcy level and male sex ($P < 0.001$). Serum Hcy level was also correlated with age ($P = 0.005$) and cigarette smoking ($P = 0.007$). Furthermore, Hcy was related to seizure manifestation and poor neurological status ($P < 0.05$ for all). Although the incidence of hemorrhage was no significant difference between Hcy quartiles ($P = 0.093$), a relatively lower risk of rupture occurred in the groups of higher Hcy concentration (Q1: 58.3%; Q2, 57.1%; Q3, 52.8%; Q4, 38.9%). The SM grade and other variables were similar across Hcy quartiles ($P > 0.05$ for all).

3.3. Analysis of Predictors for Hemorrhage of bAVMs. Predictors for the hemorrhagic presence of bAVMs were analyzed (Table 3). Univariate analysis showed that the maximum diameter of bAVM lesions and level of serum Hcy were associated with hemorrhage. After incorporating the covariables of age, male sex, smoking, prior embolization, deep location, eloquent location, deep venous drainage, and associated aneurysms into the multivariate analysis, maximum diameter (OR 0.634, 95% CI 0.479-0.839; $P = 0.001$) and serum Hcy level (OR 0.956, 95% CI 0.920-0.993; $P = 0.021$) were shown to be significantly related to hemorrhage.

Prior to adjusting for potential covariables (Figure 2), HHcy was associated with the hemorrhagic presence (OR 0.437, 95% CI 0.212-0.901; $P = 0.025$). After adjusting for age, male sex, smoking, prior embolization, deep location, eloquent location, deep venous drainage, and associated aneurysms, HHcy was correlated with a lower risk of hemorrhage (OR 0.381, 95% CI 0.165-0.881; $P = 0.024$). The curve of regression model was fitted to reveal the linear relationship between Hcy level and probability of hemorrhage (Figure 3).

4. Discussion

In this retrospective study, we identified the potential risk factors for hemorrhage of bAVMs and investigated the association between serum Hcy level and bAVMs' rupture. HHcy was observed significantly less in patients with the hemorrhagic presentation. Furthermore, we found that increased size of bAVM lesions and higher levels of Hcy were correlated with a lower risk of hemorrhage.

Although HHcy was proved to be an independent risk factor for ischemic stroke [24], the relationship between intracranial hemorrhage and HHcy has not been extensively

TABLE 3: Logistic regression analysis on the risk of hemorrhage.

Variables	Univariate analysis			Multivariate analysis		
	OR	95% CI	P value	OR	95% CI	P value
Age	0.985	0.962-1.009	0.220	0.980	0.954-1.007	0.154
Male sex	1.135	0.587-2.196	0.707	1.565	0.686-3.568	0.287
Medical history						
Hypertension	3.500	0.701-17.467	0.127			
Diabetes mellitus	1.889	0.167-21.311	0.607			
Cigarette smoking	1.108	0.473-2.598	0.813	0.974	0.325-2.914	0.962
Alcohol drinking	1.226	0.430-3.495	0.703			
Prior treatments						
Embolization	2.067	0.780-5.475	0.144	2.848	0.868-9.347	0.084
Radiosurgery	4.928	0.561-43.286	0.150			
Microsurgery	1.415	0.229-8.737	0.708			
AVM characteristics						
Maximum diameter	0.668	0.519-0.859	0.002	0.634	0.479-0.839	0.001*
Deep location	1.012	0.465-2.205	0.976	1.271	0.507-3.187	0.609
Eloquent location	1.087	0.564-2.094	0.804	1.230	0.561-2.698	0.605
Deep venous drainage	0.967	0.473-1.977	0.927	0.914	0.391-2.135	0.836
Associated aneurysms	1.030	0.408-2.603	0.950	1.184	0.415-3.380	0.753
Clinical features						
Heart rate	1.014	0.981-1.049	0.402			
SBP	1.000	0.978-1.022	>0.999			
DBP	1.013	0.981-1.046	0.432			
BMI	0.937	0.867-1.013	0.102			
Laboratory results						
Glucose	1.510	0.965-2.362	0.071			
Albumin	0.976	0.886-1.074	0.614			
Creatinine	0.978	0.957-1.000	0.051			
UA	1.000	0.999-1.001	0.964			
TC	0.912	0.638-1.305	0.616			
TG	1.052	0.764-1.449	0.756			
HDL-C	1.819	0.851-3.886	0.123			
LDL-C	0.724	0.493-1.064	0.100			
ApoA	0.916	0.272-3.089	0.888			
ApoB	0.404	0.081-2.012	0.269			
Hcy	0.965	0.934-0.998	0.038	0.956	0.920-0.993	0.021*

OR: odds ratio; CI: confidence intervals; AVM: arteriovenous malformation; SBP: systolic blood pressure; DBP: diastolic blood pressure; BMI: body mass index; UA: uric acid; TC: total cholesterol; TG: triglyceride; HDL-C: high-density lipoprotein cholesterol; LDL-C: low-density lipoprotein cholesterol; ApoA: apolipoprotein A; ApoB: apolipoprotein B; Hcy: homocysteine. * $P < 0.05$, significant difference.

studied. A previous study involving 503 patients with ICH reported that the risk of hemorrhage in patients with HHcy was 1.94-fold compared to the controls [17]. A recent meta-analysis showed that Hcy levels in patients with ICH were significantly higher than in healthy participants [19]. Various diseases are characterized by intracranial hemorrhage, including hypertension, cerebral amyloid angiopathy, intracranial aneurysms, and bAVMs. Wang et al. reported that HHcy was an independent risk factor for the formation of intracranial aneurysms in the Chinese Han population [25]. HHcy may also be associated with the rupture of intra-

cranial aneurysms in animal experiments [12]. According to the study by Kumar et al., higher serum Hcy level was observed in SAH patients as compared to healthy controls [26]. However, other studies demonstrated the contrary results. Dhandapani et al. revealed that the increased Hcy was significantly associated with favorable outcomes following SAH [27]. Moreover, a lower concentration of Hcy was verified as the predictor for hematoma expansion of ICH in cerebral small vessel diseases [28].

In our study, Hcy was proved to be associated with rupture in bAVM patients. Surprisingly, ruptured bAVMs had less

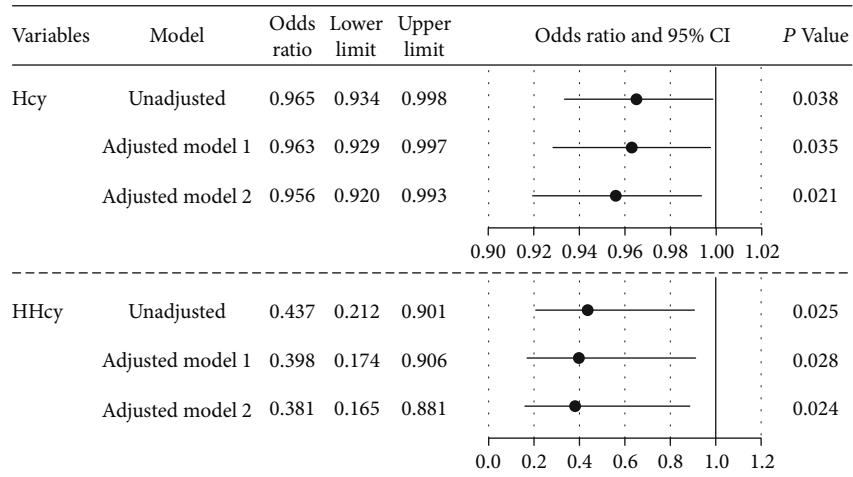


FIGURE 2: Odds ratio for hemorrhage in bAVMs, according to Hcy and HHcy. Model 1: adjusted for age, sex, cigarette smoking, eloquent location, deep venous drainage, maximum diameter of lesions, and Hcy. Model 2: additionally adjusted for prior treatment of embolization, deep location, and associated aneurysm. CI: confidence intervals; Hcy: homocysteine; HHcy: hyperhomocysteinemia.

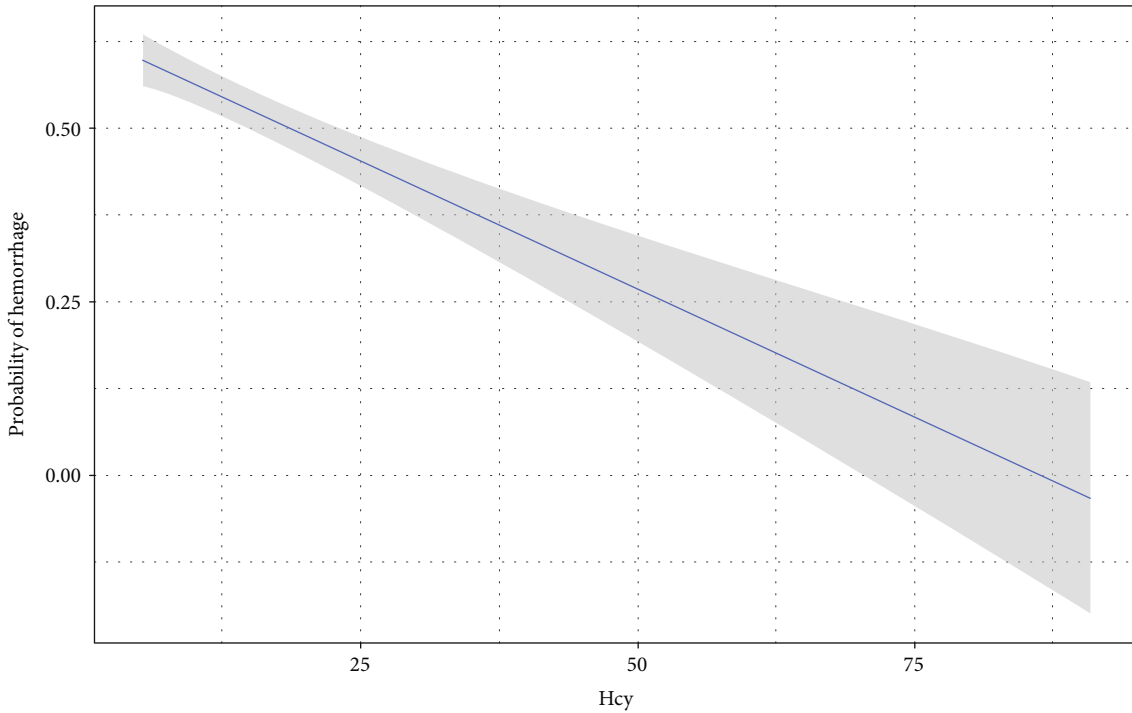


FIGURE 3: A linear relationship between Hcy level and probability of hemorrhage in the regression model. Hcy: homocysteine.

proportion of HHcy, and the level of Hcy was an independent protective factor for hemorrhage. Hcy is an amino acid involved in the metabolism of methionine and folate cycle. The permeability of cerebrovascular endothelial cells is increased with MMP-9 (matrix metalloproteinase-9) activated by Hcy, accompanied with blood-brain barrier (BBB) destruction [29]. It has been found that Hcy may further activate MMP-9 through extracellular signal-regulated kinase (ERK) pathway and inhibition of γ -aminobutyric acid (GABA) receptor in endothelial cells [30]. MMP-9 may also disrupt the BBB by degrading type IV collagenase, laminin, and fibronectin in extracellular matrix

and basement membrane; activating vascular endothelial growth factor (VEGF) and thrombin; inducing apoptosis, which exacerbates the occurrence of ICH [31]. Furthermore, increased levels of MMP-9 were observed in bAVMs. The abnormal expression of MMP-9 destabilized the vessels, which potentially leads to the rupture of bAVM lesions [32].

Alternatively, the results may be associated with hemodynamic abnormalities. Recent studies have documented the effects of Hcy on arterial hemodynamics [33–35]. Several lines of evidence suggested a converse relationship between Hcy and flow velocity for the coronary arteries [33, 35].

The elevated level of serum Hcy was connected with the phenomenon of slow flow in coronary arteries. Oxidative stress and endothelial destruction related to Hcy were suggested to be the leading cause of slow coronary flow [33, 34]. Likewise, Hcy was shown to be associated with augmented arterial resistance in patients with internal carotid stenosis [36]. The altered hemodynamics may attribute to the remodeling of arterials with the effect of HHcy. Sun et al. reported that the flow velocity of internal carotid arteries and vertebral arteries was inversely correlated with Hcy quartiles in healthy participants, despite the parameters were not significantly different after the adjustments [37]. The difference of conclusions may be related to the inaccuracy of the data collected through carotid Doppler ultrasound, instead of transcranial Doppler sonography (TCD). As described, high-flow and low-resistance arterial blood flows directly into the venous system under the conditions of insufficient intervening capillaries in bAVMs, which carries a high risk of hemorrhage [1]. In this study, we revealed that the probability of hemorrhage was decreased in bAVM patients with higher Hcy. Therefore, we supposed that hemodynamic abnormalities induced by Hcy play an important role in the pathogenesis of bAVMs' rupture. The present results highlighted the correlation between Hcy and hemorrhage in bAVMs.

Specific morphological and angioarchitectural characteristics were proved to be related to hemorrhage of brain AVMs. The SM grading scale is used as the most common classification system in bAVMs, consisting of three anatomical factors (size of nidus, relative position of eloquent location, and patterns of draining veins) [38]. The five-classified grading system is a powerful tool for predicting operative risks based on the radiological data. In the current study, the maximum diameter of bAVMs was the independent predictor for rupture. In accordance with the present results, previous studies have illustrated that the incidence of subsequent hemorrhage increased with decreasing the size of lesions in untreated bAVMs [39, 40]. A small size of bAVMs (<3 cm) were more likely to present with bleeding compared to the larger lesions. In terms of other characteristics of bAVMs, no significant relationship between deep venous drainage or eloquent location and hemorrhage was evident in the present analyses. However, these variables were considered to be the key predictors for outcomes in previous studies [38]. The negative finding may be limited by the small sample size of enrolled participants.

There are several limitations to our study. First, this was a retrospective study with relatively small sample size, and it was difficult to avoid selection bias. Second, the diet patterns and supplements of folic acid or vitamins were not taken into consideration, and the variables may influence the metabolism of Hcy and affect the results. Third, there was a lack of data regarding levels of MMP-9 and hemodynamics parameters owing to the retrospective design; the direct relation between hemodynamic status and Hcy would be concluded with the support of evidence generated from TCD or DSA hemodynamic evaluation. Fourth, the clinical data derived from a high-volume single institution may present tentative associations between risk factors and bAVMs. Further prospective studies comparing Hcy before and after hemorrhage

are required to investigate the predictive value for bAVM ruptures.

5. Conclusions

In conclusion, our results indicated that the Hcy levels were significantly associated with the risk of rupture in bAVM patients. A higher concentration of Hcy carried a lower prevalence of hemorrhage. It is recommended to monitor the factor in patients with bAVMs, which may facilitate the guidance of subsequent nutritional management strategies.

Data Availability

The data used to support the findings of this study are available from the corresponding author upon request.

Conflicts of Interest

The authors declare that they have no conflicts of interest.

Acknowledgments

This study was supported by the National Key Technologies Research and Development Program of China (2016YFC1301800), Beijing Science and Technology Supporting Plan (D161100003816005), and Beijing Municipal Administration of Hospitals' Mission Plan (SML20150501).

References

- [1] R. M. Friedlander, "Arteriovenous malformations of the brain," *The New England Journal of Medicine*, vol. 356, no. 26, pp. 2704–2712, 2007.
- [2] S. I. Nikolaev, S. Vetiska, X. Bonilla et al., "Somatic Activating KRAS Mutations in arteriovenous malformations of the brain," *The New England Journal of Medicine*, vol. 378, no. 3, pp. 250–261, 2018.
- [3] H. Kim, R. A.-S. Salman, C. E. McCulloch, C. Stapf, W. L. Young, and For the MARS Coinvestigators, "Untreated brain arteriovenous malformation: patient-level meta-analysis of hemorrhage predictors," *Neurology*, vol. 83, no. 7, pp. 590–597, 2014.
- [4] X. Lv and G. Wang, "Review of de novo cerebral arteriovenous malformation: haemorrhage risk, treatment approaches and outcomes," *The Neuroradiology Journal*, vol. 31, no. 3, pp. 224–229, 2018.
- [5] M. Holmes, P. Newcombe, J. Hubacek et al., "Effect modification by population dietary folate on the association between *MTHFR* genotype, homocysteine, and stroke risk: a meta-analysis of genetic studies and randomised trials," *The Lancet*, vol. 378, no. 9791, pp. 584–594, 2011.
- [6] C. Boushey, S. Beresford, G. Omenn, and A. Motulsky, "A quantitative assessment of plasma homocysteine as a risk factor for vascular disease. Probable benefits of increasing folic acid intakes," *JAMA*, vol. 274, no. 13, pp. 1049–1057, 1995.
- [7] I. Wiernicki, B. Millo, K. Safranow, B. Gorecka-Szyld, and P. Gutowski, "MMP-9, homocysteine and CRP circulating levels are associated with intraluminal thrombus thickness of abdominal aortic aneurysms—new implication of the old
















- biomarkers,” *Disease Markers*, vol. 31, no. 2, Article ID 783721, pp. 67–74, 2011.
- [8] M. T. Lawton, W. C. Rutledge, H. Kim et al., “Brain arteriovenous malformations,” *Nature Reviews. Disease Primers*, vol. 1, no. 1, p. 15008, 2015.
- [9] Y. Liu, J.-H. Song, X.-H. Hou et al., “Elevated homocysteine as an independent risk for intracranial atherosclerotic stenosis,” *Aging (Albany NY)*, vol. 11, no. 11, pp. 3824–3831, 2019.
- [10] T. Li, B. Yu, Z. Liu et al., “Homocysteine directly interacts and activates the angiotensin II type I receptor to aggravate vascular injury,” *Nature Communications*, vol. 9, no. 1, p. 11, 2018.
- [11] Y. Xu, Y. Tian, H. J. Wei, J. F. Dong, and J. N. Zhang, “Methionine diet-induced hyperhomocysteinemia accelerates cerebral aneurysm formation in rats,” *Neuroscience Letters*, vol. 494, no. 2, pp. 139–144, 2011.
- [12] M. Korai, K. T. Kitazato, Y. Tada et al., “Hyperhomocysteinemia induced by excessive methionine intake promotes rupture of cerebral aneurysms in ovariectomized rats,” *Journal of Neuroinflammation*, vol. 13, no. 1, p. 165, 2016.
- [13] K. J. Halazun, K. A. Bofkin, S. Asthana, C. Evans, M. Henderson, and J. I. Spark, “Hyperhomocysteinemia is associated with the rate of abdominal aortic aneurysm expansion,” *European Journal of Vascular and Endovascular Surgery*, vol. 33, no. 4, pp. 391–394, 2007, discussion 395–396.
- [14] F. Zhou, B. Chen, C. Chen et al., “Elevated homocysteine levels contribute to larger hematoma volume in patients with intracerebral hemorrhage,” *Journal of Stroke and Cerebrovascular Diseases*, vol. 24, no. 4, pp. 784–788, 2015.
- [15] T. L. Sudduth, D. K. Powell, C. D. Smith, A. Greenstein, and D. M. Wilcock, “Induction of hyperhomocysteinemia models vascular dementia by induction of cerebral microhemorrhages and neuroinflammation,” *Journal of Cerebral Blood Flow & Metabolism*, vol. 33, no. 5, pp. 708–715, 2013.
- [16] A. W. McEvoy, C. Marras, N. D. Kitchen, and A. Briddon, “Plasma total homocysteine and subarachnoid haemorrhage in a co-factor replete population,” *Amino Acids*, vol. 21, no. 3, pp. 237–241, 2001.
- [17] Z. Li, L. Sun, H. Zhang et al., “Elevated plasma homocysteine was associated with hemorrhagic and ischemic stroke, but methylenetetrahydrofolate reductase gene C677T polymorphism was a risk factor for thrombotic stroke: a multicenter case-control study in China,” *Stroke*, vol. 34, no. 9, pp. 2085–2090, 2003.
- [18] H. Iso, Y. Moriyama, S. Sato et al., “Serum total homocysteine concentrations and risk of stroke and its subtypes in Japanese,” *Circulation*, vol. 109, no. 22, pp. 2766–2772, 2004.
- [19] Z. Zhou, Y. Liang, H. Qu et al., “Plasma homocysteine concentrations and risk of intracerebral hemorrhage: a systematic review and meta-analysis,” *Scientific Reports*, vol. 8, no. 1, p. 2568, 2018.
- [20] T. H. T. Chiu, H.-R. Chang, L.-Y. Wang, C.-C. Chang, M.-N. Lin, and C.-L. Lin, “Vegetarian diet and incidence of total, ischemic, and hemorrhagic stroke in 2 cohorts in Taiwan,” *Neurology*, vol. 94, no. 11, pp. e1112–e1121, 2020.
- [21] Y. He, Y. Li, Y. Chen, L. Feng, and Z. Nie, “Homocysteine level and risk of different stroke types: a meta-analysis of prospective observational studies,” *Nutrition, Metabolism and Cardiovascular Diseases*, vol. 24, no. 11, pp. 1158–1165, 2014.
- [22] B. Van Guelpen, J. Hultdin, I. Johansson et al., “Folate, vitamin B12, and risk of ischemic and hemorrhagic stroke: a prospective, nested case-referent study of plasma concentrations and dietary intake,” *Stroke*, vol. 36, no. 7, pp. 1426–1431, 2005.
- [23] C. S. Ogilvy, P. E. Stieg, I. Awad et al., “Recommendations for the management of intracranial arteriovenous malformations: a statement for healthcare professionals from a special writing group of the stroke council, American Stroke Association,” *Circulation*, vol. 103, no. 21, pp. 2644–2657, 2001.
- [24] S.-B. Jeon, D.-W. Kang, J. S. Kim, and S. U. Kwon, “Homocysteine, small-vessel disease, and atherosclerosis: an MRI study of 825 stroke patients,” *Neurology*, vol. 83, no. 8, pp. 695–701, 2014.
- [25] Q. Wang, J. Zhang, K. Zhao, and B. Xu, “Hyperhomocysteinemia is an independent risk factor for intracranial aneurysms: a case-control study in a Chinese Han population,” *Neurosurgical Review*, vol. 43, no. 4, pp. 1127–1134, 2020.
- [26] M. Kumar, S. Goudihalli, K. Mukherjee, S. Dhandapani, and R. Sandhir, “Methylenetetrahydrofolate reductase C677T variant and hyperhomocysteinemia in subarachnoid hemorrhage patients from India,” *Metabolic Brain Disease*, vol. 33, no. 5, pp. 1617–1624, 2018.
- [27] S. Dhandapani, S. Goudihalli, K. K. Mukherjee et al., “Prospective study of the correlation between admission plasma homocysteine levels and neurological outcome following subarachnoid hemorrhage: a case for the reverse epidemiology paradox?,” *Acta Neurochirurgica*, vol. 157, no. 3, pp. 399–407, 2015.
- [28] Y. Suo, W. Chen, Y. Pan et al., “Magnetic resonance imaging markers of cerebral small vessel disease in hematoma expansion of intracerebral hemorrhage,” *Journal of Stroke and Cerebrovascular Diseases*, vol. 27, no. 7, pp. 2006–2013, 2018.
- [29] D. Lominadze, A. M. Roberts, N. Tyagi, K. S. Moshal, and S. C. Tyagi, “Homocysteine causes cerebrovascular leakage in mice,” *American Journal of Physiology. Heart and Circulatory Physiology*, vol. 290, no. 3, pp. H1206–H1213, 2006.
- [30] N. Tyagi, W. Gillespie, J. C. Vacek, U. Sen, S. C. Tyagi, and D. Lominadze, “Activation of GABA-A receptor ameliorates homocysteine-induced MMP-9 activation by ERK pathway,” *Journal of Cellular Physiology*, vol. 220, no. 1, pp. 257–266, 2009.
- [31] H. Min, J. Hong, I.-H. Cho et al., “TLR2-induced astrocyte MMP9 activation compromises the blood brain barrier and exacerbates intracerebral hemorrhage in animal models,” *Molecular Brain*, vol. 8, no. 1, p. 23, 2015.
- [32] T. Hashimoto, G. Wen, M. T. Lawton et al., “Abnormal expression of matrix metalloproteinases and tissue inhibitors of metalloproteinases in brain arteriovenous malformations,” *Stroke*, vol. 34, no. 4, pp. 925–931, 2003.
- [33] A. Riza Erbay, H. Turhan, A. S. Yasar et al., “Elevated level of plasma homocysteine in patients with slow coronary flow,” *International Journal of Cardiology*, vol. 102, no. 3, pp. 419–423, 2005.
- [34] K. Yamashita, H. Tasaki, Y. Nagai et al., “Experimental hyperhomocysteinemia impairs coronary flow velocity reserve,” *International Journal of Cardiology*, vol. 104, no. 2, pp. 163–169, 2005.
- [35] H. Tanriverdi, H. Evrengul, S. Tanriverdi et al., “Carotid intima-media thickness in coronary slow flow: relationship with plasma homocysteine levels,” *Coronary Artery Disease*, vol. 17, no. 4, pp. 331–337, 2006.
- [36] M. H. Lim, Y. I. Cho, and S. K. Jeong, “Homocysteine and pulsatility index of cerebral arteries,” *Stroke*, vol. 40, no. 10, pp. 3216–3220, 2009.
- [37] Y. Sun, C.-J. Lu, R.-C. Chen, and K.-L. Chien, “Lack of association between total serum homocysteine and extracranial

cerebral flow,” *Journal of the Formosan Medical Association*, vol. 109, no. 4, pp. 278–286, 2010.

- [38] R. F. Spetzler and N. A. Martin, “A proposed grading system for arteriovenous malformations,” *Journal of Neurosurgery*, vol. 65, no. 4, pp. 476–483, 1986.
- [39] R. F. Spetzler, R. W. Hargraves, P. W. McCormick, J. M. Zabramski, R. A. Flom, and R. S. Zimmerman, “Relationship of perfusion pressure and size to risk of hemorrhage from arteriovenous malformations,” *Journal of Neurosurgery*, vol. 76, no. 6, pp. 918–923, 1992.
- [40] M. Reitz, N. von Spreckelsen, E. Vettorazzi et al., “Angioarchitectural risk factors for hemorrhage and clinical long-term outcome in pediatric patients with cerebral arteriovenous malformations,” *World Neurosurgery*, vol. 89, pp. 540–551, 2016.

Research Article

The Genetic and Epigenetic Mechanisms Involved in Irreversible Pulp Neural Inflammation

Xiaoxi Xi ¹, Yihong Ma ², Yuzhen Xu ³, Anthony Chukwunonso Ogbuehi ⁴,
Xiangqiong Liu ⁵, Yupei Deng ⁵, Junming Xi ¹, Haitong Pan ⁶, Qian Lin ⁷, Bo Li ⁸,
Wanchen Ning ⁹, Xiao Jiang ¹⁰, Hanluo Li ¹¹, Simin Li ¹⁰, and Xianda Hu ⁵

¹Department of Stomatology, Northeast Petroleum University Affiliated Hospital, Fazhan Road, High Tech District, 163000 Daqing City, Heilongjiang Province, China

²Department of Neurology, Graduate School of Medical Sciences, Kumamoto University, Kumamoto 860-0811, Japan

³Department of Neurology, Shanghai Tenth People's Hospital, Tongji University School of Medicine, No. 301 Middle Yanchang Road, Shanghai, China

⁴Department of Physics, University of Münster, Wilhelm-Klemm-Str. 9, 48149 Münster, Germany

⁵Laboratory of Molecular Cell Biology, Beijing Tibetan Hospital, China Tibetology Research Center, 218 Anwaixiaoguanbeili Street, Chaoyang, Beijing 100029, China

⁶Department of Stomatology, Daqing Oilfield General Hospital, Zhongkang Street No. 9, Saertu District, 163000 Daqing City, Heilongjiang Province, China

⁷Department of Prosthetics, School of Stomatology, Second Affiliated Dental Hospital of Jiamusi University, Hongqi Street No. 522, Jiamusi City, Heilongjiang Province, China

⁸Department of Stomatology, South District Hospital, Daqing Oilfield General Hospital Group, Tuqiang Fourth Street No. 14, Hong Gang District, Daqing City, Heilongjiang Province, China

⁹Department of Conservative Dentistry and Periodontology, Ludwig-Maximilians-University of Munich, Goethestrasse 70, 80336 Munich, Germany

¹⁰Stomatological Hospital, Southern Medical University, 510280 Guangzhou, China

¹¹Department of Cranio Maxillofacial Surgery, University Clinic Leipzig, Liebigstr. 12, 04103 Leipzig, Germany

Correspondence should be addressed to Xianda Hu; hellocean@hotmail.com

Received 9 September 2020; Revised 2 November 2020; Accepted 13 January 2021; Published 9 March 2021

Academic Editor: Wen-Jun Tu

Copyright © 2021 Xiaoxi Xi et al. This is an open access article distributed under the Creative Commons Attribution License, which permits unrestricted use, distribution, and reproduction in any medium, provided the original work is properly cited.

Aim. To identify the critical genetic and epigenetic biomarkers by constructing the long noncoding RNA- (lncRNA-) related competing endogenous RNA (ceRNA) network involved in irreversible pulp neural inflammation (pulpitis). **Materials and Methods.** The public datasets regarding irreversible pulpitis were downloaded from the gene expression omnibus (GEO) database. The differential expression analysis was performed to identify the differentially expressed genes (DEGs) and DELncRNAs. Functional enrichment analysis was performed to explore the biological processes and signaling pathways enriched by DEGs. By performing a weighted gene coexpression network analysis (WGCNA), the significant gene modules in each dataset were identified. Most importantly, DELncRNA-DEmRNA regulatory network and DELncRNA-associated ceRNA network were constructed. A transcription factor- (TF-) DEmRNA network was built to identify the critical TFs involved in pulpitis. **Result.** Two datasets (GSE92681 and GSE77459) were selected for analysis. DEGs involved in pulpitis were significantly enriched in seven signaling pathways (i.e., NOD-like receptor (NLR), Toll-like receptor (TLR), NF-kappa B, tumor necrosis factor (TNF), cell adhesion molecules (CAMs), chemokine, and cytokine-cytokine receptor interaction pathways). The ceRNA regulatory relationships were established consisting of three genes (i.e., LCP1, EZH2, and NR4A1), five miRNAs (i.e., miR-340-5p, miR-4731-5p, miR-27a-3p, miR-34a-5p, and miR-766-5p), and three lncRNAs (i.e., XIST, MIR155HG, and LINC00630). Six transcription factors (i.e., GATA2, ETS1, FOXP3, STAT1, FOS, and JUN) were identified to play pivotal roles in pulpitis.

Conclusion. This paper demonstrates the genetic and epigenetic mechanisms of irreversible pulpitis by revealing the ceRNA network. The biomarkers identified could provide research direction for the application of genetically modified stem cells in endodontic regeneration.

1. Introduction

Pulpitis, as the neuroinflammation of the sensory trigeminal afferent axons in the dental pulp tissue, is accompanied by the pain induced by the stimulation of the pulp nerve fibers [1]. As a dynamic immune-inflammatory disease, the balance between the inflammatory and regenerative responses in the diseased pulp determines the clinical outcome, for example, from healthy pulp to reversible pulpitis, to irreversible pulpitis, and until pulp necrosis and pulp death [2]. Irreversible pulpitis is of high therapeutical relevance, as it is characterized by lingering pain that is featured by thermal stimuli, spontaneous pain, and pain at night [3]. Root canal therapy (RCT) based on pulpotomy remains the only choice for irreversible pulpitis; however, RCT can cause the teeth to be more brittle and thus more easily fractured [4]. Given this complication of RCT, researchers are attempting to use a combination of mesenchymal stem cells, biomaterial scaffolds, and growth factors to preserve dental pulp and achieve the neurovascularization of pulp tissue based on methods of modern tissue engineering. Nevertheless, pulp regeneration approaches face many challenges such as lifespan and diffusion of growth factor, as well as degradation of biomaterial. To overcome all of these challenges, genetically modified stem cells have been increasingly investigated and have also been shown to achieve better efficacy compared to using stem cells alone [5]. Since genetically modified stem cell transplantation could be promising in endodontic regeneration, it is therefore essential to have a deep understanding of the genetic and epigenetic mechanisms involved in the pathology of pulpitis.

With the advent of gene detection techniques, the genetic and epigenetic mechanisms have been shown by microarray and sequencing datasets [6, 7] to play a critical role in the immune-inflammatory response and repair response of pulpitis. As is well known, a messenger RNA (mRNA) as a protein-coding RNA can be targeted by multiple noncoding RNAs such as microRNAs (miRNAs) and long noncoding RNAs (lncRNAs) [8, 9]. Based on the competing endogenous RNA (ceRNA) hypothesis proposed by Salmena et al., lncRNAs harboring miRNA response elements (MREs) and mRNAs can compete with each other by binding to a shared miRNA, thereby acting as molecular “sponges” and inducing translational repression at the posttranscriptional level [10]. Since the ceRNA network has been demonstrated to be involved in many inflammatory conditions and cancers [11], this network is possibly also involved in pulpal inflammation and should therefore be investigated. The bioinformatic techniques integrate all of the expression profiling datasets available to the public and allow the identification of critical biomarkers involved in the ceRNA network to be possible. Up until now, there is only one study available that examined this issue; however, there are differences in terms of study designs and processes, thereby obtaining quite distinct results [12].

Therefore, the current study is aimed at identifying many genetic and epigenetic biomarkers, including significantly enriched pathways of differentially expressed genes, critical genes involved in the protein-protein interaction network and the ceRNA network, critical miRNAs and lncRNAs involved in the ceRNA network, and transcription factors involved in the TF-mRNA network. The identification of these biomarkers will be helpful for the genetic modification of stem cells and will benefit pulpal regeneration and the shift from irreversible pulpitis to reversible pulpitis.

2. Methods

2.1. Procurement of Datasets. The microarray datasets regarding irreversible pulpitis were searched from the GEO of the NCBI database [13]. The genetic datasets could be investigating mRNA expression profile or noncoding RNA expression profile. The inclusion criteria of datasets were established as follows. (1) The study design of the included datasets should be established as two groups, including normal pulp tissue as the control group and inflamed pulp tissue as the experimental group. (2) The samples were taken from the adults (18 years or older) presenting for endodontic treatment with no evidence of periapical pathoses (i.e., radiolucency, swelling, and pressure sensitivity) and no previous pulp therapy (i.e., pulp capping). (3) Normal pulp tissues in the control group of the included datasets were collected from healthy third molars or teeth extracted for orthodontic purpose. Inflamed pulp tissues in the experimental group of the included datasets were extracted from teeth diagnosed with irreversible pulpitis in accordance with the endodontics diagnoses system from the American Association of Endodontists. (4) The sample size for each group in the included datasets should be more than three. The exclusion criteria of datasets were established as follows: (1) the datasets which had the different study design; (2) the datasets which took the pulp samples from the teeth with periodontitis/incompletely developed roots; (3) the datasets which took the pulp samples from the patients who had a compromised immune system or those who were taking medications known to influence the immune response; (4) the sample size for each group in the included datasets was less than three. According to the inclusion and exclusion criteria mentioned above, two datasets (GSE92681 and GSE77459) were therefore obtained.

2.2. Procurement of miRNA-mRNA and miRNA-lncRNA Interaction Data. The human’s experimentally validated miRNA-target interaction pairs’ data that have been validated by experiments were downloaded from three databases: TarBase (version 6.0) [14], miRTarBase (version 4.5) [15], and miRecords (version 4) [16]. The human’s experimentally validated miRNA-lncRNA interaction pairs’ data were downloaded from the starBase (version 2.0) database [17].

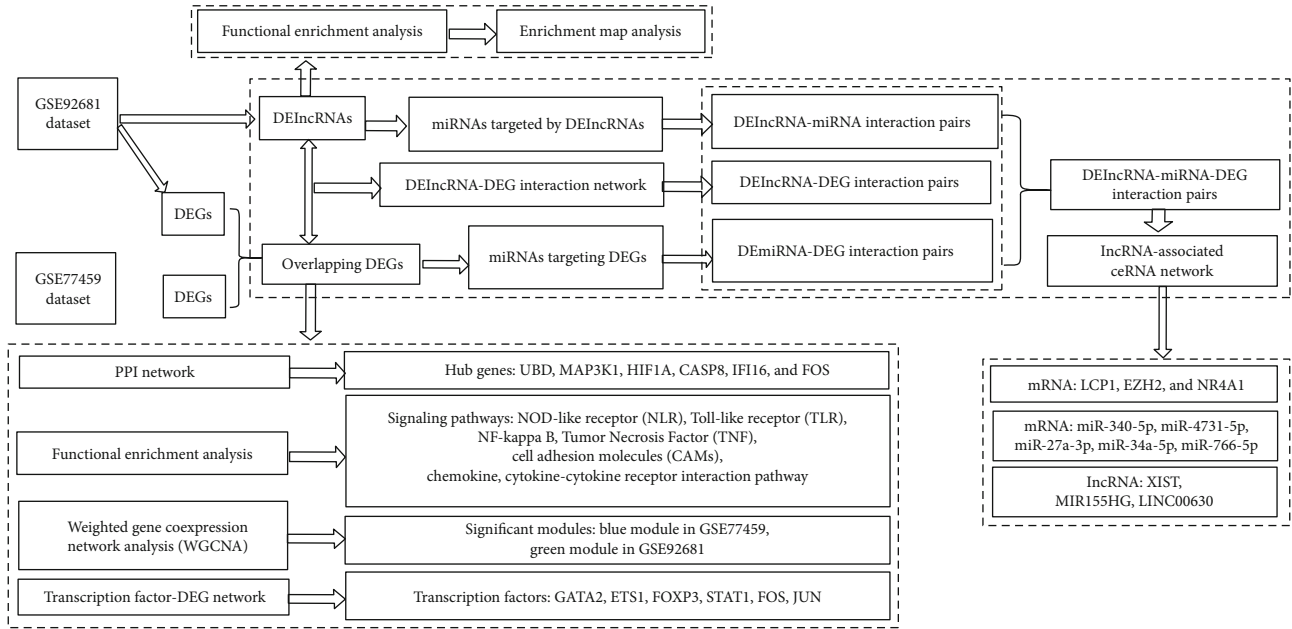


FIGURE 1: The flowchart of the present study. Two datasets (GSE92681 and GSE77459) were analyzed in this research by using varying bioinformatic analyzing methods, for example, differential expression analysis, functional enrichment analysis, weighted gene coexpression network analysis (WGCNA), enrichment map analysis, and network construction analysis (e.g., TF-DEG network, DEIncRNA-DEG network, and ceRNA network).

2.3. Differential Expression Analysis. Regarding the dataset GSE92681, the probe sequences were reannotated because the corresponding gene symbols of probes cannot be obtained. The lncRNA and mRNA data were obtained from the platform of the GSE92681 dataset after annotation. The differential expression analysis was performed by using the Linear Models for Microarray data (limma) R/Bioconductor package [18] to identify the differentially expressed genes (DEGs), and differentially expressed lncRNAs (DEIncRNAs) were identified between irreversible pulpitis samples and control healthy pulpal samples. The gene and lncRNAs that had the required cutoff criteria (p value < 0.05 and a $|\log_2$ fold change (FC)| > 1) were considered as DEGs and DEIncRNAs. The Venn diagram was used to visualize the overlapped and union DEGs identified by two datasets.

2.4. Functional Enrichment Analysis of DEGs. The DEGs overlapped by two datasets (GSE77459 and GSE92681) were used for the functional enrichment analysis in order to explore the regulated biological processes and signaling pathways that are involved by these DEGs. The functional enrichment analysis was performed by using clusterProfiler package in the Bioconductor package [19]. The functional terms with p value < 0.05 were regarded to be significant.

2.5. Construction of Protein-Protein Interaction (PPI) Network. To comprehensively analyze the functions of DEGs involved in the entire biological network of pulpitis, the union DEGs identified from two datasets were used for the PPI network analysis instead of only taking the overlapped intersection DEGs. The interacting genes of these DEGs were downloaded from HPRD [20] and the BioGRID database

TABLE 1: The pulpitis-related datasets used for the present analysis.

Datasets	Experimental type of datasets	Sample size of inflamed pulp tissue	Sample size of healthy pulp tissue
GSE92681	Noncoding RNA	7	5
GSE77459	mRNA	6	6

TABLE 2: The number of upregulated and downregulated DEGs or DEIncRNAs identified from included datasets.

Datasets	Number of upregulated factors	Number of downregulated factors	Number of total factors
GSE92681_DEIncRNA	138	136	274
GSE92681_DEG	486	178	664
GSE77459_DEG	823	278	1101

[21]. The visualization of a PPI network was performed by using Cytoscape software [22]. Several topological features (i.e., degree, average shortest path length, betweenness centrality, closeness centrality, clustering coefficient, and topological coefficient) of the nodes (protein) in this PPI network were calculated by using CytoNCA plugin in Cytoscape software to screen hub genes. The top 20 genes were selected from this network, and their topological features were listed.

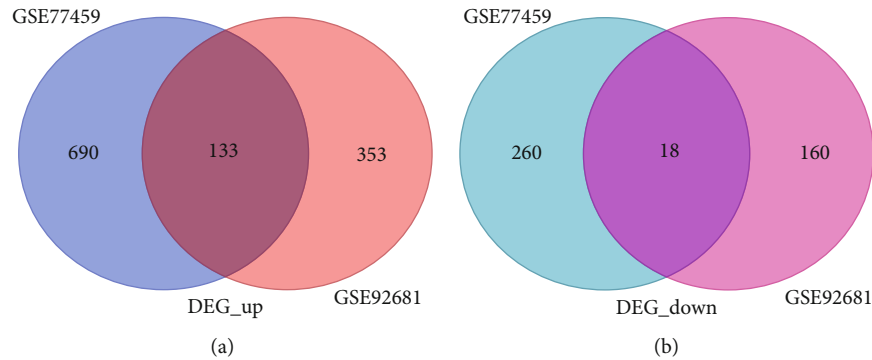


FIGURE 2: The Venn diagram shows the (a) up- and (b) downregulated DEGs identified by two datasets (GSE77459 and GSE92681). 133 upregulated DEGs and 18 downregulated DEGs were found to be overlapped between DEGs of GSE77459 and GSE92681.

2.6. Weighted Gene Coexpression Network Analysis. To further analyze the functions of interacting genes in the pathogenesis of pulpitis, the weighted gene coexpression network was constructed by using weighted gene coexpression network analysis (WGCNA). The genes with p value < 0.05 were selected, and the expression profile data of these genes were obtained. The significant gene modules were selected, and genetic interactions within each module were investigated. Based on the HPRD and BioGRID database, the PPI network of the selected significant gene modules was constructed, respectively. The top 25 gene nodes in these PPI networks were calculated and listed.

2.7. Functional Enrichment Analysis of DElncRNAs. Based on the GSE92681 dataset, the coexpression status of DElncRNAs and DEGs was calculated by using a statistical method—Pearson correlation. The significant interaction pairs with PPC (Pearson correlation coefficient) > 0.98 and p value < 0.05 were selected. The functional enrichment analysis using clusterProfiler was performed to investigate the function of DElncRNAs within the selected significant interaction pairs. The function terms with p value < 0.05 were regarded as significant function terms.

2.8. Enrichment Map Analysis. The enrichment map analysis using Cytoscape plugin was performed for functional enrichment visualization. The enrichment map organizes enriched terms into a network with edges connecting overlapping gene sets [23]. This map in the present study was constructed to show the similarity among the function terms of genes regulated by lncRNAs. The enriched functions of genes targeted by DElncRNAs can interact with each other instead of being separate and isolated; thus, the dysregulation of a certain function term may result in the aberrant regulation of its interacted functions terms. In the enrichment map, nodes represent the functional GO terms. The color intensity of nodes represents significance (p value), and the color of nodes is lighter when the p value is bigger. The edge thickness represents the degree of gene overlap that exists between two GO terms. The edge is wider when the mutual gene overlap between two GO terms is larger; that is to say, the similarity between these two GO terms is bigger.

2.9. Construction of a DElncRNA-DEG Regulatory Network. The interaction pairs of DElncRNA-DEG were obtained and used to construct a DElncRNA-DEG regulatory network. The topological characteristics of nodes in this network were calculated, and the top 20 nodes were ranked in descending order according to the degree.

2.10. Construction of a Transcription Factor- (TF-) DEG Network. First, DEGs obtained from two datasets (GSE92681 and GSE77459) were combined and used for subsequent analysis. The transcription factor- (TF-) DEG interaction pairs were then obtained from several databases, including TRANSFAC [24], TRED [25], and ORTI [26]. Based on these interaction pairs, the TF-DEG regulatory network was constructed. The topological feature of the nodes in this TF-DEG network was calculated, and the top 20 nodes were ranked in descending order according to the degree.

2.11. Construction of a ceRNA Network. The miRNAs that target DEGs and miRNAs targeted by DElncRNAs were obtained from the starBase database [17]. Afterward, we integrated coexpressed DElncRNA-mRNA interaction pairs, DElncRNA-miRNA interaction pairs, and DEG-miRNA interaction pairs. Based on these interaction pairs, a ceRNA network was constructed consisting of DElncRNA-miRNA-DEmRNA interaction pairs. The topological feature of nodes in this ceRNA network was calculated, and the top 20 nodes were listed in a descending rank according to the degree. In addition, in order to obtain the functional modules between lncRNA-mRNA interactions and miRNA-mRNA interactions, the Cytoscape plugin MCODE is used to identify the clusters in the ceRNA network.

3. Results

3.1. The Study Flowchart. The analyzing sequence of the present study is presented in Figure 1. As shown in Figure 1, two datasets regarding irreversible pulpitis were analyzed by performing differential expression analysis to identify DEGs and DElncRNAs, by carrying out functional enrichment analysis to identify signaling pathways, by constructing the DEG-TF network to identify critical TFs, and finally by building

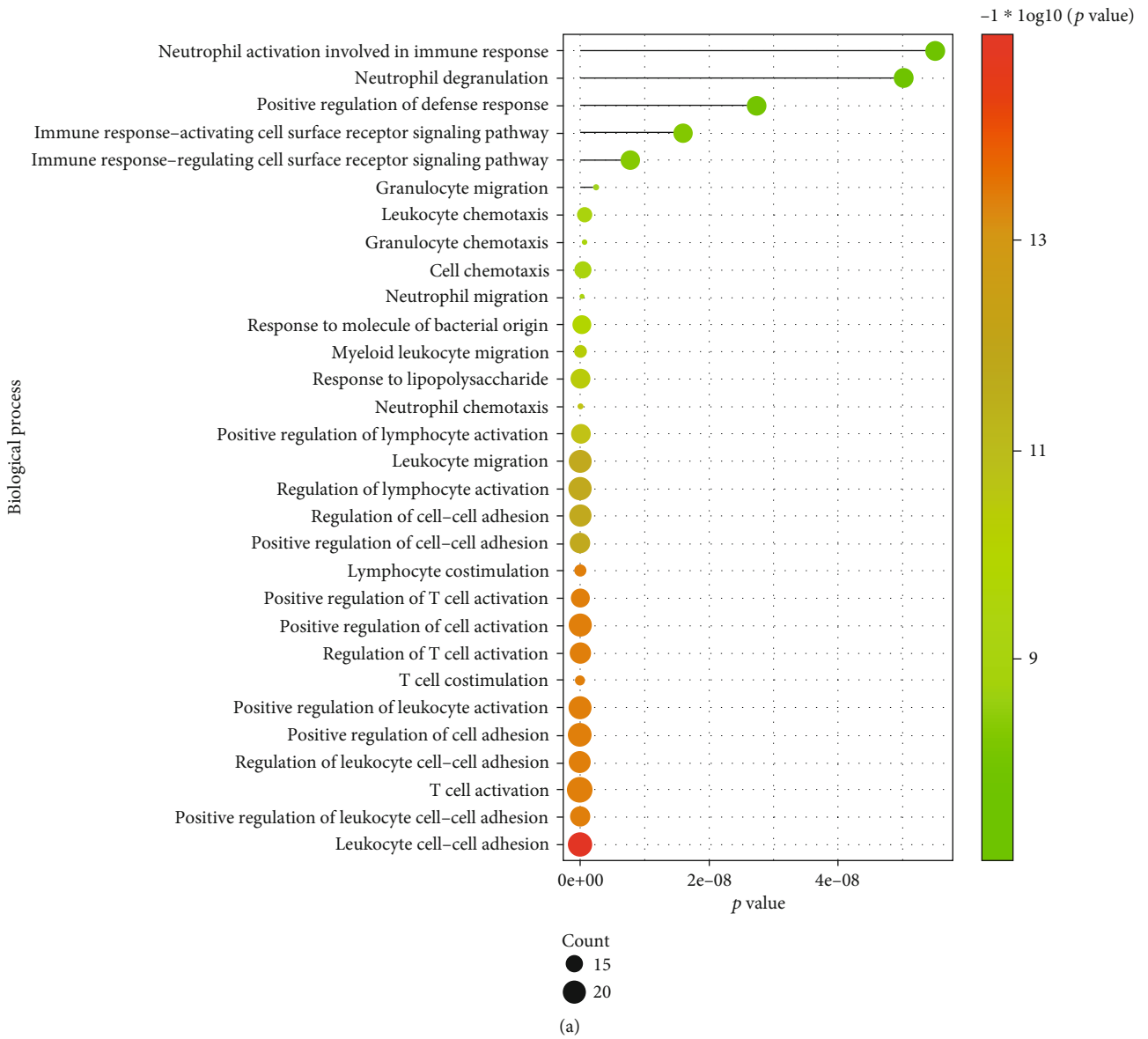


FIGURE 3: Continued.

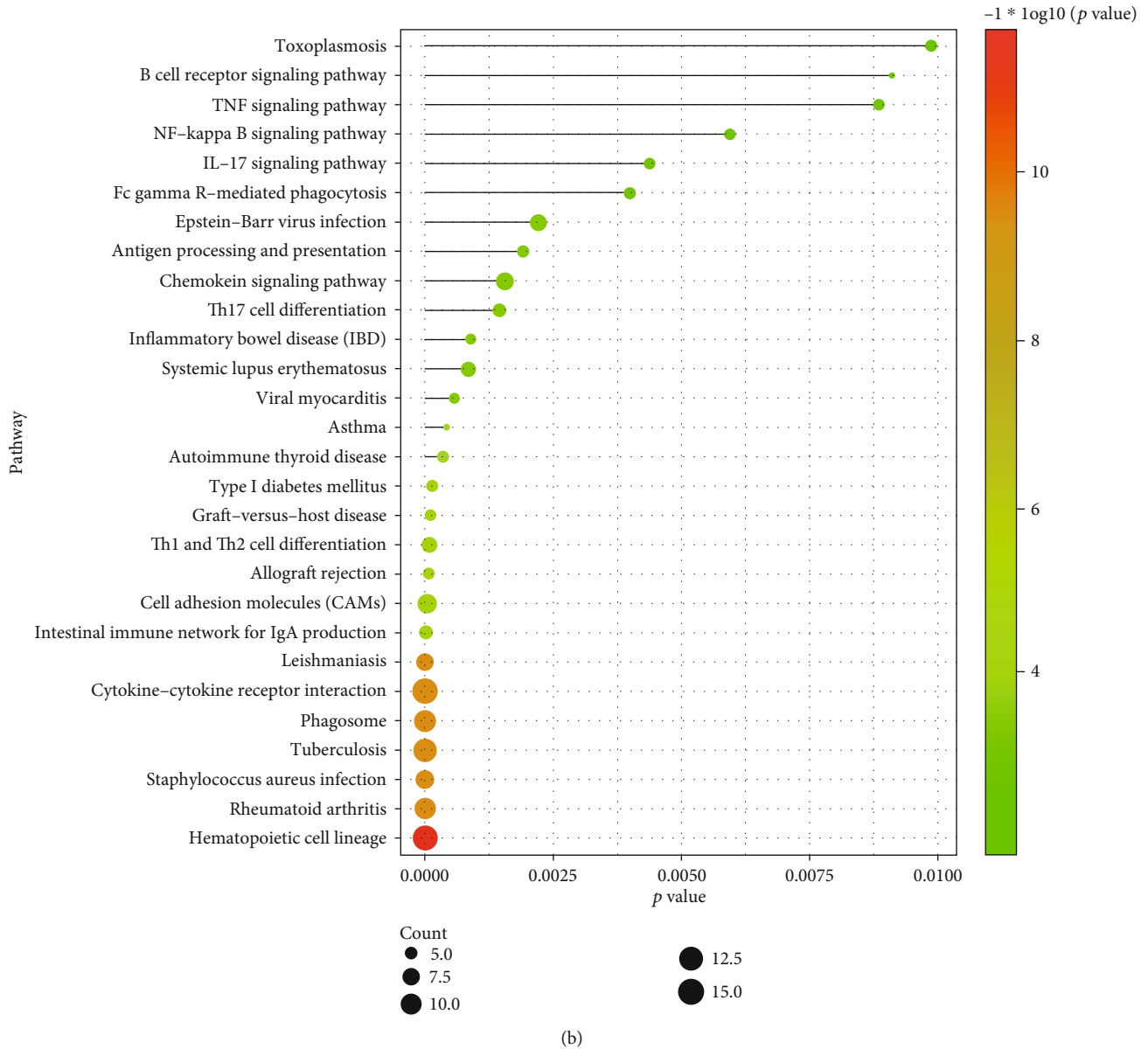


FIGURE 3: The functional enrichment analysis of DEGs overlapped in two datasets (GSE77459 and GSE92681). (a) The significantly enriched biological processes of overlapped DEGs. (b) The significantly enriched signaling pathways of overlapped DEGs.

lncRNA-associated ceRNA network to identify the critical genes, miRNAs, and lncRNAs.

3.2. Identification of DEGs. The GSE92681 dataset based on the GPL16956 platform analyzed the noncoding RNA expression profiling data of 7 inflamed pulpal tissues and 5 healthy pulpal tissues (Table 1). The GSE77459 dataset based on the GPL17692 platform analyzed the mRNA expression profiling data of 6 inflamed pulpal tissues and 6 healthy pulpal tissues (Table 1). From the dataset GSE92681, 274 DElncRNAs (138 upregulated and 136 downregulated) and 664 DEGs (486 upregulated and 178 downregulated) were identified (Table 2). From the dataset GSE77459, a total of 1,101 DEGs consisting of 823 upregulated and 278 downregulated were

identified (Table 2). In addition, the intersection parts shown in the Venn diagram (Figure 2) show that 151 DEGs including 133 upregulated DEGs and 18 downregulated DEGs were found to be overlapped by two datasets. When considering the union parts of the Venn diagram, a total of 1,176 upregulated DEGs and 438 downregulated DEGs were identified.

3.3. Biological Processes and Signaling Pathways Enriched by DEGs. As shown in Figure 3(a), DEGs were significantly involved in many biological processes, for instance, cell adhesion-related BPs, immune cells (e.g., 3T cell, neutrophil, granulocyte, leukocyte, and lymphocyte)-related BPs, and immune response-related BPs. As shown in Figure 3(b), DEGs were significantly involved in many signaling

TABLE 3: The topological characteristics of the top 20 nodes in the PPI network.

Gene name	Degree	Average shortest path length	Betweenness centrality	Closeness centrality	Clustering coefficient	Topological coefficient
UBD	656	2.700089	0.092136	0.370358	0.001564	0.003702
UBC	460	2.20363	0.309699	0.453797	0.004092	0.005551
IFI16	436	2.853032	0.052658	0.350504	0.001381	0.005531
ARRB2	369	2.872067	0.040035	0.348181	0.001915	0.007365
HLA-B	338	2.825255	0.037735	0.35395	0.002915	0.00551
EZH2	301	2.891545	0.030774	0.345836	0.00206	0.008083
SFN	296	2.903608	0.032059	0.344399	0.00213	0.00725
ADRB2	294	2.855246	0.033685	0.350233	0.003088	0.006755
LYN	243	2.795595	0.03365	0.357706	0.013332	0.008931
MAP3K1	229	2.901173	0.021399	0.344688	0.00406	0.009621
FOS	226	2.943448	0.02579	0.339738	0.00468	0.010265
RPS9	208	2.82127	0.017896	0.35445	0.009337	0.00958
KPNA2	205	2.867641	0.022731	0.348719	0.00263	0.009771
IL7R	199	2.931496	0.015151	0.341123	0.002944	0.011601
LGR4	198	3.039287	0.020276	0.329025	3.59E-04	0.010662
CASP8	196	2.906707	0.020462	0.344032	0.008791	0.010607
CD247	196	2.964697	0.024808	0.337303	0.00539	0.010402
HIF1A	174	2.950089	0.016343	0.338973	0.003123	0.013813
MYO19	173	2.93548	0.0148	0.34066	0.010687	0.00917
MNDA	168	3.236498	0.007305	0.308976	7.84E - 04	0.012766

pathways, for instance, chemokine and cytokine-related pathways (i.e., TNF, IL-17, chemokine, and cytokine-cytokine receptor interaction), T cell and B cell-related pathways (i.e., B cell receptor and Th1 and Th2 cell differentiation), NF-kappa B, and microbial infection-related pathways (i.e., Epstein-Barr virus infection and *Staphylococcus aureus* infection).

3.4. Identification of Hub Genes by Constructing the PPI Network. The PPI network of DEGs expressed in pulpitis shown in Figure 2 consisted of 9,070 gene nodes and 24,903 PPI interaction pairs. File S1 shows the topological characteristics of all DEG nodes in Figure 2. Table 3 shows the top 20 gene nodes were ranked in descending order according to their degree. It can be seen from Figure 4 that the gene UBD with the highest degree was identified to play the most important role in the network by interacting with the highest number of DEGs. Apart from the gene UBD, some other upregulated DEGs (e.g., IFI16, ARRB2, HLA-B, EZH2, ADRB2, LYN, FOS, RPS9, KPNA2, IL7R, CASP8, CD247, HIF1A, MYO19, and MNDA) and downregulated DEGs (e.g., SFN, MAP3K1, and LGR4) were also identified to play critical roles in the network.

3.5. Enriched Biological Processes of DElncRNAs. As shown in Figure 5, DElncRNAs were found to be significantly involved in many biological processes, for example, immune cells (dendritic cells, leukocytes, and T cells)-related BPs (e.g., regulation of dendritic cell differentiation, dendritic cell differ-

entiation, T cell activation involved in immune response, regulation of T cell activation, and leukocyte differentiation), cytokine-related BPs (i.e., interferon-gamma production, regulation of cytokine secretion, and negative regulation of cytokine secretion).

3.6. The Similarity of Functional Terms of DElncRNAs. As shown in Figure 6, immune cells (e.g., lymphocytes, leukocytes, and T cells)-related GO functional terms were observed to interact with cytokine-related GO terms (e.g., the cellular response of cytokine stimulus, positive regulation of cytokine production, and regulation of interleukin-1 production).

3.7. The DElncRNA-DEG Regulatory Network. As shown in Figure 7, the DElncRNA-DEG regulatory network consisted of 312 nodes and 905 edges. File S2 shows the characteristics of all nodes in the network in Figure 7. As seen from Table 4, many lncRNAs with the highest degree play critical roles in the network, such as RP11-702F3.3, RP5-963E22.4, RP11-555G19.1, CTD-2568A17.1, and PRSS29P.

3.8. Identification of Hub Transcription Factor. The TF-DEG regulatory network consisted of 1,750 nodes and 17,095 edges (Figure 8). File S3 shows the topological characteristics of all nodes in the network in Figure 8. Combining the data shown in Figure 8 and Table 5, it can be found that only one TF-FOS was differentially expressed in pulpitis among the top 20 nodes of the TF-DEG network. Although the other 19 nodes (i.e., GATA2, ETS1, YBX1, AR, FOXP3, GATA1,

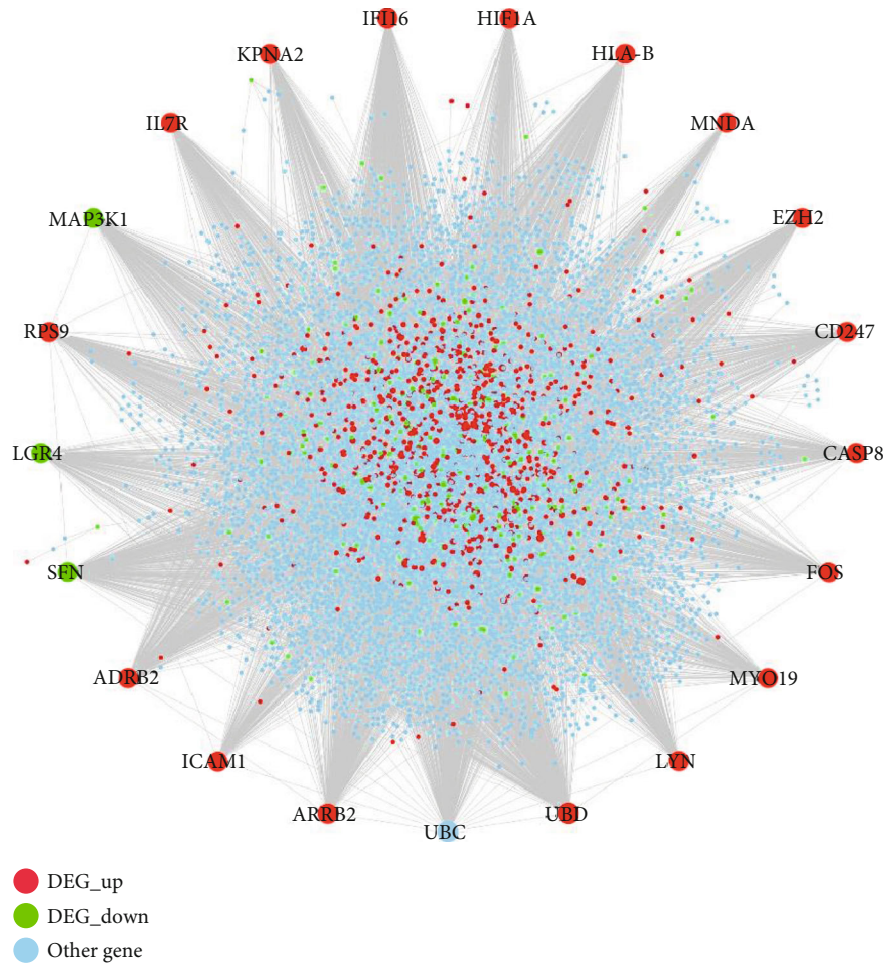


FIGURE 4: The PPI network of DEGs. The red and green circle nodes represent up- and downregulated DEGs, respectively. The sky-blue circle nodes represent the non-DEGs which interact with DEGs in the PPI network.

SP1, E2F4, PRDM14, ARNT, MIA3, JUN, CREB1, FOS, STAT1, CEBPA, AHR, E2F1, PAX5, and Pax-5) except FOS were not differentially expressed in pulpitis, they still play critical roles in the pathogenesis of pulpitis by interacting and regulating DEGs that are expressed in pulpitis. As seen from Figure 8, some other TFs were also found to be differentially expressed in pulpitis, for example, some FOSB, JUNB, EGR1, HIF1A, PLAU, MECOM, TP63, and BDNF.

3.9. Identification of Significant Gene Modules. As seen from Figure 9, five gene modules with varying colors (i.e., blue, brown, grey, turquoise, and yellow) were identified from GSE77459. Among these five coexpressed gene modules, the blue module with the lowest p value was found to be the most significant module. Regarding GSE92681, eight gene modules with various colors (i.e., black, blue, brown, green, grey, red, turquoise, and yellow) were identified, among which the green module with the lowest p value was found to be the most significant module.

3.10. Construction of PPI Network for Selected Significant Gene Modules. The PPI networks were constructed for these

two selected significant coexpressed gene modules (blue module in GSE77459 (Figure 10) and green module in GSE92681 (Figure 11)), respectively. The PPI network of the blue module within the GSE77459 dataset consisted of 3,599 gene nodes and 4,712 edges, while the PPI network of the green module within the GSE92681 dataset consisted of 930 gene nodes and 1,019 edges. Files S4 and S5 show the topological characteristics of all nodes of the network shown in Figures 10 and 11, respectively. Tables 6 and 7 show the topological characteristics of these two PPI networks depicted in Figures 10 and 11, respectively. Among the top 25 genes in the PPI network of the blue module of the GSE77459 dataset, only 3 upregulated DEGs (BIRC3, ITPR3, and PTPRB) were found; by contrast, the other 22 genes within the top 25 gene nodes were not DEGs (Table 6). Among the top 25 genes in the PPI network of the green module of the GSE92681 dataset, only one upregulated DEG (MMP-7) and one downregulated DEG (IK) were found; by contrast, the other 23 genes were not DEGs (Table 7).

3.11. The ceRNA Network. As shown in Figure 12, a ceRNA network consisting of DElncRNA-miRNA-DEmRNA

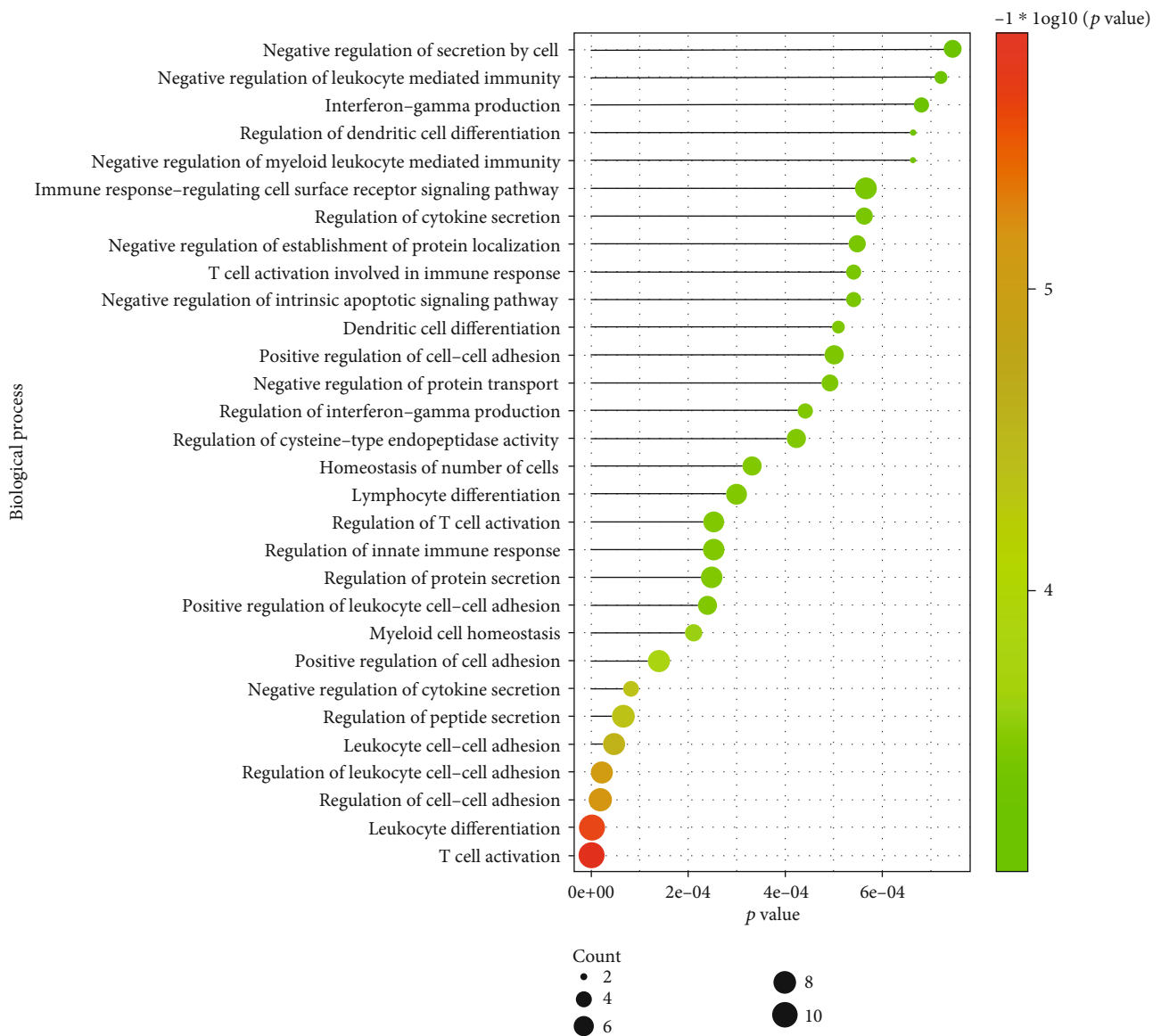


FIGURE 5: The significantly enriched biological processes of DElncRNAs. Count represents the number of genes enriched in a BP term, and $-\log_{10}[p \text{ value}]$ represents the enrichment score. The bigger size of the dots corresponding to a BP term means more genes were enriched in this term. The colored dots represent the term enrichment: green indicates low enrichment, and red indicates high enrichment.

interaction pairs was depicted. File S6 shows the topological characteristics of all nodes in the network in Figure 12. Combined with the information of the top 20 nodes shown in Table 8, it can be observed that lncRNA XIST plays the most important role in this network. Apart from lncRNA XIST, some genes (e.g., MIR155HG, LCP1, EZH2, and NR4A1) and several miRNAs (e.g., hsa-miR-340-5p, hsa-miR-4731-5p, hsa-miR-5590-3p, hsa-miR-27a-3p, hsa-miR-27b-3p, hsa-miR-329-3p, hsa-miR-362-3p, hsa-miR-494-3p, hsa-miR-424-5p, hsa-miR-2682-5p, hsa-miR-515-5p, hsa-miR-766-5p, hsa-miR-449c-5p, hsa-miR-34a-5p, and hsa-miR-449a) also play critical roles in the network. As shown in Figures 13(a)–13(c), three clusters were identified from the ceRNA network. As seen from Figure 13(c), LINC00630

can compete with two miRNAs (miR-539-3p and miR-485-3p) in targeting gene PEX5, and LINC00630 can indirectly target gene PEX5.

4. Discussion

This study identified many genetic and epigenetic biomarkers involved in the pathology of pulpitis, including six hub genes in the PPI network (i.e., UBD, MAP3K1, HIF1A, CASP8, IFI16, and FOS), several factors involved in the ceRNA network (e.g., three genes (i.e., LCP1, EZH2, and NR4A1), five miRNAs (i.e., miR-340-5p, miR-4731-5p, miR-27a-3p, miR-34a-5p, and miR-766-5p), and three lncRNAs (i.e., XIST, MIR155HG, and LINC00630)), six

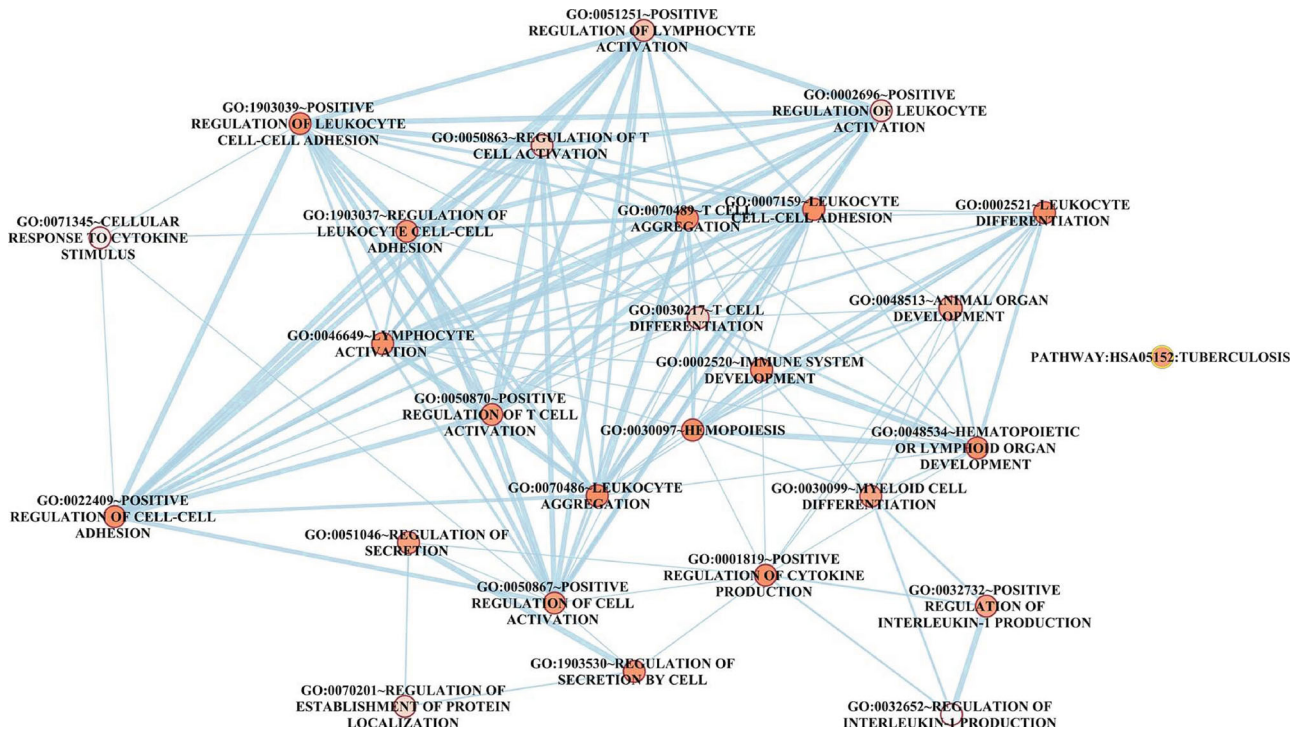


FIGURE 6: The enrichment map shows the GO interacting network of genes targeted by DELncRNAs. The orange circle node represents the significantly enriched GO terms, and the line represents the interaction between GO terms.

transcription factors (i.e., GATA2, ETS1, FOXP3, STAT1, FOS, and JUN), and seven signaling pathways (i.e., NOD-like receptor (NLR), Toll-like receptor (TLR), NF-kappa B, tumor necrosis factor (TNF), cell adhesion molecules (CAMs), chemokine, and cytokine-cytokine receptor interaction pathway). The detailed roles of these critical factors are supported by the previous scholar evidence and will be described in the following section.

Many genes are identified to be involved in the PPI network of pulpitis; however, there is still no direct evidence that can support the involvement of these genes in pulpitis. Herein, only six genes that were most investigated by previous research were described, including UBD, MAP3K1, HIF1A, CASP8, IFI16, and FOS. For the first example, UBD (Ubiquitin D) was shown to have multiple cellular processes that occurred in pulpitis: regulating NF-kappa B signaling pathway [27], mediating cell apoptosis in a caspase-dependent manner [28], and being involved in the maturation of dendritic cells [29]. Looking at the case of MAP3K1 (Mitogen-Activated Protein Kinase Kinase 1), this gene encodes a serine/threonine kinase and has been shown to be part of many signaling transduction cascades including ERK (extracellular signal-regulated kinases) [30] and JNK (c-Jun N-terminal kinase) kinase [31], NF-kappa B [32], TLR4 signaling [33], and IL-1 family signaling pathways [32]. Since these pathways mentioned here have been verified to be implicated in pulpitis [34–36], MAP3K1 can be speculated to be also involved in pulpal inflammation. Taking the case of HIF1A (hypoxia-inducible factor 1 subunit alpha), this gene encodes the alpha subunit of transcription factor

hypoxia-inducible factor-1 (HIF-1) [37]. This gene has been shown to regulate the cellular and systemic homeostatic response to the hypoxia environment by activating many genes related to angiogenesis and apoptosis [38]. Since the hypoxic environment caused by a collapse of the venous microcirculation during the pulpal inflammation could result in localized or generalized pulp necrosis and death [39], HIF1A could be a specific signal which indicates the potential deterioration risk from irreversible pulpitis to pulp necrosis and death. For example, caspase-8 and caspase-9 (encoded by CASP8 and CASP9) are cysteine proteases that play a crucial role in the signaling pathways of apoptosis, necrosis, and inflammation [40]. Since CASP9 is involved in cell apoptosis in human dental pulp stem cells from deciduous teeth [41] and also activation of caspase-9 can lead to activation of downstream caspase-8 [42], CASP8 can be therefore assumed to be involved in the signaling pathway of apoptosis in the pathogenesis of pulpitis. Another example is interferon gamma inducible protein 16 (IFI16) that is induced by IFN- γ , a member of the HIN-200 family of cytokines. A high prevalence of IFN- γ messenger RNA in inflamed pulps has been detected [43], and the methylated status of IFN- γ has been altered from total methylation in healthy pulp to partial methylation or unmethylation in the inflamed pulp. Since IFN- γ cytokine may be implicated in the immune response during the process of pulp inflammation [44], the epigenetic events of pulpitis could also be relevant to the alteration of IFI16. Looking at another example, the Fos gene family (FOS, FOSB, FOSL1, and FOSL2) has been suggested to regulate the process of cell proliferation, differentiation,

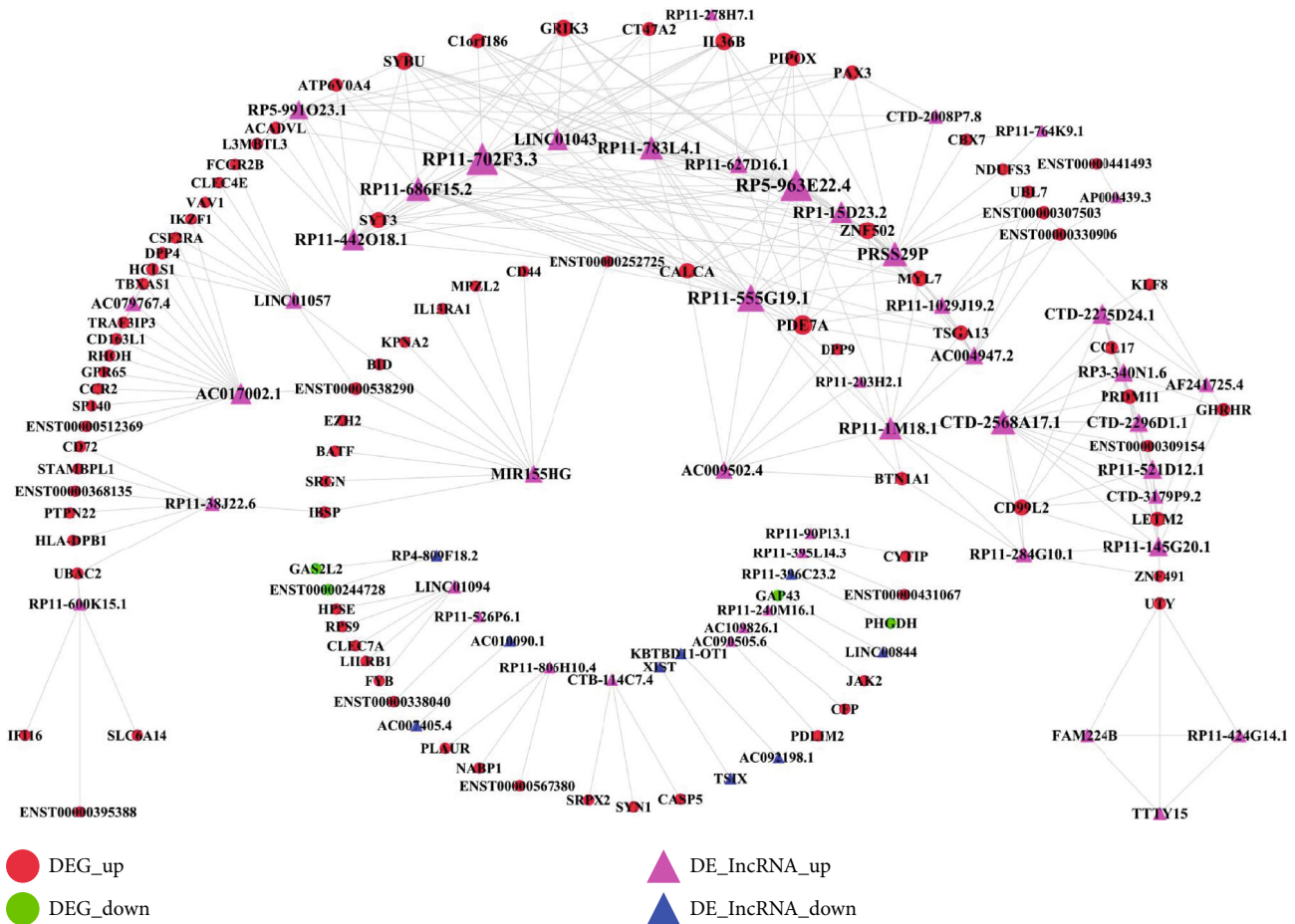


FIGURE 7: The DElncRNA-DEG regulatory network involved in pulpitis. The red circle nodes represent the upregulated DEGs, and the green circle nodes represent the downregulated DEGs. The rose-red triangle nodes represent the upregulated DElncRNA, and the blue triangle node represents the downregulated DElncRNA.

transformation, and apoptosis. The expression of the immediate-early gene product Fos was reported to be evoked by the LPS-induced pulpal inflammation in the rostral trigeminal regions of ferrets [45]. Regarding the pattern of its expression, another study using the rat model found that the expression of Fos induced by chronic tooth pulpal inflammation in dynorphin-rich regions of rat brainstem was shown to be temporal and spatial [46]. The role of almost all of the genes in pulpitis is based on speculation and thus needs to be validated in future research by designing relevant experiments.

Three genes (i.e., LCP1, EZH2, and NR4A1) are identified to be key biomarkers in the ceRNA network. For example, LCP1 (Lymphocyte Cytosolic Protein 1) is significantly enriched in a GO term named T cell activation [47]. The activation of T lymphocytes can orchestrate other types of immunocompetent cells, thereby promoting the local immune defense that occurred in the dental pulp [48]. Given this evidence, it can be assumed that LCP1 might be involved in the pathogenic mechanism of pulpitis by regulating T cell-mediated immune response. For another example, the enhancer of zeste homolog 2 (EZH2), as a catalytic subunit of PRC2 (polycomb repressor complex 2), could regulate

gene silencing via its histone methyltransferase activity, accumulation of DNA damage, and chromosome abnormalities [49]. EZH2 is suggested to be implicated in the pulp inflammation, proliferation, and regeneration by inhibiting osteogenic differentiation of human dental pulp cell (HDPCs) and enhancing inflammatory response and proliferation [50]. Another research investigating the effect of EZH2 in odontogenic differentiation of hDPCs suggested that EZH2 could impair mineralization of HDPCs under the mechanism of activating the Wnt canonical signaling pathway [51]. Taking the final example, Nuclear Receptor Subfamily 4 Group A Member 1 (NR4A1) is enriched in many pulpitis-related signaling pathways, including signaling by PDGF and EGFR, PI3K/AKT activation, and MAPK signaling pathways, and also some GO terms including positive regulation of endothelial cell proliferation and apoptotic process. The previous scholar evidence investigating the involvement of NR4A1 in inflammation showed that the overexpression of NR4A1 was associated with a chronic low-grade inflammatory state [52] and also plays a key role in mediating the anti-inflammatory effects of apoptotic cells [53]. However, the expression patterns and its regulatory mechanisms of NR4A1 remain to be researched in pulp inflammation.

TABLE 4: The topological characteristics of the top 20 nodes in the DElncRNA-DEG regulatory network.

Name	Degree	Average shortest path length	Betweenness centrality	Closeness centrality	Clustering coefficient	Topological coefficient	Regulate
RP11-702F3.3	32	2.26666667	0.09257337	0.44117647	0.36363636	0.2867215	lncRNAup
RP5-963E22.4	32	2.05	0.14685811	0.48780488	0.3982684	0.27954545	lncRNAup
RP11-555G19.1	25	2.21666667	0.08384754	0.45112782	0.37908497	0.30401235	lncRNAup
CTD-2568A17.1	21	2.56666667	0.17922917	0.38961039	0.37179487	0.26627219	lncRNAup
PRSS29P	21	2.28333333	0.18869008	0.4379562	0.20588235	0.26916221	lncRNAup
RP11-686F15.2	20	2.53333333	0.01950748	0.39473684	0.44761905	0.35757576	lncRNAup
RP11-783L4.1	19	2.58333333	0.01555518	0.38709677	0.47252747	0.37327189	lncRNAup
RP11-1M18.1	18	2.06666667	0.32645541	0.48387097	0.3030303	0.22644928	lncRNAup
LINC01043	17	2.61666667	0.01053104	0.38216561	0.43589744	0.36923077	lncRNAup
RP1-15D23.2	17	2.48333333	0.00914061	0.40268456	0.59090909	0.38333333	lncRNAup
RP11-442O18.1	17	2.66666667	0.03491119	0.375	0.3974359	0.33846154	lncRNAup
AC017002.1	16	2.35	0.51050061	0.42553191	0.05714286	0.17333333	lncRNAup
CTD-2275D24.1	14	3.23333333	0.02043004	0.30927835	0.44444444	0.41176471	lncRNAup
PDE7A	13	2.15	0.08844751	0.46511628	0.35897436	0.33208255	mRNA up
RP11-145G20.1	13	3.33333333	0.01660117	0.3	0.36111111	0.39869281	lncRNAup
RP11-521D12.1	13	3.35	0.00459174	0.29850746	0.5	0.43382353	lncRNAup
RP5-99IO23.1	13	3.03333333	0.01404135	0.32967033	0.33333333	0.31481481	lncRNAup
CTD-2296D1.1	12	3.36666667	0.00429011	0.2970297	0.5	0.453125	lncRNAup
RP3-340N1.6	12	3.35	0.0054601	0.29850746	0.57142857	0.44852941	lncRNAup
MIR155HG	11	2.55	0.41865079	0.39215686	0	0.12121212	lncRNAup

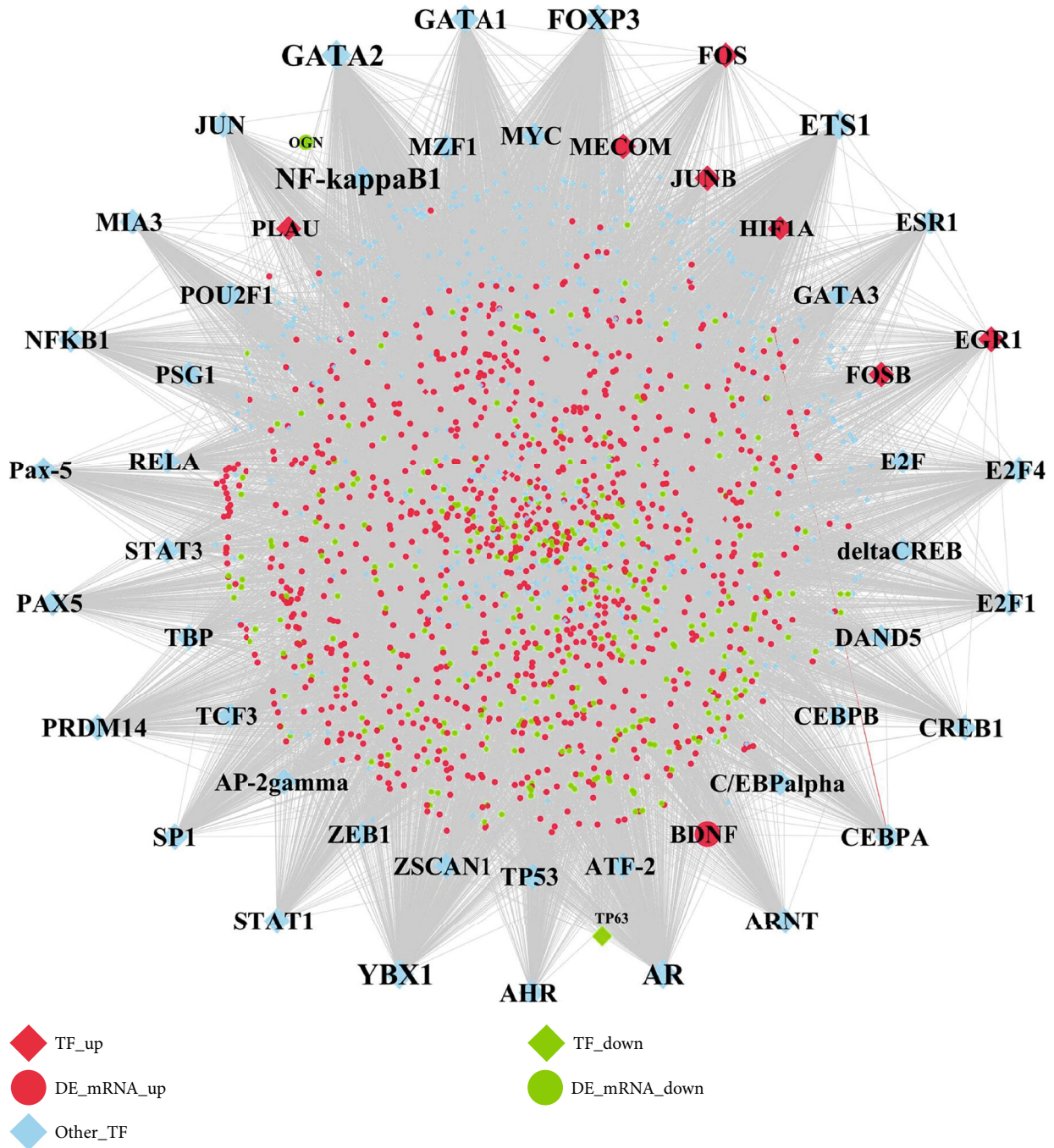


FIGURE 8: The TF-DEG regulatory network involved in pulpitis. The diamond nodes represent TFs and the circle nodes represent DEGs. For the diamond nodes, the red diamond nodes represent the upregulated TFs, the green diamond nodes represent the downregulated TFs, and the sky-blue diamond nodes represent other nondifferentially expressed TFs. For the circle nodes, red circle nodes represent the upregulated DEGs, while the green circle nodes represent the downregulated DEGs.

Many miRNAs are involved in the ceRNA network of pulpitis; however, the expression patterns and functions of almost all of them have not been investigated in pulpal inflammation. Based on the potential target genes of the miRNAs searched on the miRWalk database [54], some miRNAs (i.e., miR-340-5p, miR-4731-5p, miR-27a-3p, miR-34a-5p, and miR-766-5p) could be assumed to be implicated in pul-

pitis by targeting genes related to inflammatory response and regeneration. For the first example, miR-340-5p has been validated to target gene LIMS1 (LIM Zinc Finger Domain Containing 1), the encoded protein of which is involved in the integrin signaling [55]. Since integrin-associated signaling is implicated in the odontogenic stimulation of human dental pulp stem cells [56]; miR-340-5p might be involved in the

TABLE 5: The topological characteristics of the top 20 nodes in the TF-DEG regulatory network.

Name	Degree	Average shortest path length	Betweenness centrality	Closeness centrality	Clustering coefficient	Topological coefficient
GATA2	518	2.03887936	0.11659147	0.49046551	0.00308432	0.02016302
ETS1	508	2.05603202	0.11527216	0.48637375	0.0028654	0.02038007
YBX1	425	2.22012579	0.09284757	0.45042493	0.00137625	0.02440558
AR	414	2.18753573	0.08279112	0.45713539	0.0032635	0.02330064
FOXP3	407	2.24013722	0.09211348	0.44640123	0.00128297	0.02202286
GATA1	322	2.30360206	0.03470622	0.43410276	0.00336681	0.02811219
SP1	214	2.3619211	0.02271018	0.42338417	0.00842438	0.03168479
E2F4	203	2.50714694	0.02510997	0.39885975	0.00248744	0.03155395
PRDM14	194	2.47970269	0.01761185	0.40327415	0.00459377	0.03274385
ARNT	190	2.47970269	0.00990145	0.40327415	0.00668338	0.04482786
MIA3	182	2.51172098	0.00828163	0.39813339	0.00558557	0.04629319
JUN	179	2.45740423	0.0132459	0.40693346	0.01726194	0.03584432
CREB1	178	2.43853631	0.0134572	0.41008206	0.01314035	0.03899076
FOS	178	2.04116638	0.03258878	0.48991597	0.05986161	0.0352397
STAT1	176	2.51229274	0.01672367	0.39804279	0.00525974	0.03983636
CEBPA	168	2.58604917	0.01187163	0.38669025	0.00377816	0.04812159
AHR	168	2.53459119	0.00776619	0.39454094	0.00620188	0.04722287
E2F1	165	2.50085763	0.01123109	0.39986283	0.00657797	0.04104892
PAX5	164	2.51172098	0.00771197	0.39813339	0.00890319	0.0434212
Pax-5	161	2.56089194	0.0066902	0.39048895	0.00535714	0.04834386

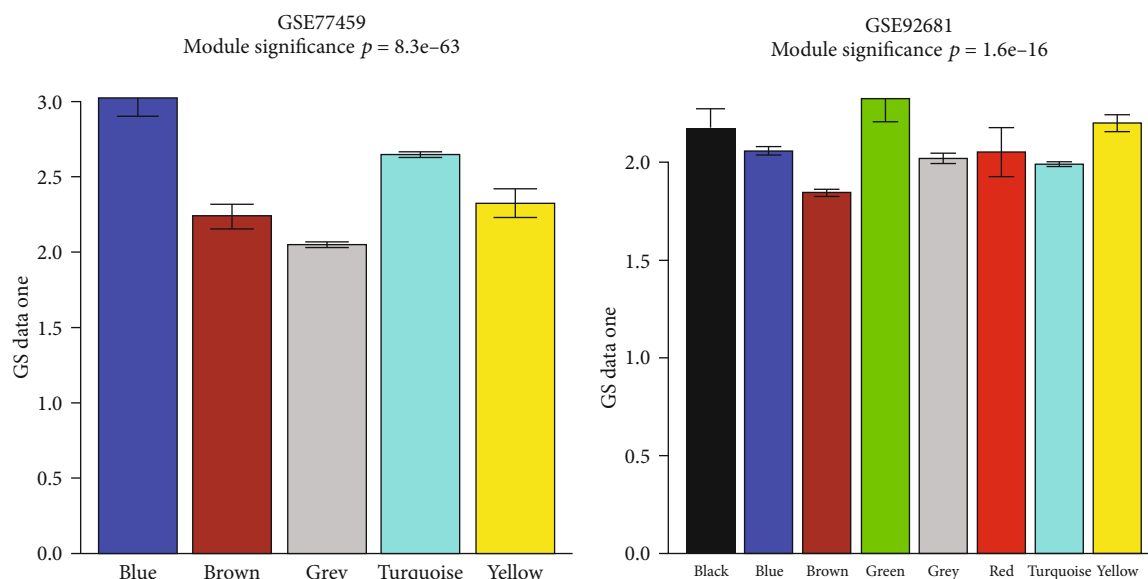


FIGURE 9: The coexpressed gene modules identified in GSE77459 and GSE92681. The horizontal axis represents each different color module; the vertical axis represents the correlation coefficient between genes in each module and disease status.

pulp healing and regeneration during the pathogenic processes of pulpitis. In the case of miR-4731-5p, it has been validated to target gene IRAK4 (Interleukin 1 Receptor-Associated Kinase 4), which encodes a kinase that can activate the upregulation of NF-kappa B [57]. Since NF-kappa B has been found to be activated by lipopolysaccharide (LPS) and tumor necrosis factor (TNF) in the dental pulp stem cells (DPSCs) and further implicated in the immune response of pulpal infection [35], miR-4731-5p could be regarded as an inflammatory biomarker during the pulpal inflammation. In the case of miR-27a-3p, it has been found to regulate the cell proliferation of vascular endothelial cells positively and further being implicated in the angiogenesis and neovascularization through ERK1 and ERK2 cascade [58]. Since an increased number of blood vessels have been found in the inflamed human dental pulp [59], miR-27a-3p could be involved in the pulpal regeneration by mediating angiogenesis during the process of pulpitis. Taking the example of miR-34a-5p, it has been validated to target the gene MAP2K1 (Mitogen-Activated Protein Kinase 1), which encodes a dual-specificity kinase that has been well-known to be involved in the ERK pathway [60]. Since the MAP/ERK pathway is implicated in the differentiation and stimulation of odontoblasts during reactionary dentinogenesis [61], miR-34a-5p might be involved in the dentinogenesis-based repair mechanism during the pathogenesis of pulpitis. In the case of miR-766-5p, it is one of the subtypes of miR-766 which is upregulated in inflamed pulpitis compared to the normal pulps [62]. miR-766 can target Heat Shock Transcription Factor 1 (HSF1), which encodes a transcription factor that can be rapidly induced after temperature stress [63]. Since thermal stresses, including hot and cold loadings, may induce the activation of tooth pain signaling [64], miR-766 could be assumed to be a sensitive biomarker of thermal exposure.

Three lncRNAs (i.e., XIST, MIR155HG, and LINC00630) are identified to be key factors involved in the ceRNA network of pulpitis. For the first example, the lncRNA X Inactive Specific Transcript (XIST), as a 17 kb long RNA transcribed by the inactive X chromosome, is involved in the X chromosome inactivation in female mammals, thus providing dosage equivalence between males and females [65]. More and more scholarly evidence has shown that XIST is dysregulated in many cancers and inflammatory conditions [66–69]. A recent study found that XIST can mediate the inflammation process of mammary epithelial cells by regulating the NF- κ B/NLRP3 inflammasome pathway [70]. In the case of the lncRNA MIR155HG (MIR155 Host Gene), it is formerly known as BIC (B-cell integration cluster) and has been shown to function as a primary micro (mi)RNA for miR-155 [71]. Since miR-155 has been established to be an ancient master regulator of the immune response [72], the MIR155HG/miR-155 axis may be involved in many physiological and pathological processes including inflammation and immunity [73]. In the case of LINC00630, this lncRNA can interact with miR-539-3p, miR-485-3p, and PEX5 gene and combinedly generate a closed regulatory loop in the ceRNA network. The gene PEX5 (Peroxisomal Biogenesis Factor 5) encodes the type 1 peroxisomal targeting signal (PTS1) receptor, which is one of 15 peroxins required for peroxisome biogenesis [74]. A recent study showed that peroxisomes could resolve microbial infection by modulating many innate immune-related pathways (reactive oxygen species (ROS) and reactive nitrogen species (RNS) signaling) and activating the stress response kinase p38 [75]. Based on the finding of the PEX5/LINC00630/miR-539-3p/miR-485-3p loop, this loop may be required for promoting the immune response in pulpal inflammation.

Several transcription factors have been identified to be involved in the TF-gene regulatory network of pulpitis,

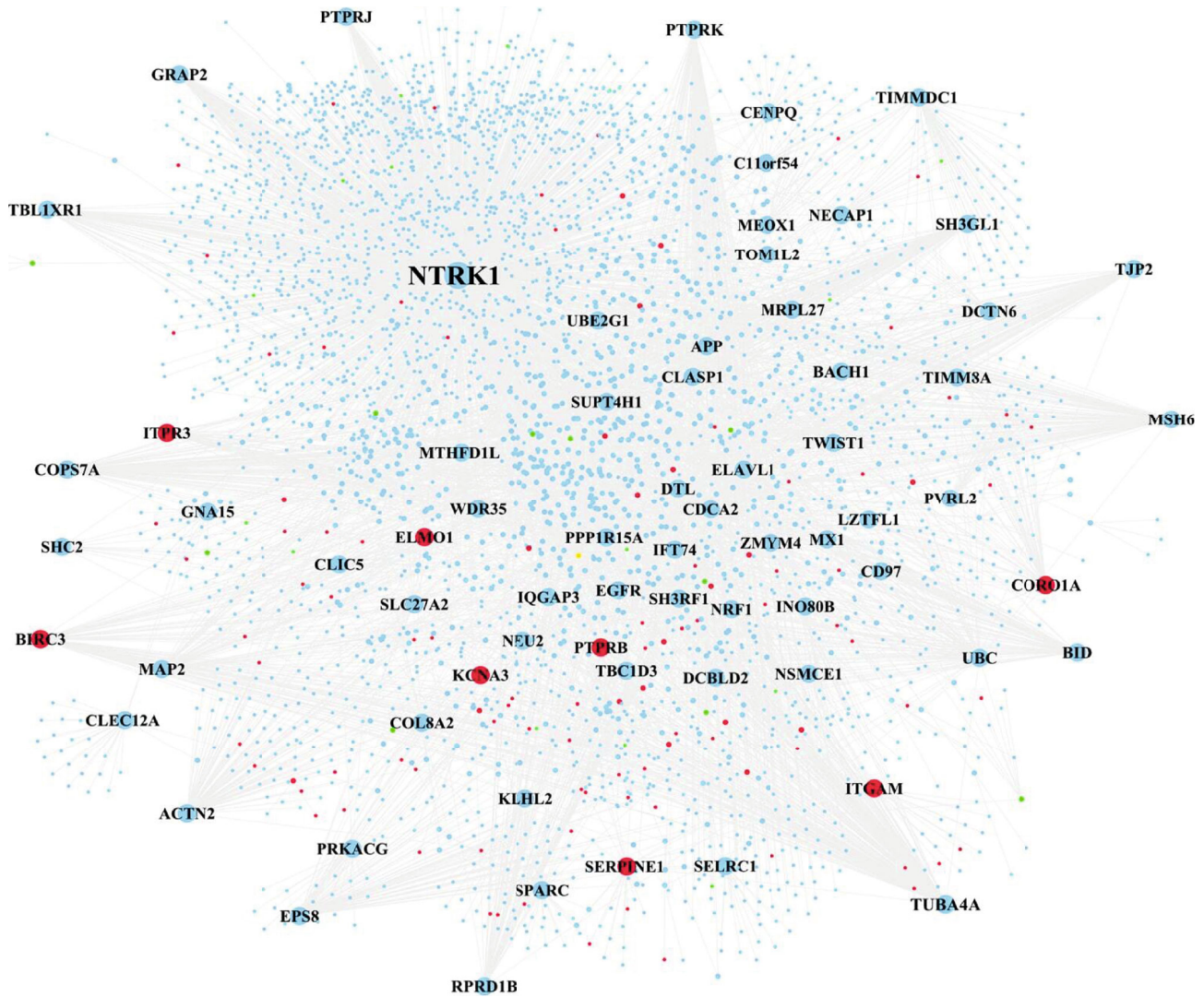


FIGURE 10: The PPI network of significant modules within the blue module in GSE77459. The red and green circle nodes represent up- and down-regulated DEGs, respectively. The sky-blue circle nodes represent the non-DEGs which interact with DEGs in the PPI network.

including GATA2, ETS1, FOXP3, STAT1, FOS, and JUN. GATA2 (Endothelial Transcription Factor GATA-2) is a transcriptional activator that regulates the expression of the endothelin-1 gene in endothelial cells [76]. It has been shown that endothelial cells can influence DPSCs by secreting endothelin-1 and further promoting the odontogenic differentiation of DPSCs [77]; thus, GATA2 can be assumed to be involved in the restoration and regeneration of dental pulp. Taking the example of ETS1, it could be speculated to be involved in the inflammation and regeneration of pulp based on its dual functions: controlling the expression of many cytokines as well as chemokine genes [78], being implicated in angiogenesis by regulating the expression of genes that are associated with migration and invasion of endothelial cells [79]. Taking the case of FOXP3 (Forkhead Box P3), it is the most specific biomarker of regulatory T cells (Treg) [80, 81]. Treg as a subset of T lymphocytes has been playing a pivotal role in the immune and inflammatory

response of pulpitis by secreting anti-inflammatory cytokines, including interleukin-10 and transforming growth factor b (TGF-b) [82]. Based on this, FOXP3 can be speculated to be involved in the inflammatory response by regulating the cytokine genes. In the case of STAT1 (Signal Transducer And Activator Of Transcription 1), it has been shown to play a critical role in mediating the cellular responses to many inflammatory mediators involved in pulpitis, including interferons (IFNs), cytokines (IL1, IL6, and KITLG/SCF), and growth factors (epidermal growth factors (EGF) and platelet-derived growth factor (PDGF)) [83]. For example, IFN-gamma has been shown to be a feasible modulator to improve the dentinogenic and immunosuppressive functions of irreversible pulpitis-DPSCs [84]; cytokines as a crucial part of host response could be regarded as diagnostic markers of pulpal inflammation [85, 86]; and growth factors can contribute to the angiogenic response of pulp tissue and enhance the regeneration of pupal-like tissue [87, 88]. Taking the final

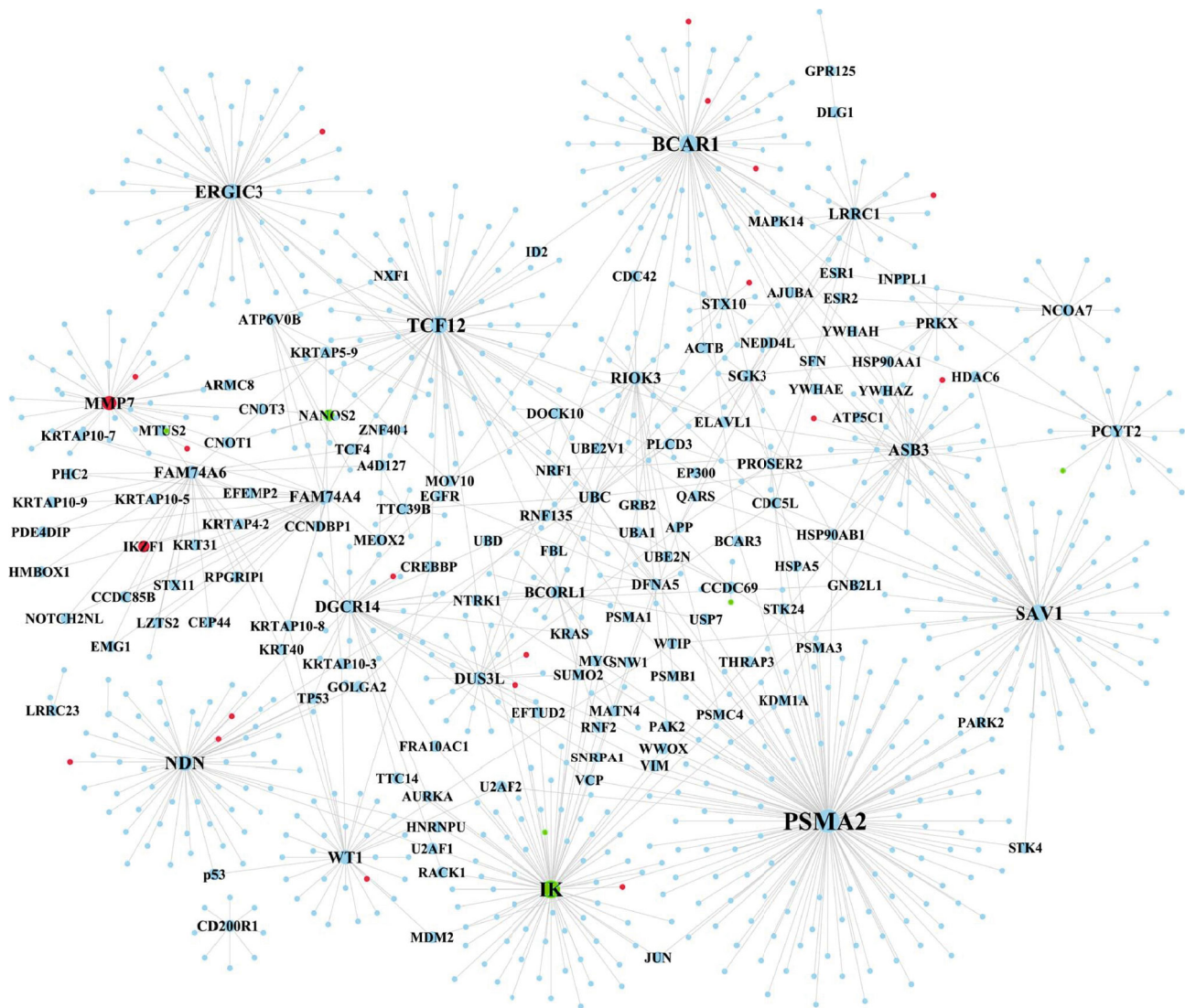


FIGURE 11: The PPI network of significant modules within the green module in GSE92681. The red and green circle nodes represent up- and downregulated DEGs, respectively. The sky-blue circle nodes represent the non-DEGs which interact with DEGs in the PPI network.

example, AP-1 complex consisting of c-JUN and c-FOS can synergize with Smad3/Smad4 protein and further cooperatively mediate the transforming growth factor-beta (TGF-beta) signaling pathway [89]. Since TGF-beta has been well known to stimulate odontoblast cells to secrete reactionary dentin [90], JUN and FOS can be speculated to play a role in the repair and regeneration process of the dental pulp.

Seven signaling pathways have been identified to be significantly enriched in the pathogenesis of pulpitis, for example, NOD-like receptor (NLR), Toll-like receptor (TLR), NF-kappa B, tumor necrosis factor (TNF), cell adhesion molecules (CAMs), chemokine, and cytokine-cytokine receptor interaction pathways. All of the pathways listed above have been well supported by previous studies. In the first example, the nucleotide-binding oligomerization domain- (NOD-) like receptors (NLRs) and Toll-like receptors (TLRs) are two members of the pattern recognition receptor (PRR) family. It has been shown/demonstrated by authors that PRR

family members can recognize carries pathogen-associated molecular patterns (PAMPs) and play crucial roles in the initiation of dental pulp innate immunity [91]. In another example, the downregulation of the NF-kappa B gene was suggested to enhance the odontogenic differentiation of DPSCs and the formation of the collagen matrix, indicating that NF-kappa B could be a potential target for promoting pulp tissue regeneration [92]. Taking the tumor necrosis factor- α (TNF- α) as an example, it has been shown that TNF- α is a pleiotropic cytokine that is upregulated in pulpal tissues of teeth with irreversible pulpitis [93]. Not only does TNF- α play a role in promoting inflammation by recruiting leukocytes and stimulating the production of proinflammatory cytokines, but it may also cause pain hypersensitivity by directly acting on nociceptive neurons [94]. In the case of cell adhesion molecules (CAMs), diverse CAM molecules (e.g., platelet-endothelial cell adhesion molecule-1 (PECAM-1), intercellular adhesion molecule-1 (ICAM-1), intercellular

TABLE 6: The topological characteristics of the top 25 gene nodes in the PPI network of the blue module within the GSE77549 dataset.

Name	Degree	Betweenness centrality	Closeness centrality	Clustering coefficient	Topological coefficient	Regulate
NTRK1	1981	0.797678	0.550769	$8.10E-05$	0.00147	Other_gene
TUBA4A	182	0.057422	0.34576	$2.46E-04$	0.012097	Other_gene
PTPRK	110	0.048111	0.334924	$5.10E-04$	0.017763	Other_gene
ACTN2	101	0.04028	0.340466	$8.08E-04$	0.012519	Other_gene
MSH6	98	0.029296	0.414544	0.009211	0.011399	Other_gene
COPS7A	87	0.027065	0.331267	0	0.024951	Other_gene
BIRC3	79	0.030191	0.33259	0	0.022419	mRNA up
SH3GL1	79	0.025169	0.330228	0	0.023044	Other_gene
EPS8	78	0.030772	0.33259	0	0.022436	Other_gene
PTPRJ	76	0.02319	0.408163	0.008288	0.014223	Other_gene
UBC	75	0.16533	0.47619	0.005405	0.017173	Other_gene
RPRD1B	71	0.019601	0.329863	0	0.026232	Other_gene
TJP2	68	0.019477	0.328079	0	0.027715	Other_gene
BID	65	0.018865	0.33035	0	0.030769	Other_gene
TBL1XR1	62	0.023597	0.409283	0.010929	0.017196	Other_gene
GRAP2	59	0.019032	0.330838	$6.05E-04$	0.027809	Other_gene
MAP2	57	0.016676	0.406541	0.014935	0.018914	Other_gene
TIMMDC1	53	0.022335	0.327539	$7.54E-04$	0.025227	Other_gene
BACH1	48	0.013952	0.327929	0	0.036859	Other_gene
DTL	48	0.009929	0.332961	0.006475	0.032282	Other_gene
CORO1A	46	0.016515	0.327929	0	0.029927	mRNA up
MX1	43	0.013576	0.329347	0	0.037265	Other_gene
TWIST1	41	0.011401	0.290915	0	0.053215	Other_gene
ITPR3	39	0.011085	0.327419	0	0.039683	mRNA up
PTPRB	36	0.007233	0.37609	0.018487	0.029667	mRNA up

TABLE 7: The topological characteristics of the top 25 gene nodes in the PPI network of the green module within the GSE92681 dataset.

Name	Degree	Average shortest path length	Betweenness centrality	Closeness centrality	Clustering coefficient	Topological coefficient	Regulate
PMA2	145	2.84572072	0.30956005	0.35140483	0	0.01436782	Other gene
IK	83	3.14752252	0.16898579	0.3177102	0	0.02628697	mRNA down
BCAR1	82	3.0731982	0.18704239	0.32539392	0	0.02264808	Other gene
TCF12	77	2.88400901	0.27221312	0.34673955	0	0.01974026	Other gene
SAV1	74	3.6768018	0.14809265	0.2719755	0	0.02402402	Other gene
NDN	61	3.29391892	0.12878792	0.30358974	0	0.02157032	Other gene
ERGIC3	55	3.31644144	0.11672478	0.30152801	0	0.02121212	Other gene
ASB3	38	3.51914414	0.07839935	0.28416	0	0.03827751	Other gene
MMP7	37	4.70157658	0.08120061	0.21269461	0	0.04054054	mRNA up
WT1	35	3.74887387	0.08035061	0.26674677	0	0.04642857	Other gene
DGCR14	32	3.37274775	0.05414526	0.29649416	0	0.05208333	Other gene
RIOK3	28	3.19256757	0.06657298	0.31322751	0	0.05844156	Other gene
DUS3L	26	3.3704955	0.04976931	0.29669228	0	0.05668016	Other gene
FAM74A4	26	4.65202703	0.02931155	0.21496006	0	0.19230769	Other gene
FAM74A6	25	4.65427928	0.0262998	0.21485604	0	0.19333333	Other gene
LRRC1	23	3.20157658	0.05583233	0.31234611	0	0.06126482	Other gene
PCYT2	21	3.31869369	0.04192798	0.30132338	0	0.05555556	Other gene
UBC	18	2.51351351	0.42421401	0.39784946	0	0.06050955	Other gene
BCORL1	16	3.4786036	0.02550435	0.28747167	0	0.08455882	Other gene
NCOA7	13	4.68581081	0.02298401	0.21341024	0	0.07692308	Other gene
STX10	13	3.48536036	0.02685944	0.28691438	0	0.07692308	Other gene
SGK3	12	3.35472973	0.03075664	0.29808661	0	0.11507937	Other gene
PRKX	11	4.67004505	0.01823525	0.2141307	0	0.18181818	Other gene
RNF135	10	4.73536036	0.01245585	0.21117717	0	0.2	Other gene
DFNA5	9	3.49436937	0.01078561	0.28617467	0	0.16339869	Other gene

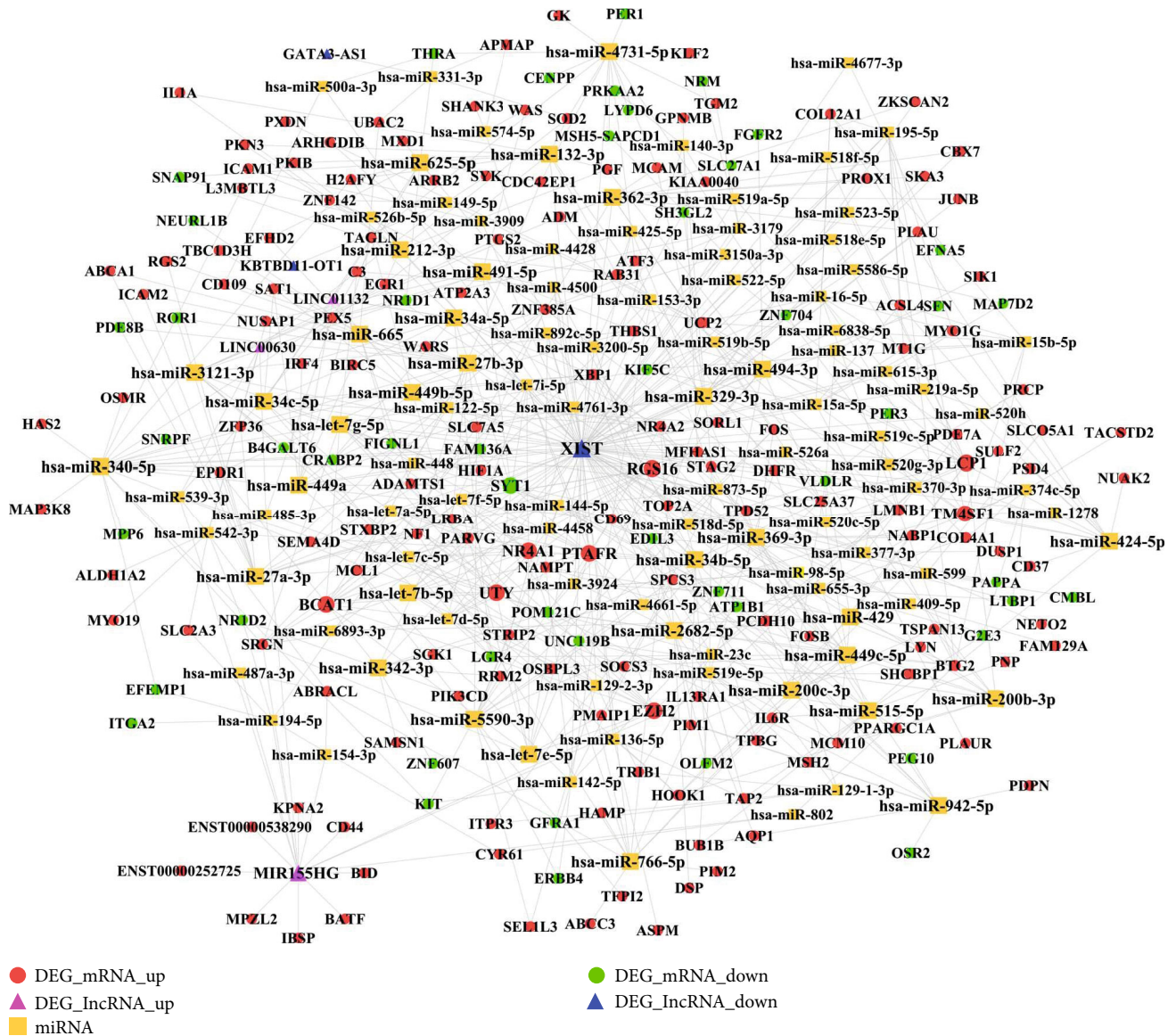


FIGURE 12: The ceRNA network consisting of DElncRNA-miRNA-DEG interaction pairs. The red circle nodes represent the upregulated DEGs, and the green circle nodes represent the downregulated DEGs. The yellow square nodes represent miRNA. The rose-red triangle nodes represent the upregulated DElncRNA, and the blue triangle node represents the downregulated DElncRNA.

adhesion molecule-3 (ICAM-3), and vascular cell adhesion molecule-1 (VCAM-1)) were shown to be expressed in the vascular endothelium of the inflamed human dental pulp, by playing roles in promoting transendothelial migration of leukocytes from the bloodstream into tissue [95]. Finally, chemokines and cytokines are kinds of inflammatory mediators suggested being involved in the innate immune response of pulpitis, playing protective roles in attracting varying inflammatory cells, inducing antibacterial reactions by the production of antimicrobial peptides such as defensins, and further killing cariogenic microbial [96]. All of the signaling pathways listed above can form complicated interactions and are involved in the inflammatory immune response of pulpitis. However, it is also worthwhile to note that the path-

ways identified in this study have also been documented as the classic pathways involved in all inflammatory diseases and are not specific for pulpitis. It is therefore questionable to regard these pathways as therapeutic targets that can inhibit the progression of pulpitis.

Some limitations should be acknowledged in this study. First, only expression profiling datasets of lncRNAs and genes could be obtained, and there were no miRNA expression profile datasets related to pulpitis in the GEO dataset. It was therefore impossible to predict the expression tendency of miRNAs in the pathology of pulpitis. This also means that miRNA sequencing technology needs to be applied to investigate the alteration of miRNAs in pulpitis. Second, the sample size of the datasets included was small

TABLE 8: The topological characteristics of the top 20 nodes in the ceRNA network.

Name	Degree	Average shortest path length	Betweenness centrality	Closeness centrality	Topological coefficient
XIST	95	1.85534591	0.78103311	0.53898305	0.03168803
hsa-miR-340-5p	21	2.58490566	0.07287356	0.38686131	0.06802721
MIR155HG	17	3.73899371	0.06134578	0.26745164	0.09207161
hsa-miR-4731-5p	15	2.7327044	0.05609297	0.36593786	0.07777778
hsa-miR-5590-3p	15	2.71069182	0.03529256	0.36890951	0.09122807
hsa-miR-27a-3p	14	2.75157233	0.02751162	0.36342857	0.0924812
hsa-miR-27b-3p	14	2.75157233	0.02751162	0.36342857	0.0924812
hsa-miR-329-3p	14	2.71698113	0.03095743	0.36805556	0.09323308
hsa-miR-362-3p	13	2.72327044	0.02835696	0.36720554	0.09797571
LCPI	13	3.71069182	0.0012642	0.26949153	0.36153846
hsa-miR-494-3p	13	2.72955975	0.03199119	0.36635945	0.10576923
hsa-miR-424-5p	12	2.71698113	0.02811	0.36805556	0.12152778
hsa-miR-2682-5p	12	2.72327044	0.02462859	0.36720554	0.12457045
hsa-miR-515-5p	12	2.78301887	0.02610732	0.35932203	0.10283688
hsa-miR-766-5p	12	2.70440252	0.04407579	0.36976744	0.11139456
hsa-miR-449c-5p	12	2.72327044	0.01602592	0.36720554	0.13058419
EZH2	11	3.40880503	0.01905647	0.29335793	0.27548209
NR4A1	11	3.46226415	0.01590906	0.28882834	0.30976431
hsa-miR-34a-5p	11	2.77044025	0.01309547	0.36095346	0.13492823
hsa-miR-449a	11	2.77044025	0.01309547	0.36095346	0.13492823

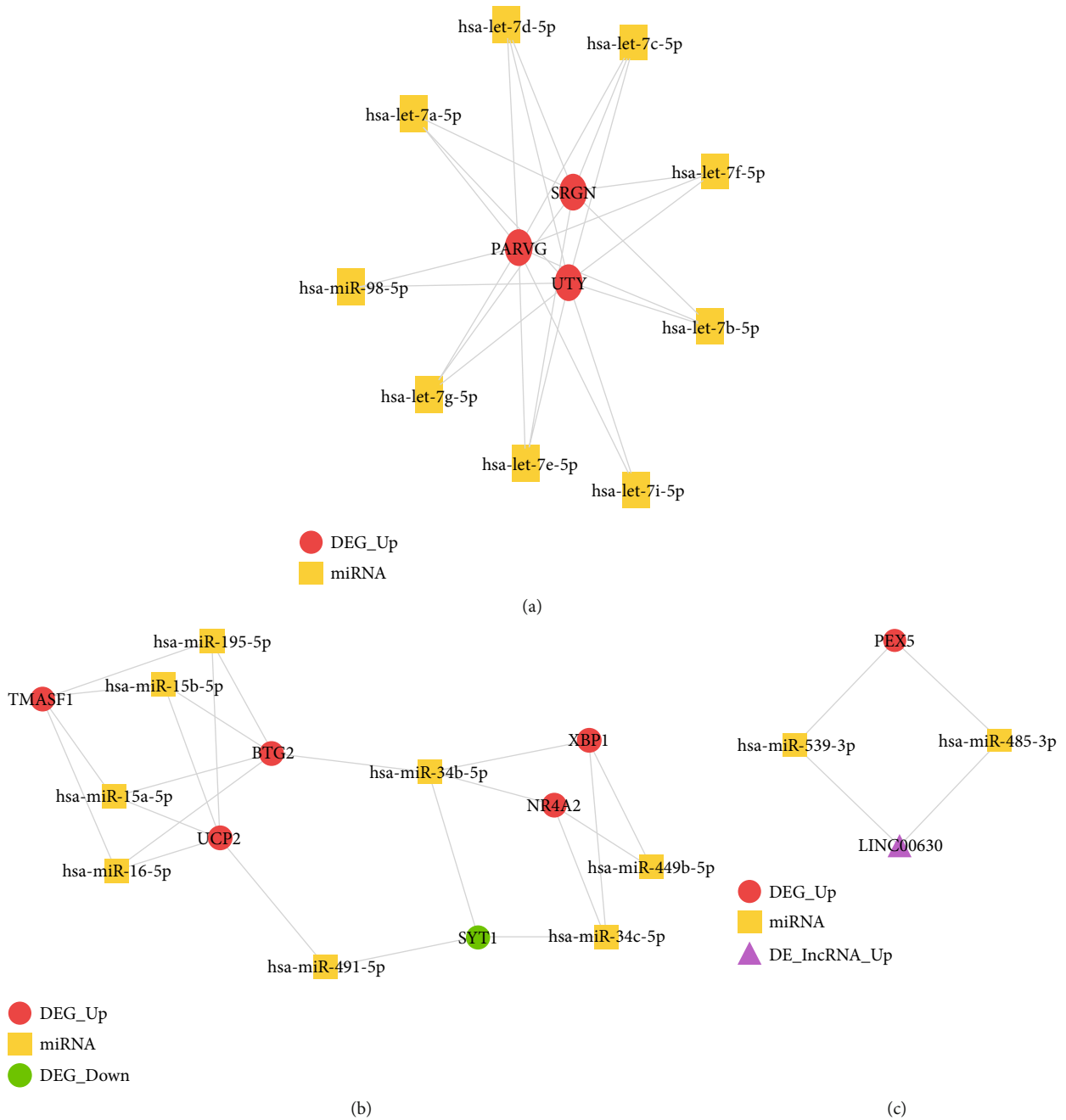


FIGURE 13: Three clusters identified in the ceRNA network. The red circle nodes represent the upregulated DEGs, and the green circle nodes represent the downregulated DEGs. The yellow square nodes represent miRNA. The rose-red triangle nodes represent the upregulated DElncRNA.

(GSE92681: 12; GSE77459: 12), and the analysis based on this limited sample data may result in a decrease of the prediction accuracy. Third, it should be noted that only bioinformatic techniques were employed. And because of limited funding, no clinical experiments were performed to validate the expression of the RNA molecules predicted in pulpitis. Although this study has some limitations, the findings also provide some direction for future research. First, the biomarkers identified could be promising therapeutic targets

that can lay the groundwork for future experimental research design. Second, the identification of these biomarkers can benefit the research of pulp tissue engineering, based on the evidence that genetically modified stem cells will receive better treatment efficacy compared with stem cells alone. The combined application of these genetic and epigenetic biomarkers modified DPSCs and already validated biomaterial scaffold (e.g., collagen, poly (lactic) acid, and fibrin) is promising for future regenerative endodontic therapy.

Data Availability

The data used to support the findings of this study are available from the corresponding author upon reasonable request.

Ethical Approval

As this study only applied bioinformatic techniques based on computational analyses, all of the data from pulp tissue samples were obtained from the public datasets, and original human samples were not analyzed. Therefore, this study does not require ethical approval.

Consent

Consent for publication is not applicable in this study because no individual person's data was used.

Conflicts of Interest

The authors declare no potential conflict of interest with respect to the authorship and publication of this paper.

Authors' Contributions

Dr. Wanchen Ning (email: wanchenning0627@gmail.com) and Dr. Xiao Jiang (email: jiangxiao_524@163.com) are equally the senior authors. Dr. Hanluo Li (email: ala1004@gmail.com), Dr. Simin Li (email: simin.li.dentist@gmail.com), and Prof. Dr. Xianda Hu (email: hellocean@hotmail.com) are equally the corresponding authors.

Acknowledgments

Dr. Wanchen Ning received doctoral study support from the China Scholarship Council (CSC) (CSC No. 201608080112) at Ludwig-Maximilians-University of Munich. Dr. Simin Li was funded by the Science Research Cultivation Program of Stomatological Hospital, Southern Medical University (Guangdong Provincial Stomatological Hospital) (No. PY2020004).

Supplementary Materials

Supplementary 1. File S1: the topological characteristics of all DEG nodes in the PPI network shown in Figure 4.

Supplementary 2. File S2: the topological characteristics of all nodes in the DElncRNA-DEG interaction network.

Supplementary 3. File S3: the topological characteristics of all nodes in the TF-DEG interaction network.

Supplementary 4. File S4: the topological characteristics of all DEG nodes in the PPI network for the significant blue module of GSE77459 dataset.

Supplementary 5. File S5: the topological characteristics of all DEG nodes in the PPI network for the significant green module of GSE92681 dataset.

Supplementary 6. File S6: the topological characteristics of all nodes in the ceRNA network.

References

- [1] N. Jain, A. Gupta, and N. Meena, "An insight into neurophysiology of pulpal pain: facts and hypotheses," *The Korean journal of pain*, vol. 26, no. 4, pp. 347–355, 2013.
- [2] P. R. Cooper, I. J. Chicca, M. J. Holder, and M. R. Milward, "Inflammation and regeneration in the dentin-pulp complex: net gain or net loss?," *Journal of Endodontia*, vol. 43, no. 9, pp. S87–s94, 2017.
- [3] A. Agnihotry, W. Thompson, Z. Fedorowicz, E. J. van Zuuren, and J. Sprakel, "Antibiotic use for irreversible pulpitis," *Cochrane Database Syst Rev*, vol. 5, article Cd004969, no. 5, 2019.
- [4] C. A. Murray and W. P. Saunders, "Root canal treatment and general health: a review of the literature," *International Endodontic Journal*, vol. 33, no. 1, pp. 1–18, 2000.
- [5] S.-B. Yong, J. Y. Chung, Y. Song, and Y. H. Kim, "Recent challenges and advances in genetically-engineered cell therapy," *Journal of Pharmaceutical Investigation*, vol. 48, no. 2, pp. 199–208, 2018.
- [6] X. Huang and K. Chen, "Differential expression of long non-coding RNAs in normal and inflamed human dental pulp," *Journal of Endodontia*, vol. 44, no. 1, pp. 62–72, 2018.
- [7] J. L. McLachlan, A. J. Smith, I. J. Bujalska, and P. R. Cooper, "Gene expression profiling of pulpal tissue reveals the molecular complexity of dental caries," *Biochimica et Biophysica Acta*, vol. 1741, no. 3, pp. 271–281, 2005.
- [8] X. Dong, W. Gao, L. V. Xiaoling et al., "Association between lncRNA GAS5, MEG3, and PCAT-1 polymorphisms and cancer risk: a meta-analysis," *Disease Markers*, vol. 2020, Article ID 6723487, 2020.
- [9] W.-n. Hu, H.-x. Ding, Q. Xu, X.-y. Zhang, D.-t. Yang, and Y.-z. Jin, "Relationship between long noncoding RNA H19 polymorphisms and risk of coronary artery disease in a Chinese population: a case-control study," *Disease Markers*, vol. 2020, Article ID 9839612, 2020.
- [10] L. Salmena, L. Poliseno, Y. Tay, L. Kats, and P. P. Pandolfi, "A _ceRNA_ Hypothesis: The Rosetta Stone of a Hidden RNA Language?," *Cell*, vol. 146, no. 3, pp. 353–358, 2011.
- [11] Y. Yao, T. Zhang, L. Qi et al., "Competitive endogenous RNA network construction and comparison of lung squamous cell carcinoma in smokers and nonsmokers," *Disease Markers*, vol. 2019, Article ID 5292787, 2019.
- [12] F. Lei, H. Zhang, and X. Xie, "Comprehensive analysis of an lncRNA-miRNA-mRNA competing endogenous RNA network in pulpitis," *PeerJ*, vol. 7, article e7135, 2019.
- [13] E. Clough and T. Barrett, "The Gene Expression Omnibus database," *Methods in Molecular Biology*, vol. 1418, pp. 93–110, 2016.
- [14] P. Sethupathy, B. Corda, and A. G. Hatzigeorgiou, "TarBase: a comprehensive database of experimentally supported animal microRNA targets," *RNA*, vol. 12, no. 2, pp. 192–197, 2006.
- [15] S. D. Hsu, F. M. Lin, W. Y. Wu et al., "miRTarBase: a database curates experimentally validated microRNA-target interactions," *Nucleic Acids Research*, vol. 39, suppl_1, pp. D163–D169, 2011.
- [16] F. Xiao, Z. Zuo, G. Cai, S. Kang, X. Gao, and T. Li, "miRecords: an integrated resource for microRNA-target interactions," *Nucleic Acids Research*, vol. 37, no. Database, pp. D105–D110, 2009.

- [17] J. H. Yang, J. H. Li, P. Shao, H. Zhou, Y. Q. Chen, and L. H. Qu, "starBase: a database for exploring microRNA-mRNA interaction maps from Argonaute CLIP-Seq and Degradome-Seq data," *Nucleic Acids Research*, vol. 39, suppl_1, pp. D202–D209, 2011.
- [18] M. E. Ritchie, B. Phipson, D. Wu et al., "limma powers differential expression analyses for RNA-sequencing and microarray studies," *Nucleic Acids Research*, vol. 43, no. 7, pp. e47–e47, 2015.
- [19] G. Yu, L. G. Wang, Y. Han, and Q. Y. He, "clusterProfiler: an R package for comparing biological themes among gene clusters," *OmicS: a journal of integrative biology*, vol. 16, no. 5, pp. 284–287, 2012.
- [20] S. Peri, "Human protein reference database as a discovery resource for proteomics," *Nucleic Acids Research*, vol. 32, no. 90001, pp. 497D–4501, 2004.
- [21] R. Oughtred, C. Stark, B. J. Breitkreutz et al., "The BioGRID interaction database: 2019 update," *Nucleic Acids Research*, vol. 47, no. D1, pp. D529–d541, 2019.
- [22] P. Shannon, A. Markiel, O. Ozier et al., "Cytoscape: a software environment for integrated models of biomolecular interaction networks," *Genome Research*, vol. 13, no. 11, pp. 2498–2504, 2003.
- [23] D. Merico, R. Isserlin, O. Stueker, A. Emili, and G. D. Bader, "Enrichment map: a network-based method for gene-set enrichment visualization and interpretation," *PLoS One*, vol. 5, no. 11, article e13984, 2010.
- [24] E. Wingender, P. Dietze, H. Karas, and R. Knüppel, "TRANSFAC: a database on transcription factors and their DNA binding sites," *Nucleic Acids Research*, vol. 24, no. 1, pp. 238–241, 1996.
- [25] C. Jiang, Z. Xuan, F. Zhao, and M. Q. Zhang, "TRED: a transcriptional regulatory element database, new entries and other development," *Nucleic Acids Research*, vol. 35, no. Database, pp. D137–D140, 2007.
- [26] F. Vafaee, J. R. Krycer, X. Ma, T. Burykin, D. E. James, and Z. Kuncic, "ORTI: an open-access repository of transcriptional interactions for interrogating mammalian gene expression data," *PLoS One*, vol. 11, no. 10, article e0164535, 2016.
- [27] I. E. Wertz and V. M. Dixit, "Signaling to NF-kappaB: regulation by ubiquitination," *Cold Spring Harbor Perspectives in Biology*, vol. 2, no. 3, p. a003350, 2010.
- [28] S. Raasi, G. Schmidtke, and M. Groettrup, "The ubiquitin-like protein FAT10 forms covalent conjugates and induces apoptosis," *Journal of Biological Chemistry*, vol. 276, no. 38, pp. 35334–35343, 2001.
- [29] F. Ebstein, N. Lange, S. Urban, U. Seifert, E. Krüger, and P. M. Kloetzel, "Maturation of human dendritic cells is accompanied by functional remodelling of the ubiquitin-proteasome system," *The International Journal of Biochemistry & Cell Biology*, vol. 41, no. 5, pp. 1205–1215, 2009.
- [30] T. Yujiri, S. Sather, G. R. Fanger, and G. L. Johnson, "Role of MEKK1 in cell survival and activation of JNK and ERK pathways defined by targeted gene disruption," *Science*, vol. 282, no. 5395, pp. 1911–1914, 1998.
- [31] F. S. Lee, J. Hagler, Z. J. Chen, and T. Maniatis, "Activation of the IκBα kinase complex by MEKK1, a kinase of the JNK pathway," *Cell*, vol. 88, no. 2, pp. 213–222, 1997.
- [32] R. Al-Sadi, D. Ye, H. M. Said, and T. Y. Ma, "IL-1β-induced increase in intestinal epithelial tight junction permeability is mediated by MEKK-1 activation of canonical NF-κB pathway," *The American Journal of Pathology*, vol. 177, no. 5, pp. 2310–2322, 2010.
- [33] A. J. Resler, K. E. Malone, L. G. Johnson et al., "Genetic variation in TLR or NFkappaB pathways and the risk of breast cancer: a case-control study," *BMC Cancer*, vol. 13, no. 1, 2013.
- [34] S. Sun, J. Sun, W. Jiang, W. Wang, and L. Ni, "Nav1.7 via promotion of ERK in the trigeminal ganglion plays an important role in the induction of pulpitis inflammatory pain," *BioMed Research International*, vol. 2019, Article ID 6973932, 2019.
- [35] J. Chang, C. Zhang, N. Tani-Ishii, S. Shi, and C. Y. Wang, "NF-κB activation in human dental pulp stem cells by TNF and LPS," *Journal of Dental Research*, vol. 84, no. 11, pp. 994–998, 2005.
- [36] A. M. Hashemi, S. S. Kahnemouii, H. Aghajani et al., "Quercetin decreases Th17 production by down-regulation of MAPK-TLR4 signaling pathway on T cells in dental pulpitis," *Journal of Dentistry*, vol. 19, no. 4, p. 259, 2018.
- [37] F. Cimmino, M. Avitabile, V. A. Lasorsa et al., "HIF-1 transcription activity: HIF1A driven response in normoxia and in hypoxia," *BMC Medical Genetics*, vol. 20, no. 1, p. 37, 2019.
- [38] A. J. Majmundar, W. J. Wong, and M. C. Simon, "Hypoxia-inducible factors and the response to hypoxic stress," *Molecular Cell*, vol. 40, no. 2, pp. 294–309, 2010.
- [39] P. M. Dixon, N. Toitdu, and I. T. Dacre, *CHAPTER 10- equine dental pathology, in Equine Dentistry (Third Edition)*, J. Easley, P. M. Dixon, and J. Schumacher, Eds., W.B. Saunders, Edinburgh, 2011.
- [40] D. R. McIlwain, T. Berger, and T. W. Mak, "Caspase functions in cell death and disease," *Cold Spring Harbor Perspectives in Biology*, vol. 5, no. 4, article a008656, 2013.
- [41] H. Qian, Q. Huang, Y.-X. Chen, Q. Liu, J.-X. Fang, and M.-W. Ye, "Caspase-9 was involved in cell apoptosis in human dental pulp stem cells from deciduous teeth," *Molecular Medicine Reports*, vol. 18, no. 1, pp. 1067–1073, 2018.
- [42] V. Viswanath, Y. Wu, R. Boonplueang et al., "Caspase-9 activation results in downstream caspase-8 activation and bid cleavage in 1-methyl-4-phenyl-1, 2, 3, 6-tetrahydropyridine-induced Parkinson's disease," *Journal of Neuroscience*, vol. 21, no. 24, pp. 9519–9528, 2001.
- [43] C.-L. Hahn, A. M. Best, and J. G. Tew, "Cytokine induction by Streptococcus mutans and pulpal pathogenesis," *Infection and Immunity*, vol. 68, no. 12, pp. 6785–6789, 2000.
- [44] F. P. Cardoso, M. B. Viana, A. P. R. Sobrinho et al., "Methylation pattern of the *_IFN_*-γ gene in human dental pulp," *Journal of Endodontics*, vol. 36, no. 4, pp. 642–646, 2010.
- [45] S. C. Chattipakorn, A. Sigurdsson, A. R. Light, M. Narhi, and W. Maixner, "Trigeminal c-Fos expression and behavioral responses to pulpal inflammation in ferrets," *Pain*, vol. 99, no. 1, pp. 61–69, 2002.
- [46] M. R. Byers, E. H. Chudler, and M. J. Iadarola, "Chronic tooth pulp inflammation causes transient and persistent expression of Fos in dynorphin-rich regions of rat brainstem," *Brain Research*, vol. 861, no. 2, pp. 191–207, 2000.
- [47] G. . H. Wabnitz, T. Köcher, P. Lohneis et al., "Costimulation induced phosphorylation of L-plastin facilitates surface transport of the T cell activation molecules CD69 and CD25," *European Journal of Immunology*, vol. 37, no. 3, pp. 649–662, 2007.
- [48] M. Jontell, T. Okiji, U. Dahlgren, and G. Bergenholtz, "Immune defense mechanisms of the dental pulp," *Critical Reviews in Oral Biology and Medicine*, vol. 9, no. 2, pp. 179–200, 1998.

- [49] R. Cao and Y. Zhang, "The functions of E(Z)/EZH2-mediated methylation of lysine 27 in histone H3," *Current Opinion in Genetics & Development*, vol. 14, no. 2, pp. 155–164, 2004.
- [50] T. Hui, P. A. Y. Zhao et al., "EZH2, a potential regulator of dental pulp inflammation and regeneration," *Journal of Endodontia*, vol. 40, no. 8, pp. 1132–1138, 2014.
- [51] B. Li, F. Yu, F. Wu et al., "EZH2 impairs human dental pulp cell mineralization via the Wnt/ β -catenin pathway," *Journal of Dental Research*, vol. 97, no. 5, pp. 571–579, 2018.
- [52] Q. I. HUANG, J. U. N. L. I. XUE, R. U. N. M. E. I. ZOU et al., "NR4A1 is associated with chronic low-grade inflammation in patients with type 2 diabetes," *Experimental and Therapeutic Medicine*, vol. 8, no. 5, pp. 1648–1654, 2014.
- [53] N. Ipseiz, S. Uderhardt, C. Scholtysek et al., "The nuclear receptor Nr4a1 mediates anti-inflammatory effects of apoptotic cells," *Journal of Immunology*, vol. 192, no. 10, pp. 4852–4858, 2014.
- [54] H. Dweep, C. Sticht, P. Pandey, and N. Gretz, "miRWalk - database: prediction of possible miRNA binding sites by "walking" the genes of three genomes," *Journal of Biomedical Informatics*, vol. 44, no. 5, pp. 839–847, 2011.
- [55] Y. Li, C. Dai, C. Wu, and Y. Liu, "PINCH-1 promotes tubular epithelial-to-mesenchymal transition by interacting with integrin-linked kinase," *J Am Soc Nephrol*, vol. 18, no. 9, pp. 2534–2543, 2007.
- [56] S.-Y. Lee, H. M. Yun, R. A. Perez et al., "Nanotopological-tailored calcium phosphate cements for the odontogenic stimulation of human dental pulp stem cells through integrin signaling," *RSC Advances*, vol. 5, no. 78, pp. 63363–63371, 2015.
- [57] D. De Nardo, K. R. Balka, Y. C. Gloria, V. R. Rao, E. Latz, and S. L. Masters, "Interleukin-1 receptor-associated kinase 4 (IRAK4) plays a dual role in myddosome formation and Toll-like receptor signaling," *The Journal of Biological Chemistry*, vol. 293, no. 39, pp. 15195–15207, 2018.
- [58] Q. Zhou, R. Gallagher, R. Ufret-Vincenty, X. Li, E. N. Olson, and S. Wang, "Regulation of angiogenesis and choroidal neovascularization by members of microRNA-23~27~24 clusters," *Proceedings of the National Academy of Sciences of the United States of America*, vol. 108, no. 20, pp. 8287–8292, 2011.
- [59] K. Takahashi, "Pulpal vascular changes in inflammation," *Proc Finn Dent Soc*, 1992, Suppl 1:381-5.
- [60] A. Hindley and W. Kolch, "Extracellular signal regulated kinase (ERK)/mitogen activated protein kinase (MAPK)-independent functions of Raf kinases," *Journal of Cell Science*, vol. 115, Part 8, pp. 1575–1581, 2002.
- [61] S. Simon, A. J. Smith, A. Berdal, P. J. Lumley, and P. R. Cooper, "The MAP kinase pathway is involved in odontoblast stimulation via p38 phosphorylation," *Journal of Endodontia*, vol. 36, no. 2, pp. 256–259, 2010.
- [62] S. Zhong, S. Zhang, E. Bair, S. Nares, and A. A. Khan, "Differential expression of microRNAs in normal and inflamed human pulps," *Journal of Endodontia*, vol. 38, no. 6, pp. 746–752, 2012.
- [63] B. E. Dayanc, S. Bansal, A. O. Gure, S. O. Gollnick, and E. A. Repasky, "Enhanced sensitivity of colon tumour cells to natural killer cell cytotoxicity after mild thermal stress is regulated through HSF1-mediated expression of MICA," *International Journal of Hyperthermia*, vol. 29, no. 5, pp. 480–490, 2013.
- [64] I. Z. Oskui, M. N. Ashtiani, A. Hashemi, and H. Jafarzadeh, "Effect of thermal stresses on the mechanism of tooth pain," *Journal of Endodontia*, vol. 40, no. 11, pp. 1835–1839, 2014.
- [65] D. B. Pontier and J. Gribnau, "Xist regulation and function explored," *Human Genetics*, vol. 130, no. 2, pp. 223–236, 2011.
- [66] X. Wu, X. Dinglin, X. Wang et al., "Long noncoding RNA XIST promotes malignancies of esophageal squamous cell carcinoma via regulation of miR-101/EZH2," *Oncotarget*, vol. 8, no. 44, pp. 76015–76028, 2017.
- [67] Q. Zhou, W. Hu, W. Zhu et al., "Long non coding RNA XIST as a prognostic cancer marker - a meta-analysis," *Clinica Chimica Acta*, vol. 482, pp. 1–7, 2018.
- [68] L. Ma, Y. Zhou, X. Luo, H. Gao, X. Deng, and Y. Jiang, "Long non-coding RNA XIST promotes cell growth and invasion through regulating miR-497/MACC1 axis in gastric cancer," *Oncotarget*, vol. 8, no. 3, pp. 4125–4135, 2017.
- [69] B. Shenoda, Y. Tian, G. Alexander, E. Aradillas-Lopez, R. Schwartzman, and S. Ajit, "miR-34a-mediated regulation of XIST in female cells under inflammation," *Journal of Pain Research*, vol. Volume 11, pp. 935–945, 2018.
- [70] M. Ma, Y. Pei, X. Wang, J. Feng, Y. Zhang, and M. Q. Gao, "LncRNA XIST mediates bovine mammary epithelial cell inflammatory response via NF- κ B/NLRP3 inflammasome pathway," *Cell Proliferation*, vol. 52, no. 1, article e12525, 2019.
- [71] K. Vargova, N. Curik, P. Burda et al., "MYB transcriptionally regulates the miR-155 host gene in chronic lymphocytic leukemia," *Blood*, vol. 117, no. 14, pp. 3816–3825, 2011.
- [72] E. Vigorito, S. Kohlhaas, D. Lu, and R. Leyland, "miR-155: an ancient regulator of the immune system," *Immunological Reviews*, vol. 253, no. 1, pp. 146–157, 2013.
- [73] X. Wu, Y. Wang, T. Yu et al., "Blocking MIR155HG/miR-155 axis inhibits mesenchymal transition in glioma," *Neuro-Oncology*, vol. 19, no. 9, pp. 1195–1205, 2017.
- [74] G. Dodt and S. J. Gould, "Multiple PEX genes are required for proper subcellular distribution and stability of Pex5p, the PTS1 receptor: evidence that PTS1 protein import is mediated by a cycling receptor," *The Journal of Cell Biology*, vol. 135, no. 6, pp. 1763–1774, 1996.
- [75] F. Di Cara, A. Sheshachalam, N. E. Braverman, R. A. Rachubinski, and A. J. Simmonds, "Peroxisome-mediated metabolism is required for immune response to microbial infection," *Immunity*, vol. 48, no. 4, pp. 832–833, 2018.
- [76] D. M. Dorfman, D. B. Wilson, G. A. Bruns, and S. H. Orkin, "Human transcription factor GATA-2. Evidence for regulation of preproendothelin-1 gene expression in endothelial cells," *The Journal of Biological Chemistry*, vol. 267, no. 2, pp. 1279–1285, 1992.
- [77] M. Liu, L. Zhao, J. Hu et al., "Endothelial cells and endothelin-1 promote the odontogenic differentiation of dental pulp stem cells," *Molecular Medicine Reports*, vol. 18, no. 1, pp. 893–901, 2018.
- [78] R. P. Panganiban, B. M. Vonakis, F. T. Ishmael, and C. Stellato, "Coordinated post-transcriptional regulation of the chemokine system: messages from CCL2," *Journal of Interferon & Cytokine Research*, vol. 34, no. 4, pp. 255–266, 2014.
- [79] J. S. Yordy, O. Moussa, H. Pei, D. Chaussabel, R. Li, and D. K. Watson, "SP100 inhibits ETS1 activity in primary endothelial cells," *Oncogene*, vol. 24, no. 5, pp. 916–931, 2005.
- [80] W. Chen, W. Jin, N. Hardegen et al., "Conversion of peripheral CD4+CD25- naive T cells to CD4+CD25+ regulatory T cells by TGF-beta induction of transcription factor Foxp3," *The*

Journal of Experimental Medicine, vol. 198, no. 12, pp. 1875–1886, 2003.

- [81] Y. Zheng and A. Y. Rudensky, “Foxp3 in control of the regulatory T cell lineage,” *Nature Immunology*, vol. 8, no. 5, pp. 457–462, 2007.
- [82] K. F. Bruno, J. A. Silva, T. A. Silva, A. C. Batista, A. H. G. Alencar, and C. Estrela, “Characterization of inflammatory cell infiltrate in human dental pulpitis,” *International Endodontic Journal*, vol. 43, no. 11, pp. 1013–1021, 2010.
- [83] D. Bayarsaihan, “Epigenetic mechanisms in inflammation,” *Journal of Dental Research*, vol. 90, no. 1, pp. 9–17, 2010.
- [84] S. Sonoda, H. Yamaza, L. Ma et al., “Interferon-gamma improves impaired dentinogenic and immunosuppressive functions of irreversible pulpitis-derived human dental pulp stem cells,” *Scientific Reports*, vol. 6, no. 1, 2016.
- [85] M. Elsalhy, F. Azizieh, and R. Raghupathy, “Cytokines as diagnostic markers of pulpal inflammation,” *International Endodontic Journal*, vol. 46, no. 6, pp. 573–580, 2013.
- [86] M. Zehnder, N. Delaleu, Y. du, and M. Bickel, “Cytokine gene expression—part of host defence in pulpitis,” *Cytokine*, vol. 22, no. 3–4, pp. 84–88, 2003.
- [87] K. Derringer and R. Linden, “Epidermal growth factor released in human dental pulp following orthodontic force,” *European Journal of Orthodontics*, vol. 29, no. 1, pp. 67–71, 2007.
- [88] M. Zhang, F. Jiang, X. Zhang et al., “The effects of platelet-derived growth factor-BB on human dental pulp stem cells mediated dentin-pulp complex regeneration,” *Stem Cells Translational Medicine*, vol. 6, no. 12, pp. 2126–2134, 2017.
- [89] Y. Zhang, X. H. Feng, and R. Derynck, “Smad3 and Smad4 cooperate with c-Jun/c-Fos to mediate TGF- β -induced transcription,” *Nature*, vol. 394, no. 6696, pp. 909–913, 1998.
- [90] T. Haniastuti, P. Nunez, and A. Djais, “The role of transforming growth factor beta in tertiary dentinogenesis,” *Dental Journal (Majalah Kedokteran Gigi)*, vol. 41, 2015.
- [91] J.-H. Jang, H. W. Shin, J. M. Lee, H. W. Lee, E. C. Kim, and S. H. Park, “An overview of pathogen recognition receptors for innate immunity in dental pulp,” *Mediators of Inflammation*, vol. 2015, 12 pages, 2015.
- [92] N. S. T. Hozhabri, M. D. Benson, M. D. Vu et al., “Decreasing NF- κ B expression enhances odontoblastic differentiation and collagen expression in dental pulp stem cells exposed to inflammatory cytokines,” *PLoS One*, vol. 10, no. 1, article e0113334, 2015.
- [93] A. B. Kokkas, A. Goulas, K. Varsamidis, V. Mirtsou, and D. Tziafas, “Irreversible but not reversible pulpitis is associated with up-regulation of tumour necrosis factor-alpha gene expression in human pulp,” *International Endodontic Journal*, vol. 40, no. 3, pp. 198–203, 2007.
- [94] B. E. Hall, L. Zhang, Z. J. Sun et al., “Conditional TNF- α overexpression in the tooth and alveolar bone results in painful pulpitis and osteitis,” *Journal of Dental Research*, vol. 95, no. 2, pp. 188–195, 2016.
- [95] Y. Sawa, S. Yoshida, K. I. Shibata, M. Suzuki, and A. Mukaida, “Vascular endothelium of human dental pulp expresses diverse adhesion molecules for leukocyte emigration,” *Tissue and Cell*, vol. 30, no. 2, pp. 281–291, 1998.
- [96] H. Yumoto, K. Hirao, Y. Hosokawa et al., “The roles of odontoblasts in dental pulp innate immunity,” *Japanese Dental Science Review*, vol. 54, no. 3, pp. 105–117, 2018.

Research Article

Differentially Expressed Circular RNA Profile in an Intracranial Aneurysm Group Compared with a Healthy Control Group

Yonggang Ma ^{1,2,3}, Baoqing Zhang ⁴, Dong Zhang ^{1,2,3}, Shuo Wang ^{1,2,3},
Maogui Li ^{1,2,3} and Jizong Zhao ^{1,2,3}

¹Department of Neurosurgery, Beijing Tiantan Hospital, Capital Medical University, Beijing, China

²China National Clinical Research Center for Neurological Diseases, Beijing, China

³Center of Stroke, Beijing Institute for Brain Disorders, Beijing, China

⁴Department of Neurosurgery, Weifang Yidu Central Hospital, 4138 Linglongshan Road, Qingzhou, Shandong Province, 262500, China

Correspondence should be addressed to Jizong Zhao; zhaojz205@163.com

Received 24 September 2020; Revised 12 November 2020; Accepted 9 January 2021; Published 29 January 2021

Academic Editor: Yuzhen Xu

Copyright © 2021 Yonggang Ma et al. This is an open access article distributed under the Creative Commons Attribution License, which permits unrestricted use, distribution, and reproduction in any medium, provided the original work is properly cited.

Objective. Intracranial aneurysm (IA) is a fatal disease owing to vascular rupture and subarachnoid hemorrhage. Much attention has been given to circular RNAs (circRNAs) because they may be potential biomarkers for many diseases, but their mechanism in the formation of IA remains unknown. **Methods.** circRNA expression profile analysis of blood samples was conducted between patients with IA and controls. Overall, 235 differentially expressed circRNAs were confirmed between IA patients and the control group. The reliability of the microarray results was demonstrated by quantitative real-time polymerase chain reaction (qRT-PCR). **Results.** Of 235 differentially expressed genes, 150 were upregulated, while the other 85 were downregulated. Five miRNAs matched to every differential expression of circRNAs, and related MREs were predicted. We performed gene ontology (GO) analysis to identify the functions of their targeted genes, with the terms “Homophilic cell adhesion via plasma membrane adhesion molecules” and “Positive regulation of cellular process” showing the highest fold enrichment. **Conclusions.** This study demonstrated the role of circRNA expression profiling in the formation of IA and revealed that the mTOR pathway can be a latent therapeutic strategy for IA.

1. Introduction

Intracranial aneurysm (IA) is a disease characterized by abnormal dilatation of the intracranial artery as an abnormal bulge. Increasing numbers of asymptomatic unruptured IAs have been discovered recently using computed tomography (CT) or magnetic resonance imaging (MRI). It has been proposed that 3% to 5% of individuals harbor an IA [1]. The pathogenesis and etiology of IA are not yet clearly understood. The possible factors for IA formation include inflammation, hemodynamics, genetics, hormones, and the environment [2–4]. A high proportion of subarachnoid hemorrhage (SAH) is due to IA rupture due to its high mortality rate. Smoking and high blood pressure were considered to be risk factors for IA rupture [5]. Several studies

have confirmed several loci contributing to IA formation and rupture [6–17]. Among them, 4 loci, including 1p34.3–p36.13, 7q11, 19q13.3, and Xp22, have been replicated in different studies [8, 10, 11, 18, 19]. Recent studies have observed that circular RNAs (circRNAs) are linked to cerebrovascular diseases such as moyamoya disease, atherosclerosis, and ischemic stroke. Nevertheless, the pathogenesis of IA formation and rupture remains poorly understood.

circRNAs are noncoding circular RNAs that are single stranded without free terminals [20]. They bond continuous loops by connecting their 3' - and 5' -ends and are abundant in eukaryotic cells [20]. In light of the literature, circRNAs are associated with the pathogenesis of a number of diseases, such as moyamoya disease and stroke. circRNAs can modulate the gene expression during transcriptional

or posttranscriptional processes through three main pathways: acting as microRNA (miRNA) sponges, holding RNA binding proteins (RBPs), and controlling alternative splicing and parental gene expression [20, 21]. Previous research has suggested that circRNAs are deeply related in many vascular diseases [22]. For instance, circular antisense noncoding RNA is linked to atherosclerosis by regulating inhibitors of cellular factor expression [23]. Moreover, Zheng et al. found that one circRNA was highly expressed in aortic tissues of patients with aortic aneurysm compared with healthy tissue. However, the connection between circRNAs and IA is still unknown. To examine how circRNAs regulate the formation of IA and identify the potential molecules contributing to IA rupture, we carried out this study to analyze circRNA profiles among unruptured IA patients (UIA) and ruptured IA (RIA) patients and controls.

2. Materials and Method

2.1. Study Population and Blood Sample. From January to March 2019, we recruited 5 healthy people aged 20 to 60 years old. All 5 healthy controls had undergone computed tomography angiography (CTA) examination and healthy check-ups within half a year. Participants diagnosed with IA from January to March 2019 in our institute were also included in this study. All enrolled participants underwent CTA or digital subtraction angiography (DSA) examination. Furthermore, computed tomography (CT) plain scanning was conducted to evaluate whether IAs ruptured among all IA patients. Based on plain CT imaging, we divided the IA patients into two subgroups: unruptured IA patients and ruptured IA patients. Patients with other serious cardiovascular or cerebrovascular diseases were eliminated to avoid confounding results. Our research was permitted by the Ethics Committee Review Board of Beijing Tiantan Hospital. Informed consent was acquired from all enrolled participants before blood sample collection.

Blood samples were drawn from individuals and subsequently collected in vacuum collecting tubes. Samples were centrifuged at 1500 g/min for 15 minutes, and blood cells were removed. To remove cell debris, the clear supernatant was transferred into a new centrifuge tube (RNase-free) and centrifuged at 10000 g/min for 10 min. We transferred the supernatant into a new RNase-free centrifuge tube and stored it at -80°C immediately.

2.2. RNA Isolation and Purification. Five samples of normal peripheral blood, five samples of UIA patients' peripheral blood and five samples of RIA patients' peripheral blood were prepared for RNA extraction. The nurse drew a 5 ml volume of blood from each subject by venipuncture and collected them in K 2 EDTA-coated vacutainer tubes (BD Biosciences, Franklin Lakes, NJ, USA). Total RNA was extracted from the blood samples using TRIzol reagent (Invitrogen, Carlsbad, CA, USA) based on the manufacturer's protocols. A NanoDrop ND-1000 (Thermo Fisher Scientific, Wilmington, DE, USA) was used to quantify the total RNA. RNA integrity was checked by agarose gel electrophoresis.

RNase R (Epicentre, Inc.) was used to discard linear RNAs and enrich circular RNAs.

2.3. RNA Labeling and Hybridization. RNA was amplified and labeled by the Arraystar Super RNA Labeling Kit (Arraystar) according to the manufacturer's protocols, and then, we purified the labeled cRNA using a RNeasy mini kit (Qiagen, Hilden, Germany). The concentration and specific activity of the labeled cRNAs (pmol Cy3/ μg cRNA) were determined by a NanoDrop ND-1000. Subsequently, the qualified labeled cRNA samples (yield $> 1.65 \mu\text{g}$ and specific activity > 9.0) were hybridized onto Arraystar Human circRNA Arrays (V2, Arraystar Inc.) Then, the microarray slides were incubated for 17 hours at 65°C in a hybridization oven (Agilent Technologies, Inc., Santa Clara, CA, USA). Hybridized arrays were washed, fixed, and scanned with a G2505C scanner (Agilent Technologies).

2.4. Data Analysis and Bioinformatics. Original data were fetched by Feature Extraction software v. 11.0.1.1 (Agilent Technologies). We performed quantile normalization of the raw data and subsequent data processing using the limma package in R v.3.3 software. After quantile normalization of the raw data, low-intensity filtering was conducted, and the circRNAs that had at least 5 out of 15 samples with flags in "Present" or "Marginal" (defined by GeneSpring software) were retained for further differential analysis.

When we compared the two groups of profile discrepancies (the IA group versus the control group), the "fold change" (i.e., the ratio of the group averages) between the groups for each circRNA was computed. The statistical significance of the difference was estimated by *t*-test. circRNAs with fold changes of ≥ 1.3 and *P* values of < 0.05 were selected as obviously differentially expressed.

Several studies have shown that circRNAs play a crucial role in regulating gene expression, which fine tunes the level of miRNA by sequestering miRNAs. Their reciprocity with diseases related to miRNAs suggests that circRNAs are crucial for disease occurrence. In our study, the circRNA/miRNA interactive relationship was predicted with Arraystar's homemade miRNA target prediction software based on TargetScan [24] and miRanda [25], and we annotated at length the differential expression circRNAs among all the groups based on circRNA/miRNA interactive information. All differentially expressed circRNAs were evaluated by GO (Gene Ontology) and KEGG (Kyoto Encyclopedia of Genes and Genomes) pathway analyses. To identify the target genes for the predicted miRNA sponge, we used the network visualization and analysis tool Cytoscape v.3.4 to generate circRNA-miRNA networks. Furthermore, pathway network analysis was performed to evaluate reciprocal relationships among the pathways and visualize the network using Cytoscape v.3.4 software.

2.5. Quantitative Real-Time (qRT)-PCR. qRT-PCR was carried out to identify the microarray results. We synthesized cDNA from the total RNA using Super Script III reverse transcriptase (Invitrogen) based on the manufacturer's protocol. The PCR thermocycling conditions of predenaturation

TABLE 1: Clinical characteristics of all participants.

Variable	IA patients			Control	P value
	UIA	RIA			
Number	5	5		5	
Age	55.60 ± 8.562	53.80 ± 8.585		45.60 ± 6.309	0.113
Size	6.20 ± 1.304	9.00 ± 0.743		NA	0.153
Location of IA				NA	
MCA	3	3			
ACA	2	2			
Shape (saccular)	5	5		NA	
Smoking	0	0		0	
Drinking	0	0		0	

were set at 95°C for 10 minutes, followed by 40 cycles (95°C for 10 seconds and 60°C for 60 seconds). We assigned the housekeeping gene β -actin as the internal reference. All reactions were performed in triplicate, and the $2^{-\Delta\Delta Ct}$ method was used to calculate the expression level of circRNAs.

2.6. Statistical Analysis. Student's *t*-test (two tailed) and chi-squared test were used to assess the statistical significance between groups. Statistical analysis was conducted using SPSS 22.0 (SPSS Inc., Chicago, IL, USA). A *P* value of < 0.05 was considered statistically significant.

3. Results

3.1. Analysis of circRNA Expression Profiles. We implemented microarray analysis of five samples from the UIA group, five from RIA patients, and five samples from matched normal controls. The general information and clinical baseline data of all participants are shown in Table 1. To prevent other probable risk factors from confounding the results, we matched the size, shape, and location of aneurysms between UIA patients and RIA patients. The expression of 12546 circRNAs was evaluated in the three groups by microarray analysis. The difference in circRNA expression profiles between the IA patients and healthy group and between the UIA group and RIA group were revealed by hierarchical clustering. Volcano, scatter, and box plots were generated to demonstrate the differentially expressed circRNAs (Figures 1(a)–1(d)). Of all differentially expressed circRNAs, 150 were upregulated, and 85 were downregulated between the two compared groups (IA group and control group). Seven upregulated and 3 downregulated differentially expressed circRNAs were validated between the UIA group and RIA group (fold difference of ≥ 1.3 and *P* value of < 0.05) [26].

3.2. qRT-PCR Validation of Differential Expression of circRNAs. Five circRNAs (hsa_circRNA_000139, hsa_circRNA_101321, hsa_circRNA_072697, hsa_circRNA_069101, and hsa_circRNA_103677) were selected for qRT-PCR to confirm the microarray analysis data in fifteen IA and control samples. The qRT-PCR results were in accordance with the

microarray expression data, indicating the high reliability of the microarray analysis (Figure 2).

3.3. ceRNA Network Construction and GO and KEGG Pathway Analyses. circRNAs can modulate gene expression during transcriptional or posttranscriptional processes by functioning as inhibitors of miRNA bonding sponges or partners. We predicted that the five feasible miRNAs matched to every differentially expressed circRNA and MRE. Additionally, we evaluated 2465 circRNA-miRNA pairs with one or more binding sites. The interactive network between circRNAs and miRNAs was predicted for verified circRNAs, and GO analysis was carried out to identify the role of targeted genes. The top ten enriched GO terms in biological process are shown in Figure 3 with terms “Homophilic cell adhesion via plasma membrane adhesion molecules” and “Positive regulation of cellular process” showing the greatest fold enrichment. The KEGG pathway evaluation proclaimed 10 obviously enriched pathways in correspondence to the targeted genes. The most significant pathways included hepatocellular carcinoma, proteoglycans in cancer, and the mammalian target of rapamycin (mTOR) signaling pathway (Figure 4).

4. Discussion

The formation mechanism of IA is still unknown. Previous research has reported that inflammation and hemodynamic, genetic, hormonal, and environmental factors may contribute to IA [10–12]. In addition, several studies have confirmed that circRNAs are relevant to cerebrovascular diseases such as moyamoya disease, atherosclerosis, and ischemic stroke. In this study, we used a circRNA microarray to demonstrate 235 differentially expressed circRNAs in IA patients compared a matched control group.

Noncoding RNAs are crucial regulators of gene expression. Studies have revealed that they can act on different cellular processes and biological functions by controlling gene regulation [27]. Noncoding RNAs, including linear RNAs and circRNAs, could serve as competing endogenous RNAs (ceRNAs) by competitively binding miRNA response elements. circRNAs mainly originate from genes that code for protein synthesis and are generally composed of exons [28].

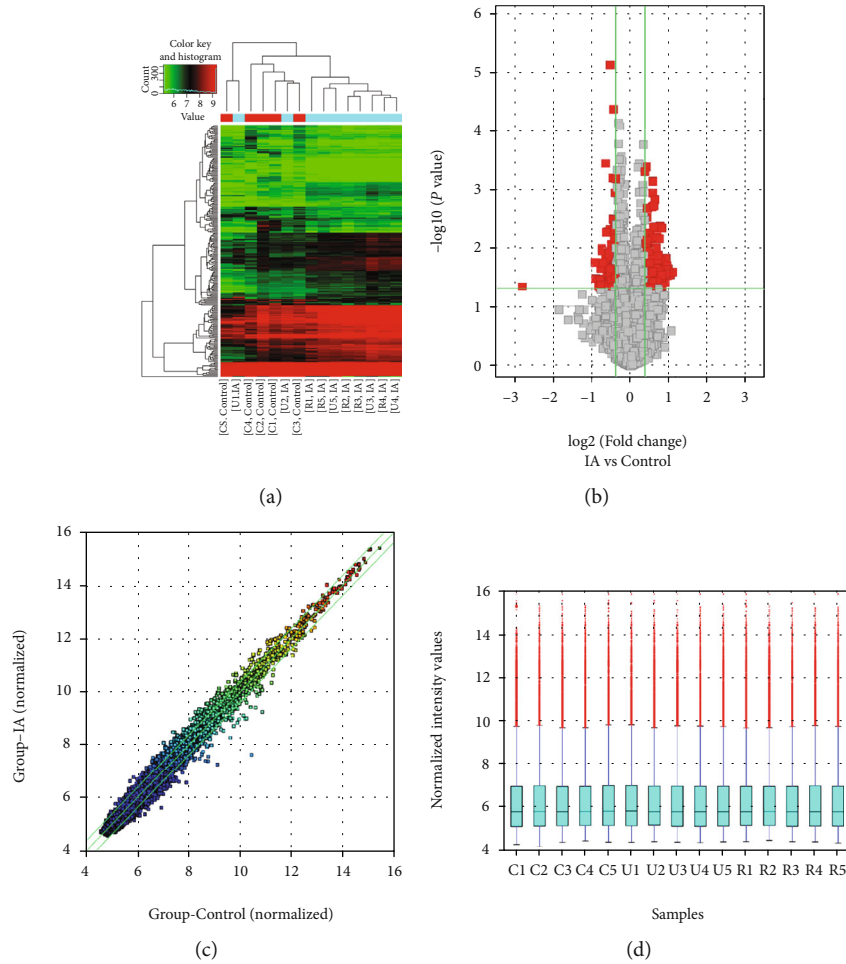


FIGURE 1: circRNA expression profile comparison among three groups. (a) Hierarchical clustering demonstrates a difference in circRNA expression profiling between the three groups. (b) Volcano plot shows differential circRNA expression between the IA patients and control groups, and the red points represent the circRNAs with log 2.0-fold changes (upregulated and downregulated) with statistical significance ($P < 0.05$). (c) Scattered plot shows the circRNA expression variation between the IA patients and control groups. (d) Box plot shows the distribution of circRNA expression patterns of three groups. IA: aneurysm.

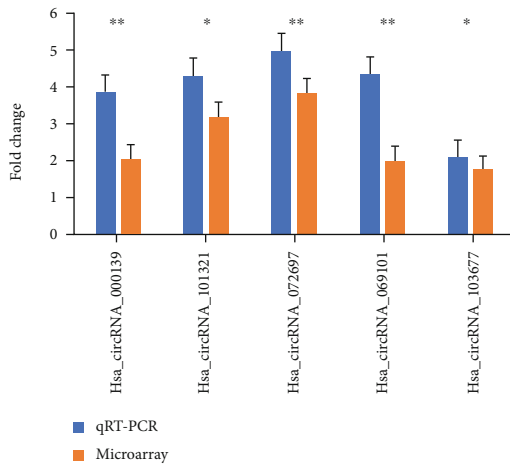
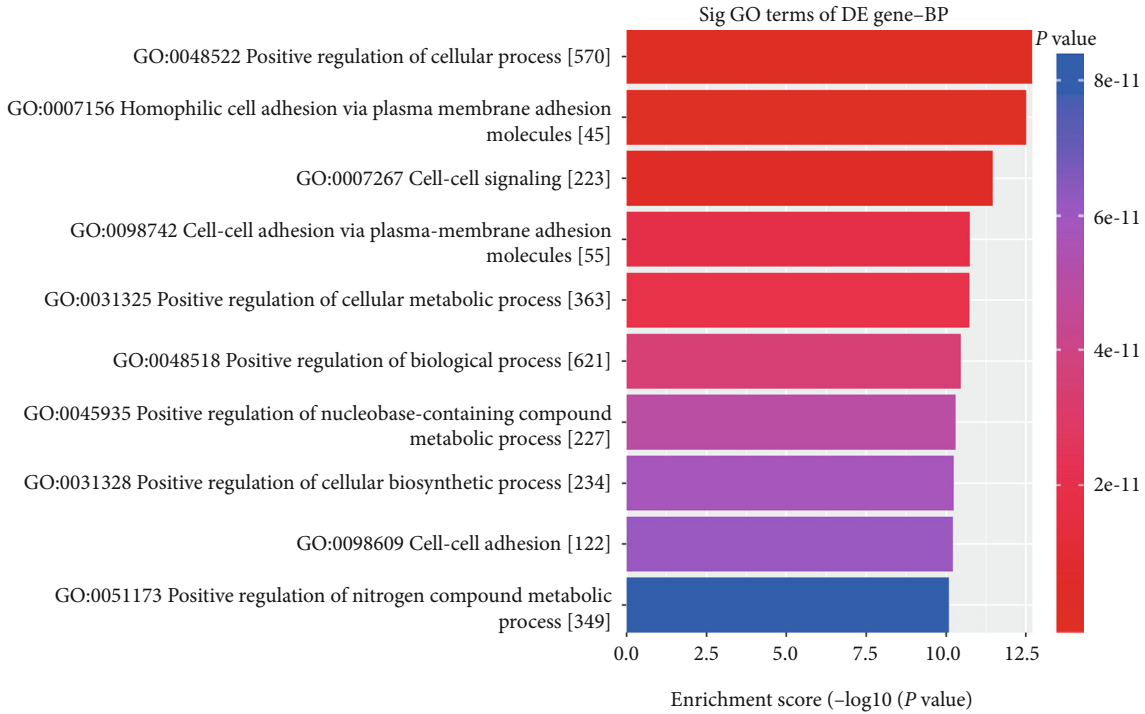
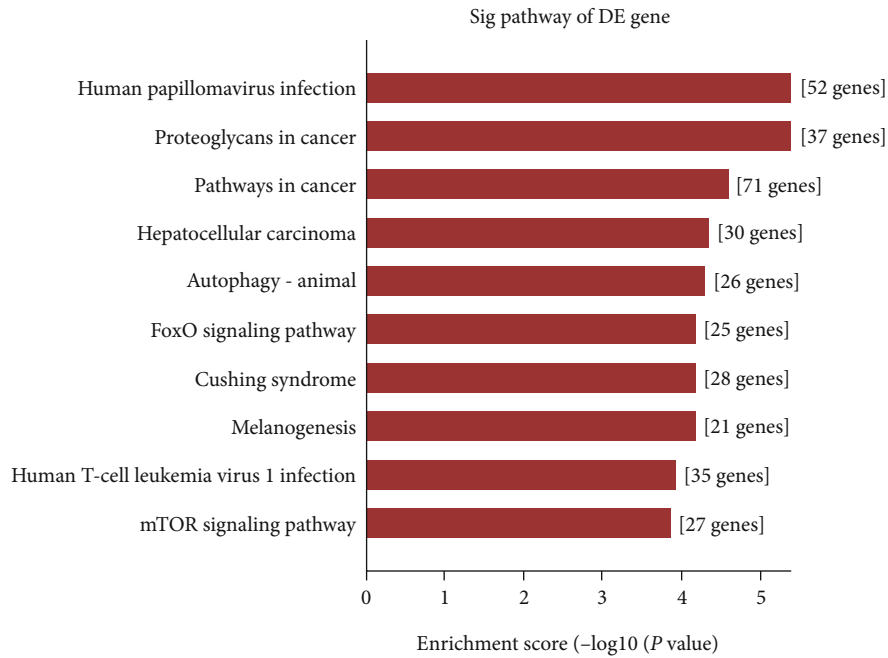


FIGURE 2: qRT-PCR validation of the differentially expressed circRNAs.

It has been reported that circRNAs can exist in every tissue and organ; however, they are also tissue enriched in some situations [28, 29]. circRNAs could not be decomposed by RNase R because their 3'- and 5'-ends form a circle. Their stable characteristics are attributed to this special structure. Furthermore, researchers have appealed that circRNAs are conserved between species, and the expression levels of circRNAs are commonly cell or tissue specific, suggesting that circRNAs could be disease markers. Previous studies have demonstrated the crucial role of circRNAs in the occurrence of various cardiovascular diseases by regulating cytodifferentiation, proliferation, necrosis, and apoptosis [30]. Several experts have harbored the idea that heart-related circRNA could prevent the heart from hypertrophy and failure [31]. It could bind with miR-223, which downregulates the level of apoptosis repressor [31]. It was previously described that Cdr1as could sequester miR-7 in neurocytes via sequence complementarity [32, 33]. Moreover, Cdr1as has been demonstrated to have the capacity to regulate myocardial infarction by binding to miR-7a in mouse cardiomyocytes [34].



(a)



(b)

FIGURE 3: GO and KEGG pathway analyses of the differential expression circRNAs. (a), Top ten GO biological processes. (b), KEGG pathways of differential expression circRNAs. GO: Gene Ontology; KEGG: Kyoto Encyclopedia of Genes and Genomes.

Wang et al. described that circRNAs are indicative of the regulation of heart mitochondrial dynamics and myocardial cell apoptosis [30]. Liu et al. reported the relationship between circR-284 and cerebrovascular ischemic stroke associated with the carotid artery. It has been found that the levels of circR-284 were higher in patients with carotid-related ischemia than in a control group [35].

circRNAs are also linked to various diseases, including Alzheimer’s disease. It has been shown that circRNA ciRS-7/CDR1as is associated with amyloid peptide clearance by regulating miRNA miR-7 [36, 37]. Additionally, circRNAs have been proven and proposed to be related to several kinds of tumors. One research group revealed that high expression of circ-100338 could promote the proliferation of hepatocellular

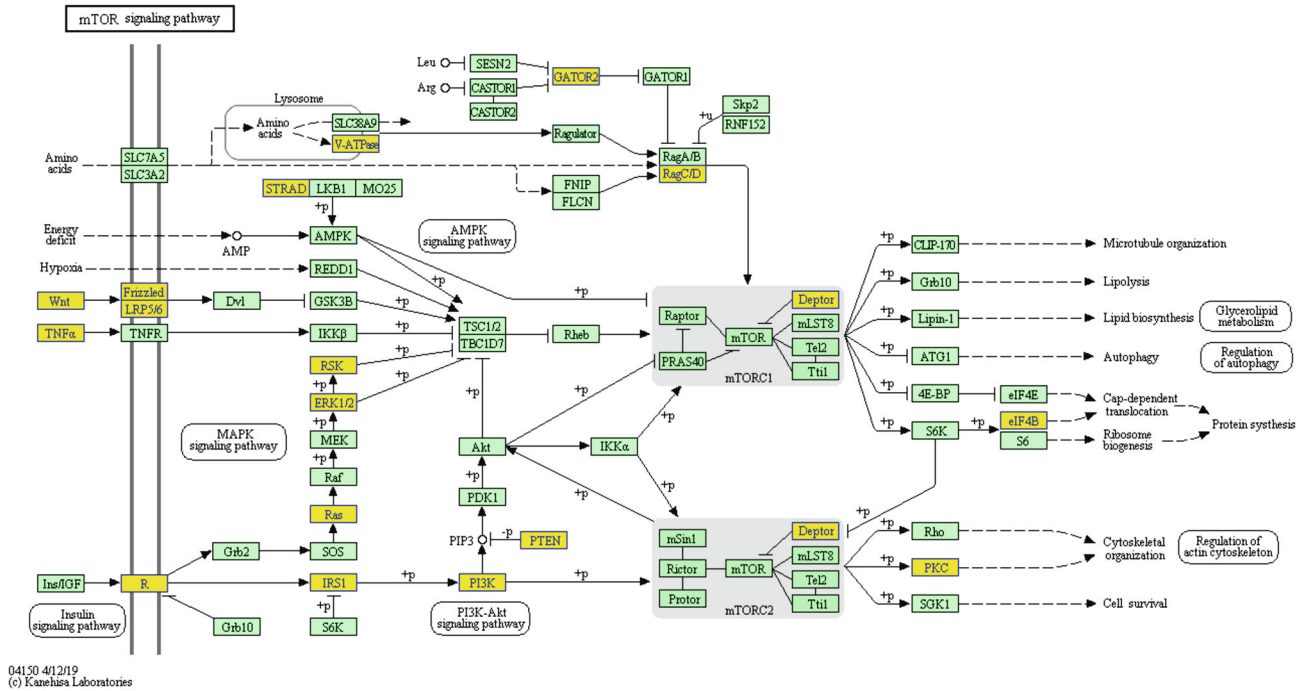


FIGURE 4: Target genes in the mTOR signaling pathway. mTOR: mammalian target of rapamycin.

carcinoma cells [38]. In another study, Pang et al. determined that circ_0072309 could retard the progression of NSCLC by inhibiting the expression of miR-580-3p [39].

In our experiments, we analyzed circRNA levels in whole blood samples using a circRNA microarray. circRNA profiling was performed using five samples from every group. In total, 235 differentially expressed circRNAs were verified; 150 were upregulated versus 85 were downregulated between the two IA groups and the control group, whereas 7 upregulated versus 3 downregulated differentially expressed circRNAs were confirmed between the UIA group and the RIA group. The results implied that circRNAs were associated with the formation of IA. The interaction network between circRNAs and miRNAs was predicted for verified circRNAs, and GO analysis was carried out to identify the role of their targeted genes. We demonstrated that the term “homophilic cell adhesion via plasma membrane adhesion molecules” was the top enriched term in the analysis. This provided overwhelming evidence for the involvement of circRNAs in the formation of IA because previous studies have described the correlation between IA and cell adhesion. Peters et al. discovered that SPARC was highly expressed in aneurysms and is a counteradhesive glycoprotein that is expressed in a variety of tissues [40]. mTOR signaling is at the core of the pathway-pathway interaction network and is linked to the genes associated with IA.

This pathway modulates translation initiation of protein synthesis, and biological processes, such as cell size and proliferation, are regulated by this pathway, which could coordinately integrate nutrient sufficiency signals from mTOR with growth factor signals [41]. Similarly, the phospho-mTOR levels were decreased in ruptured IAs compared to unruptured IAs [42].

5. Conclusion

In conclusion, our study predicted the function of circRNAs in IA formation and expanded the body of knowledge on the pathogenesis of IA. We demonstrated that circRNAs are linked to the formation of IA by modulating the mTOR signaling pathway. Our results revealed a list of potential diagnostic biomarkers for IA and suggested that differentially expressed circRNAs or the mTOR pathway can be latent therapeutic strategies for IA.

Data Availability

The raw data used to support the findings of this study are available from the corresponding author upon request.

Conflicts of Interest

The authors have no financial conflicts of interest.

Acknowledgments

This work was supported by the “13th Five-Year Plan” National Science and Technology Supporting Plan (2015BAI12B04), National Natural Science Foundation of China (81371292), Beijing Municipal Administration of Hospitals’ Mission Plan (code: SML20150501), program of the National Natural Science Foundation of China (81870904), and the Program of Natural Science Foundation of Capital Medical University (PYZ2017068).

Supplementary Materials

The supplementary materials include three files. The primer file lists the primer sequences, lengths, and target genes. The sample file shows the quality and concentration of the 15 perineal blood samples. In addition, the network file shows the circRNA-miRNA networks. (*Supplementary Materials*)

References

- [1] M. H. Vlak, A. Algra, R. Brandenburg, and G. J. Rinkel, "Prevalence of unruptured intracranial aneurysms, with emphasis on sex, age, comorbidity, country, and time period: a systematic review and meta-analysis," *Lancet Neurology*, vol. 10, no. 7, pp. 626–636, 2011.
- [2] N. Chalouhi, M. S. Ali, P. M. Jabbour et al., "Biology of intracranial aneurysms: role of inflammation," *Journal of Cerebral Blood Flow and Metabolism*, vol. 32, no. 9, pp. 1659–1676, 2012.
- [3] T. Aoki, H. Kataoka, R. Ishibashi, K. Nozaki, K. Egashira, and N. Hashimoto, "Impact of monocyte chemoattractant protein-1 deficiency on cerebral aneurysm formation," *Stroke*, vol. 40, no. 3, pp. 942–951, 2009.
- [4] R. M. Koffie, C. J. Stapleton, C. M. Torok, A. J. Yoo, T. M. Leslie-Mazwi, and P. J. Codd, "Rapid growth of an infectious intracranial aneurysm with catastrophic intracranial hemorrhage," *Journal of Clinical Neuroscience*, vol. 22, no. 3, pp. 603–605, 2015.
- [5] V. Feigin, V. Parag, C. M. Lawes et al., "Smoking and elevated blood pressure are the most important risk factors for subarachnoid hemorrhage in the asia-pacific region: an overview of 26 cohorts involving 306, 620 participants," *Stroke*, vol. 36, no. 7, pp. 1360–1365, 2005.
- [6] J. M. Farnham, N. J. Camp, S. L. Neuhausen et al., "Confirmation of chromosome 7q11 locus for predisposition to intracranial aneurysm," *Hum Genet*, vol. 114, no. 3, pp. 250–255, 2004.
- [7] Y. B. Roos, G. Pals, P. M. Struycken et al., "Genome-wide linkage in a large dutch consanguineous family maps a locus for intracranial aneurysms to chromosome 2p13," *Stroke*, vol. 35, no. 10, pp. 2276–2281, 2004.
- [8] S. Yamada, M. Utsunomiya, K. Inoue et al., "Genome-wide scan for Japanese familial intracranial aneurysms: linkage to several chromosomal regions," *Circulation*, vol. 110, no. 24, pp. 3727–3733, 2004.
- [9] A. K. Ozturk, B. V. Nahed, M. Bydon et al., "Molecular genetic analysis of two large kindreds with intracranial aneurysms demonstrates linkage to 11q24-25 and 14q23-31," *Stroke*, vol. 37, no. 4, pp. 1021–1027, 2006.
- [10] H. Onda, H. Kasuya, T. Yoneyama et al., "Genomewide-linkage and haplotype-association studies map intracranial aneurysm to chromosome 7q11," *American Journal of Human Genetics*, vol. 69, no. 4, pp. 804–819, 2001.
- [11] B. V. Nahed, A. Seker, B. Guclu et al., "Mapping a Mendelian form of intracranial aneurysm to 1p34.3-p36.13," *American Journal of Human Genetics*, vol. 76, no. 1, pp. 172–179, 2005.
- [12] E. Biros and J. Golledge, "Meta-analysis of whole-genome linkage scans for intracranial aneurysm," *Neuroscience Letters*, vol. 431, no. 1, pp. 31–35, 2008.
- [13] D. Woo and J. Broderick, "Genetics of intracranial aneurysm," *Journal of Stroke and Cerebrovascular Diseases*, vol. 11, no. 5, pp. 230–240, 2002.
- [14] L. R. Sauerbeck, R. Hornung, C. J. Moomaw et al., "The effects of study participation in the familial intracranial aneurysm study on cigarette smoking," *Journal of Stroke and Cerebrovascular Diseases*, vol. 17, no. 6, pp. 370–372, 2008.
- [15] J. R. Ren, S. H. Ren, B. Ning et al., "Hyperhomocysteinemia as a risk factor for saccular intracranial aneurysm: a cohort study in a Chinese Han population," *Journal of Stroke and Cerebrovascular Diseases*, vol. 26, no. 12, pp. 2720–2726, 2017.
- [16] P. J. Hui, Y. H. Yan, S. M. Zhang et al., "Intraoperative microvascular Doppler monitoring in intracranial aneurysm surgery," *Chinese Medical Journal*, vol. 126, no. 13, pp. 2424–2429, 2013.
- [17] Y. X. Gu, X. C. Chen, D. L. Song, B. Leng, and F. Zhao, "Risk factors for intracranial aneurysm in an ethnic population," *Chinese Medical Journal*, vol. 119, no. 16, pp. 1359–1364, 2006.
- [18] Y. Mineharu, K. Inoue, S. Inoue et al., "Model-based linkage analyses confirm chromosome 19q13.3 as a susceptibility locus for intracranial aneurysm," *Stroke*, vol. 38, no. 4, pp. 1174–1178, 2007.
- [19] L. Liu, Q. Zhang, X. Y. Xiong, Q. W. Gong, M. F. Liao, and Q. W. Yang, "Tlr 4 gene polymorphisms rs 11536889 is associated with intracranial aneurysm susceptibility," *Journal of Clinical Neuroscience*, vol. 53, pp. 165–170, 2018.
- [20] J. W. Fischer and A. K. Leung, "CircRNAs: a regulator of cellular stress," *Critical Reviews in Biochemistry and Molecular Biology*, vol. 52, no. 2, pp. 220–233, 2017.
- [21] N. R. Pamudurti, O. Bartok, M. Jens et al., "Translation of circrnas," *Molecular Cell*, vol. 66, no. 1, pp. 9–21.e7, 2017, e27.
- [22] M. Zhao, F. Gao, D. Zhang et al., "Altered expression of circular RNAs in moyamoya disease," *Journal of the Neurological Sciences*, vol. 381, pp. 25–31, 2017.
- [23] C. E. Burd, W. R. Jeck, Y. Liu, H. K. Sanoff, Z. Wang, and N. E. Sharpless, "Expression of linear and novel circular forms of an INK 4/ARF-associated non-coding RNA correlates with atherosclerosis risk," *PLoS Genetics*, vol. 6, no. 12, p. e1001233, 2010.
- [24] A. J. Enright, B. John, U. Gaul, T. Tuschl, C. Sander, and D. S. Marks, "MicroRNA targets in drosophila," *Genome Biology*, vol. 5, no. 1, p. R1, 2003.
- [25] A. E. Pasquinelli, "MicroRNAs and their targets: recognition, regulation and an emerging reciprocal relationship," *Nature Reviews. Genetics*, vol. 13, no. 4, pp. 271–282, 2012.
- [26] J. P. Bennett and P. M. Keeney, "RNA-sequencing reveals similarities and differences in gene expression in vulnerable brain tissues of Alzheimer's and Parkinson's diseases," *Journal of Alzheimer's Disease Reports*, vol. 2, no. 1, pp. 129–137, 2018.
- [27] A. F. Gabriel, M. C. Costa, and F. J. Enguita, "Interactions among regulatory non-coding RNAs involved in cardiovascular diseases," *Advances in Experimental Medicine and Biology*, vol. 1229, pp. 79–104, 2020.
- [28] W. R. Jeck, J. A. Sorrentino, K. Wang et al., "Circular RNAs are abundant, conserved, and associated with alu repeats," *RNA*, vol. 19, no. 2, pp. 141–157, 2013.
- [29] J. Salzman, C. Gawad, P. L. Wang, N. Lacayo, and P. O. Brown, "Circular RNAs are the predominant transcript isoform from hundreds of human genes in diverse cell types," *PLoS One*, vol. 7, no. 2, p. e30733, 2012.
- [30] K. Wang, T. Y. Gan, N. Li et al., "Circular RNA mediates cardiomyocyte death via miRNA-dependent upregulation of MTP 18 expression," *Cell Death and Differentiation*, vol. 24, no. 6, pp. 1111–1120, 2017.

- [31] K. Wang, B. Long, F. Liu et al., "A circular RNA protects the heart from pathological hypertrophy and heart failure by targeting miR-223," *European Heart Journal*, vol. 37, no. 33, pp. 2602–2611, 2016.
- [32] T. B. Hansen, T. I. Jensen, B. H. Clausen et al., "Natural RNA circles function as efficient microRNA sponges," *Nature*, vol. 495, no. 7441, pp. 384–388, 2013.
- [33] S. Memczak, M. Jens, A. Elefsinioti et al., "Circular RNAs are a large class of animal RNAs with regulatory potency," *Nature*, vol. 495, no. 7441, pp. 333–338, 2013.
- [34] H. H. Geng, R. Li, Y. M. Su et al., "The circular RNA Cdr1as promotes myocardial infarction by mediating the regulation of mir-7a on its target genes expression," *PLoS One*, vol. 11, no. 3, p. e0151753, 2016.
- [35] X. Liu, Y. Cheng, S. Zhang, Y. Lin, J. Yang, and C. Zhang, "A necessary role of miR-221 and miR-222 in vascular smooth muscle cell proliferation and neointimal hyperplasia," *Circulation Research*, vol. 104, no. 4, pp. 476–487, 2009.
- [36] W. J. Lukiw, "Circular RNA (circRNA) in Alzheimer's disease (AD)," *Frontiers in Genetics*, vol. 4, p. 307, 2013.
- [37] Z. Shi, T. Chen, Q. Yao et al., "The circular RNA ciRS-7 promotes APP and BACE 1 degradation in an NF-kappaB-dependent manner," *The FEBS Journal*, vol. 284, no. 7, pp. 1096–1109, 2017.
- [38] X. Cheng, P. Tian, W. Zheng, and X. Yan, "Piplartine attenuates the proliferation of hepatocellular carcinoma cells via regulating hsa_circ_100338 expression," *Cancer Medicine*, vol. 9, no. 12, pp. 4265–4273, 2020.
- [39] W. Pang, F. Huang, X. Zhang et al., "Circular RNA hsa_circ_0072309 inhibits non-small cell lung cancer progression by sponging miR-580-3p," *Bioscience Reports*, vol. 40, no. 5, 2020.
- [40] D. G. Peters, A. B. Kassam, E. Feingold et al., "Molecular anatomy of an intracranial Aneurysm," *STROKE*, vol. 32, no. 4, pp. 1036–1042, 2001.
- [41] A. C. Gingras, B. Raught, and N. Sonenberg, "mTOR signaling to translation," *Current Topics in Microbiology and Immunology*, vol. 279, pp. 169–197, 2004.
- [42] E. Laaksamo, M. Ramachandran, J. Frösen et al., "Intracellular signaling pathways and size, shape, and rupture history of human intracranial aneurysms," *NEUROSURGERY*, vol. 70, no. 6, pp. 1565–1573, 2012.

Research Article

Identification of miRNAs as the Crosstalk in the Interaction between Neural Stem/Progenitor Cells and Endothelial Cells

Xin Wang ¹, Simin Li ², Yihong Ma ³, Yuzhen Xu ⁴,
Anthony Chukwunonso Ogbuehi ⁵, Xianda Hu ⁶, Aneesha Acharya ⁷, Rainer Haak ²,
Dirk Ziebolz ², Gerhard Schmalz ², Hanluo Li ⁸, Sebastian Gaus ⁸, Bernd Lethaus ⁸,
Vuk Savkovic ⁸ and Zhiqiang Su ¹

¹Department of Neurology, First Affiliated Hospital of Harbin Medical University, Harbin 150001, China

²Department of Cariology, Endodontology and Periodontology, University Leipzig, Liebigstr. 12, 04103 Leipzig, Germany

³Department of Neurology, Graduate School of Medical Sciences, Faculty of Life Sciences, Kumamoto University, Kumamoto, Japan

⁴Department of Neurology, Shanghai Tenth People's Hospital, Tongji University School of Medicine, No. 301 Middle Yanchang Road, Shanghai, China

⁵Faculty of Physics, University of Münster, Wilhelm-Klemm-Straße 9, 48149 Münster, Germany

⁶Laboratory of Molecular Cell Biology, Beijing Tibetan Hospital, China Tibetology Research Center, 218 Anwaixiaoguanbeili Street, Chaoyang, Beijing 100029, China

⁷Faculty of Dentistry, University of Hong Kong, Hong Kong, China

⁸Department of Cranio Maxillofacial Surgery, University Clinic Leipzig, Liebigstr. 12, 04103 Leipzig, Germany

Correspondence should be addressed to Zhiqiang Su; suzhiqiang2020@126.com

Received 9 October 2020; Revised 22 November 2020; Accepted 24 November 2020; Published 16 December 2020

Academic Editor: Wen-Jun Tu

Copyright © 2020 Xin Wang et al. This is an open access article distributed under the Creative Commons Attribution License, which permits unrestricted use, distribution, and reproduction in any medium, provided the original work is properly cited.

Aim. This study is aimed at identifying genetic and epigenetic crosstalk molecules and their target drugs involved in the interaction between neural stem/progenitor cells (NSPCs) and endothelial cells (ECs). **Materials and Methods.** Datasets pertaining to reciprocal mRNA and noncoding RNA changes induced by the interaction between NSPCs and ECs were obtained from the GEO database. Differential expression analysis (DEA) was applied to identify NSPC-induced EC alterations by comparing the expression profiles between monoculture of ECs and ECs grown in EC/NSPC cocultures. DEA was also utilized to identify EC-induced NSPC alterations by comparing the expression profiles between monoculture of NSPCs and NSPCs grown in EC/NSPC cocultures. The DEGs and DEmiRNAs shared by NSPC-induced EC alterations and EC-induced NSPC alterations were then identified. Furthermore, miRNA crosstalk analysis and functional enrichment analysis were performed, and the relationship between DEmiRNAs and small molecular drug targets/environment chemical compounds was investigated. **Results.** One dataset (GSE29759) was included and analyzed in this study. Six genes (i.e., MMP14, TIMP3, LOXL1, CCK, SMAD6, and HSPA2), three miRNAs (i.e., miR-210, miR-230a, and miR-23b), and three pathways (i.e., Akt, ERK1/2, and BMPs) were identified as crosstalk molecules. Six small molecular drugs (i.e., depropine, fluphenazine, lycorine, quinostatin, resveratrol, and thiamazole) and seven environmental chemical compounds (i.e., folic acid, dexamethasone, choline, doxorubicin, thalidomide, bisphenol A, and titanium dioxide) were identified to be potential target drugs of the identified DEmiRNAs. **Conclusion.** To conclude, three miRNAs (i.e., miR-210, miR-230a, and miR-23b) were identified to be crosstalks linking the interaction between ECs and NSPCs by implicating in both angiogenesis and neurogenesis. These crosstalk molecules might provide a basis for devising novel strategies for fabricating neurovascular models in stem cell tissue engineering.

1. Introduction

It is well known that the neurovascular unit (NVU) comprises a collection of cells (e.g., endothelial, neural, and glial cells), which can control interactions between neurons and the vasculature. Based on the concept of NVU, the construction of 3D neurovascular tissue has emerged as a promising approach in the field of tissue engineering [1, 2]. Constructing 3D neurovascular tissues by combining neurogenesis and angiogenesis models is viewed as a potentially effective strategy to facilitate functional recovery in ischemic stroke [3]. Increasing evidence has shown that the cell contact-dependent interactions between neural stem/progenitor cells (NSPCs) and endothelial cells (ECs) can drive the coupling of neurogenesis and angiogenesis. On the one hand, NSPCs can promote morphogenesis and angiogenesis of ECs by expressing angiogenic factors such as vascular endothelial growth factor (VEGF) [4]. In turn, VEGF has been demonstrated to promote neurogenesis, neuronal patterning, neuroprotection, and glial growth of NSPCs [5]. On the other hand, ECs can also stimulate survival, proliferation, neuronal differentiation, and neurogenesis of NSPCs by secreting neurotrophic factors such as brain-derived neurotrophic factor (BDNF) [6–8]. Conversely, BDNF has been shown to support the cell-cell contacts and survival of ECs, suggesting that it plays a critical role in maintaining vessel stabilization and mediating angiogenesis [9]. Overall, current evidence indicates that the interactions between NSPCs and ECs are governed by several common crosstalk factors that regulate both the neurogenic and angiogenic processes.

A previous study using microarray analysis investigated the molecular mechanisms underlying the interaction between NSPCs and ECs at the mRNA and miRNA levels [10]. This study focused on investigating the NSPC-induced molecular alterations in the angiogenesis of ECs and the EC-induced molecular alterations in the neurogenesis of NSPCs. However, this study did not explore the genetic and epigenetic crosstalks underlying the reciprocal regulations between NSPCs and ECs from a systemic and comprehensive perspective. Bioinformatics techniques can be used to analyze and interpret data obtained by microarray datasets in order to identify the crosstalk between NSPCs and ECs at the gene and microRNA (miRNA) levels. Since targeting miRNAs with small molecules and environmental chemical compounds is a promising therapeutic strategy for human diseases [11, 12], it is necessary to identify the molecules and compounds that might be utilized in targeted drug delivery to construct neurovascular tissue. To the authors' knowledge, this is the first report using bioinformatics techniques to identify the crosstalk genes, signaling pathways, and miRNAs, as well as the crosstalk miRNA targeting drugs that are involved in the reciprocal regulation between NSPCs and ECs. As crosstalk molecules and their related drugs identified in this study are implicated in regulating neurogenic and angiogenic processes, their identification can potentially enable the development of novel strategies for fabricating neurovascular models using 3D tissue engineering.

2. Materials and Methods

2.1. Procurement of Microarray Datasets. A single dataset (GSE29759) using the *Mus musculus* model was retrieved from the Gene Expression Omnibus (GEO) database [10]. This dataset investigated both the mRNA and miRNA expression profiling. The study design of this dataset was established with four groups: monoculture of ECs (group A), ECs grown in EC/NSPC cocultures (group B), monoculture of NSPCs (group C), and NSPCs grown in EC/NSPC cocultures (group D).

These four groups were divided into two categories. First, the NSPC-induced EC alterations were analyzed by comparing expression profiles between groups A and B. In the comparison between groups A and B, group A was considered the control group, while group B was regarded as the experimental group. Second, the EC-induced NSPC changes were analyzed by comparing groups C and D. Likewise, in the comparison between groups C and D, group C was considered the control group, while group D was regarded as the experimental group.

2.2. Differential Expression Analysis. Differential expression analysis was performed using the R package “limma” [13] for identifying differentially expressed genes (DEGs) and differentially expressed miRNAs (DEmiRNAs) relevant to EC-induced NSPC changes and NSPC-induced EC changes, respectively. Genes and miRNAs with P value < 0.05 and $|\log_2 \text{FC}| \geq 0.5$ were considered DEGs and DEmiRNAs. Overlapping DEGs and DEmiRNAs between these two categories were determined using Venn diagrams.

2.3. Functional Enrichment Analysis of DEGs. Functional enrichment analysis of the overlapping DEGs was based on Gene Ontology (GO) terms, especially biological process (BP), as well as KEGG (Kyoto Encyclopedia of Genes and Genomes) pathways. This analysis was conducted by using the clusterProfiler package in the R program (significance level $P < 0.05$) [14].

2.4. The Construction of a PPI Network. Protein-protein interaction (PPI) pairs corresponding to DEGs were obtained using the STRING database [15]. Protein-protein interaction (PPI) networks of NSPC-induced EC changes (EC-PPI) and EC-induced NSPC changes (NSPC-PPI) were constructed with the “Cytoscape” software platform [16]. The topological characteristics of each PPI network were determined using the “NetworkAnalyzer” tool. A Venn diagram was used to identify the overlapping DEGs between the EC-PPI network and the NSPC-PPI network.

2.5. Identification of Transcription Factors-Target DEGs. To identify regulatory transcription factors (TFs) that control the DEGs at a transcriptional level, TF-target DEG interactions were obtained using the Transcriptional Regulatory Relationships Unraveled by Sentence-based Text mining (TRRUST) database Version 2 [17]. The TF-target DEG interaction networks, respectively, for the DEGs involved in the EC-induced NSPC alteration and NSPC-induced EC alteration, were constructed based on these TF-target DEG

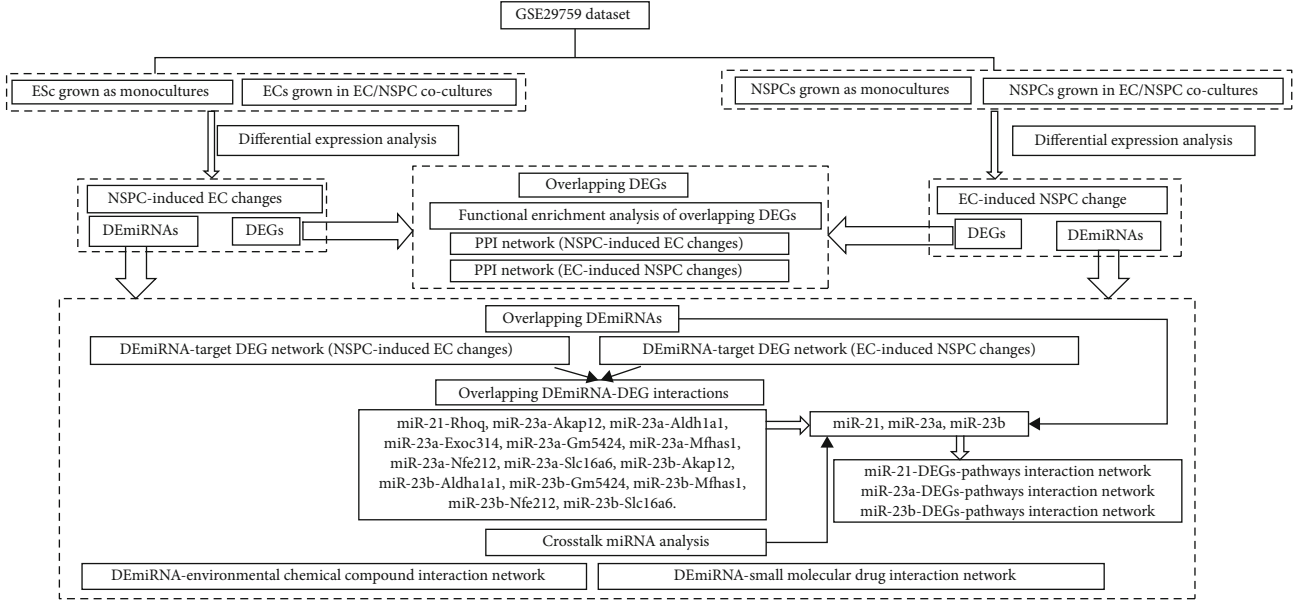


FIGURE 1: The flowchart of the present study.

TABLE 1: The number of up- and downregulated DEGs and DEmiRNAs that are, respectively, involved in NSPC-induced EC alterations and EC-induced NSPC alterations.

Coculture-induced genetic and epigenetic alteration in one type of cells	Number of DEmRNAs (DEGs)			Number of DEmiRNAs		
	Upregulated DEGs	Downregulated DEGs	Total	Upregulated DEmiRNAs	Downregulated DEmiRNAs	Total
NSPC-induced alterations in ECs	399	345	744	5	13	18
EC-induced alterations in NSPCs	425	710	1135	5	3	8

interaction pairs. The topological characteristics (e.g., degree and betweenness centrality) of the nodes in the networks were also calculated.

2.6. Prediction of miRNA Targets. The experimentally validated gene targets of DEmiRNAs were obtained by three databases, including miRTarBase [18], miRecords [19], and TarBase v7 [20]. The computationally predicted gene targets of DEmiRNAs were obtained from eight databases including TargetScan [21], starBase [22], miRNAMap [23], miRDB [24], miRWalk [25], RNAhybrid [26], and miRanda [24]. Combining the experimentally validated and computationally predicted gene targets, a set of gene targets of the DEmiRNAs was obtained. From these, differentially expressed gene targets were identified and termed as miRNA-DEtarget. The DEmiRNA-target network involved in the EC-induced NSPC alteration and NSPC-induced EC alteration was constructed, respectively, using the clusterProfiler package in the R program [14]. The topological characteristics of nodes in this network were also calculated.

The DEmiRNA-DEtargets for each category were subjected to functional enrichment analysis in order to identify the signaling pathways with significant involvement. Corre-

sponding miR-DEG-pathway interaction networks for each miRNA were constructed to examine DEtarget genes and their relevant enriched functional pathways.

2.7. The Relationship between DEmiRNAs and Small Molecular Drugs. The DEmiRNAs determined using the mouse genome were assigned corresponding Homo sapiens gene identities and further converted to the names of probes based on the HG-U133A platform. The human probe identities were uploaded to the Cmap web tool [27], and small molecular signatures of the selected DEmiRNAs were calculated by the following three formulas:

$$\begin{aligned}
 a &= \text{Max}_{j=1}^t \left[\frac{j}{t} - \frac{V(j)}{N} \right], \\
 b &= \text{Max}_{j=1}^t \left[\frac{V(j)}{N} - \frac{(j-1)}{t} \right], \\
 \text{KS}_{\text{up/down}} &= \begin{cases} a(a > b) \\ -b(b > a) \end{cases}.
 \end{aligned} \tag{1}$$

The variable t represents the number of DEmiRNAs which could be either upregulated or downregulated; j represents the j th gene based on the rank of the differential

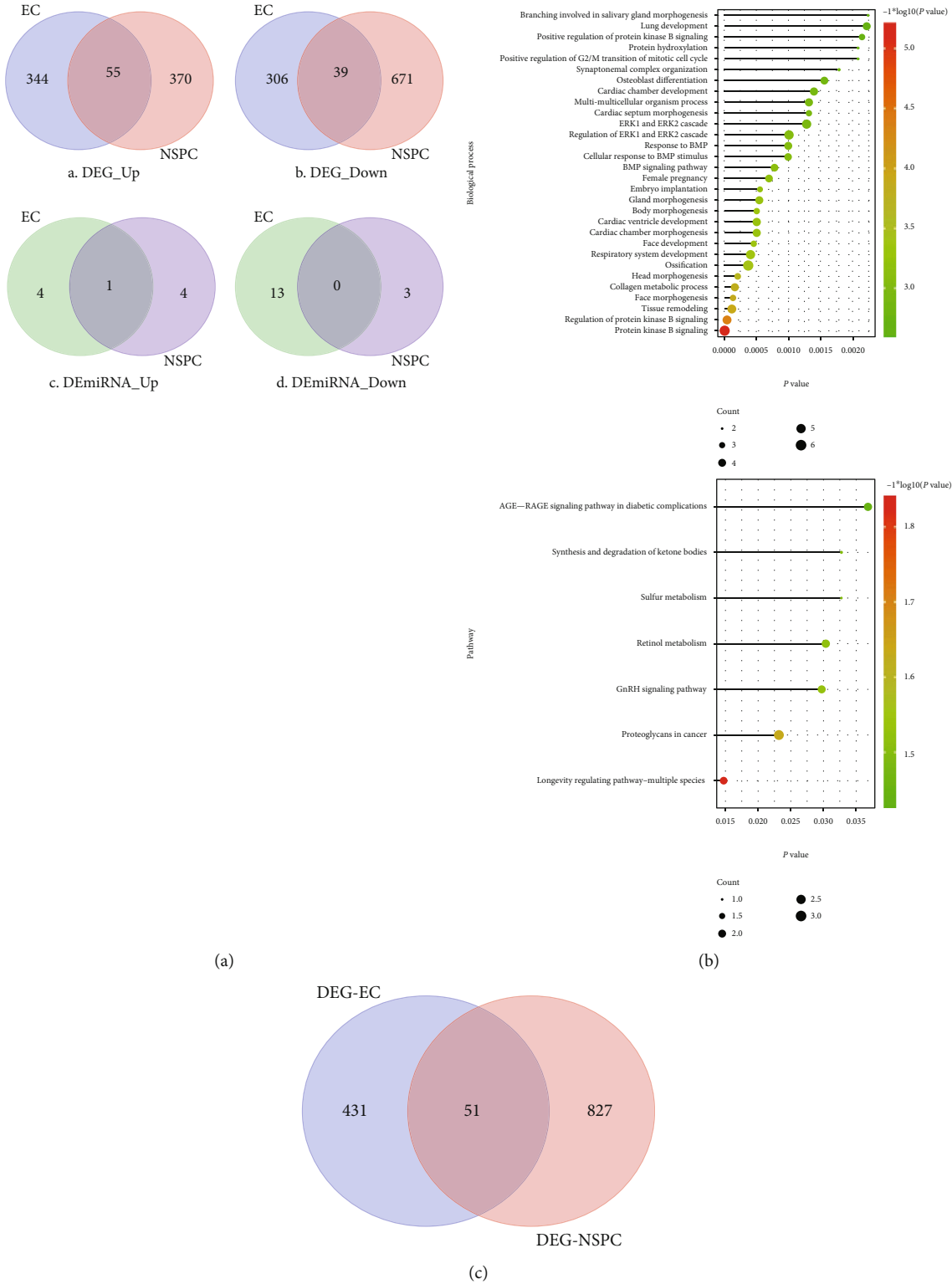


FIGURE 2: The DEGs identified to be involved in the EC-induced NSPC alterations and NSPC-induced EC alterations and the functions in which these DEGs were involved. (a) Venn diagram showing the overlapped DEGs and DEMiRNAs that hold the same expression patterns (either up- or downregulated) in EC-induced NSPC alterations and NSPC-induced EC alterations. (b) The top 30 BPs (A) and top signaling pathways (B) in which overlapped DEGs were enriched. The overlapped DEGs are shared between the NSPC-induced EC alterations and the EC-induced NSPC alterations. (c) The Venn diagram shows the DEGs overlapped between the DEGs involved in the EC-PPI network (PPI network involved in the NSPC-induced EC genetic alteration) and the NSPC-PPI network (PPI network involved in the EC-induced NSPC genetic alteration).

TABLE 2: The top 30 DEGs involved in the NSPC-induced alterations in ECs, ranked by the ascending order of P value.

Gene	logFC	AveExpr	t value	P value	Adj. P value	B value	Regulation pattern
Matn2	-0.95204	0.491256	-10.0494	$3.86E-06$	0.025782	4.509474	Down
Fmod	-1.02587	0.511182	-10.011	$3.98E-06$	0.025782	4.485352	Down
LOC102641248///Maf	-1.1636	0.572078	-9.81371	$4.69E-06$	0.025782	4.359141	Down
Csf2	0.946405	-0.49723	9.80391	$4.73E-06$	0.025782	4.352778	Up
Cyr61	1.916043	-0.90785	9.163675	$8.19E-06$	0.035735	3.917772	Up
Rad54b	0.884623	-0.50864	8.718932	$1.22E-05$	0.038883	3.591553	Up
Hmgb3	1.027877	-0.53931	8.697135	$1.25E-05$	0.038883	3.575027	Up
Srpx2	-1.03053	0.491458	-8.532	$1.45E-05$	0.039663	3.448146	Down
Ces1g	-1.12288	0.585271	-8.39761	$1.65E-05$	0.040014	3.342658	Down
Glis3	-0.82208	0.370708	-8.27324	$1.86E-05$	0.040548	3.243204	Down
Negr1	-0.85748	0.4562	-8.03571	$2.34E-05$	0.041325	3.048246	Down
C1ra	-0.80236	0.398421	-7.9815	$2.47E-05$	0.041325	3.002814	Down
Smarcal1	-0.90427	0.471865	-7.90938	$2.65E-05$	0.041325	2.941813	Down
Gmnn	0.868301	-0.43587	7.834033	$2.86E-05$	0.041325	2.877409	Up
Tex30	1.021454	-0.5467	7.64017	$3.48E-05$	0.041325	2.708438	Up
Steap4	-0.90097	0.356113	-7.58391	$3.68E-05$	0.041325	2.658512	Down
Rbms3	-0.79877	0.399764	-7.5764	$3.71E-05$	0.041325	2.651814	Down
Cdo1	-0.87123	0.459852	-7.51396	$3.96E-05$	0.041325	2.595861	Down
Col3a1	-0.72967	0.358484	-7.49893	$4.02E-05$	0.041325	2.582317	Down
3632451O06Rik	-0.99083	0.395715	-7.37964	$4.55E-05$	0.041325	2.47378	Down
C3	-0.8261	0.446644	-7.36875	$4.61E-05$	0.041325	2.463774	Down
Thsd7a	-1.00741	0.566198	-7.34217	$4.74E-05$	0.041325	2.439301	Down
Mad2l1	0.769878	-0.43152	7.272629	$5.10E-05$	0.041325	2.374807	Up
Ccne2	0.891927	-0.50969	7.268195	$5.12E-05$	0.041325	2.370674	Up
Adamts2	-0.9331	0.460263	-7.23757	$5.29E-05$	0.041325	2.342049	Down
AI506816	0.79492	-0.41645	7.222375	$5.38E-05$	0.041325	2.327797	Up
Timm8a1	0.742468	-0.41919	7.211119	$5.44E-05$	0.041325	2.317221	Up
Ccnb2	0.6736	-0.32421	7.16572	$5.71E-05$	0.041325	2.274388	Up
Tyms///Tyms-ps	0.676379	-0.36727	7.152192	$5.80E-05$	0.041325	2.26157	Up
5730414N17Rik	-0.79662	0.418908	-7.14794	$5.82E-05$	0.041325	2.257534	Down

expression; N denotes the magnitude of the ranked small molecular signature; the element $V(j)$ of a vector V is the position of the j th target gene in the ordered small molecular signature. The corresponding KS_{up} and KS_{down} generated were integrated into the S score as follows: S is equal to 0 when KS_{up} and KS_{down} have the same sign and is equal to $KS_{up} - KS_{down}$ otherwise.

2.8. Predicting the Relationship between DE miRNAs and Environmental Chemical Compounds. The relationship between environmental chemical compounds and DE miRNAs was determined by downloading the corresponding interaction pairs from the Comparative Toxicogenomics Database (CTD) [28]. Highly correlated DE miRNAs-environmental chemical compounds were then determined

by filtering using a hypergeometric test. The formula of the hypergeometric test is as follows:

$$P(k, N, M, n) = \frac{\binom{M}{k} * \binom{N-M}{n-k}}{\binom{N}{n}}, \quad k = 0, 1, 2, 3, \dots, M. \quad (2)$$

N represents the total number of DE miRNAs; n represents the number of DE miRNAs corresponding to a specific chemical compound; M represents the number of the target genes of a specific miRNA; k represents the genes which

TABLE 3: The top 30 DEGs involved in the EC-involved alterations in NSPCs, ranked by the ascending order of P value.

Gene	logFC	AveExpr	t value	P value	Adj. P value	B value	Regulation pattern
Pcolce2	-3.29485	1.6351	-45.4871	2.08E-11	4.55E-07	13.2377	Down
Dbp	-2.00859	1.062409	-26.2015	2.14E-09	2.34E-05	11.11723	Down
AU020206	-1.63296	0.821066	-21.5827	1.08E-08	7.32E-05	10.05187	Down
F3	-1.6611	0.850706	-20.9105	1.41E-08	7.32E-05	9.863187	Down
Tpi1	-1.68121	0.830618	-20.4734	1.68E-08	7.32E-05	9.73502	Down
Gm2115	-1.53464	0.719453	-19.4163	2.60E-08	9.46E-05	9.405935	Down
Ldha	-1.78095	0.900045	-18.2662	4.32E-08	0.000134	9.014231	Down
Sorl1	-1.45704	0.706881	-17.7044	5.59E-08	0.000135	8.808873	Down
Dct	-1.30765	0.669351	-17.6998	5.60E-08	0.000135	8.807132	Down
Klf9	-1.86306	0.937896	-17.4915	6.17E-08	0.000135	8.728473	Down
Pgk1	-1.18385	0.609345	-16.5411	9.78E-08	0.000194	8.351213	Down
Gypc	-1.22407	0.595138	-16.039	1.26E-07	0.000207	8.139031	Down
Aldoa	-1.26041	0.65786	-15.9803	1.30E-07	0.000207	8.113603	Down
Plekhf1	-1.317	0.690027	-15.8197	1.41E-07	0.000207	8.043409	Down
4-Sep	-1.14394	0.579925	-15.6971	1.50E-07	0.000207	7.989137	Down
Aldh1a1	-2.80632	1.506176	-15.6785	1.52E-07	0.000207	7.980857	Down
Plin3	-1.2668	0.589403	-15.1096	2.06E-07	0.000264	7.720663	Down
Parp9	-1.23876	0.648245	-14.7499	2.50E-07	0.000303	7.549197	Down
Cldn12	-1.28813	0.622674	-14.0937	3.63E-07	0.000408	7.221524	Down
Gpi1	-1.00716	0.517518	-14.0417	3.74E-07	0.000408	7.194653	Down
Htra1	-1.19764	0.56397	-13.8878	4.09E-07	0.000409	7.114509	Down
Srd5a1	-1.16578	0.561656	-13.8718	4.13E-07	0.000409	7.106129	Down
Dlx5	1.127851	-0.58715	13.43145	5.37E-07	0.000478	6.87001	Up
ND5	1.058484	-0.52334	13.36773	5.58E-07	0.000478	6.835023	Up
Rbp1	-1.12775	0.585747	-13.3416	5.67E-07	0.000478	6.820608	Down
Atp1b2	-1.03892	0.500454	-13.3344	5.69E-07	0.000478	6.816639	Down
Clybl	-1.27083	0.618039	-13.1367	6.42E-07	0.000519	6.706417	Down
Sox8	-1.02853	0.485142	-12.9808	7.08E-07	0.000551	6.617969	Down
Srprb//Trf	-1.18478	0.624131	-12.8262	7.80E-07	0.000586	6.52904	Down
Hspb6	-0.93188	0.490732	-12.7078	8.40E-07	0.000594	6.459985	Down

not only belong to the target genes of DE miRNAs but also are related to chemical compounds.

2.9. Crosstalk miRNA Analysis. The crosstalk miRNAs were explored using the “Meet/Min” score based on the gene targets, small molecules (DE miRNA-molecule interaction pairs), environmental chemical compounds, signaling pathways, and biological processes in GO terms. The “Meet/Min” score was calculated as follows:

$$\text{Score}(i, j) = \frac{|\text{targets}(i) \cap \text{targets}(j)|}{\min(|\text{targets}(i)|, |\text{targets}(j)|)}. \quad (3)$$

For one miRNA pair, i and j , their differentially expressed target gene sets were $\text{targets}(i)$ and $\text{targets}(j)$, respectively.

The number of common differentially expressed targets of the two miRNAs was divided by the size of the smaller target set. Interaction pairs of miRNAs were identified through filtering based on interaction with a measurement of 0 or without common features (e.g., environmental chemical compounds, small molecular drugs). Thereafter, a miRNA crosstalk network was constructed.

3. Results

3.1. The Flowchart of the Present Study. The study design of the present research is shown in Figure 1. As shown in Figure 1, the differential expression analysis was performed to investigate the DEGs and DE miRNAs involved in the NSPC-induced EC alteration and EC-induced NSPC

TABLE 4: The topological characteristics of the top 30 nodes in the PPI network of NSPC-induced EC genetic alterations. NA means not overlapped between the EC-PPI and NSPC-PPI networks.

DEGs	Overlap	Regulate	Degree	Average shortest path length	Betweenness centrality	Closeness centrality	Topological coefficient
Cdk1	NA	Up	72	2.737069	0.056051	0.365354	0.179894
Mad2l1	NA	Up	63	2.844828	0.019572	0.351515	0.211029
Ccnb1	NA	Up	60	2.706897	0.084386	0.369427	0.195539
Il6	NA	Up	58	2.872845	0.111663	0.348087	0.08938
Rad51	NA	Up	58	2.855603	0.04335	0.350189	0.232014
Birc5	NA	Up	56	2.732759	0.058321	0.365931	0.213803
Ccnb2	NA	Up	54	2.922414	0.006045	0.342183	0.255649
Ncapg	NA	Up	52	3.032328	0.008236	0.32978	0.282051
Rrm2	NA	Up	52	2.931034	0.018658	0.341176	0.262327
Zwilch	NA	Up	52	2.974138	0.008695	0.336232	0.26455
Esp11	NA	Up	51	2.961207	0.010195	0.3377	0.265609
Hells	NA	Up	51	2.967672	0.006265	0.336964	0.268318
Cdca5	NA	Up	49	2.971983	0.002445	0.336476	0.279941
Cenpa	NA	Up	49	2.997845	0.016442	0.333573	0.260875
Cenpe	NA	Up	49	2.961207	0.018044	0.3377	0.257355
Hmmr	NA	Up	49	3.040948	0.009178	0.328845	0.288843
Pbk	NA	Up	49	3.006466	0.002026	0.332616	0.287645
Prim1	NA	Up	49	2.935345	0.019553	0.340675	0.251913
Nuf2	NA	Up	48	2.974138	0.00309	0.336232	0.275905
Sgol1	NA	Up	48	2.997845	0.002882	0.333573	0.28125
Cenpi	NA	Up	47	2.99569	0.017411	0.333813	0.26534
Kif20a	NA	Up	47	3.0625	0.001547	0.326531	0.30589
Orc1	NA	Up	47	2.989224	0.022176	0.334535	0.25024
Tacc3	NA	Up	46	2.939655	0.025243	0.340176	0.287225
H2afz	NA	Up	45	3.002155	0.040379	0.333094	0.188816
Cep55	NA	Up	44	3.071121	0.000625	0.325614	0.323656
Cks2	NA	Up	43	2.980603	0.001636	0.335503	0.301077
Lrr1	NA	Up	43	3.047414	0.025254	0.328147	0.28961
Spag5	NA	Up	42	3.096983	0.000598	0.322895	0.327866
Arhgap11a	NA	Up	41	3.090517	0.043119	0.32357	0.316706

alteration. As regards DEGs, the DEGs overlapped between DEGs involved in NSPC-induced EC alteration and EC-induced NSPC alteration were identified, and then the functional enrichment analysis was performed to investigate the biological processes and signaling pathways in which these overlapping DEGs were involved. Based on the DEGs, respectively, involved in the NSPC-induced EC alteration and EC-induced NSPC alteration, the corresponding PPI network was constructed. As regards DEMiRNAs, the DEMiRNAs overlapped between DEMiRNAs expressed in the NSPC-induced EC alteration and EC-induced NSPC alteration were identified to be mmu-miR-23a, mmu-miR-23b, and mmu-miR-210. Afterward, the DEMiRNA-DEG interaction networks were constructed, respectively, for the NSPC-induced EC alteration and EC-induced NSPC alteration, from which the overlapping DEMiRNA-DEG interaction pairs were found. The crosstalk miRNA analysis was

performed and validated the crosstalk role of three DEMiRNAs (mmu-miR-23a, mmu-miR-23b, and mmu-miR-210) in the interaction between ECs and NSPCs. The corresponding miRNA-DEG-pathway network, respectively, for these three DEMiRNAs was constructed. In addition, the chemical compounds and small molecular drugs which regulate the expression patterns of DEMiRNAs were also identified by constructing the DEMiRNA-environmental chemical compound interaction network and DEMiRNA-small molecular drug interaction network.

3.2. Identification of DEGs and DEMiRNAs. Table 1 and Figure 2(a) show that 94 DEGs consisting of 55 upregulated DEGs and 39 downregulated DEGs were overlapping. Tables 2 and 3 list the differential expression values (e.g., logFC, AveExpr, t value, P value, adj. P value, B value, and regulation pattern (up/down)) of the top 30 DEGs which

TABLE 5: The topological characteristics of the top 30 nodes in the PPI network of EC-induced NSPC genetic alterations. NA means not overlapped between the EC-PPI and NSPC-PPI networks.

Gene	Overlap	Regulate	Degree	Average shortest path length	Betweenness centrality	Closeness centrality	Topological coefficient
Gapdh	NA	Down	129	2.303797	0.21952	0.434066	0.040603
Fn1	NA	Down	83	2.586881	0.062983	0.386566	0.054676
Vegfa	NA	Down	64	2.638665	0.041079	0.37898	0.063087
Decr1	NA	Down	59	2.609896	0.066189	0.383157	0.059219
Cd44	NA	Down	57	2.693901	0.029026	0.371209	0.069522
Ccnd1	NA	Down	54	2.703107	0.040282	0.369945	0.065015
Gfap	NA	Down	51	2.663982	0.042334	0.375378	0.070175
Gad1	NA	Up	47	2.837745	0.023163	0.352393	0.075753
Cxcr4	NA	Down	45	2.805524	0.015376	0.35644	0.091761
Pkm	NA	Down	45	2.780207	0.042856	0.359685	0.072881
Anxa5	NA	Down	41	2.817031	0.007322	0.354984	0.091351
Timp1	NA	Down	41	2.805524	0.010114	0.35644	0.09083
Agt	NA	Down	40	2.857307	0.014755	0.34998	0.0945
Cav1	NA	Down	40	2.788262	0.021742	0.358646	0.081866
H6pd	Overlap	Down	39	2.905639	0.018002	0.344158	0.081197
Calb1	NA	Up	39	2.827388	0.022978	0.353683	0.082931
Ctgf	NA	Down	38	2.79977	0.019484	0.357172	0.08851
Pdgfrb	NA	Down	38	2.840046	0.010704	0.352107	0.092062
Snap25	NA	Up	38	2.840046	0.026457	0.352107	0.071554
Fos	NA	Down	37	2.757192	0.026678	0.362688	0.086654
Gad2	NA	Up	37	2.842348	0.016537	0.351822	0.0868
Anxa1	NA	Down	36	2.912543	0.010209	0.343343	0.091158
Tpi1	NA	Down	36	2.905639	0.015808	0.344158	0.086608
Gria1	NA	Up	35	2.837745	0.033782	0.352393	0.079529
Ldha	NA	Down	35	2.933257	0.010636	0.340918	0.096276
Thy1	NA	Down	35	2.886076	0.018426	0.346491	0.090796
Tubb3	NA	Up	35	2.829689	0.013785	0.353396	0.087982
Npy	NA	Up	34	2.906789	0.010344	0.344022	0.099831
Sst	NA	Up	34	2.921749	0.012787	0.342261	0.101852
Gng3	NA	Up	32	3.179517	0.007673	0.314513	0.107118

were, respectively, differentially expressed in the NSPC-induced EC alteration and EC-induced NSPC alteration. Three DE miRNAs found to be overlapped between the EC-induced NSPC alteration and NSPC-induced EC alteration categories (i.e., mmu-miR-23a, mmu-miR-23b, and mmu-miR-210) were selected for further investigation. The expression pattern of mmu-miR-210 was similar in both EC-induced NSPC alterations and NSPC-induced EC alterations. However, the expression patterns of mmu-miR-23a and mmu-miR-23b differed in both situations.

3.3. Functions of Overlapping DEGs. Figure 2(b) depicts the biological processes and pathways in which overlapping DEGs were enriched. As seen in Figure 2(b) A, the overlapping DEGs were found to be involved in several biological processes, for instance, positive regulation of protein kinase B (PKB, also known as Akt), ERK1/2 cascade, response to

BMP, collagen metabolic process, and tissue remodeling. The overlapping DEGs were found to be involved in several signaling pathways including synthesis and degradation of ketone bodies, sulfur metabolism, retinol metabolism, and GnRH signaling (Figure 2(b) B).

3.4. EC-PPI Network and NSPC-PPI Network. The PPI network consisting of DEGs involved in NSPC-induced EC alteration (EC-PPI network) was constructed and included 482 nodes with 2,679 edges (Figure 3(a)), while the PPI network consisting of DEGs involved in EC-induced NSPC alteration (NSPC-PPI network) showed 878 nodes and 3,795 edges (Figure 3(b)). The characteristics of the top 30 nodes of EC-PPI as well as NSPC-PPI network are listed in descending order of degree (Tables 4 and 5).

By construction of a Venn diagram, 51 DEGs were overlapping between the EC-PPI network and the NSPC-PPI

TABLE 6: The topological characteristics of overlapped DEGs in the PPI network of NSPC-induced EC genetic alterations. The overlapped DEGs mean these DEGs were overlapped between the PPI network of NSPC-induced EC alteration and the PPI network of EC-induced NSPC alteration.

Overlapped DEGs	Regulate	Degree	Average shortest path length	Betweenness centrality	Closeness centrality	Topological coefficient
Timp3	Down	21	3.394397	0.012355	0.294603	0.193591
Mmp14	Down	15	3.321121	0.006668	0.301103	0.213333
Col11a1	Down	14	3.681034	0.000966	0.271663	0.265873
H3f3b	Up	13	3.793103	3.40E - 05	0.263636	0.329522
Loxl1	Down	13	3.568966	0.001462	0.280193	0.254605
Ccp110	Up	12	3.497845	0.007609	0.28589	0.324906
Rpl30	Up	12	3.715517	0.001937	0.269142	0.208333
Irs1	Down	11	3.103448	0.01987	0.322222	0.171937
Aldh1a1	Down	9	3.403017	0.022894	0.293857	0.139918
P4ha2	Down	9	3.913793	0.00226	0.255507	0.381313
Cck	Up	8	3.579741	0.011327	0.27935	0.194444
Plod2	Down	8	4.118534	7.55E - 06	0.242805	0.428977
Rhoq	Down	8	4.008621	0.012817	0.249462	0.156863
H6pd	Down	7	3.534483	0.017785	0.282927	0.159664
Luc7l3	Up	7	3.571121	0.009536	0.280024	0.188065
Dlx5	Up	6	3.784483	0.007836	0.264237	0.215278
Rcn3	Down	6	3.525862	0.008417	0.283619	0.330247
F3	Down	5	3.56681	7.31E - 06	0.280363	0.413514
Hspa2	Down	5	3.221983	0.000827	0.310368	0.275229
Tgm2	Down	5	3.538793	0.005005	0.282582	0.379221
Aldh1a7	Down	4	4.165948	0.000317	0.240041	0.416667
Irgm2	Down	4	4.290948	0.000557	0.233049	0.3125
Smad6	Down	4	3.928879	0.002692	0.254526	0.289474
Bmper	Down	3	4.810345	0.000753	0.207885	0.433333
Daam2	Down	3	3.87931	0.008654	0.257778	0.333333
Rras	Down	3	4.3125	0.000343	0.231884	0.439394
Syde1	Down	3	4.939655	0.000344	0.202443	0.545455
Tns1	Down	3	4.286638	0.002258	0.233283	0.355556
Fcgrt	Down	2	4.157328	0	0.240539	0.576923
Rin2	Down	2	4.681034	0.000218	0.213628	0.5
Sdpr	Down	2	4.275862	0.000187	0.233871	0.5
Slc2a10	Down	2	4.176724	0	0.239422	0.738095

network (Figure 2(c)). The topological features of the overlapping DEGs in the EC-PPI network and the NSPC-PPI network are listed in Tables 6 and 7, respectively.

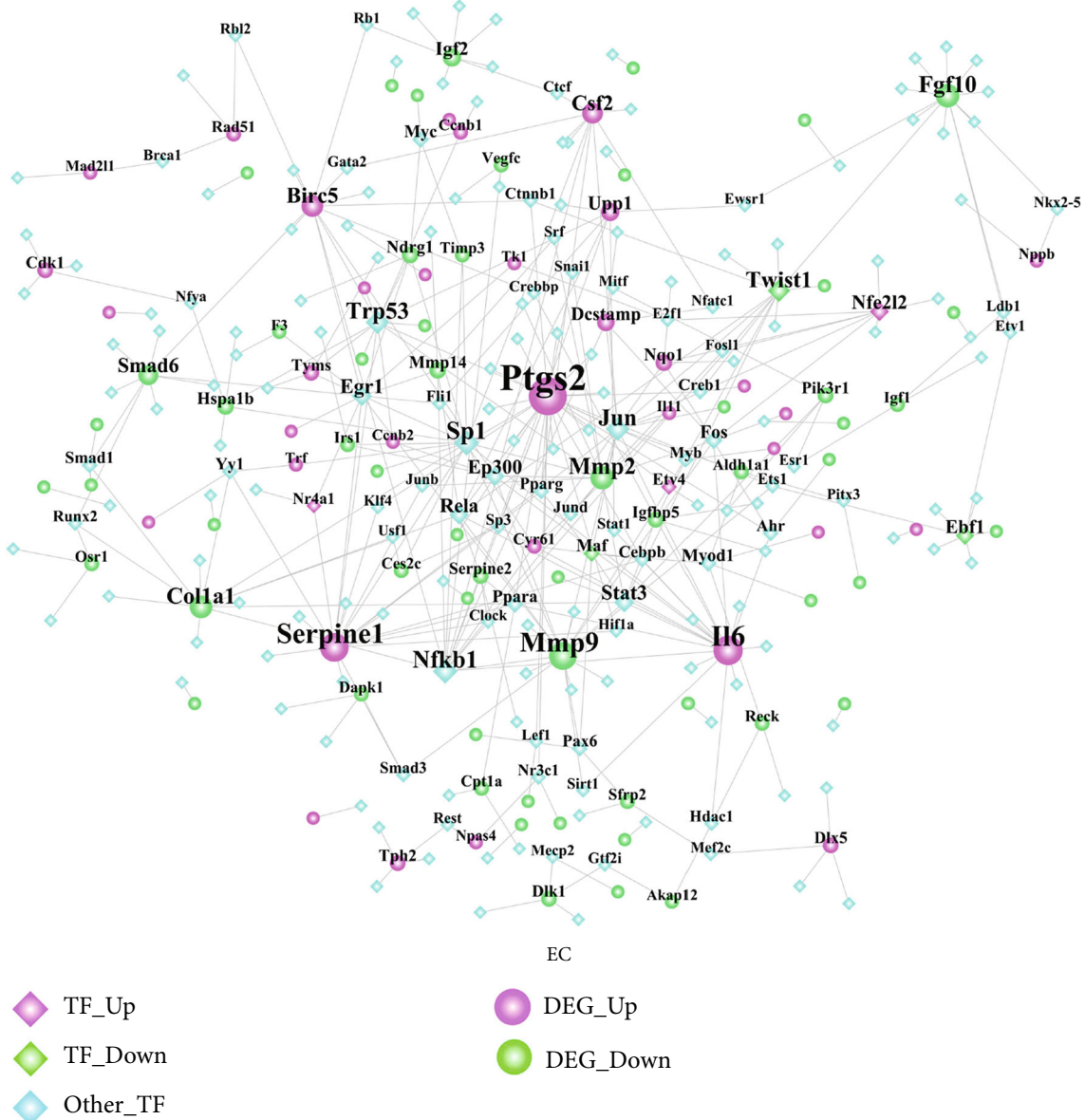
3.5. The Transcription Factor-Target DEG Interaction Network. The TF-target DEG network was constructed, respectively, for the DEGs involved in the NSPC-induced EC alteration (Figure 4(a)) and EC-induced NPSC alteration (Figure 4(b)). Figure 4(a) consists of 285 nodes and 363 edges, while Figure 4(b) consists of 451 nodes and 668 edges. As shown in Figure 4(a) and Table 8, several TFs (e.g., Sp1, Nfkb1, Trp53, Jun, Twist1, and Stat3) were identified to be hub transcription factors targeting the greatest number of DEGs involved in the NSPC-induced EC alteration. As

shown in Figure 4(b) and Table 9, several TFs (e.g., Ccnd1, Sp1, Fos, Hes1, Nfkb1, and Cebpb) were identified to be hub transcription factors targeting the greatest number of DEGs involved in the EC-induced NPSC alteration.

3.6. The DE miRNAs-Target DEGs and Their Functions. The number of experimentally validated, computationally predicted, and total miRNA-DE targets for ECs and NSPCs is listed in Table 10. As evident here, 14 interaction pairs of miRNA-DE targets were determined. The DE miRNA-target network involved in NSPC-induced EC alteration was constructed and included 5,916 nodes with 22,664 edges (Figure 5(a)), while the DE miRNA-target network involved in NSPC-induced EC alteration showed 4,962 nodes and

TABLE 7: The topological characteristics of overlapped DEGs in the PPI network of EC-induced NSPC genetic alterations. The overlapped DEGs mean these DEGs were overlapped between the PPI network of NSPC-induced EC alteration and the PPI network of EC-induced NSPC alteration.

Overlapped DEGs	Regulate	Degree	Average shortest path length	Betweenness centrality	Closeness centrality	Topological coefficient
H6pd	Down	39	2.905639	0.018002	0.344158	0.081197
Mmp2	Down	30	2.905639	0.009375	0.344158	0.111791
Cck	Up	24	3.161105	0.002392	0.316345	0.14388
Irs1	Down	24	2.90794	0.011375	0.343886	0.090661
Igfbp5	Down	18	3.002302	0.001391	0.333078	0.145524
Loxl1	Down	18	3.331415	0.002588	0.300173	0.154147
Mmp14	Down	18	2.958573	0.006212	0.338001	0.147655
Aldh1a1	Down	16	3.079402	0.008487	0.324738	0.124419
Plod2	Down	16	3.535098	0.002197	0.282878	0.168269
Col11a1	Down	15	3.464902	0.007219	0.288608	0.154386
Timp3	Down	15	3.065593	0.004764	0.326201	0.152648
Irgm2	Down	14	3.910242	4.82E - 05	0.255739	0.348397
P4ha2	Down	14	3.637514	0.001633	0.274913	0.177721
Rhoq	Down	13	3.673188	0.001094	0.272243	0.173382
F3	Down	11	3.150748	0.00066	0.317385	0.188776
Dlx5	Up	10	3.500575	0.001701	0.285667	0.221359
Hspa2	Down	10	3.356732	0.009675	0.297909	0.113084
Luc7l3	Up	9	3.771001	0.004972	0.265182	0.17284
Syde1	Down	9	3.562716	0.005367	0.280685	0.202822
Tgm2	Down	9	3.103567	0.002864	0.32221	0.194714
Rras	Down	8	3.651323	0.00461	0.273873	0.227113
Sdpr	Down	8	3.372842	0.002511	0.296486	0.180118
Aldh1a7	Down	7	3.686997	0.000587	0.271223	0.221254
Ccp110	Up	7	3.982739	0.002565	0.251084	0.159664
Cdc7	Up	7	3.821634	0.000152	0.261668	0.313589
Rcn3	Down	7	3.697353	0.000432	0.270464	0.249433
Tns1	Down	7	3.397008	0.005802	0.294377	0.188729
Zcchc12	Up	6	3.775604	0.006142	0.264858	0.217391
Akap12	Down	5	3.422325	0.002599	0.292199	0.261111
Daam2	Down	5	3.658228	0.000694	0.273356	0.303226
H3f3b	Up	5	4.362486	6.29E - 05	0.229227	0.5125
Rpl30	Up	5	4.084005	0.000687	0.244858	0.3
Sema3c	Down	5	3.528193	0.002593	0.283431	0.2075
Smad6	Down	5	3.510932	0.001004	0.284825	0.284848
Bmper	Down	4	4.210587	0.00075	0.237497	0.26
Rin2	Down	4	3.874568	0.002452	0.258093	0.25
Gem	Down	3	3.882624	0.002302	0.257558	0.42735
Selenbp1	Down	3	4.462601	0.000293	0.224085	0.458333
Fcgrt	Down	2	3.943613	3.45E - 05	0.253575	0.5
Slc2a10	Down	2	3.864212	6.35E - 05	0.258785	0.5
Sytl2	Down	2	3.759494	0.000207	0.265993	0.5
Fam102a	Down	1	5.730725	0	0.174498	0
Macrodl	Down	1	5.880322	0	0.170059	0
Pdgfrl	Down	1	4.286536	0	0.233289	0



(a)

FIGURE 4: Continued.

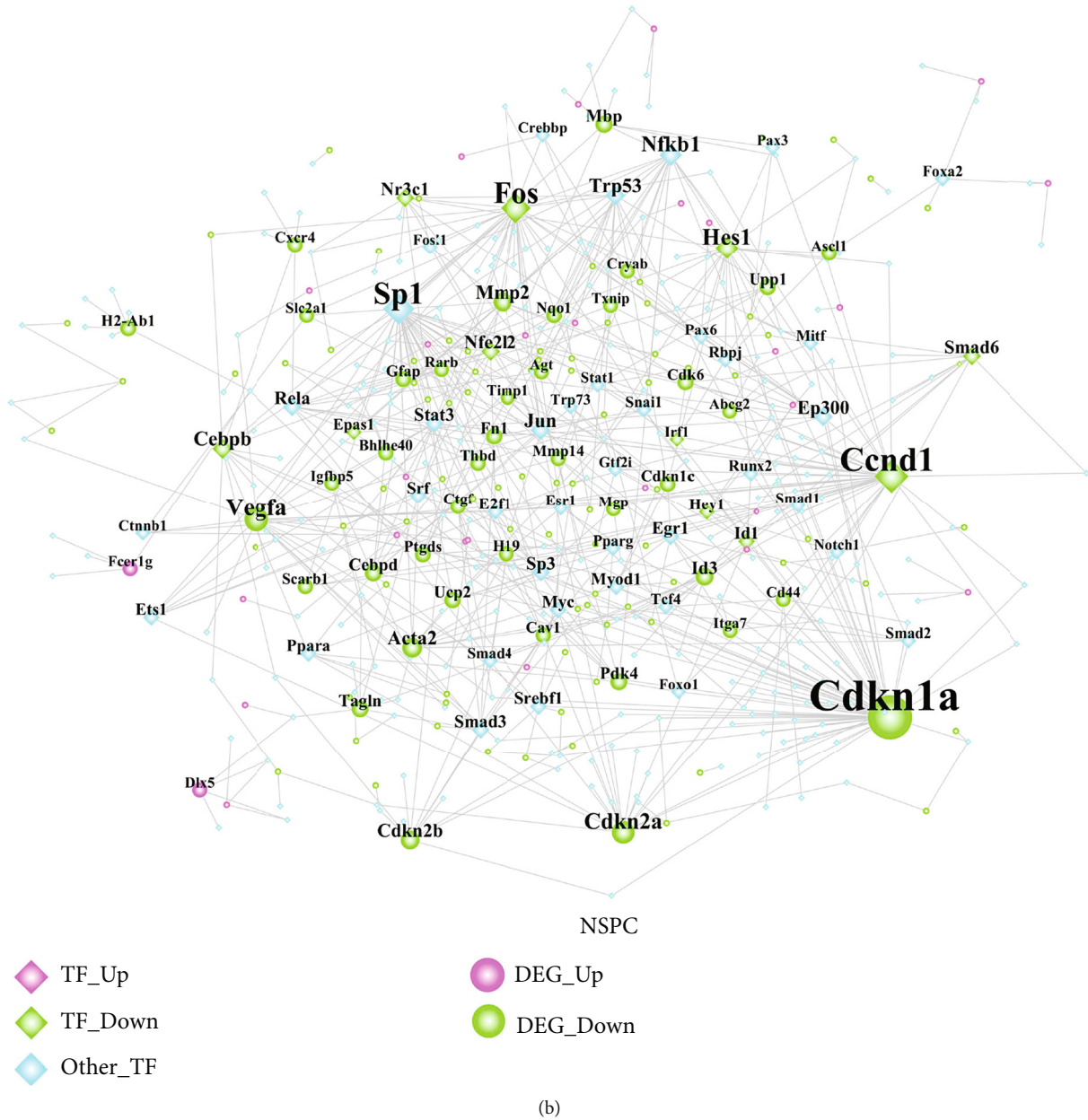


FIGURE 4: The transcription factor-target DEG interaction network. (a) The TF-target DEG network involved in the NSPC-induced EC alteration. (b) The TF-target DEG network involved in the EC-induced NSPC alteration.

11,675 edges (Figure 5(b)). The characteristics of the top 30 nodes of these two networks are listed in descending order of degree (Tables 11 and 12).

The miR-DEG-pathway network for three selected miRNAs (miR-210 (Figure 6(a)), miR-23a (Figure 6(b)), and miR-23b (Figure 6(c))) is depicted in Figure 6. As shown in Figure 6(a), miR-210 targets the Rhoq gene which was found to be downregulated in both NSPC-induced EC alteration and EC-induced NSPC alteration. The Rhoq gene was shown to be involved in the insulin signaling pathway. As shown in Figure 6(b), miR-23a targets the Aldh1a1 gene which was found to be downregulated in both NSPC-induced EC alteration and EC-induced NSPC alteration. The Aldh1a1 gene was shown to be involved in the retinol metabolism and met-

abolic pathway. It could be observed from Figure 6(c) that the target genes of miR-23b were almost the same as those of miR-23a. miR-23b can target the Igf1 gene which was found to be downregulated in NSPC-induced EC alteration. The Igf1 gene was involved in many signaling pathways including AMPK, Rap1, HIF-1, p53, and FoxO signaling.

3.7. Identifying Significant Small Molecular Drugs. Figure 7 shows the DEmiRNA-small molecular drug network involved in the NSPC-induced EC alterations (Figure 7(a)) and EC-induced NSPC alterations (Figure 7(b)). Upon comparing the small molecules relevant to NSPC-induced EC alteration and EC-induced NSPC alteration, a total of 16 small drug molecules were found to be overlapped and

TABLE 8: The topological characteristics of the top 30 nodes in the TF-target DEG interaction network involved in the NSPC-induced EC alteration.

Name	Label	Degree	Average shortest path length	Betweenness centrality	Closeness centrality	Topological coefficient
Ptgs2	Upregulated DEG	30	3.17073171	0.25370241	0.31538462	0.07348485
Il6	Upregulated DEG	20	3.31300813	0.16071429	0.30184049	0.10921053
Serpine1	Upregulated DEG	19	3.40650407	0.10638454	0.29355609	0.09078947
Mmp9	Downregulated DEG	18	3.25203252	0.16761464	0.3075	0.11243386
Sp1	TF	15	3.17479675	0.15105709	0.31498079	0.10813008
Nfkb1	TF	14	2.99593496	0.17606132	0.33378562	0.11316212
Mmp2	Downregulated DEG	13	3.45121951	0.05861543	0.28975265	0.16008316
Fgf10	Downregulated DEG	13	4.18699187	0.10945704	0.23883495	0.07692308
Trp53	TF	13	3.42276423	0.10326907	0.29216152	0.10697115
Jun	TF	13	3.14634146	0.14436348	0.31782946	0.12725546
Twist1	Downregulated DEG_ TF	12	3.50406504	0.13470851	0.28538283	0.13288288
Col1a1	Downregulated DEG	12	3.4796748	0.11936909	0.28738318	0.13709677
Birc5	Upregulated DEG	11	3.53252033	0.1098108	0.283084	0.13636364
Csf2	Upregulated DEG	10	3.51626016	0.08268292	0.28439306	0.16071429
Smad6	Downregulated DEG	9	4.94715447	0.04322026	0.2021364	0.12698413
Stat3	TF	9	3.43495935	0.09055949	0.29112426	0.15065913
Egr1	TF	9	3.76829268	0.05361397	0.26537217	0.13947991
Nfe2l2	Upregulated DEG_TF	8	3.89430894	0.03472983	0.25678497	0.15972222
Rela	TF	8	3.33333333	0.05841757	0.3	0.18382353
Ep300	TF	8	3.52439024	0.04168611	0.28373702	0.19067797
Upp1	Upregulated DEG	7	3.58536585	0.04680464	0.27891156	0.1978022
Igf2	Downregulated DEG	7	5.18292683	0.04071495	0.19294118	0.14285714
Ebfl	Downregulated DEG_ TF	7	4.57723577	0.04361263	0.21847247	0.14285714
Fos	TF	6	3.82926829	0.01974273	0.2611465	0.22727273
Dcstamp	Upregulated DEG	6	3.75203252	0.02000123	0.26652221	0.25396825
Nqo1	Upregulated DEG	5	3.83333333	0.02317522	0.26086957	0.21904762
Ndr1	Downregulated DEG	5	3.83333333	0.02104419	0.26086957	0.27142857
Mmp14	Downregulated DEG	5	3.81707317	0.01378142	0.26198083	0.29
Maf	Downregulated DEG_ TF	5	3.84146341	0.0340471	0.26031746	0.28571429
Hspa1b	Downregulated DEG	5	3.88211382	0.05662735	0.25759162	0.24545455

significantly enriched (Table 13). Table 13 shows that 6 small molecular drugs (e.g., depropine, fluphenazine, lycorine, quinostatin, resveratrol, and thiamazole) had similar regulatory roles in the process of EC-induced NSPC alteration and NSPC-induced EC alteration, indicating simultaneous upregulation or downregulation.

3.8. The miRNA-Environmental Chemical Compound Network. There were 60 environmental chemical compounds highly correlated with the DE miRNAs expressed during NSPC-induced EC alteration and EC-induced NSPC alteration (Figure 8). As shown from Figure 8, miR-210 was significantly related to many compounds such as bisphenol A, titanium dioxide, choline, dietary

fats, folic acid, and methionine. miR-23b was found to be significantly related to many compounds such as dexamethasone, potassium dichromate, sodium fluoride, thalidomide, cadmium chloride, and soot.

3.9. Crosstalk miRNAs Linking the EC-Induced NSPC Alteration Process and NSPC-Induced EC Alteration Process. A total of 54 interaction pairs of miRNAs were determined and are listed in Table 14. As shown in Figure 9, three miRNAs (miR-23a, miR-23b, and miR-210) were determined to perform critical bridging roles in the link between the EC-induced NSPC alteration process and the NSPC-induced EC alteration process.

TABLE 9: The topological characteristics of the top 30 nodes in the TF-target DEG interaction network involved in the EC-induced NSPC alteration.

Name	Label	Degree	Average shortest path length	Betweenness centrality	Closeness centrality	Topological coefficient
Cdkn1a	Downregulated DEG	65	2.73913043	0.30858346	0.36507937	0.0283698
Ccnd1	Downregulated DEG_ TF	44	2.90096618	0.18721585	0.34471274	0.0390556
Sp1	TF	38	2.75120773	0.18665254	0.36347673	0.04086687
Fos	Downregulated DEG_ TF	37	2.89855072	0.15489676	0.345	0.05012705
Vegfa	Downregulated DEG	24	3.09178744	0.1032236	0.3234375	0.06904762
Hes1	Downregulated DEG_ TF	21	3.26328502	0.093159	0.30643967	0.06776557
Cdkn2a	Downregulated DEG	20	3.16183575	0.06806015	0.31627196	0.0622093
Nfkb1	TF	19	2.83091787	0.10896078	0.35324232	0.078356
Cebpb	Downregulated DEG_ TF	15	3.01690821	0.0630859	0.33146517	0.07979003
Acta2	Downregulated DEG	14	3.41062802	0.04841393	0.29320113	0.10449735
Trp53	TF	14	3.23188406	0.04815141	0.30941704	0.09895151
Jun	TF	14	3.25603865	0.03607564	0.30712166	0.10204082
Mmp2	Downregulated DEG	13	3.08937198	0.03126342	0.32369038	0.11609687
Ep300	TF	12	3.13043478	0.05353532	0.31944444	0.11131841
Cdkn2b	Downregulated DEG	12	3.80917874	0.03041314	0.26252378	0.10714286
Nfe2l2	Downregulated DEG_ TF	12	3.26570048	0.04141463	0.30621302	0.10585586
Rela	TF	11	3.21497585	0.03799736	0.31104433	0.118411
Nr3c1	Downregulated DEG_ TF	11	3.24637681	0.03066868	0.30803571	0.11162255
Smad6	Downregulated DEG_ TF	11	3.73671498	0.02413405	0.26761474	0.11004785
Sp3	TF	10	3.35990338	0.01668852	0.29762761	0.12268041
Stat3	TF	10	3.33816425	0.03841092	0.29956585	0.13235294
Id3	Downregulated DEG	10	3.82125604	0.02673839	0.26169406	0.10869565
Smad3	TF	9	3.72463768	0.03330304	0.26848249	0.14403292
Egr1	TF	9	3.57004831	0.03896833	0.28010825	0.12007168
Mbp	Downregulated DEG	9	3.52415459	0.02687184	0.283756	0.13888889
Srebf1	TF	8	3.59903382	0.0307691	0.27785235	0.13380282
Myc	TF	8	3.36231884	0.02336862	0.29741379	0.14650538
Id1	Downregulated DEG_ TF	8	3.2826087	0.02185908	0.30463576	0.13903061
Cebpd	Downregulated DEG	8	3.43236715	0.01679448	0.29134412	0.16163793
Pdk4	Downregulated DEG	8	3.61111111	0.01282401	0.27692308	0.19396552

TABLE 10: The number of experimentally validated, computationally predicted, and total miRNA-target DEG interaction pairs during the NSPC-induced EC alteration and EC-induced NSPC alteration.

Coculture-induced alterations in one type of cells	Validated miRNA-target DEG pairs	Predicted miRNA-target DEG pairs	Total miRNA-target DEG pairs (including validated and predicted)	Overlapped miRNA-target DEG interaction pairs (overlapped between NSPC-induced EC alteration and EC-induced NSPC alteration)
NSPC-induced EC alteration	536	391	810	The overlapped 14 interaction pairs are as follows: miR-21-Rhoq, miR-23a-Akap12, miR-23a-Aldh1a1, miR-23a-Exoc3l4, miR-23a-Gm5424, miR-23a-Mfhas1, miR-23a-Nfe2l2, miR-23a-Slc16a6, miR-23b-Akap12, miR-23b-Aldh1a1, miR-23b-Gm5424, miR-23b-Mfhas1, miR-23b-Nfe2l2, and miR-23b-Slc16a6.
EC-induced NSPC alteration	571	243	711	

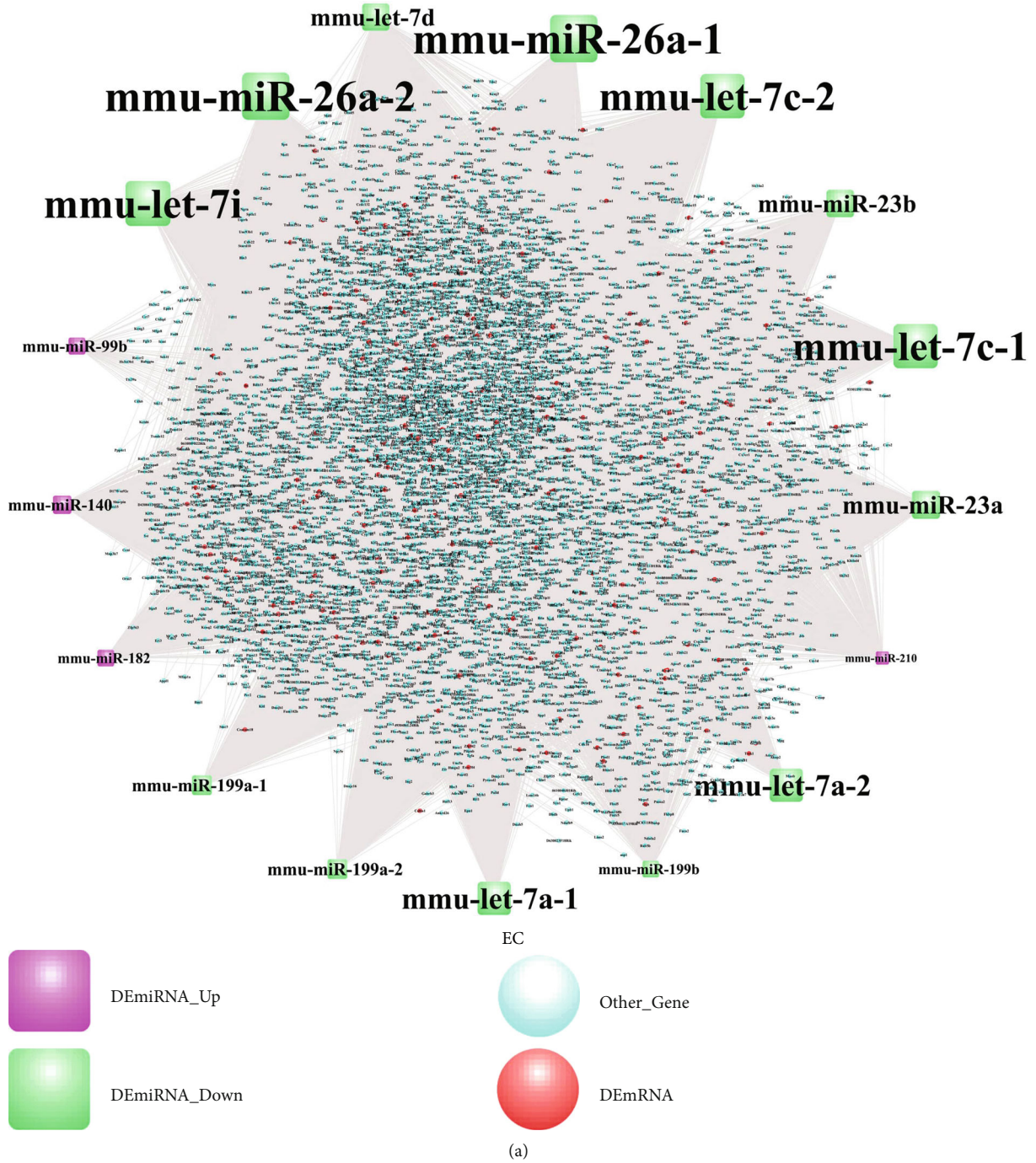


FIGURE 5: Continued.

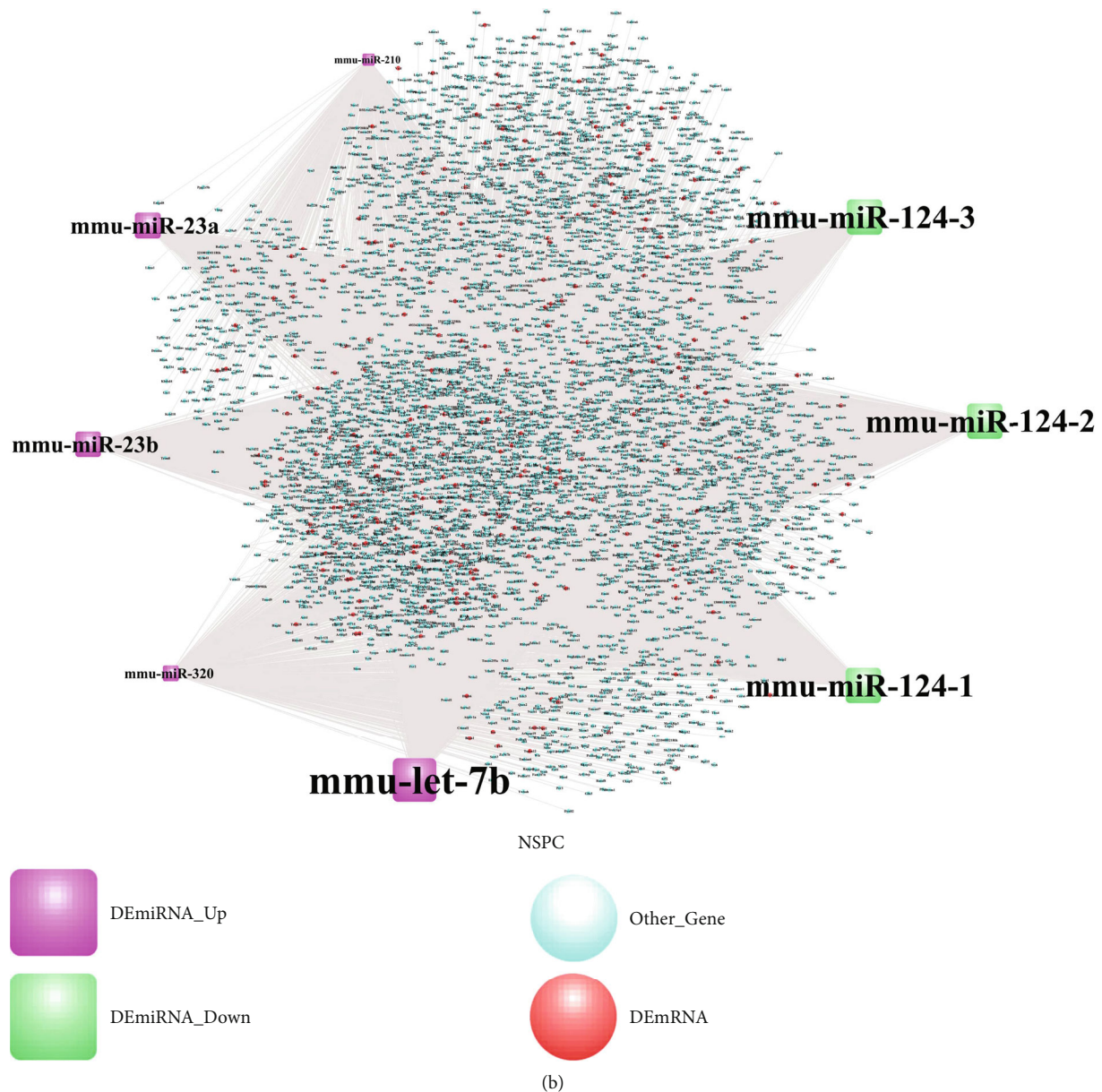


FIGURE 5: The DEmiRNA-target network involved in the NSPC-induced EC alteration (a) and EC-induced NSPC alteration (b).

4. Discussion

This study identified three miRNAs (i.e., miR-210, miR-230a, and miR-23b) to be crosstalks involved in the interaction between ECs and NSPCs. The roles of these miRNAs in regulating the interactions between ECs and NSPCs will be discussed in the following sections by using the previous related evidence.

miR-210 is identified to be involved in the interaction between ECs and NSPCs by targeting many genes (e.g., Rhoq, Fn1, and Pard3) and pathways (e.g., insulin, PI3K/Akt, and chemokine signaling pathway) (Figure 3(a)), and its regulating roles will be discussed in this and next paragraph. Rhoq (Ras Homolog (Rho) Family Member Q) was identified to

be downregulated during the process of EC-induced NSPC alteration and NSPC-induced EC alteration; however, Rhoq has not been investigated to regulate NSPCs and ECs. As another member of the Rho family, RhoA was found to influence the proliferation and fate of NSPCs by mediating mechanotransduction and cellular stiffness [29, 30], as well as impact the migration and angiogenesis of ECs by mediating the cytoskeletal changes [31]. The insulin signaling pathway targeted by RhoA could promote angiogenic processes via mediating the migration and proliferation of ECs as well as in vitro tubular structure formation [32]. The insulin-mediated pathway could also regulate the self-renewal, neurogenesis, cognition, and sensory function, as well as homeostasis of NSPCs [33].

TABLE 11: The topological characteristics of the top 30 nodes in the DEmiRNA-target network involved in the NSPC-induced EC alteration.

Name	lab2	Degree	Average shortest path length	Betweenness centrality	Closeness centrality	Topological coefficient
mmu-miR-26a-2	DEmiRNA	2371	2.195604	0.216585	0.455455	0.221505
mmu-miR-26a-1	DEmiRNA	2371	2.195604	0.216585	0.455455	0.221505
mmu-let-7i	DEmiRNA	2244	2.238546	0.131513	0.446719	0.323641
mmu-let-7c-2	DEmiRNA	2202	2.252747	0.110037	0.443902	0.332539
mmu-let-7c-1	DEmiRNA	2202	2.252747	0.110037	0.443902	0.332539
mmu-let-7a-2	DEmiRNA	1585	2.461369	0.051855	0.406278	0.376735
mmu-let-7a-1	DEmiRNA	1585	2.461369	0.051855	0.406278	0.376735
mmu-miR-23a	DEmiRNA	1297	2.558749	0.106936	0.390816	0.247494
mmu-miR-23b	DEmiRNA	1269	2.568216	0.100185	0.389375	0.248916
mmu-let-7d	DEmiRNA	1252	2.573965	0.063356	0.388506	0.353484
mmu-miR-199a-2	DEmiRNA	839	2.713609	0.055721	0.368513	0.273838
mmu-miR-199a-1	DEmiRNA	839	2.713609	0.055721	0.368513	0.273838
mmu-miR-140	DEmiRNA	760	2.740321	0.114496	0.364921	0.175411
mmu-miR-182	DEmiRNA	668	2.771429	0.088383	0.360825	0.194891
mmu-miR-199b	DEmiRNA	660	2.774134	0.048537	0.360473	0.278883
mmu-miR-210	DEmiRNA	468	2.839053	0.061318	0.35223	0.195913
mmu-miR-99b	DEmiRNA	52	2.979713	0.006853	0.335603	0.234375
Celf1	Target gene	16	2.004227	0.002733	0.498946	0.24026
Taok1	Target gene	15	2.179374	0.001948	0.458847	0.263894
Ubn2	Target gene	14	2.137447	0.001613	0.467848	0.279439
Suco	Target gene	14	2.137447	0.001613	0.467848	0.279439
Mtf2	Target gene	14	2.186475	0.001497	0.457357	0.28312
Map3k2	Target gene	14	2.162468	0.001485	0.462435	0.282045
Kdm6a	Target gene	14	2.162468	0.001485	0.462435	0.282045
Ino80d	Target gene	14	2.137109	0.001824	0.467922	0.267984
Celf2	Target gene	14	2.090786	0.001937	0.478289	0.265165
Ankrd44	Target gene	14	2.186475	0.001497	0.457357	0.28312
Tnpo1	Target gene	13	2.196281	0.001334	0.455315	0.291288
Rfx7	Target gene	13	2.144548	0.001367	0.466299	0.28419
Kmt2a	Target gene	13	2.263567	0.001442	0.441781	0.289898

During the interactions between ECs and NSPCs, the genes dysregulated by a certain type of cell might influence the biological behavior and processes of another type of cell. For instance, the addition of ECs into NSPCs induced the

downregulation of the gene Fn1 (fibronectin-1) in NSPCs. While fibronectin was shown to regulate the survival and migration of primary NSPCs [34], its dysregulation in NSPCs can modulate the functions of ECs by influencing survival

TABLE 12: The topological characteristics of the top 30 nodes in the DEmiRNA-target network involved in the EC-induced NSPC alteration.

Name	lab2	Degree	Average shortest path length	Betweenness centrality	Closeness centrality	Topological coefficient
mmu-let-7b	DEmiRNA_up	2362	2.046362	0.551173	0.488672	0.170618
mmu-miR-124-1	DEmiRNA_down	1863	2.247531	0.154513	0.444933	0.394448
mmu-miR-124-2	DEmiRNA_down	1863	2.247531	0.154513	0.444933	0.394448
mmu-miR-124-3	DEmiRNA_down	1863	2.247531	0.154513	0.444933	0.394448
mmu-miR-23a	DEmiRNA_up	1297	2.475711	0.158061	0.403924	0.306091
mmu-miR-23b	DEmiRNA_up	1269	2.486999	0.14813	0.402091	0.309242
mmu-miR-320	DEmiRNA_up	690	2.720419	0.141572	0.36759	0.217805
mmu-miR-210	DEmiRNA_up	468	2.809917	0.093463	0.355882	0.206654
Ino80d	Target gene	8	1.998387	0.0024	0.500403	0.294443
Adam10	Target gene	8	1.998387	0.0024	0.500403	0.294443
Mtf2	Target gene	8	1.998387	0.0024	0.500403	0.294443
Pcdh19	DEmRNA	7	2.085467	0.001524	0.479509	0.337695
Rora	DEmRNA	7	2.545051	0.001403	0.392919	0.369491
Ago2	Target gene	7	2.1282	0.00156	0.469881	0.338576
Ago3	Target gene	7	2.1282	0.00156	0.469881	0.338576
Col4a1	Target gene	7	2.085467	0.001524	0.479509	0.337695
Cpd	Target gene	7	2.085467	0.001524	0.479509	0.337695
Map3k1	Target gene	7	2.085467	0.001524	0.479509	0.337695
Mecp2	Target gene	7	2.085467	0.001524	0.479509	0.337695
Etnk1	Target gene	7	2.085467	0.001524	0.479509	0.337695
Kpna1	Target gene	7	2.085467	0.001524	0.479509	0.337695
Yod1	Target gene	7	2.085467	0.001524	0.479509	0.337695
Prtg	Target gene	7	2.085467	0.001524	0.479509	0.337695
Slc36a1	Target gene	7	2.1282	0.00156	0.469881	0.338576
Tet2	Target gene	7	2.1282	0.00156	0.469881	0.338576
Ahctf1	Target gene	7	2.1282	0.00156	0.469881	0.338576
Qser1	Target gene	7	2.085467	0.001524	0.479509	0.337695
Wnk1	Target gene	7	2.085467	0.001524	0.479509	0.337695
Slc7a2	Target gene	7	2.085467	0.001524	0.479509	0.337695
Aldh1l2	Target gene	7	2.545051	0.001403	0.392919	0.369491

and angiogenesis in both the integrin-dependent and integrin-independent manners [35]. The PI3K/Akt pathway targeted by Fn1 has been established as a classic pathway in regulating both angiogenesis and neurogenesis. This pathway plays a mediating role in neural regeneration by controlling the survival, proliferation, differentiation, and migration of NSPCs [36]. The link between this pathway and angiogenesis has been highlighted since it can modulate the expression of many angiogenic factors such as vascular endothelial growth factor (VEGF), nitric oxide, and angiopoietins [37]. As another example, the addition of NSPCs to ECs induced a decreased expression of the gene Pard3 (Par-3 Family Cell Polarity Regulator) in ECs. Pard3 can not only determine the cell polarity of ECs [38] but also modulate the sprouting behavior of ECs during the process of angiogenesis [39]. Conversely,

the dysregulation of cell polarity regulators can influence the behavior and functions of NSPCs in terms of architecture and shape, interkinetic nuclear migration, proliferation and differentiation potential, and asymmetric cell division [40]. The chemokine signaling pathway targeted by Pard3 was shown to promote neovascularization by stimulating the migration and proliferation of ECs, as well as recruiting endothelial progenitor cells [41]. Regarding the role of chemokine in regulating NSPCs, chemokines were shown to promote the quiescence and survival of NSPCs [42], as well as regulate the migration of NSPCs toward the sites of neuroinflammation [43]. Overall, based on this existing evidence, it can be assumed that miR-210 plays a critical role in the interaction between ECs and NSPCs by targeting genes and pathways associated with both neurogenesis and angiogenesis.

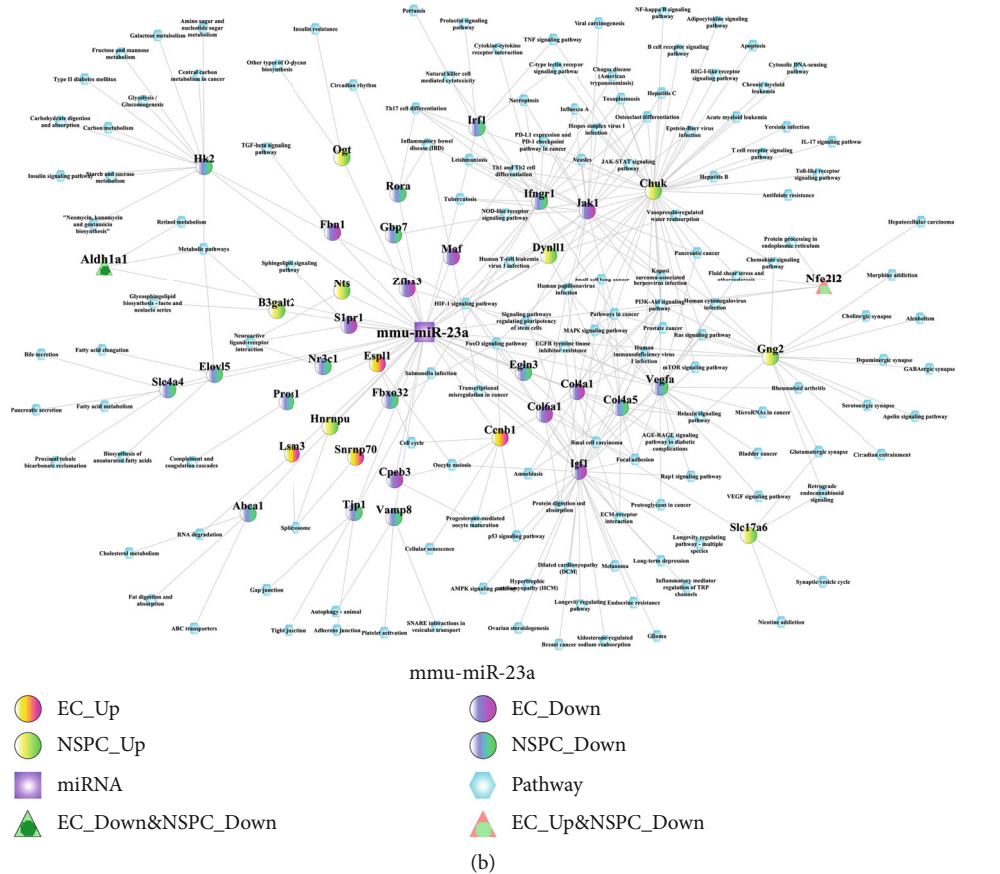
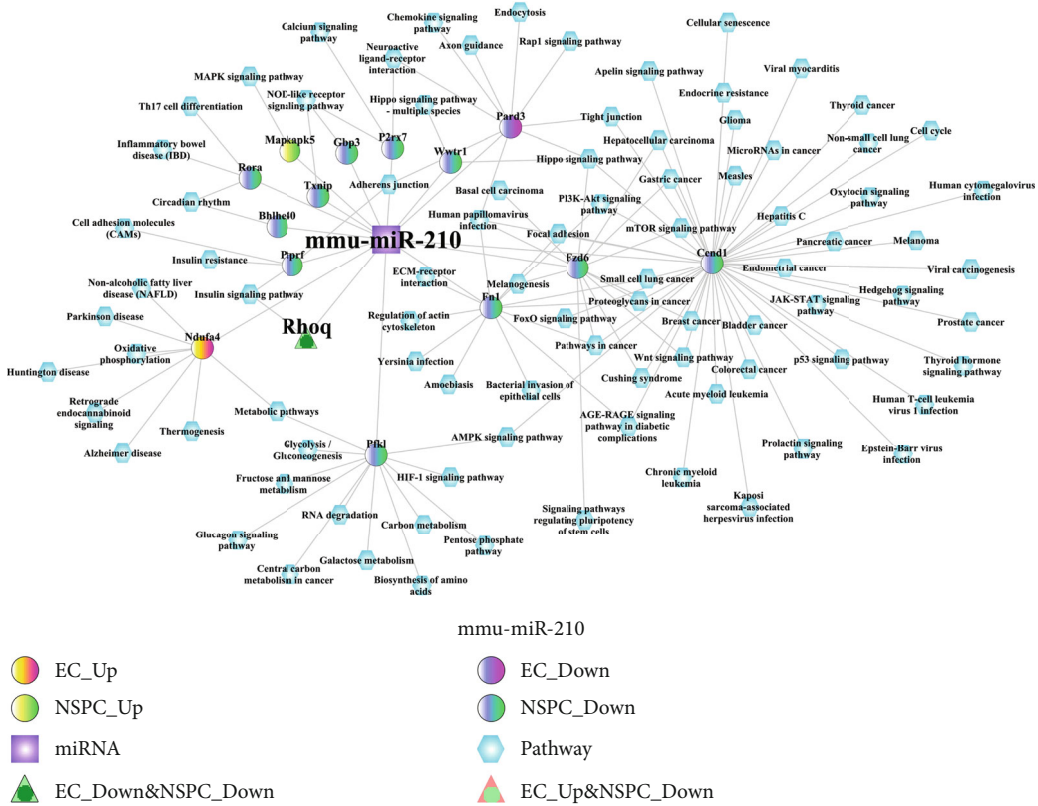


FIGURE 6: Continued.

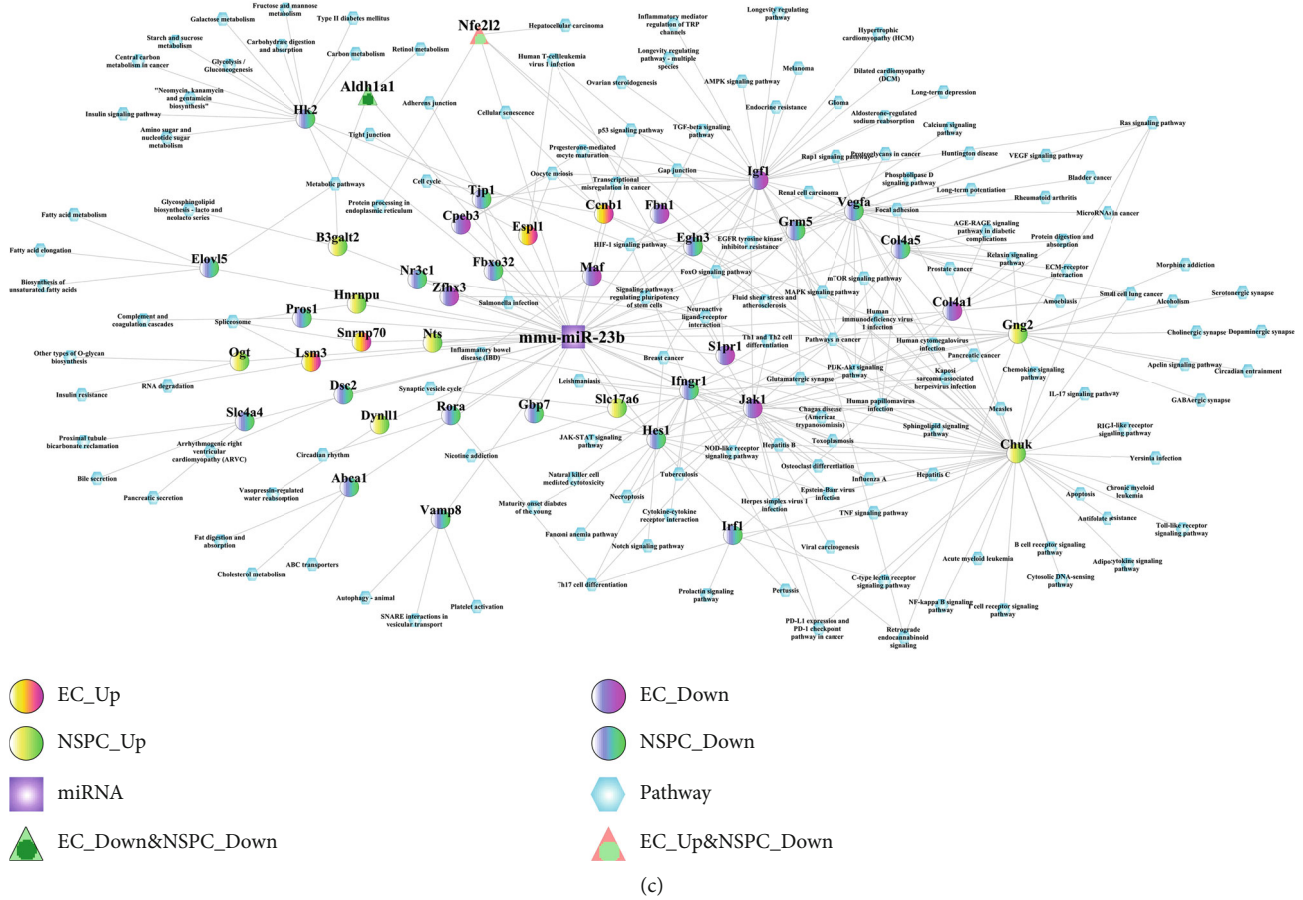
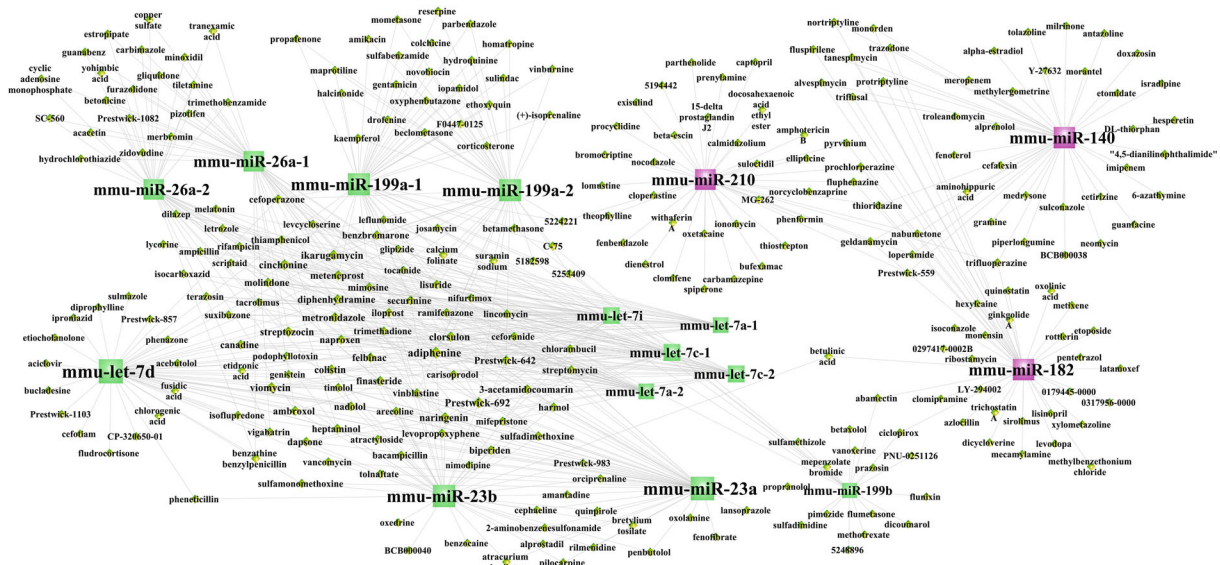


FIGURE 6: The miRNA-DEG-pathway interaction network. (a) mmu-miR-210, (b) mmu-miR-23a, and (c) mmu-miR-23b.

The mechanisms of two miRNAs (miR-23a and miR-23b) involved in the interaction between ECs and NSPCs are almost similar, and the regulatory roles of miR-23a will be therefore an example to discuss in this and next paragraph. As shown in Figure 3(b), miR-23a is involved in the interaction between ECs and NSPCs by targeting many genes (e.g., Aldh1a1, Fbn1, and Chuk) and pathways (e.g., retinol metabolism, TGF-beta, and NF- κ B pathway). For example, the Aldh1a1 (Aldehyde Dehydrogenase 1 Family Member A1) gene targeted by miR-23a was found to be simultaneously downregulated during the process of EC-induced NSPC alteration and NSPC-induced EC alteration. High activity of aldehyde dehydrogenase (ALDH) in tumor ECs and its function in promoting angiogenesis in tumor progression have been reported [44]; however, so far, there is no evidence supporting the angiogenic role of ALDH in stem cell-like ECs. A recent review [45] reported that aldehyde dehydrogenase (ALDH) not only represents an intracellular and metabolic marker of stem cells including NSPCs and endothelial progenitor cells (EPCs) but also acts as a functional regulator of stem cells mainly by mediating the metabolic pathway of retinoic acid (RA). The retinol metabolism pathway targeted by Aldh1a1 was shown to be involved at the early stage of neurogenesis and antiangiogenic response. In terms of neurogenesis, RA has been commonly applied for differentiating NSPCs due to its function in promoting the acquisition of a neuronal fate [46]. In terms of antiangiogenic

response, RA has been shown to selectively block vascular permeability factor/vascular endothelial growth factor (VPF/VEGF), thereby further inhibiting these angiogenic factors that induced microvascular permeability [47].

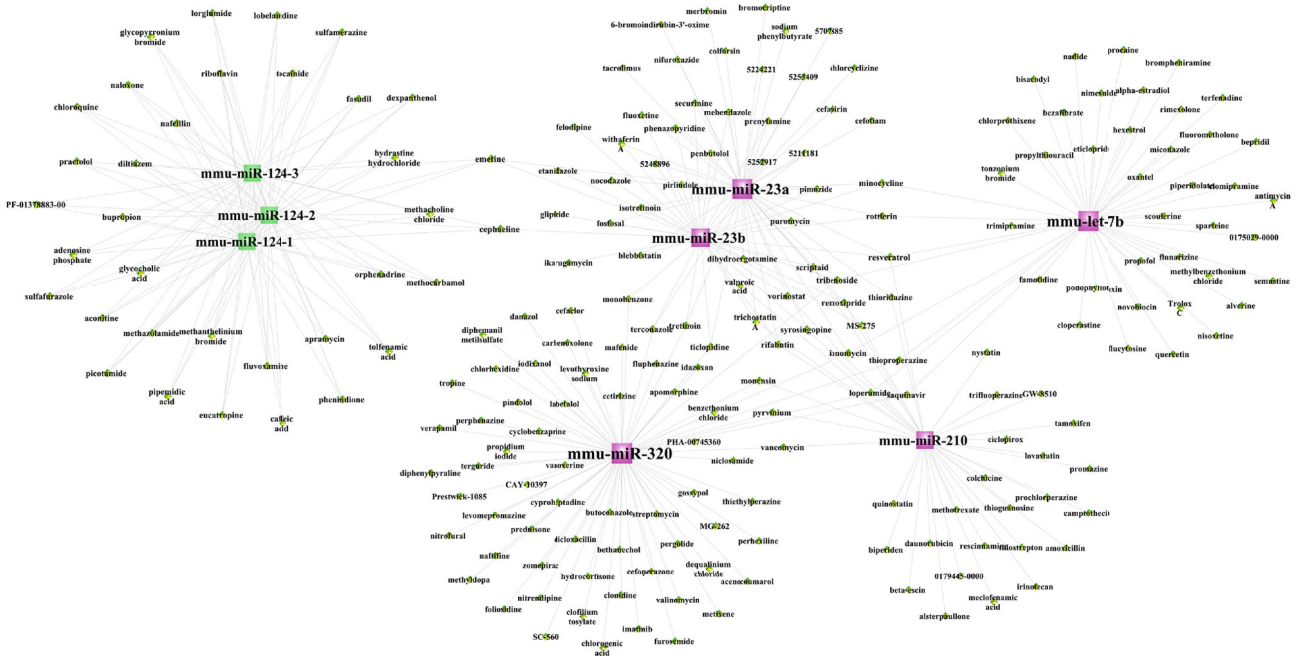
The interaction of ECs and NSPCs supports the angiogenesis of ECs by influencing the expression of angiogenesis-related genes in ECs; likewise, this interaction also supports the neurogenesis of NSPCs by impacting the neurogenesis-associated genes in NSPCs. For instance, the addition of NSPCs into ECs resulted in the downregulation of Fbn1 (Fibrillin 1) in ECs. The encoded protein of gene Fbn1 is a large extracellular matrix (ECM) glycoprotein, which assembles to form 10-12 nm microfibrils in ECM. ECM has been demonstrated as a hard player in regulating angiogenesis via interacting/restoring a variety of growth factors (e.g., fibroblast growth factor (FGF), platelet-derived growth factor (PDGF), hepatocyte growth factor (HGF), and VEGF) [48]. In addition to its involvement in angiogenesis, ECM was shown to regulate the proliferation and differentiation of NSPCs by inducing the local alterations in the substrate stiffness [30]. The TGF-beta signaling pathway targeted by Fbn1 has been regarded as an indispensable player in facilitating interactions between ECs and NSPCs based on its function in vasculogenesis and angiogenesis by upregulating the expression of angiogenic factors [49], as well as its function in neurogenesis by modulating the temporal specification and progenitor potency of NSPCs [50]. As another



EC

- DEmiRN_Up
- DEmiRNA_Down
- ◆ Enrichment

(a)



- DEmiRN_Up
- DEmiRNA_Down
- ◆ Enrichment

(b)

FIGURE 7: The DEmiRNA-small molecular drug network involved in the NSPC-induced EC alterations (a) and EC-induced NSPC alterations (b). Red squares represent upregulated miRNAs, green squares indicate downregulated miRNAs, and yellow diamonds indicate miRNA-related small molecular drugs.

example, the addition of ECs into NSPCs was noted to cause the upregulation of the gene *Chuk* (Component of Inhibitor of Nuclear Factor Kappa B Kinase) in NSPCs. The encoded

protein of *Chuk* is a component of a cytokine-activated protein complex that acts as an inhibitor of the transcription factor NF- κ B complex [51]. The *Chuk* gene overexpressed in

TABLE 13: The 16 small molecular drugs that were overlapped between NSPC-induced EC genetic alteration and EC-induced NSPC genetic alteration.

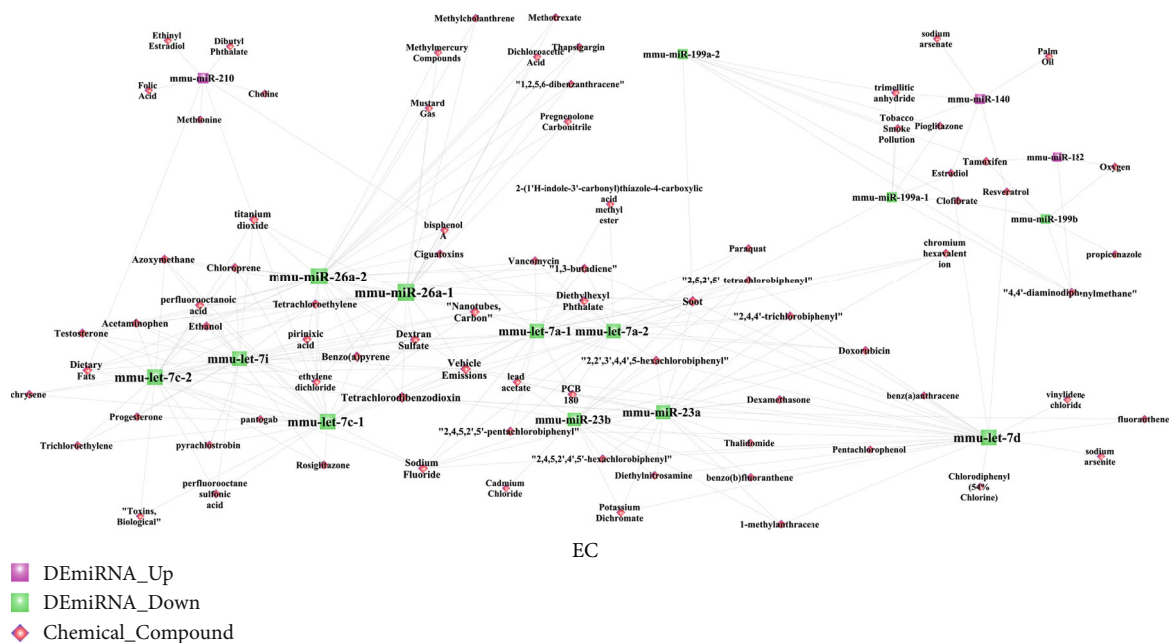
Small molecular drugs	Enrichment in the NSPC-induced EC alteration	Enrichment in the EC-induced NSPC alteration
2-Aminobenzenesulfonamide	0.629	-0.682
Adiphenine	0.748	-0.693
Deptropine	-0.677	-0.672
Diphenhydramine	0.67	-0.573
Felbinac	0.719	-0.697
Fludrocortisone	0.503	-0.496
Fluphenazine	-0.357	-0.378
Ikarugamycin	0.811	-0.838
Lycorine	0.633	0.776
Milrinone	-0.779	0.73
PHA-00745360	0.567	-0.514
Podophyllotoxin	0.661	-0.933
Quinostatin	-0.992	-0.954
Resveratrol	-0.479	-0.504
Thiamazole	0.726	0.543
Triflupromazine	0.694	-0.71

NSPCs might be a crosstalk gene in promoting interactions between NSPCs and ECs, based on the function of the Chuk-targeted NF- κ B pathway in regulating neurogenesis [52] and angiogenesis [53]. The activation of the NF- κ B pathway is known to be involved in angiogenesis by increasing the proliferating potential of vascular ECs and increasing the expression levels of vascular growth factors [53]. In addition, the regulatory function of the NF- κ B pathway in neurogenesis is reflected in its role in initiating the early differentiation of NSPCs [52]. In summary, previous evidence supports the notion that miR-23a plays a role in promoting the interactions between ECs and NSPCs by targeting genes and pathways relevant to angiogenesis and neurogenesis.

The research value of the current research should be highlighted by the comparison between the previously published paper based on the same dataset GSE29759 [10] and the results obtained by the current research. In the previously published paper [10], the authors performed differential expression analysis and have listed the up- and downregulated DE miRNAs which were differentially expressed in NSPC-induced EC alteration and EC-induced NSPC alteration, respectively. However, further deep investigation about the crosstalk miRNAs linking the interaction between NSPCs and ECs is lacking. In order to remedy this research gap, the present research made full use of this valuable dataset with reasonable study design by performing a series of comprehensive bioinformatics analysis and finally obtained the main results showing the crosstalk role of three miRNAs (miR-210, miR-230a, and miR-23b) in the reciprocal interaction between ECs and NSPCs. Apart from this main finding, the present research also identified that some other genetic biomarkers (i.e., six genes (i.e., MMP14, TIMP3, LOXL1, CCK, SMAD6, and HSPA2) and three pathways (i.e., Akt,

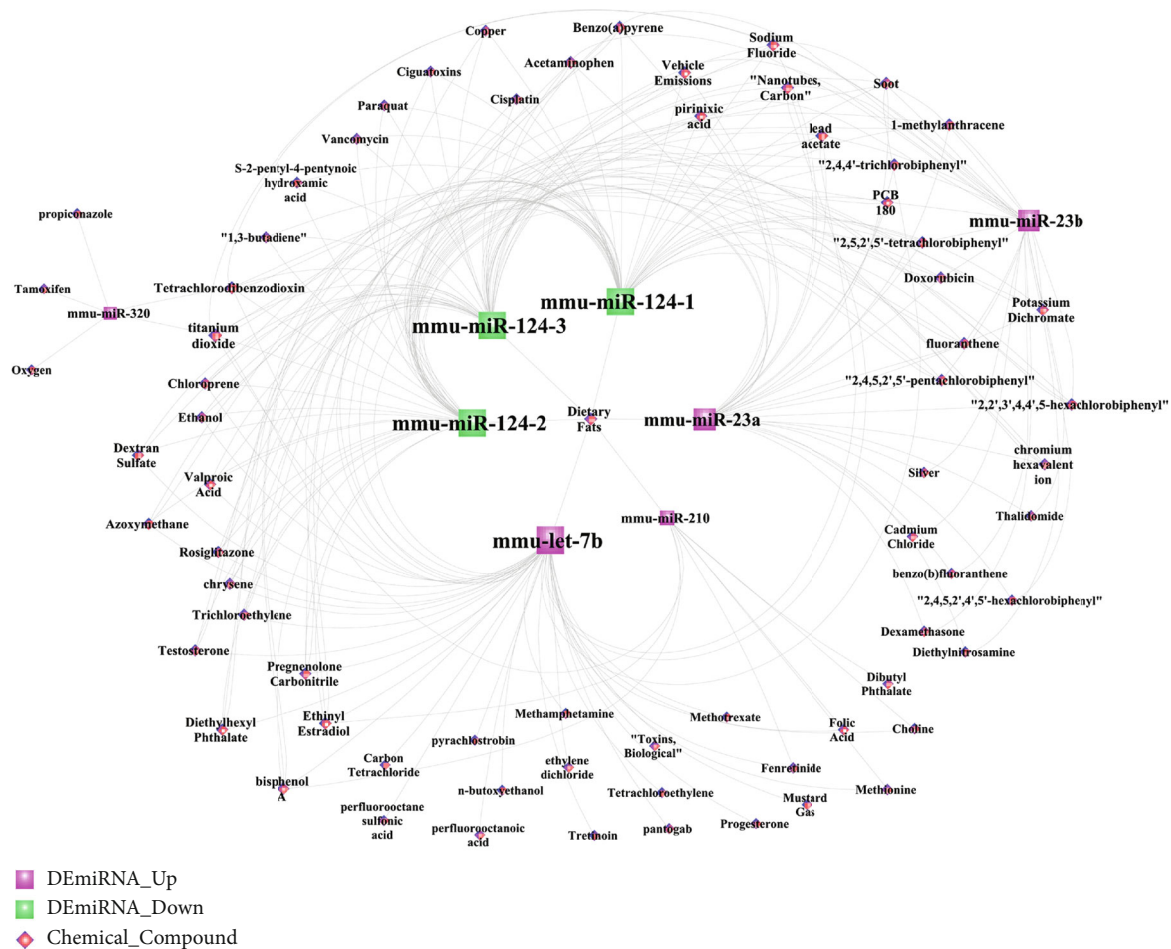
ERK1/2, and BMPs)) play critical roles in the interaction of ECs and NSPCs. And also, some target drugs (six small molecular drugs (i.e., deptropine, fluphenazine, lycorine, quinostatin, resveratrol, and thiamazole) and seven environmental chemical compounds (i.e., folic acid, dexamethasone, choline, doxorubicin, thalidomide, bisphenol A, and titanium dioxide)) were identified to influence angiogenesis and neurogenesis by regulating the expression of DE miRNAs. These results obtained by the current research not only fully explained the underlying information of the dataset GSE29759 but also facilitated neurology researchers to have a better understanding of the genetic and epigenetic mechanisms involved in the interaction between ECs and NSPCs.

It is important to acknowledge the limitation of this research. The first limitation is lacking experimental validation using quantitative real-time polymerase chain reaction (qRT-PCR) to verify the dysregulation of biomarkers identified during the reciprocal alterations between ECs and NSPCs; however, investigating the expression patterns and detailed functions of these biomarkers (especially 3 miRNAs (miR-210, miR-230a, and miR-23b)) as the crosstalks between ECs and NSPCs could be a separate research study and within the research plan of our team. The second limitation is only one dataset (GSE29759) related to this research topic was included, which means the sample size that was analyzed was comparatively limited. This indicates that the future RNA-sequencing study could follow the same study design; if so, more datasets could be combined and analyzed together, which could increase the prediction accuracy of the results identified by bioinformatics analyses. The third limitation is the dataset (GSE29759) only examined the messenger RNA and miRNA expression profiles. Since noncoding RNAs contain miRNAs, long noncoding RNAs (lncRNAs),



EC

(a)



(b)

FIGURE 8: The DE miRNA-chemical compound network involved in the NSPC-induced EC alterations (a) and EC-induced NSPC alterations (b). Red squares represent upregulated miRNAs, green squares indicate downregulated miRNAs, and pink diamonds indicate miRNA-related chemical compounds.

TABLE 14: The scores of the crosstalk miRNA interaction pairs under five conditions including the target genes, small molecular drugs, chemical compounds, signaling pathways, and biological processes. These crosstalk miRNAs link the EC-induced NSPC alteration process and NSPC-induced EC alteration process. The scores were calculated by the “Meet/Min” formula.

miRNAs involved in the NSPC-induced EC alteration	miRNAs involved in the EC-induced NSPC alteration	Score_target	Score_molecular	Score_chemical	Score_pathway	Score_bp
mmu-miR-210	mmu-miR-210	1	0.166667	1	1	1
mmu-miR-23b	mmu-miR-23b	1	0.075	1	1	1
mmu-miR-23b	mmu-miR-23a	0.966903	0.022222	1	0.946667	0.931284
mmu-miR-23a	mmu-miR-23b	0.966903	0.05	0.95	0.946667	0.931284
mmu-let-7d	mmu-let-7b	0.834665	0.021739	0.2	1	0.862256
mmu-miR-26a-1	mmu-miR-23a	0.393215	0.05	0.321429	0.936709	0.614696
mmu-miR-26a-2	mmu-miR-23a	0.393215	0.05	0.321429	0.936709	0.614696
mmu-miR-26a-1	mmu-miR-23b	0.389283	0.025	0.307692	0.946667	0.615335
mmu-miR-26a-2	mmu-miR-23b	0.389283	0.025	0.307692	0.946667	0.615335
mmu-miR-26a-1	mmu-miR-210	0.344017	0.027778	0.333333	0.8	0.689956
mmu-miR-26a-2	mmu-miR-210	0.344017	0.027778	0.333333	0.8	0.689956
mmu-miR-26a-1	mmu-miR-320	0.337681	0.05	0.4	0.885714	0.708661
mmu-miR-26a-2	mmu-miR-320	0.337681	0.05	0.4	0.885714	0.708661
mmu-miR-23a	mmu-let-7b	0.312259	0.021739	0.25	0.772152	0.595539
mmu-let-7i	mmu-miR-23b	0.3026	0.074074	0.318182	0.693333	0.592737
mmu-let-7i	mmu-miR-23a	0.302236	0.074074	0.363636	0.708861	0.590143
mmu-miR-199a-1	mmu-let-7b	0.299166	0.022222	0.142857	0.728395	0.65798
mmu-miR-199a-2	mmu-let-7b	0.299166	0.022222	0.142857	0.728395	0.65798
mmu-let-7c-1	mmu-miR-23b	0.29866	0.071429	0.32	0.72	0.587937
mmu-let-7c-2	mmu-miR-23b	0.29866	0.071429	0.32	0.72	0.587937
mmu-let-7i	mmu-miR-210	0.297009	0.037037	0.222222	0.8	0.609898
mmu-miR-210	mmu-let-7b	0.292735	0.073171	0.875	0.8	0.63901
mmu-let-7c-1	mmu-miR-124-1	0.285561	0.035714	0.72	0.709302	0.623492
mmu-let-7c-1	mmu-miR-124-2	0.285561	0.035714	0.72	0.709302	0.623492
mmu-let-7c-1	mmu-miR-124-3	0.285561	0.035714	0.72	0.709302	0.623492
mmu-let-7c-2	mmu-miR-124-1	0.285561	0.035714	0.72	0.709302	0.623492
mmu-let-7c-2	mmu-miR-124-2	0.285561	0.035714	0.72	0.709302	0.623492
mmu-let-7c-2	mmu-miR-124-3	0.285561	0.035714	0.72	0.709302	0.623492
mmu-let-7a-1	mmu-miR-23b	0.239559	0.041667	0.619048	0.706667	0.616536
mmu-let-7a-2	mmu-miR-23b	0.239559	0.041667	0.619048	0.706667	0.616536
mmu-let-7a-1	mmu-miR-23a	0.2367	0.041667	0.666667	0.721519	0.610834
mmu-let-7a-2	mmu-miR-23a	0.2367	0.041667	0.666667	0.721519	0.610834
mmu-miR-23b	mmu-miR-124-1	0.230102	0.028571	0.666667	0.8	0.527677
mmu-miR-23b	mmu-miR-124-2	0.230102	0.028571	0.666667	0.8	0.527677
mmu-miR-23b	mmu-miR-124-3	0.230102	0.028571	0.666667	0.8	0.527677
mmu-miR-23a	mmu-miR-124-1	0.229761	0.028571	0.75	0.759494	0.523207
mmu-miR-23a	mmu-miR-124-2	0.229761	0.028571	0.75	0.759494	0.523207
mmu-miR-23a	mmu-miR-124-3	0.229761	0.028571	0.75	0.759494	0.523207
mmu-miR-23a	mmu-miR-320	0.226087	0.04	0.2	0.714286	0.755906
mmu-miR-23b	mmu-miR-320	0.22029	0.043478	0.2	0.628571	0.76378
mmu-miR-199a-1	mmu-miR-23a	0.212157	0.066667	0.142857	0.594937	0.619707
mmu-miR-199a-2	mmu-miR-23a	0.212157	0.066667	0.142857	0.594937	0.619707
mmu-miR-199a-1	mmu-miR-23b	0.205006	0.05	0.142857	0.626667	0.618078
mmu-miR-199a-2	mmu-miR-23b	0.205006	0.05	0.142857	0.626667	0.618078
mmu-miR-210	mmu-miR-23a	0.202991	0.170732	0.25	0.8	0.660844
mmu-miR-210	mmu-miR-23b	0.196581	0.075	0.125	0.8	0.672489

TABLE 14: Continued.

miRNAs involved in the NSPC-induced EC alteration	miRNAs involved in the EC-induced NSPC alteration	Score_target	Score_molecular	Score_chemical	Score_pathway	Score_bp
mmu-let-7d	mmu-miR-23b	0.183706	0.025	0.64	0.666667	0.675705
mmu-let-7d	mmu-miR-23a	0.182109	0.022222	0.64	0.717949	0.671367
mmu-let-7d	mmu-miR-320	0.176812	0.057692	0.2	0.485714	0.531496
mmu-miR-199a-1	mmu-miR-320	0.127536	0.022222	0.2	0.771429	0.616142
mmu-miR-199a-2	mmu-miR-320	0.127536	0.022222	0.2	0.771429	0.616142
mmu-miR-182	mmu-miR-320	0.115269	0.093023	0.666667	0.828571	0.555118
mmu-miR-199b	mmu-miR-320	0.109091	0.090909	0.6	0.714286	0.543307
mmu-miR-210	mmu-miR-320	0.087607	0.121951	0.2	0.2	0.358268

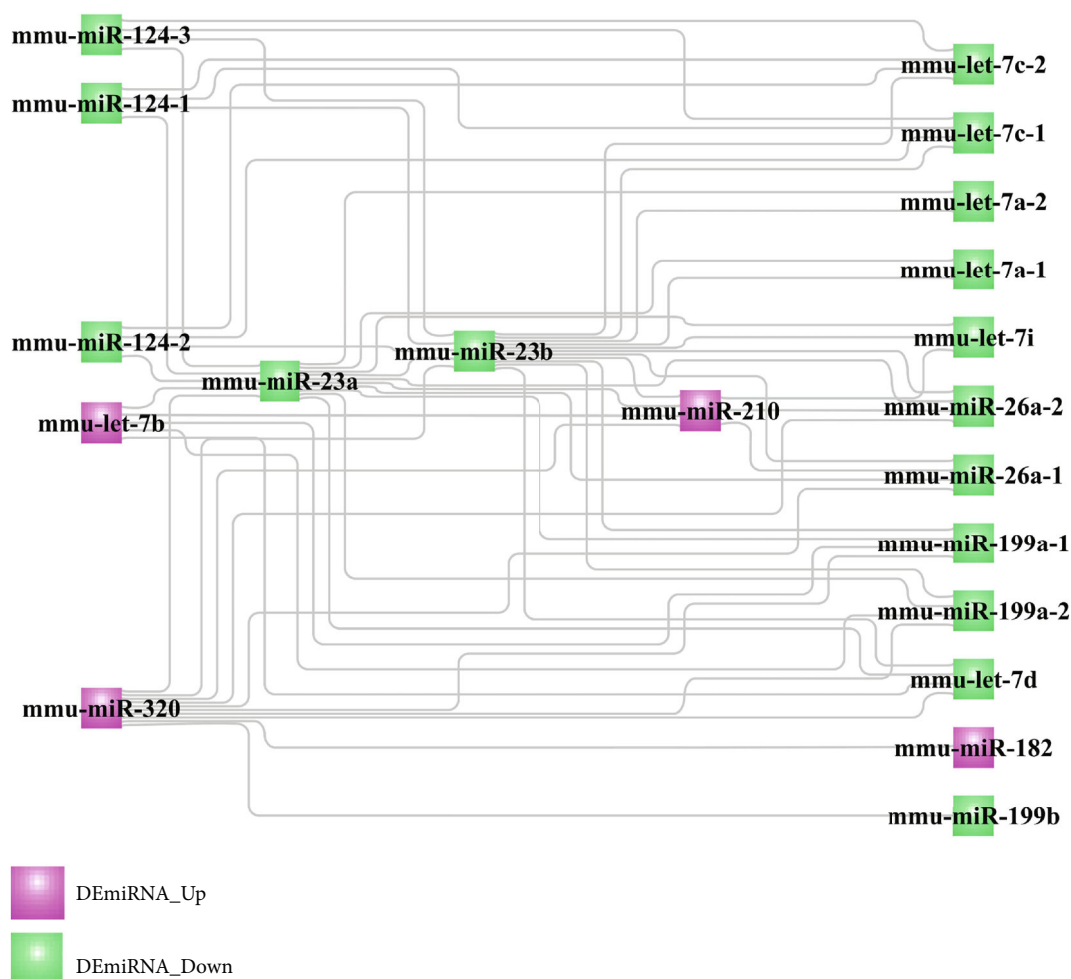


FIGURE 9: The crosstalk DEmiRNA interaction network involved in the link between the EC-induced NSPC alteration process and the NSPC-induced EC alteration process.

circular RNAs (circRNAs), and Piwi-interacting RNA (piRNA), the future research with the same study design could further examine the other noncoding RNA expression profile alterations that occurred during the reciprocal changes in the interactions between ECs and NPSCs. If more datasets with the design of examining the other noncoding RNA expression profiles were included in this analysis, then

constructing a circRNA/lncRNA-miRNA-mRNA competitive endogenous RNA (ceRNA) interaction network will be more meaningful for investigating the genetic and epigenetic crosstalks involved in the reciprocal interactions between ECs and NPSCs.

Although limitations exist in this research, the present study also provides implications for future research. First,

the genetic and epigenetic linkage mechanisms as well as drugs that are involved in the interactions between ECs and NSPCs could translate to novel gene/drug delivery strategies for constructing 3D neurovascular tissue. With the rapid advancements in genome-editing techniques, it may be possible to perform the gene modifications on stem cells (i.e., endothelial stem-like cells and NSPCs) specific to the crosstalk genes and miRNAs identified in this study. The small molecular drugs and chemical compounds are relevant to nanoparticle research for controlled drug delivery to exert sustained effects on the neurogenic and angiogenic processes of ECs and NSPCs. Another noteworthy issue that should be investigated is the dose and concentration of drugs and chemical compounds, especially considering their toxicity and degradation rate. In addition, several of the identified entities are candidates for future research for the purpose of experimental validation, as these have not been investigated in the context of interactions between ECs and NSPCs.

In addition, the present research has potential clinical transfer values for ischemic stroke therapy. Since the current clinical treatments (e.g., intravenous administration of tissue-type plasminogen activator, early motor training, and physical therapy) could not result in complete functional recovery in ischemic stroke patients [54], construction of a multicellular EC-NPSC-based 3D neurovascular unit model might be an alternative tissue engineering approach for regeneration of stroke-affected neuronal tissue. However, there are still no clinical trials using the biomaterial scaffolds carried with ECs and NPSCs in stroke therapy. Although tissue engineering is currently fraught with many challenges [55, 56], the identification of genetic and epigenetic mechanisms and drugs in facilitating the interactions between ECs and NSPCs might be potentially used for the genetic/epigenetic modification of ECs/NSPCs and drug delivery of biomaterial scaffolds and thereby enhance the effects of angiogenesis and neurogenesis. By performing these modifications, the success rate of constructing a 3D neurovascular unit model might be significantly increased. Therefore, the findings of the present research may be regarded as a preliminary step providing a theoretical basis to further research toward a promising stem cell-based stroke therapy.

5. Conclusions

This bioinformatics study identified 3 miRNAs (miR-210, miR-230a, and miR-23b) as crosstalk entities involved in the interaction between ECs and NSPCs. These 3 miRNAs may be relevant to the arena of stem cell modification to further promote angiogenesis and neurogenesis within the field of stem cell tissue engineering.

Data Availability

The data used to support the findings of this study are available from the corresponding author upon request.

Conflicts of Interest

The authors declare no potential conflict of interest with respect to the authorship and publication of this paper.

Authors' Contributions

Bernd Lethaus and Vuk Savkovic contributed equally as senior authors.

Acknowledgments

The first author Xin Wang received financial support from the Research Fund of Heilongjiang Provincial Education Department, Heilongjiang Province, China (Grant No. 31041180068).

References

- [1] V. Muoio, P. B. Persson, and M. M. Sendeski, "The neurovascular unit - concept review," *Acta Physiologica*, vol. 210, no. 4, pp. 790–798, 2014.
- [2] G. Potjewyd, S. Moxon, T. Wang, M. Domingos, and N. M. Hooper, "Tissue engineering 3D neurovascular units: a biomaterials and bioprinting perspective," *Trends in Biotechnology*, vol. 36, no. 4, pp. 457–472, 2018.
- [3] O. Rajkovic, G. Potjewyd, and E. Pinteaux, "Regenerative medicine therapies for targeting neuroinflammation after stroke," *Frontiers in Neurology*, vol. 9, p. 734, 2018.
- [4] T. Roitbak, L. Li, and L. A. Cunningham, "Neural stem/progenitor cells promote endothelial cell morphogenesis and protect endothelial cells against ischemia via HIF-1 α -regulated VEGF signaling," *Journal of Cerebral Blood Flow and Metabolism*, vol. 28, no. 9, pp. 1530–1542, 2008.
- [5] J. M. Rosenstein, J. M. Krum, and C. Ruhrberg, "VEGF in the nervous system," *Organogenesis*, vol. 6, no. 2, pp. 107–114, 2014.
- [6] O. A. Levada, N. V. Cherednichenko, A. V. Trailin, and A. S. Troyan, "Plasma brain-derived neurotrophic factor as a biomarker for the main types of mild neurocognitive disorders and treatment efficacy: a preliminary study," *Disease Markers*, vol. 2016, Article ID 4095723, 7 pages, 2016.
- [7] N. Nakagomi, T. Nakagomi, S. Kubo et al., "Endothelial cells support survival, proliferation, and neuronal differentiation of transplanted adult ischemia-induced neural stem/progenitor cells after cerebral infarction," *Stem Cells*, vol. 27, no. 9, pp. 2185–2195, 2009.
- [8] Q. Shen, S. K. Goderie, L. Jin et al., "Endothelial cells stimulate self-renewal and expand neurogenesis of neural stem cells," *Science*, vol. 304, no. 5675, pp. 1338–1340, 2004.
- [9] M. J. Donovan, M. I. Lin, P. Wiegand et al., "Brain derived neurotrophic factor is an endothelial cell survival factor required for intramyocardial vessel stabilization," *Development*, vol. 127, no. 21, pp. 4531–4540, 2000.
- [10] T. Roitbak, O. Bragina, J. L. Padilla, and G. G. Pickett, "The role of microRNAs in neural stem cell-supported endothelial morphogenesis," *Vascular Cell*, vol. 3, no. 1, p. 25, 2011.
- [11] S. Zhang, L. Chen, E. J. Jung, and G. A. Calin, "Targeting microRNAs with small molecules: from dream to reality," *Clinical Pharmacology and Therapeutics*, vol. 87, no. 6, pp. 754–758, 2010.

- [12] X. Wu and Y. Song, "Preferential regulation of miRNA targets by environmental chemicals in the human genome," *BMC Genomics*, vol. 12, no. 1, p. 244, 2011.
- [13] J. Reinhardt, J. Landsberg, J. L. Schmid-Burgk et al., "MAPK signaling and inflammation link melanoma phenotype switching to induction of CD73 during immunotherapy," *Cancer Research*, vol. 77, no. 17, pp. 4697–4709, 2017.
- [14] G. Yu, L. G. Wang, Y. Han, and Q. Y. He, "clusterProfiler: an R package for comparing biological themes among gene clusters," *OMICS*, vol. 16, no. 5, pp. 284–287, 2012.
- [15] D. Szklarczyk, A. L. Gable, D. Lyon et al., "STRING v11: protein-protein association networks with increased coverage, supporting functional discovery in genome-wide experimental datasets," *Nucleic Acids Research*, vol. 47, no. D1, pp. D607–D613, 2019.
- [16] P. Shannon, A. Markiel, O. Ozier et al., "Cytoscape: a software environment for integrated models of biomolecular interaction networks," *Genome Research*, vol. 13, no. 11, pp. 2498–2504, 2003.
- [17] H. Han, J.-W. Cho, S. Lee et al., "TRRUST v2: an expanded reference database of human and mouse transcriptional regulatory interactions," *Nucleic Acids Research*, vol. 46, no. D1, pp. D380–D386, 2018.
- [18] H.-Y. Huang, Y.-C.-D. Lin, J. Li et al., "miRTarBase 2020: updates to the experimentally validated microRNA–target interaction database," *Nucleic Acids Research*, vol. 48, no. D1, pp. D148–D154, 2020.
- [19] F. Xiao, Z. Zuo, G. Cai, S. Kang, X. Gao, and T. Li, "miRecords: an integrated resource for microRNA–target interactions," *Nucleic Acids Research*, vol. 37, no. Database, pp. D105–D110, 2009.
- [20] I. S. Vlachos, M. D. Paraskevopoulou, D. Karagkouni et al., "DIANA-TarBase v7. 0: indexing more than half a million experimentally supported miRNA: mRNA interactions," *Nucleic Acids Research*, vol. 43, no. D1, pp. D153–D159, 2015.
- [21] V. Agarwal, G. W. Bell, J.-W. Nam, and D. P. Bartel, "Predicting effective microRNA target sites in mammalian mRNAs," *eLife*, vol. 4, article e05005, 2015.
- [22] J.-H. Yang, J.-H. Li, P. Shao, H. Zhou, Y.-Q. Chen, and L.-H. Qu, "starBase: a database for exploring microRNA–mRNA interaction maps from Argonaute CLIP-Seq and Degradome-Seq data," *Nucleic Acids Research*, vol. 39, Supplement 1, pp. D202–D209, 2011.
- [23] S.-D. Hsu, C.-H. Chu, A.-P. Tsou et al., "miRNAMap 2.0: genomic maps of microRNAs in metazoan genomes," *Nucleic Acids Research*, vol. 36, Supplement 1, pp. D165–D169, 2007.
- [24] Y. Chen and X. Wang, "miRDB: an online database for prediction of functional microRNA targets," *Nucleic Acids Research*, vol. 48, no. D1, pp. D127–D131, 2020.
- [25] H. Dweep, C. Sticht, P. Pandey, and N. Gretz, "miRWalk - database: prediction of possible miRNA binding sites by "walking" the genes of three genomes," *Journal of Biomedical Informatics*, vol. 44, no. 5, pp. 839–847, 2011.
- [26] J. Krüger and M. Rehmsmeier, "RNAhybrid: microRNA target prediction easy, fast and flexible," *Nucleic Acids Research*, vol. 34, Supplement 2, pp. W451–W454, 2006.
- [27] J. Lamb, E. D. Crawford, D. Peck et al., "The connectivity map: using gene-expression signatures to connect small molecules, genes, and disease," *Science*, vol. 313, no. 5795, pp. 1929–1935, 2006.
- [28] A. P. Davis, C. J. Grondin, R. J. Johnson et al., "The comparative toxicogenomics database: update 2019," *Nucleic Acids Research*, vol. 47, no. D1, pp. D948–D954, 2019.
- [29] K.-I. Katayama, J. Melendez, J. M. Baumann et al., "Loss of RhoA in neural progenitor cells causes the disruption of adherens junctions and hyperproliferation," *Proceedings of the National Academy of Sciences of the United States of America*, vol. 108, no. 18, pp. 7607–7612, 2011.
- [30] A. J. Keung, E. M. de Juan-Pardo, D. V. Schaffer, and S. Kumar, "Rho GTPases mediate the mechanosensitive lineage commitment of neural stem cells," *Stem Cells*, vol. 29, no. 11, pp. 1886–1897, 2011.
- [31] G. P. van Nieuw Amerongen, P. Koolwijk, A. Versteilen, and V. W. M. van Hinsbergh, "Involvement of RhoA/Rho kinase signaling in VEGF-induced endothelial cell migration and angiogenesis in vitro," *Arteriosclerosis, Thrombosis, and Vascular Biology*, vol. 23, no. 2, pp. 211–217, 2003.
- [32] C. A. Escudero, K. Herlitz, F. Troncoso et al., "Pro-angiogenic role of insulin: from physiology to pathology," *Frontiers in Physiology*, vol. 8, p. 204, 2017.
- [33] A. N. Ziegler, S. W. Levison, and T. L. Wood, "Insulin and IGF receptor signalling in neural-stem-cell homeostasis," *Nature Reviews Endocrinology*, vol. 11, no. 3, pp. 161–170, 2015.
- [34] M. C. Tate, D. A. Shear, S. W. Hoffman, D. G. Stein, D. R. Archer, and M. C. Laplaca, "Fibronectin promotes survival and migration of primary neural stem cells transplanted into the traumatically injured mouse brain," *Cell Transplantation*, vol. 11, no. 3, pp. 283–295, 2002.
- [35] V. B. S. Kumar, R. I. Viji, M. S. Kiran, and P. R. Sudhakaran, "Angiogenic response of endothelial cells to fibronectin," *Advances in Experimental Medicine and Biology*, vol. 749, pp. 131–151, 2012.
- [36] S. H. Koh and E. H. Lo, "The role of the PI3K pathway in the regeneration of the damaged brain by neural stem cells after cerebral infarction," *Journal of Clinical Neurology*, vol. 11, no. 4, pp. 297–304, 2015.
- [37] J. Karar and A. Maity, "PI3K/AKT/mTOR pathway in angiogenesis," *Frontiers in Molecular Neuroscience*, vol. 4, p. 51, 2011.
- [38] K. Ebneth, M. Aurrand-Lions, A. Kuhn et al., "The junctional adhesion molecule (JAM) family members JAM-2 and JAM-3 associate with the cell polarity protein PAR-3: a possible role for JAMs in endothelial cell polarity," *Journal of Cell Science*, vol. 116, no. 19, pp. 3879–3891, 2003.
- [39] T. Hikita, F. Mirzapourshafiyi, P. Barbacena et al., "PAR-3 controls endothelial planar polarity and vascular inflammation under laminar flow," *EMBO Reports*, vol. 19, no. 9, 2018.
- [40] Y. Arai and E. Taverna, "Neural progenitor cell polarity and cortical development," *Frontiers in Cellular Neuroscience*, vol. 11, p. 384, 2017.
- [41] R. J. Bodnar, "Chemokine regulation of angiogenesis during wound healing," *Advances in Wound Care*, vol. 4, no. 11, pp. 641–650, 2015.
- [42] M. D. Krathwohl and J. L. Kaiser, "Chemokines promote quiescence and survival of human neural progenitor cells," *Stem Cells*, vol. 22, no. 1, pp. 109–118, 2004.
- [43] A. Belmadani, P. B. Tran, D. Ren, and R. J. Miller, "Chemokines regulate the migration of neural progenitors to sites of neuroinflammation," *The Journal of Neuroscience*, vol. 26, no. 12, pp. 3182–3191, 2006.

- [44] K. Hida, N. Maishi, K. Akiyama et al., "Tumor endothelial cells with high aldehyde dehydrogenase activity show drug resistance," *Cancer Science*, vol. 108, no. 11, pp. 2195–2203, 2017.
- [45] G. Vassalli, "Aldehyde dehydrogenases: not just markers, but functional regulators of stem cells," *Stem Cells International*, vol. 2019, Article ID 3904645, 15 pages, 2019.
- [46] J. Takahashi, T. D. Palmer, and F. H. Gage, "Retinoic acid and neurotrophins collaborate to regulate neurogenesis in adult-derived neural stem cell cultures," *Journal of Neurobiology*, vol. 38, no. 1, pp. 65–81, 1999.
- [47] S. Pal, M. L. Iruela-Arispe, V. S. Harvey et al., "Retinoic acid selectively inhibits the vascular permeabilizing effect of VPF/VEGF, an early step in the angiogenic cascade," *Microvascular Research*, vol. 60, no. 2, pp. 112–120, 2000.
- [48] M. Mongiat, E. Andreuzzi, G. Tarticchio, and A. Paulitti, "Extracellular matrix, a hard player in angiogenesis," *International Journal of Molecular Sciences*, vol. 17, no. 11, p. 1822, 2016.
- [49] P. A. Guerrero and J. H. McCarty, "TGF- β activation and signaling in angiogenesis," in *Physiologic and Pathologic Angiogenesis - Signaling Mechanisms and Targeted Therapy*, 2017.
- [50] J. M. Dias, Z. Alekseenko, J. M. Applequist, and J. Ericson, "Tgf β signaling regulates temporal neurogenesis and potency of neural stem cells in the CNS," *Neuron*, vol. 84, no. 5, pp. 927–939, 2014.
- [51] Y. Xie, K. Xie, Q. Gou, and N. Chen, "I κ B kinase α functions as a tumor suppressor in epithelial-derived tumors through an NF- κ B-independent pathway (review)," *Oncology Reports*, vol. 34, no. 5, pp. 2225–2232, 2015.
- [52] Y. Zhang, J. Liu, S. Yao et al., "Nuclear factor Kappa B signaling initiates early differentiation of neural stem cells," *Stem Cells*, vol. 30, no. 3, pp. 510–524, 2012.
- [53] X. Sui, "Inhibition of the NF- κ B signaling pathway on endothelial cell function and angiogenesis in mice with acute cerebral infarction," *Journal of Biological Regulators and Homeostatic Agents*, vol. 33, no. 2, pp. 375–384, 2019.
- [54] J. Wang, W. Yang, H. Xie, Y. Song, Y. Li, and L. Wang, "Ischemic stroke and repair: current trends in research and tissue engineering treatments," *Regenerative Medicine Research*, vol. 2, no. 1, p. 3, 2014.
- [55] M. Singh, P. K. Pandey, A. Bhasin, M. V. Padma, and S. Mohanty, "Application of stem cells in stroke: a multifactorial approach," *Frontiers in Neuroscience*, vol. 14, 2020.
- [56] O. Y. Bang, E. H. Kim, J. M. Cha, and G. J. Moon, "Adult stem cell therapy for stroke: challenges and progress," *Journal of Stroke*, vol. 18, no. 3, pp. 256–266, 2016.

Research Article

Responsive Expression of MafF to β -Amyloid-Induced Oxidative Stress

Xiaoxuan Wang, Yu Zhang, Xinkun Wan, Chenjia Guo, Jing Cui, Jing Sun, and Liang Li 

Department of Pathology, School of Basic Medical Sciences, Capital Medical University, Beijing 100069, China

Correspondence should be addressed to Liang Li; liliang8698@yeah.net

Received 24 June 2020; Revised 13 October 2020; Accepted 9 November 2020; Published 7 December 2020

Academic Editor: Donald H. Chace

Copyright © 2020 Xiaoxuan Wang et al. This is an open access article distributed under the Creative Commons Attribution License, which permits unrestricted use, distribution, and reproduction in any medium, provided the original work is properly cited.

The small musculoaponeurotic fibrosarcoma (sMaf) proteins MafF, MafG, and MafK are basic region leucine zipper- (bZIP-) type transcription factors and display tissue- or stimulus-specific expression patterns. As the oxidative stress reactive proteins, sMafs are implicated in various neurological disorders. In the present study, the expressions of sMafs were investigated across five databases gathering transcriptomic data from 74 Alzheimer's disease (AD) patients and 66 controls in the Gene Expression Omnibus (GEO) database. The expression of MafF was increased in the hippocampus of AD patients, which was negatively correlated with the expression of the glutamate cysteine ligase catalytic subunit (GCLC). Furthermore, MafF was significantly increased in patients with Braak stage V-VI, compared to those with Braak stage III-IV. β -Amyloid ($A\beta$), a strong inducer of oxidative stress, plays a crucial role in the pathogenesis of AD. The responsive expressions of sMafs to $A\beta$ -induced oxidative stress were studied in the APP/PS1 mouse model of AD, $A\beta$ intrahippocampal injection rats, and several human cell lines from different tissue origins. This study revealed that only the induction of MafF was accompanied with reduction of GCLC and glutathione (GSH). MafF knockdown suppressed the increase of GSH induced by $A\beta$. Among sMafs, MafF is the most responsive to $A\beta$ -induced oxidative stress and might potentiate the inhibition of antioxidation. These results provide a better understanding of sMaf modulation in AD and highlight MafF as a potential therapeutic target in AD.

1. Introduction

The musculoaponeurotic fibrosarcoma (Maf) proteins belong to the family of the basic region leucine zipper- (bZIP-) type transcription factors, also including activator protein- (AP-) 1 factors, CREB/ATF, CNC, C/EBP, and PAR [1, 2]. There are two groups in the Maf family. The large Maf proteins, including v-Maf, c-Maf, MafB, and Nrl, contain a distinctive acidic domain suggestive of transcriptional activation properties. The small Maf (sMaf) proteins, including MafF, MafG, and MafK, present high degrees of homology. They are predominantly localized in the nucleus and have emerged as important transcription regulators, although they lack activation domains [3, 4]. Nuclear factor (erythroid-derived 2)-like 2 (Nrf2) belongs to the bZIP family and is a master regulator of antioxidant and xenobiotic metabolizing enzymes [5–7]. Because Nrf2 cannot bind to the DNA, sMafs are indispensable partners that are required by Nrf2 to exert its functions. In response to oxidative and

electrophilic stresses, Nrf2 translocates to the nucleus and heterodimerizes with sMafs to activate specific target genes such as glutamate cysteine ligase catalytic subunit (GCLC). This activation promotes the production of antioxidants such as glutathione (GSH). sMafs can also form homodimers that act as transcriptional repressors [8, 9]. One study suggested that all three sMaf genes play important roles in oxidative stress. Yet, even though the three genes can be coexpressed in the same cell line, their expressions seem to be regulated by distinct mechanisms [10].

Many studies reported the relevance of sMafs in a broad range of human pathologies, such as neurological disorders [11], chronic myeloid leukemia [12], diabetes [13], lung cancers [14], and hepatocellular carcinoma [15]. Although the causes of neurodegenerative diseases remain unclear, growing evidences point toward oxidative injury as an important pathogenic mechanism. Alzheimer's disease (AD) manifests by cognitive dysfunction and memory impairment. The pathological characteristics of AD are the formations of

extracellular β -amyloid ($A\beta$) plaques and intraneuronal deposits of neurofibrillary tangles (NFTs). $A\beta$ is produced by cleavage of the transmembrane glycoprotein amyloid precursor protein (APP) through the sequential actions of β -secretases and presenilin-dependent γ -secretases [16]. $A\beta$ is a strong oxidative stress inducer that promotes the formation of free radicals and causes damages to nerve cells [17]. Extensive data demonstrate that $A\beta$ overproduction in the brains of AD patients and APP/PS1 mice is positively correlated with the level of oxidative stress [18] and that the Nrf2-sMaf signal pathway is severely inhibited in late AD patients [19–21]. Despite the potential link between oxidative stress, sMafs, and AD, the functions of sMafs in the brain, especially in AD conditions, are rarely documented.

In the present study, we compared the transcriptomes of 74 AD patients and 66 controls taken from five databases. Since $A\beta$ is a main cause for the various pathological changes observed in AD, we investigated the expression levels of MafF, MafG, and MafK in APP/PS1 transgenic mice, $A\beta$ intrahippocampal injection rat model, and $A\beta$ -treated several human cell lines from different tissue.

2. Materials and Methods

2.1. Data Collection. Transcriptomic data from 74 AD patients and 66 controls were collected from the databases GSE29378 (<https://www.ncbi.nlm.nih.gov/geo/query/acc.cgi?acc=GSE29378>), GSE36980 (<https://www.ncbi.nlm.nih.gov/geo/query/acc.cgi?acc=GSE36980>), GSE28146 (<https://www.ncbi.nlm.nih.gov/geo/query/acc.cgi?acc=GSE28146>), GSE48350 (<https://www.ncbi.nlm.nih.gov/geo/query/acc.cgi?acc=GSE48350>), and GSE5281 (<https://www.ncbi.nlm.nih.gov/geo/query/acc.cgi?acc=GSE5281>). The cross-platform normalized data were downloaded from the Alz-Data database [22–27]. The basal clinical information related to the samples was provided in Supplement Table S1.

2.2. Animals. Nine-month-old male APP^{swe}/PS1^{dE9} (APP/PS1) mice (Ethical approval AEEI-2019-081, Beijing HFK Bioscience Co., Ltd. Beijing, China) and 12-week-old adult male Sprague-Dawley (SD) rats (Ethical approval AEET-2017-103, Beijing Vital River Experimental Animal Technology Co., Ltd. Beijing, China) were used in this study. All animals were housed in the Experimental Animal Center of the Capital Medical University (Beijing, China) under standard laboratory conditions (22°C–24°C, 40%–60% relative humidity) with regular 12 h light/dark cycles. All experimental procedures were performed in compliance with the Guidance for the Care and Use of Laboratory Animals formulated by the Ministry of Science and Technology of China.

2.3. Cell Culture and Treatment. SH-SY5Y neuroblastoma, HepG2 liver hepatocellular carcinoma, and A549 alveolar basal epithelial human cell lines were cultured in Dulbecco minimum essential medium (DMEM) (Gibco, USA) containing 10% fetal bovine serum (Gibco) at 37°C in incubator supplied with 5% CO₂. Both $A\beta_{1-42}$ peptides (China Peptides Co., Ltd.) and scrambled $A\beta$ peptides with the same amino acid composition as $A\beta_{1-42}$ but in randomized sequences

were aggregated before use by incubation in dimethyl sulfoxide (DMSO) at 37°C for 72 h [28]. The oligomerization of $A\beta$ was verified by electronic microscopy. $A\beta_{1-42}$ or scrambled $A\beta$ peptides were added to the medium and incubated for 48 h. Hydrogen peroxide (H₂O₂, Beijing Shiji, Beijing, China) or phosphate buffer saline (PBS) was added to the medium and incubated for 24 h.

2.4. Stereotaxic Injection of $A\beta$. Rats anesthetized with 2%–3% isoflurane with an animal anesthesia ventilator system (RWD Life Science Co. Ltd., Shenzhen, China) were placed onto a stereotaxic frame (RWD Life Science Co. Ltd., Shenzhen, China). A microsyringe was implanted stereotactically to the hippocampus (4.3 mm posterior to the bregma; 3.5 mm lateral from midline; and 3.3 mm ventral to bregma). A volume of 3 μ l containing 20 μ g of $A\beta_{1-42}$ or scrambled $A\beta$ was delivered with a stepper-motorized 10 μ l microsyringe at a rate of 1 μ l/min [28].

2.5. Quantitative Real-Time PCR (q-PCR). Total RNAs were extracted from tissues and cells using RNAsimple Total RNA kit (Tiangen, Beijing, China). Reverse transcriptions were performed using FastQuant kit with gDNase (Tiangen). The q-PCR reactions were performed as previously described [28]. Each q-PCR assay was run in triplicate in a CFX96 Touch system (Bio-Rad, Hercules, CA, USA). Data were analyzed using the $2^{-\Delta\Delta C_t}$ method with glyceraldehyde-3-phosphate dehydrogenase (GAPDH) or beta-actin (β -actin) as controls. The primer sequences are listed in Table 1.

2.6. Western Blot. Cells or hippocampal tissues were harvested and homogenized in RIPA buffer containing a cocktail of protease inhibitors (MedChemExpress, NJ, USA). Whole-cell lysates were prepared for western blot analysis as described before [29]. The primary antibodies were as follows: rabbit anti-GCLC antibody (1:10000, Abcam, UK), rabbit anti-MafF antibody (1:1000, Proteintech Group, Rosemont, IL, USA), rabbit anti-MafG antibody (1:2000, Novus Biologicals, CO, USA), rabbit anti-MafK antibody (1:5000, Abcam), and mouse GAPDH monoclonal antibody (1:5000, Proteintech Group). Signals were quantified with Alpha FluorChem FC3 system (Protein Simple, San Francisco, CA, USA) and analyzed with ImageJ 16.0 (NIH, Bethesda, MD, USA).

2.7. Determination of GSH. Quantitative analysis of GSH levels was performed with Reduced GSH Assay kit (Nanjing Jiancheng Bioengineering Institute, Nanjing, China) according to the manufacturer's instructions. The absorbance was measured using a microplate reader (Thermo Scientific, Waltham, MA, USA) at a wavelength of 405 nm.

2.8. Cell Transfection. MafF siRNA was purchased from Hanbio (Shanghai, China). SH-SY5Y cells were seeded in 6-well plates. Two milliliters of transfection solution containing RNAFit and 10 nM of MafF siRNA or scrambled siRNA used as a negative control (NC) were added to the cultures. Cells were collected 48 h after transfection.

TABLE 1: Primer sequences used in q-PCR.

Species	Gene	Forward primer	Reverse primer
Mice	MafF	5'-TGGGCgATGGATCTAGCCAC-3'	5'-CAACTCGCGCTTGACCTTCA-3'
	MafG	5'-GAGTGCCTGCTCACTGTGT-3'	5'-AGGTGCTGGTTCAACTCTCG-3'
	MafK	5'-GAGTCGGAACGAGAAGTCCG-3'	5'-CAGGACGGAACCACCAGAAA-3'
	GAPDH	5'-GGTTGTCTCCTGCGACTTCA-3'	5'-GGTGGTCCAGGGTTTCTTACTC-3'
	MafF	5'-GCCTCAGCTCCCTCCCAAAGTG-3'	5'-ACCCCAGGCCAACCCAGAGG-3'
	MafG	5'-AGTAAAGTCCAAGACGGATGC-3'	5'-GAAGAGAAGGAAACAGAGGGAC-3'
Human	MafK	5'-AGCTACGAGTTCCAGGGAG-3'	5'-ATGGACACCAGCTCATCATC-3'
	β -Actin	5'-GCACTCTTCCAGCCTTCC-3'	5'-TGTCCACGTCACACTTCATG-3'
	GAPDH	5'-TGGGTGTGAACCATGAGAAG-3'	5'-GAGTCCTTCCACGATACCAAAG-3'

2.9. Statistical Analysis. Statistical analysis was carried out using the unpaired two-tailed Student *t*-test or variance analysis (ANOVA) followed by a Tukey's post hoc test using GraphPad Prism 6 software (GraphPad Software, San Diego, CA, USA) [28]. Pearson correlations were considered statistically significant from $p < 0.05$, with r representing the correlation coefficient. All data are presented as mean \pm standard error of the mean (SEM).

3. Results

3.1. Analysis of sMaf Expressions in the Hippocampus of AD Patients. In order to study the expression changes of the three sMaf genes between the brains of AD patients and controls, the transcriptomic data from 74 AD patients and 66 controls from five databases were analyzed. All patients were diagnosed with AD according to stringent clinical and pathological criteria. The control group also underwent strict enrollment examinations, including cognitive and other functional tests. There was no significant difference in the mean age between the two groups. Detailed information is shown in Supplement Table S1. Compared with the control group, a significant increase in MafF expression was found in the hippocampus of AD patients (Figure 1(a)), while there were no significant changes in the expressions of MafG and MafK (Figures 1(b) and 1(c)). Furthermore, the sMaf expressions were analyzed in AD patients with definite Braak stages. We found that MafF was significantly increased in the hippocampus of patients with Braak stage V-VI, compared to those with Braak stage III-IV (Figure 1(d)). Moreover, the results of Pearson correlation analysis showed that the expressions of sMafs were negatively correlated with GCLC expression in AD patients (Figures 1(h)-1(j)). These results gave us an important reminder that MafF might participate in the pathological process of AD.

3.2. Constitutive Expressions of sMafs in Different Tissues. Since there were less reports on the basal expressions of sMafs in tissues, especially in the brain, to document the expression of the mRNAs encoding sMafs, q-PCR was performed to determine the mRNA expressions of MafF, MafG,

and MafK in different mouse brain areas, including the hippocampus, cortex, cerebellum, and brainstem, as well as from other tissues including liver, lung, and kidney. Constitutive expressions of sMafs were the highest in the lungs and relatively low in the brain (Figures 2(a)-2(c)). Basal expression levels of the three genes varied significantly in different regions of the brain. The expressions of both MafF and MafG were the highest in the cerebellum, intermediate in the cortex and the brainstem, and lowest in the hippocampus. MafF and MafG expressions were, respectively, 4-7 and 7-15 times lower in the hippocampus than in other regions of the brain (Figures 2(a) and 2(b)). MafK expression was the highest in the brainstem, intermediate in the cerebellum, and lowest in the hippocampus and the cortex. The expression of MafK in the hippocampus was similar to that found in the cortex (Figure 2(c)). Overall, the expressions of the three sMafs were lower in the brain, particularly in the hippocampus, than in other tissues.

3.3. MafF Expression Was Increased in response to $A\beta$ -Induced Oxidative Injury. As $A\beta$ -induced oxidative stress is a main cause in the development of AD, we investigated the potential changes of sMaf expressions under $A\beta$ insult. First, 9-month-old APP/PS1 transgenic mice with numerous amyloid plaques deposited in the hippocampus were assessed to observe the expressions of sMafs under long-term $A\beta$ insult. As shown in Figure 3(a), the MafF level was increased by 22.96% compared with that in C57 control mice, but there were no significant changes in MafG and MafK levels between the two groups of mice (Figure 3(a)). Furthermore, $A\beta$ intrahippocampal injection rat models and $A\beta$ -treated SH-SY5Y cells were employed to obtain the similar findings that MafF protein was upregulated by 37.63% and 19.07%, respectively (Figures 3(b) and 3(c)), and there were no significant changes in the expressions of MafG and MafK (Figures 3(b) and 3(c)).

3.4. MafF Might Be Involved in the Inhibition of Antioxidation Caused by $A\beta$ -Induced Oxidative Stress. sMaf nuclear factors are important transcriptional regulators, and in particular, Nrf2/sMafs is a main endogenous pathway operating against oxidative stress [8]. This signal pathway is

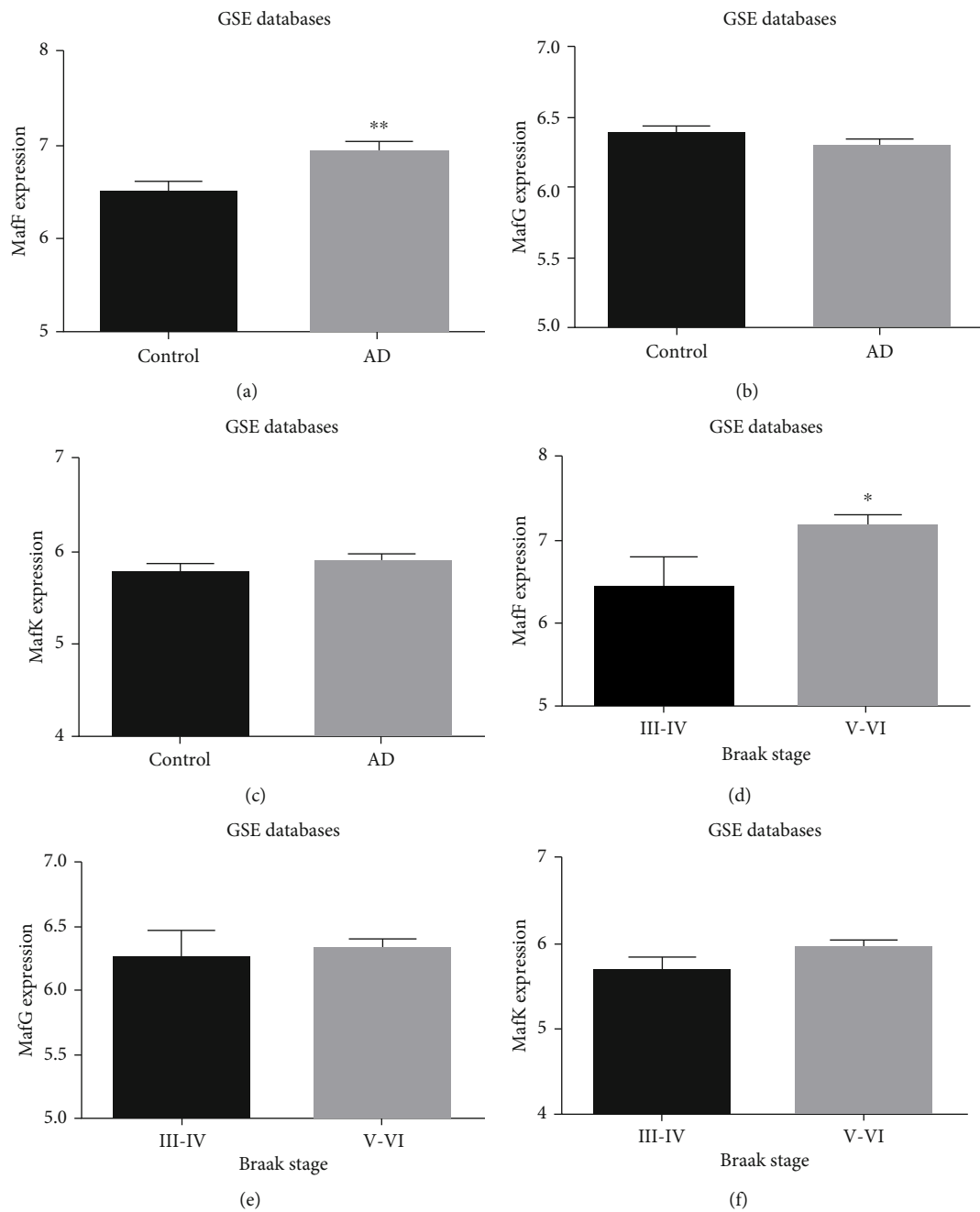


FIGURE 1: Continued.

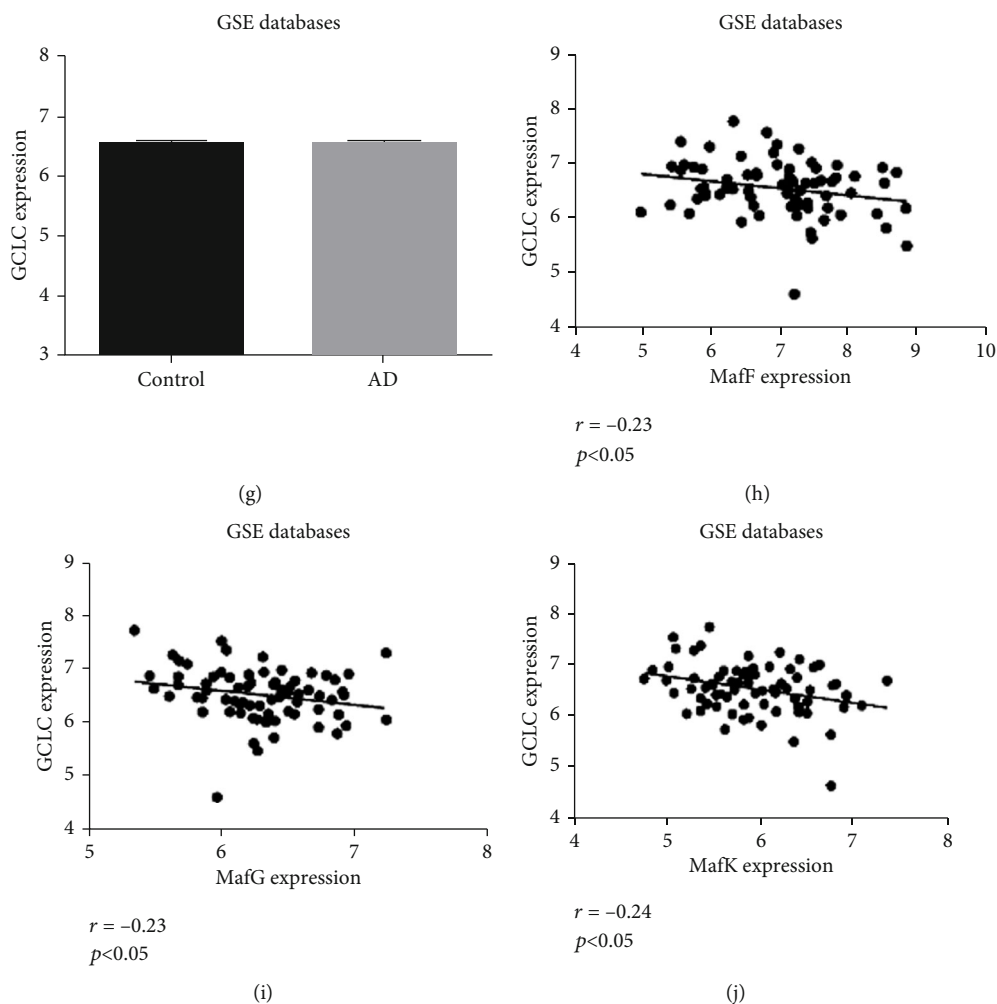


FIGURE 1: Analysis of sMaf expressions in the hippocampus of AD patients. The mRNA expressions of (a) MafF, (b) MafG, and (c) MafK in the hippocampus of AD patient databases. The mRNA expressions of (d) MafF, (e) MafG, and (f) MafK in the hippocampus of AD patients under Braak stages III-IV and V-VI. The correlations between (h) MafF, (i) MafG, and (j) MafK and GCLC in the hippocampus of AD patient databases. All data were presented as mean \pm SEM. * $p < 0.05$ and ** $p < 0.01$ versus the control group or the Braak stage III-IV group.

severely inhibited in AD patients [19]. In APP/PS1 transgenic mice, the expression of the GCLC protein was reduced by 14.89% (Figure 4(a)) and was accompanied with reduced GSH level (Figure 4(b)). In $A\beta$ intrahippocampal injection rat models, GCLC expression was reduced by 18.21% (Figure 4(c)), and GSH was decreased by 25.56% (Figure 4(d)). Similarly, in SH-SY5Y cells treated with $A\beta$, GCLC was reduced by 25.59% (Figure 4(e)) and GSH level was dropped by 11.71% (Figure 4(f)).

To further investigate whether MafF was involved in GSH generation under $A\beta$ treatment, the expression of MafF was knocked down by MafF siRNA transfection in the *in vitro* study. MafF silencing did not affect the expressions of MafG and MafK (Figure 4(g)). GSH level was increased under $A\beta$ treatment for 6h, but this increase was suppressed when MafF was knocked down (Figure 4(h)). The expression of MafF was closely related to the production of GSH under $A\beta$ treatment. These results consistently suggested that MafF might be involved in the oxidative stress caused by $A\beta$.

3.5. MafF Was More Susceptible to $A\beta$ -Induced Oxidative Stress. Furthermore, to investigate the specific effects of $A\beta$ -induced oxidative stress on the expressions of sMafs, three different cell lines (including SH-SY5Y, HepG2, and A549) were used in the *in vitro* studies. First, we tested the constitutive expressions of MafF, MafG, and MafK mRNAs in the three cell lines. MafF, MafG, and MafK expressions were the highest in A549 cells (Figures 5(a)–5(c)). MafF expression was the lowest in SH-SY5Y cells while MafG was the lowest in HepG2 cells (Figures 5(a) and 5(b)). To determine the optimal concentration of $A\beta$ in cell culture, we titrated the toxic effects of $A\beta$ (Supplement Figure S1). MafF was increased by 143.99% after $A\beta$ treatment in HepG2 cells (Figure 5(d)), whereas no significant changes were observed in the expressions of MafG and MafK. None of the protein expressions of the sMafs was significantly affected in A549 cells (Figure 5(e)). In SH-SY5Y cells, only MafF showed an increase under $A\beta$ treatment (Figure 3(c)). These results suggested that MafF might be more susceptible to $A\beta$.

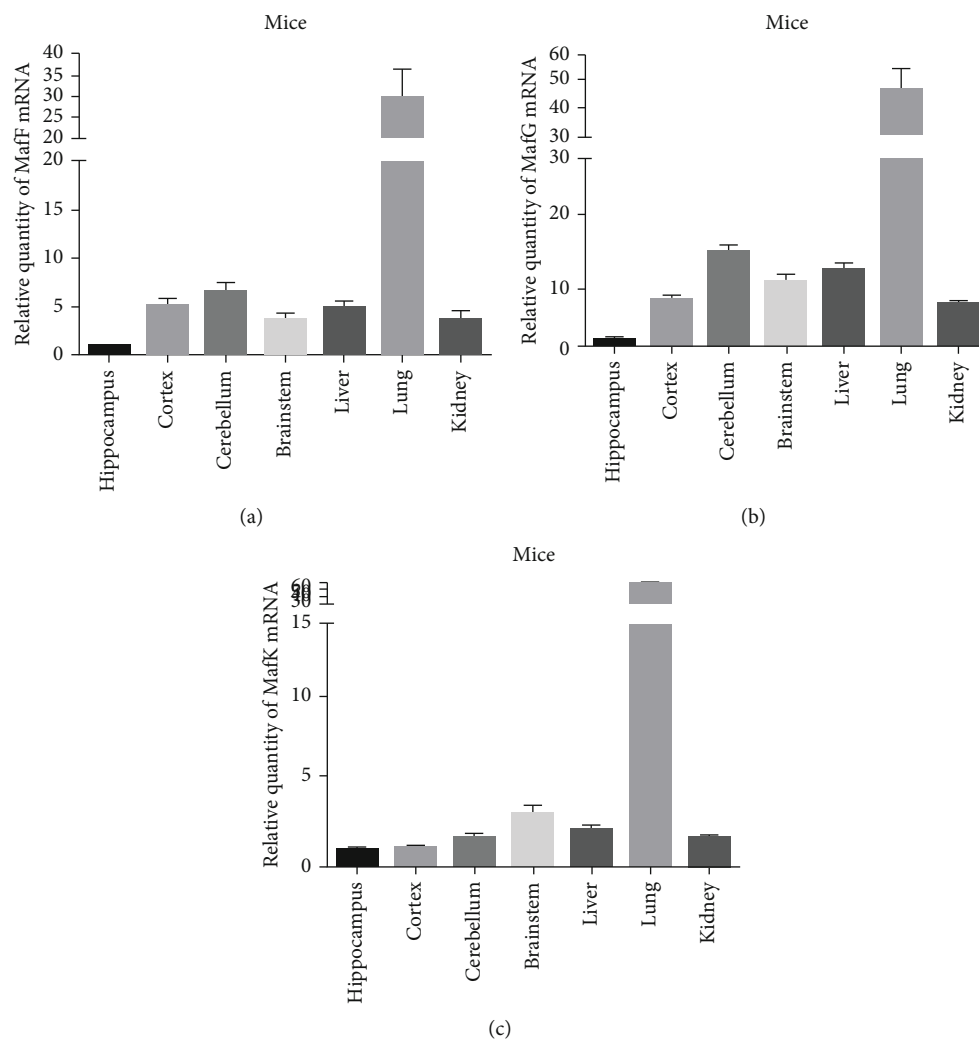


FIGURE 2: Constitutive expressions of sMafs in different tissues. The mRNA expressions of (a) MafF, (b) MafG, and (c) MafK in the brain (hippocampus, cerebral cortex, cerebellum, and brainstem), liver, lung, and kidney. The relative expressions of sMafs were normalized to GAPDH ($n = 3$). All data were presented as mean \pm SEM.

A strong oxidizing agent, H_2O_2 , is usually used as a non-specific oxidative stress inducer. We treated all three cell lines with H_2O_2 for 24 h. The applied concentrations of H_2O_2 were determined by CCK8 assay (Supplement Fig. S2). MafF was upregulated by 69.34% in SH-SY5Y cells (Figure 5(f)), while MafG and MafK remained unchanged. In HepG2 cells, MafF and MafG levels increased by 1.81-fold and 39.8%, respectively (Figure 5(g)). In A549 cells, similar to HepG2 cells, MafF and MafG levels increased by 3.75-fold and 1.31-fold, respectively, while MafK remained unchanged (Figure 5(h)). These data indicated that the expressions of sMafs are oxidative factor-specific.

4. Discussion

MafF, MafG, and MafK are conserved among vertebrates, including humans, mice, and rats [3]. sMaf triple-knockout mice are embryonic lethal, indicating that sMafs are indispensable during development [30]. MafF, MafG, and MafK are expressed broadly in various tissues. In this study, the

tissue-specific expression profiles of the three sMaf genes were detected, which were in keeping with the reported results in mice [31]. In mouse, each sMaf gene harbors multiple first exons, which partly contribute to their tissue-specific or stimulus-specific expression patterns [3]. To our knowledge, here we for the first time reported differential expressions of sMafs in different brain regions of the mouse. The expressions of the three sMaf genes were the lowest in the hippocampus. sMafs participate in the development of diseases by affecting the level of oxidative stress. Postmortem analyses of the brain of patients with AD have documented impaired antioxidant defenses with reduction of GSH [32]. However, some postmortem studies reported elevation or no changes of GSH levels. These inconsistent results may be due to the heterogeneity of the disease stages in patients enrolled in AD [33, 34], which may also be the reason why no changes of GCLC expression in the AD patients enrolled in the studies reported in GSE databases. The growing recognition of the role of low GSH levels in AD supports the use of this characteristic as a biomarker [35]. Our present study

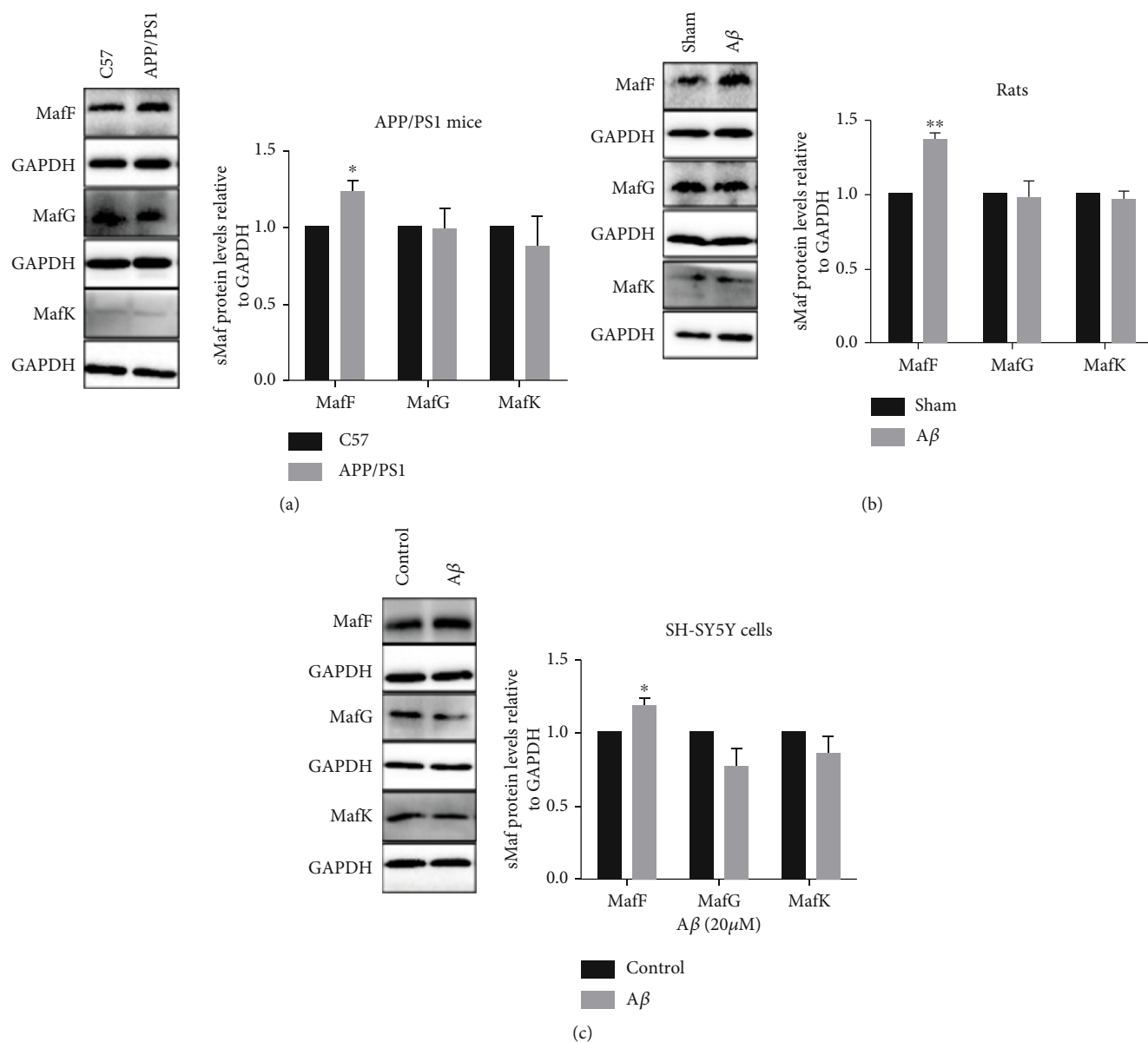


FIGURE 3: MafF expression was increased in response to A β -induced oxidative injury. The protein expressions of MafF, MafG, and MafK in the (a) hippocampus from APP/PS1 mice and in the (b) hippocampus from SD rats after A β injection and in (c) SH-SY5Y cells treated with A β (20 μ M, 48 h) ($n = 3 - 5$). The relative expressions of proteins were normalized to GAPDH. All data were presented as mean \pm SEM; * $p < 0.05$ and ** $p < 0.01$ versus the C57 group, the sham group, or the control group.

revealed that A β treatment lowers the levels of GCLC and GSH, suggesting that A β -induced oxidative injuries played a key role in the development of AD. The results of data analysis from the AD patient databases show that all sMafs are negatively correlated with the expression of GCLC, which matches the capabilities of sMafs that they all can form homodimers to inhibit the expression of downstream GCLC [36]. However, only MafF expression is increased either in data analysis from AD patient databases or in the studies from *in vivo* and *in vitro*. Although sMafs have highly similar structures, they have distinctive functions. Torocsik et al. reported that MafK plays a crucial role in neurite outgrowth and maintenance, while MafG does not have this effect. MafF plays a crucial role in neuronal differentiation via abating epi-

dermal growth factor- (EGF-) induced MAPK signaling [37]. In Parkinson's disease, MafF is differentially regulated in olfactory neurosphere-derived cells [38]. Our results suggest that only MafF is involved in A β -induced inhibition of oxidative stress. Massrieh et al. reported that MafF can be induced by interleukin-1 beta (IL-1 β) and tumor necrosis factor (TNF) in myometrial cells, while MafG and MafK genes are not modulated by these cytokines [39]. Our earlier experiments confirmed that the levels of TNF- α and IL-1 β in the hippocampus were significantly increased in A β intrahippocampal injection rat models, as well as in cultured cells treated with A β . We propose that the increases of TNF- α and IL-1 β could lead to high expression of MafF under A β treatment, but the regulatory mechanisms of sMaf

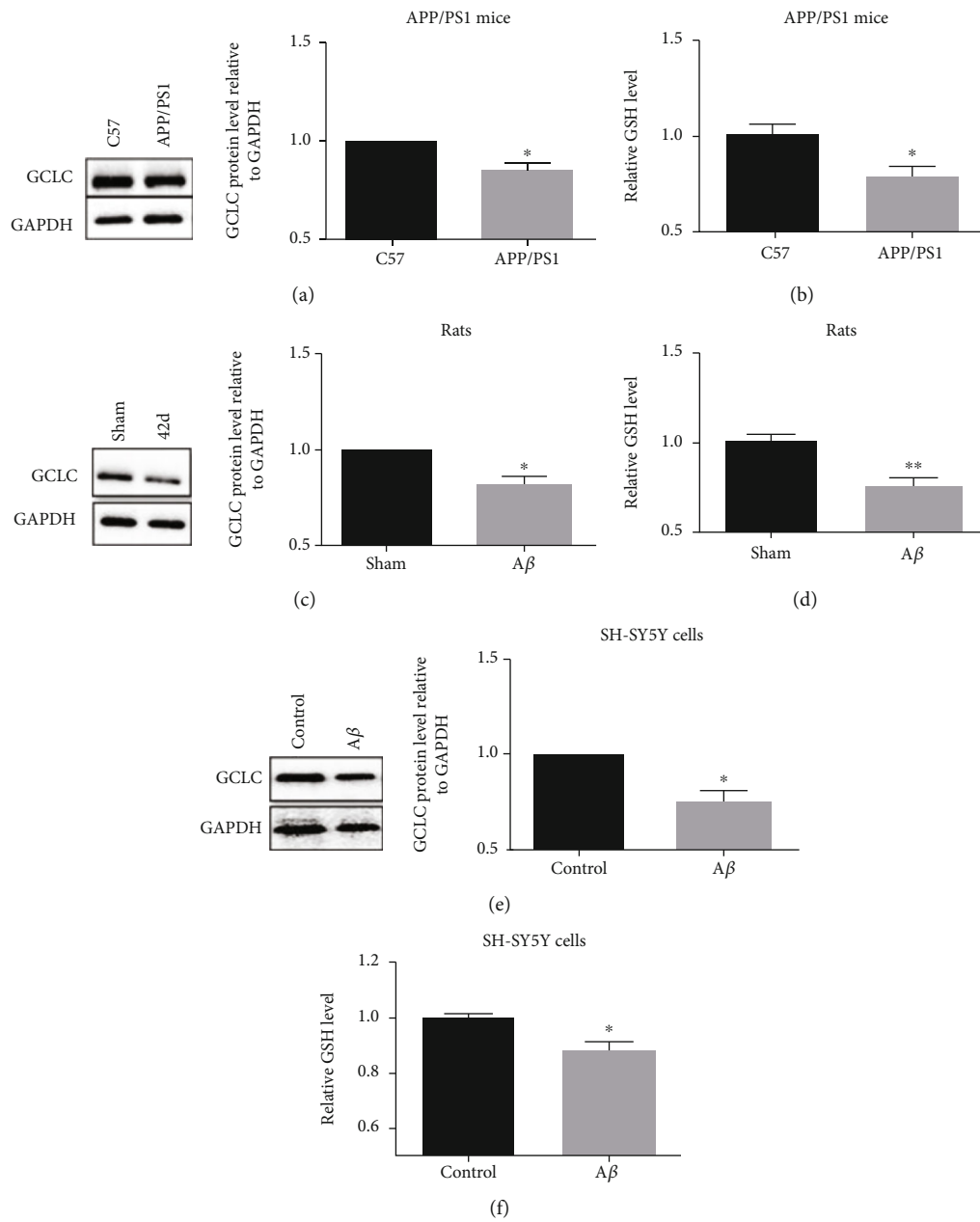


FIGURE 4: Continued.

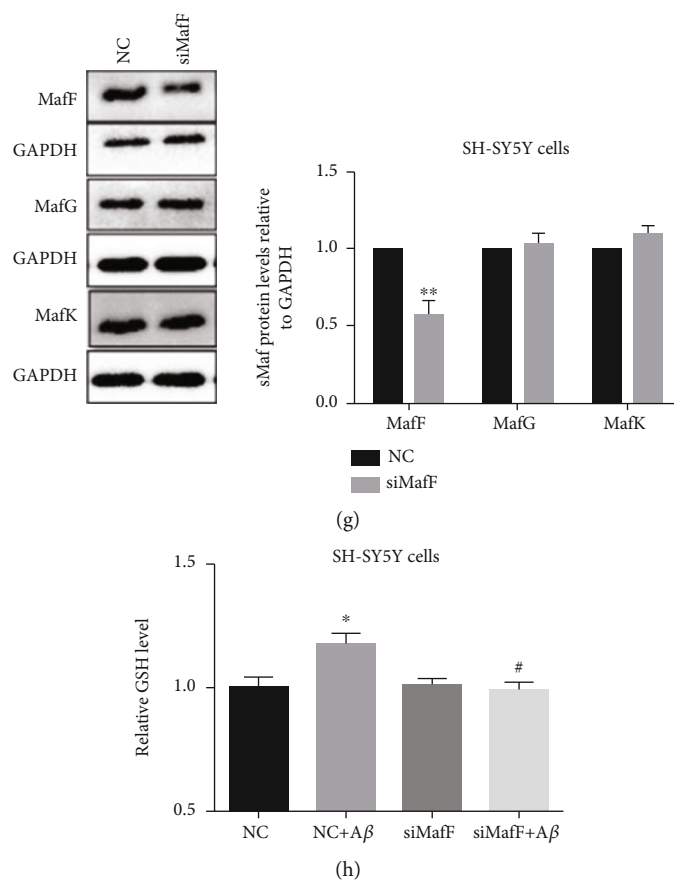


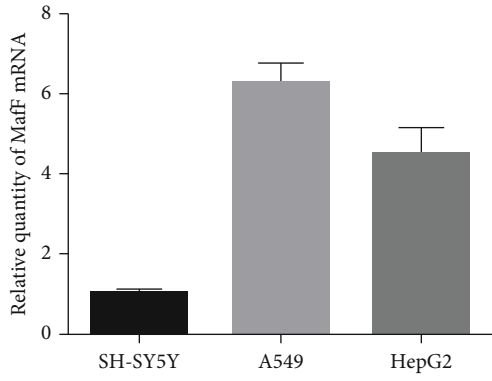
FIGURE 4: MafF expression participated in the oxidative stress caused by $A\beta$. The protein expressions of GCLC in the (a) hippocampus from APP/PS1 mice and in the (c) hippocampus from SD rats after $A\beta$ injection and in (e) SH-SY5Y cells treated with $A\beta$ ($20 \mu\text{M}$, 48 h). The GSH levels in the (b) hippocampus from APP/PS1 mice and in the (d) hippocampus from SD rats after $A\beta$ injection and in (f) SH-SY5Y cells treated with $A\beta$ ($20 \mu\text{M}$, 48 h). The protein expressions of MafF, MafG, and MafK in SH-SY5Y cells transfected with MafF siRNA for 48 h (g). GSH level in SH-SY5Y cells transfected with MafF siRNA (10 nM) for 48 h with or without $A\beta$ ($20 \mu\text{M}$) treatment (6 h) (h) ($n = 3 - 7$). The relative expressions of proteins were normalized to GAPDH. All data were presented as mean \pm SEM; * $p < 0.05$ and ** $p < 0.01$ versus the C57 group, the sham group, the control group, or the NC group; # $p < 0.05$ versus the NC+A β group.

expressions need further investigation. Some peripheral biomarkers of inflammation and oxidative stress such as monomeric c-reactive protein, matrix metalloproteinases, and neutrophil-to-lymphocyte ratio have been already shown to be significantly associated with the course of disorders affecting the brain [40–43]. In the future, the expression of MafF and its relationship with peripheral biomarkers can be detected in animal models and patients at different stages of AD, and this would allow identification of a potential easy way to stage and monitor AD progression in clinical practice.

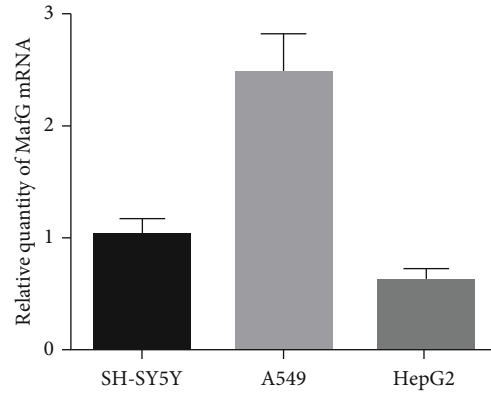
sMafs can act as transcriptional activators when they form heterodimers with Nrf2, but act as repressors when they form homodimers among themselves [36, 44, 45]. In previous studies, we found that the changes of GSH levels were varied under different time points of $A\beta$ treatment. The level of GSH was increased at the short-term treatment of $A\beta$ (6 h) and decreased at the long-term treatment (48 h). We speculate that the short-term treatment of $A\beta$ increases heterodimer formation between MafF and Nrf2 and promotes the transcription of target genes, whereas the long-term treatment enhances MafF

expression and promotes the formation of homodimeric repressors. GSH level increased under short-term treatment of $A\beta$. MafF knockdown suppressed this increase of GSH induced by $A\beta$, suggesting that MafF contributed to this antioxidative pathway. Moreover, MafF knockdown had no effect on the expression of MafG and MafK, which suggested that there was no complementarity between the three sMaf proteins. In addition, it has been reported that the formation of sMaf heterodimers depends on the levels of SUMOylation; it can promote the formation of sMaf heterodimers [46, 47]. Furthermore, the synthesis of GSH also depends on the supply of its substrate, such as cysteine.

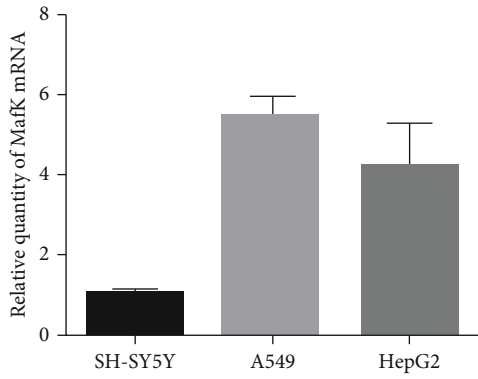
According to the NCBI Reference Sequence (Ref Seq) and UCSC EST databases, human sMaf genes also have multiple alternative first exons. MafF, MafG, and MafK are expressed broadly in various tissues, but each sMaf gene has a distinctive expression profile [3]. We found that the expression patterns of the sMaf genes across different human cell lines were different. Circulating $A\beta$ is mainly cleared by degradation in hepatocytes. Liver tissues from AD patients contain less $A\beta$ than those from healthy



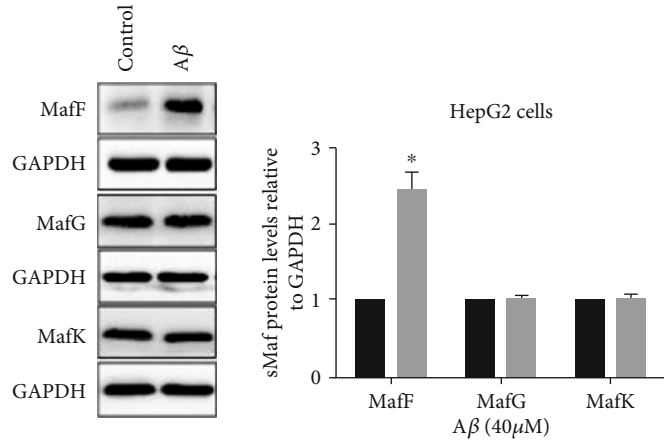
(a)



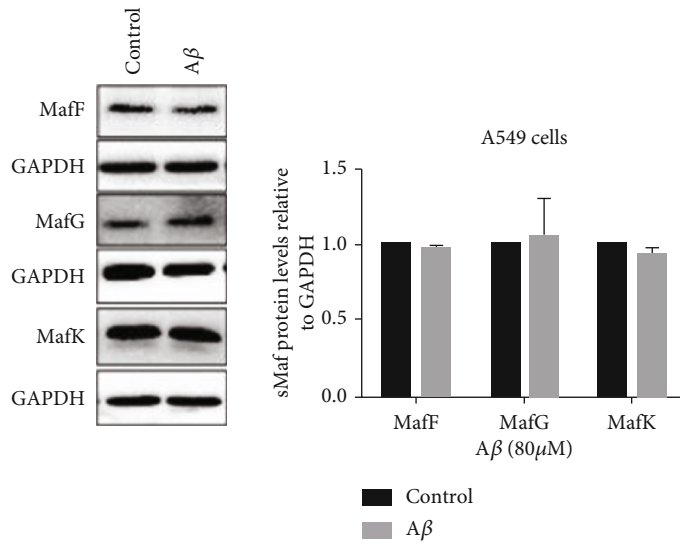
(b)



(c)



(d)



(e)

FIGURE 5: Continued.

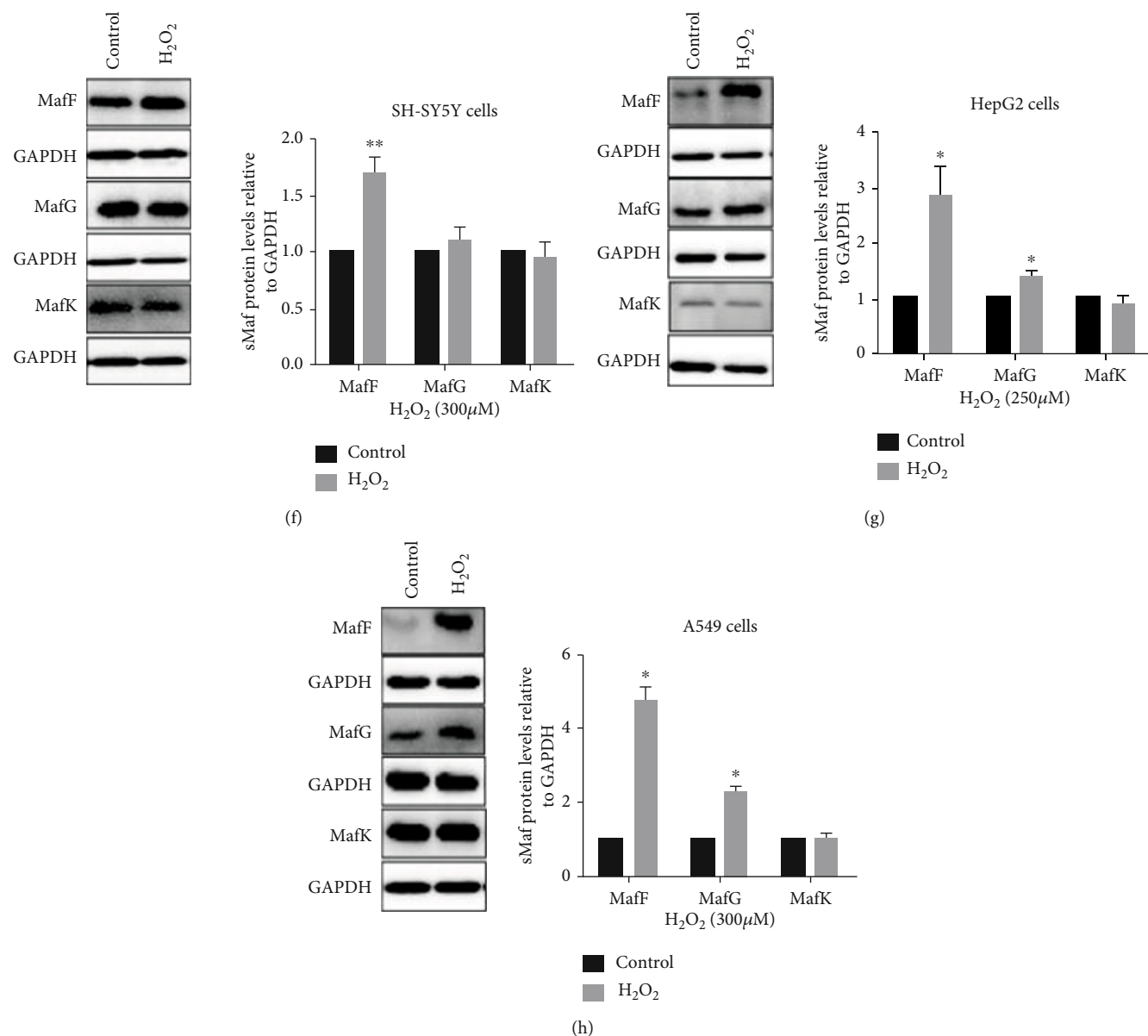


FIGURE 5: The expressions of sMafs in basal or under A β /H₂O₂ treatment in different cell lines. The constitutive expressions of (a) MafF, (b) MafG, and (c) MafK in SH-SY5Y cells, HepG2 cells, and A549 cells. The protein levels of MafF, MafG, and MafK in (f) SH-SY5Y cells, (d, g) HepG2 cells, and (e, h) A549 cells treated with A β for 48 h or H₂O₂ for 24 h ($n = 3 - 5$). The relative expressions of sMafs were normalized to β -actin/GAPDH. All data were presented as mean \pm SEM; * $p < 0.05$ and ** $p < 0.01$ versus the control group.

individuals, which implies that the A β -clearance function of the liver is compromised in AD patients [48]. We observed a significant increase in MafF in HepG2 cells stimulated by A β . This may cause inhibition of the antioxidant capacity of liver cells. Pavliukeviciene et al. reported that A β oligomers inhibit the growth of A549 cells [49]. We also found that high concentrations of A β can significantly reduce the activity of A549 cells, but we did not observe expression changes of sMafs in A549 cell lines caused by A β . H₂O₂ is widely used as an oxidizing agent for its strong oxidation ability. A β can trigger the production of reactive oxygen species (ROS) as well as the accumulation of H₂O₂. Godoy et al. reported that quercetin completely prevents neuronal loss, ROS increase, and

mitochondrial impairment in neurons exposed to H₂O₂. However, A β -induced neurotoxic effects are only partially prevented by coincubation with quercetin, which suggests that amyloid species induce neuronal damage via additional pathways [50]. Given the variability of the changes in sMaf expressions induced by A β and H₂O₂ across different cell lines, it is likely that the modulation of sMaf responses by these treatments is multifactorial. As general mechanisms, we propose that only MafF intervenes in A β -induced oxidative stress responses, while MafF and MafG are involved in oxidative stress responses caused by H₂O₂. These new hypotheses have medical implications and call for further research on the functions and regulations of sMafs. In clinical aspect, the occurrence of AD

can be found by detecting the expression of MafF, and the ability of antioxidative stress can be enhanced by targeting the expression of MafF protein, thus inhibiting the further progress of AD.

5. Conclusion

In summary, sMafs have distinctive expression profiles in different tissues. MafF is involved in A β -induced oxidative stress and antioxidative pathways. The role of MafF in AD deserves further research as MafF might represent a target for AD therapy.

Data Availability

Transcriptomic data from 74 AD patients and 66 controls were collected from the databases GSE29378 (<https://www.ncbi.nlm.nih.gov/geo/query/acc.cgi?acc=GSE29378>), GSE36980 (<https://www.ncbi.nlm.nih.gov/geo/query/acc.cgi?acc=GSE36980>), GSE28146 (<https://www.ncbi.nlm.nih.gov/geo/query/acc.cgi?acc=GSE28146>), GSE48350 (<https://www.ncbi.nlm.nih.gov/geo/query/acc.cgi?acc=GSE48350>), and GSE5281 (<https://www.ncbi.nlm.nih.gov/geo/query/acc.cgi?acc=GSE5281>). The cross-platform normalized data were downloaded from AlzData database. The clinical information related to the samples was provided in Supplement Table S1.

Conflicts of Interest

There is no conflict of interest in this manuscript.

Acknowledgments

This work was supported by the National Natural Science Foundation of China (81870827). We thank the GSE29378, GSE36980, GSE28146, GSE48350, and GSE5281 and the AlzData databases for sharing large amounts of data.

Supplementary Materials

Supplement Table S1: AD patient information in databases. Figure S1: the cell viability under A β treatment in different cell lines. Figure S2: the cell viability under H₂O₂ treatment in different cell lines. (*Supplementary Materials*)

References

- [1] M. Nishizawa, K. Kataoka, N. Goto, K. T. Fujiwara, and S. Kawai, "v-maf, a viral oncogene that encodes a "leucine zipper" motif," *Proceedings of the National Academy of Sciences*, vol. 86, no. 20, pp. 7711–7715, 1989.
- [2] C. Vinson, A. Acharya, and E. J. Taparowsky, "Deciphering B-ZIP transcription factor interactions in vitro and in vivo," *Biochimica et Biophysica Acta (BBA) - Gene Structure and Expression*, vol. 1759, no. 1–2, pp. 4–12, 2006.
- [3] F. Katsuoka and M. Yamamoto, "Small Maf proteins (MafF, MafG, MafK): history, structure and function," *Gene*, vol. 586, no. 2, pp. 197–205, 2016.
- [4] M. B. Kannan, V. Solovieva, and V. Blank, "The small MAF transcription factors MAFF, MAFG and MAFK: current knowledge and perspectives," *Biochimica et Biophysica Acta (BBA) - Molecular Cell Research*, vol. 1823, no. 10, pp. 1841–1846, 2012.
- [5] M. Nezu and N. Suzuki, "Roles of Nrf2 in protecting the kidney from oxidative damage," *International Journal of Molecular Sciences*, vol. 21, no. 8, p. 2951, 2020.
- [6] Z. Guo and Z. Mo, "Keap1-Nrf2 signaling pathway in angiogenesis and vascular diseases," *Journal of Tissue Engineering and Regenerative Medicine*, vol. 14, no. 6, pp. 869–883, 2020.
- [7] L.-C. Chang, C.-W. Fan, W.-K. Tseng et al., "The ratio of Hmox1/Nrf2 mRNA level in the tumor tissue is a predictor of distant Metastasis in colorectal cancer," *Disease Markers*, vol. 2016, Article ID 8143465, 6 pages, 2016.
- [8] I. Bellezza, I. Giambanco, A. Minelli, and R. Donato, "Nrf2-Keap1 signaling in oxidative and reductive stress," *Biochimica et Biophysica Acta (BBA) - Molecular Cell Research*, vol. 1865, no. 5, pp. 721–733, 2018.
- [9] A. Otsuki, M. Suzuki, F. Katsuoka et al., "Unique cistrome defined as CsMBE is strictly required for Nrf2-sMaf heterodimer function in cytoprotection," *Free Radical Biology & Medicine*, vol. 91, pp. 45–57, 2016.
- [10] J. A. Moran, E. L. Dahl, and R. T. Mulcahy, "Differential induction of maff, mafg and mafk expression by electrophile-response-element activators," *The Biochemical Journal*, vol. 361, no. 2, pp. 371–377, 2002.
- [11] Q. Wang, W. X. Li, S. X. Dai et al., "Meta-analysis of Parkinson's disease and Alzheimer's disease revealed commonly impaired pathways and dysregulation of NRF2-dependent genes," *Journal of Alzheimer's Disease*, vol. 56, no. 4, pp. 1525–1539, 2017.
- [12] A. Martínez-Hernández, H. Gutierrez-Malacatt, K. Carrillo-Sánchez et al., "Small MAF genes variants and chronic myeloid leukemia," *European Journal of Haematology*, vol. 92, no. 1, pp. 35–41, 2014.
- [13] H. Shimohata, K. Yoh, A. Fujita et al., "MafA-deficient and beta cell-specific MafK-overexpressing hybrid transgenic mice develop human-like severe diabetic nephropathy," *Biochemical and Biophysical Research Communications*, vol. 389, no. 2, pp. 235–240, 2009.
- [14] X. Wang, B. N. Chorley, G. S. Pittman et al., "Genetic variation and antioxidant response gene expression in the bronchial airway epithelium of smokers at risk for lung cancer," *PLoS One*, vol. 5, no. 8, article e11934, 2010.
- [15] T. Liu, H. Yang, W. Fan et al., "Mechanisms of MAFG dysregulation in cholestatic liver injury and development of liver cancer," *Gastroenterology*, vol. 155, no. 2, pp. 557–571.e14, 2018, e514.
- [16] R. L. Nussbaum and C. E. Ellis, "Alzheimer's disease and Parkinson's disease," *The New England Journal of Medicine*, vol. 348, no. 14, pp. 1356–1364, 2003.
- [17] T. Jiang, Q. Sun, and S. Chen, "Oxidative stress: a major pathogenesis and potential therapeutic target of antioxidative agents in Parkinson's disease and Alzheimer's disease," *Progress in Neurobiology*, vol. 147, pp. 1–19, 2016.
- [18] G. Zuliani, A. Passaro, C. Bosi et al., "Testing a combination of markers of systemic redox status as a possible tool for the diagnosis of late onset Alzheimer's disease," *Disease Markers*, vol. 2018, Article ID 2576026, 9 pages, 2018.

- [19] J. Tong, P. S. Fitzmaurice, A. Moszczynska et al., "Do glutathione levels decline in aging human brain?," *Free Radical Biology & Medicine*, vol. 93, pp. 110–117, 2016.
- [20] D. A. Butterfield and D. Boyd-Kimball, "Oxidative stress, amyloid- β peptide, and altered key molecular pathways in the pathogenesis and progression of Alzheimer's disease," *Journal of Alzheimer's Disease*, vol. 62, no. 3, pp. 1345–1367, 2018.
- [21] S. Dong, X. Huang, J. Zhen et al., "Dietary vitamin E status dictates oxidative stress outcomes by modulating effects of fish oil supplementation in Alzheimer disease model APPswe/PS1dE9 mice," *Molecular Neurobiology*, vol. 55, no. 12, pp. 9204–9219, 2018.
- [22] M. Hokama, S. Oka, J. Leon et al., "Altered expression of diabetes-related genes in Alzheimer's disease brains: the Hisayama study," *Cerebral Cortex*, vol. 24, no. 9, pp. 2476–2488, 2014.
- [23] J. A. Miller, R. L. Woltjer, J. M. Goodenbour, S. Horvath, and D. H. Geschwind, "Genes and pathways underlying regional and cell type changes in Alzheimer's disease," *Genome Medicine*, vol. 5, no. 5, p. 48, 2013.
- [24] M. Xu, D. F. Zhang, R. Luo et al., "A systematic integrated analysis of brain expression profiles reveals YAP1 and other prioritized hub genes as important upstream regulators in Alzheimer's disease," *Alzheimers Dement*, vol. 14, no. 2, pp. 215–229, 2018.
- [25] E. M. Blalock, H. M. Buechel, J. Popovic, J. W. Geddes, and P. W. Landfield, "Microarray analyses of laser-captured hippocampus reveal distinct gray and white matter signatures associated with incipient Alzheimer's disease," *Journal of Chemical Neuroanatomy*, vol. 42, no. 2, pp. 118–126, 2011.
- [26] N. C. Berchtold, D. H. Cribbs, P. D. Coleman et al., "Gene expression changes in the course of normal brain aging are sexually dimorphic," *Proceedings of the National Academy of Sciences of the United States of America*, vol. 105, no. 40, pp. 15605–15610, 2008.
- [27] W. S. Liang, E. M. Reiman, J. Valla et al., "Alzheimer's disease is associated with reduced expression of energy metabolism genes in posterior cingulate neurons," *Proceedings of the National Academy of Sciences of the United States of America*, vol. 105, no. 11, pp. 4441–4446, 2008.
- [28] D. Cao, J. Cui, D. Cao et al., "S-Adenosylmethionine reduces the inhibitory effect of A β on BDNF expression through decreasing methylation level of BDNF exon IV in rats," *Biochemical and Biophysical Research Communications*, vol. 495, no. 4, pp. 2609–2615, 2018.
- [29] X. Gu, J. Sun, S. Li, X. Wu, and L. Li, "Oxidative stress induces DNA demethylation and histone acetylation in SH-SY5Y cells: potential epigenetic mechanisms in gene transcription in A β production," *Neurobiology of Aging*, vol. 34, no. 4, pp. 1069–1079, 2013.
- [30] H. Yamazaki, F. Katsuoka, H. Motohashi, J. D. Engel, and M. Yamamoto, "Embryonic lethality and fetal liver apoptosis in mice lacking all three small Maf proteins," *Molecular and Cellular Biology*, vol. 32, no. 4, pp. 808–816, 2012.
- [31] K. Onodera, J. A. Shavit, H. Motohashi et al., "Characterization of the murine mafF gene," *Journal of Biological Chemistry*, vol. 274, no. 30, pp. 21162–21169, 1999.
- [32] C. Venkateshappa, G. Harish, A. Mahadevan, M. M. Srinivas Bharath, and S. K. Shankar, "Elevated oxidative stress and decreased antioxidant function in the human hippocampus and frontal cortex with increasing age: implications for neurodegeneration in Alzheimer's disease," *Neurochemical Research*, vol. 37, no. 8, pp. 1601–1614, 2012.
- [33] T. L. Perry, V. W. Yong, C. Bergeron, S. Hansen, and K. Jones, "Amino acids, glutathione, and glutathione transferase activity in the brains of patients with Alzheimer's disease," *Annals of Neurology*, vol. 21, no. 4, pp. 331–336, 1987.
- [34] J. D. Adams, L. K. Klaidman, I. N. Odunze, H. C. Shen, and C. A. Miller, "Alzheimer's and Parkinson's disease," *Molecular and Chemical Neuropathology*, vol. 14, no. 3, pp. 213–226, 1991.
- [35] P. K. Mandal, S. Saharan, M. Tripathi, and G. Murari, "Brain glutathione levels—a novel biomarker for mild cognitive impairment and Alzheimer's disease," *Biological Psychiatry*, vol. 78, no. 10, pp. 702–710, 2015.
- [36] S. Dhakshinamoorthy and A. K. Jaiswal, "Small maf (MafG and MafK) proteins negatively regulate antioxidant response element-mediated expression and antioxidant induction of the NAD(P)H:quinone oxidoreductase1 gene," *The Journal of Biological Chemistry*, vol. 275, no. 51, pp. 40134–40141, 2000.
- [37] I. Amit, A. Citri, T. Shay et al., "A module of negative feedback regulators defines growth factor signaling," *Nature Genetics*, vol. 39, no. 4, pp. 503–512, 2007.
- [38] A. L. Cook, A. M. Vitale, S. Ravishankar et al., "NRF2 activation restores disease related metabolic deficiencies in olfactory neurosphere-derived cells from patients with sporadic Parkinson's disease," *PLoS One*, vol. 6, no. 7, article e21907, 2011.
- [39] W. Massrieh, A. Derjuga, F. Doualla-Bell, C. Y. Ku, B. M. Sanborn, and V. Blank, "Regulation of the MAFF transcription factor by proinflammatory cytokines in myometrial cells," *Biology of Reproduction*, vol. 74, no. 4, pp. 699–705, 2006.
- [40] M. Di Napoli, M. Slevin, A. Popa-Wagner, P. Singh, S. Lattanzi, and A. A. Divani, "Monomeric C-reactive protein and cerebral hemorrhage: from bench to bedside," *Frontiers in Immunology*, vol. 9, p. 1921, 2018.
- [41] S. Lattanzi, M. Di Napoli, S. Ricci, and A. A. Divani, "Matrix metalloproteinases in acute intracerebral hemorrhage," *Neurotherapeutics*, vol. 17, no. 2, pp. 484–496, 2020.
- [42] S. Lattanzi, F. Brigo, E. Trinka, C. Cagnetti, M. di Napoli, and M. Silvestrini, "Neutrophil-to-lymphocyte ratio in acute cerebral hemorrhage: a system review," *Translational Stroke Research*, vol. 10, no. 2, pp. 137–145, 2019.
- [43] J. Long, G. Pan, E. Ifeachor, R. Belshaw, and X. Li, "Discovery of novel biomarkers for Alzheimer's disease from blood," *Disease Markers*, vol. 2016, Article ID 4250480, 9 pages, 2016.
- [44] V. Blank and N. C. Andrews, "The Maf transcription factors: regulators of differentiation," *Trends in Biochemical Sciences*, vol. 22, no. 11, pp. 437–441, 1997.
- [45] K. Igarashi, K. Kataokata, K. Itoh, N. Hayashi, M. Nishizawa, and M. Yamamoto, "Regulation of transcription by dimerization of erythroid factor NF-E2 p45 with small Maf proteins," *Nature*, vol. 367, no. 6463, pp. 568–572, 1994.
- [46] M. L. Tomasi, M. Ryoo, H. Yang, A. Iglesias Ara, K. S. Ko, and S. C. Lu, "Molecular mechanisms of lipopolysaccharide-mediated inhibition of glutathione synthesis in mice," *Free Radical Biology & Medicine*, vol. 68, pp. 148–158, 2014.
- [47] K. Ramani, M. L. Tomasi, H. Yang, K. Ko, and S. C. Lu, "Mechanism and significance of changes in glutamate-cysteine ligase expression during hepatic fibrogenesis," *The Journal*

of Biological Chemistry, vol. 287, no. 43, pp. 36341–36355, 2012.

- [48] M. Ankarcona, B. Winblad, C. Monteiro et al., “Current and future treatment of amyloid diseases,” *Journal of Internal Medicine*, vol. 280, no. 2, pp. 177–202, 2016.
- [49] B. Pavliukeviciene, A. Zentelyte, M. Jankunec et al., “Amyloid β oligomers inhibit growth of human cancer cells,” *PLoS One*, vol. 14, no. 9, article e0221563, 2019.
- [50] J. A. Godoy, C. B. Lindsay, R. A. Quintanilla, F. J. Carvajal, W. Cerpa, and N. C. Inestrosa, “Quercetin exerts differential neuroprotective effects against H_2O_2 and $A\beta$ aggregates in hippocampal neurons: the role of mitochondria,” *Molecular Neurobiology*, vol. 54, no. 9, pp. 7116–7128, 2017.

Research Article

Prognostic Significance of Homocysteine Level on Neurological Outcome in Brain Arteriovenous Malformations

Fa Lin ^{1,2,3,4}, Chaofan Zeng ^{1,2,3,4}, Peicong Ge ^{1,2,3,4}, Dong Zhang,^{1,2,3,4}
Shuo Wang ^{1,2,3,4} and Jizong Zhao ^{1,2,3,4,5}

¹Department of Neurosurgery, Beijing Tiantan Hospital, Capital Medical University, No. 119 South Fourth Ring Rd West, Fengtai District, Beijing 100070, China

²China National Clinical Research Center for Neurological Diseases, Beijing 100070, China

³Center of Stroke, Beijing Institute for Brain Disorders, Beijing 100070, China

⁴Beijing Key Laboratory of Translational Medicine for Cerebrovascular Disease, Beijing 100070, China

⁵Savaid Medical School, University of the Chinese Academy of Sciences, Beijing, China

Correspondence should be addressed to Jizong Zhao; zhaojz205@163.com

Received 15 October 2020; Revised 9 November 2020; Accepted 11 November 2020; Published 30 November 2020

Academic Editor: Wen-Jun Tu

Copyright © 2020 Fa Lin et al. This is an open access article distributed under the Creative Commons Attribution License, which permits unrestricted use, distribution, and reproduction in any medium, provided the original work is properly cited.

Objective. We aimed to investigate the serum homocysteine (Hcy) level in patients with brain arteriovenous malformation (bAVM) and their impact on neurological outcome during hospitalization. **Method.** We retrospectively reviewed patients diagnosed with bAVMs in Beijing Tiantan Hospital from January 2019 to August 2020. Patients were divided into two groups according to the mRS (modified Rankin Scale) score at discharge. Clinical and laboratory characteristics were compared. Logistic regression analyses were performed to identify the potential risk factors for short-term neurological outcome. **Results.** A total of 175 bAVM patients were enrolled in the study, including 139 patients with favorable outcome (mRS ≤ 2) and 36 patients with unfavorable outcome (mRS > 2). Hyperhomocysteinemia was identified in 32.6% of cases ($n = 57$). Serum Hcy level was related to seizure manifestation ($P = 0.034$) and short-term neurological outcome ($P = 0.027$). Logistic regression analysis showed that serum glucose (OR 1.897, 95% CI 1.115-3.229; $P = 0.018$) and Hcy level (OR 0.838, 95% CI 0.720-0.976; $P = 0.023$) were significantly associated with short-term disability. **Conclusion.** Our results indicated that the lower serum Hcy level is strongly associated with in-hospital unfavorable outcome. Further prospective studies of Hcy natural history and managements in bAVMs are required, which would be valuable for evaluating the disease-modifying efficacy of oral nutritional supplements in bAVM patients.

1. Introduction

Brain arteriovenous malformations (bAVMs) are well known as congenitally abnormal conglomerations of dilated feeding arteries and draining veins without intervening capillary beds [1, 2]. Although bAVM occurs in approximately 15/100,000 persons, it is still the leading cause of hemorrhagic stroke in young people and often results in a high incidence of neurological morbidity and mortality [2]. Prediction of outcomes is mostly based on demographic, clinical, and radiographic markers, while the information on routine laboratory examinations is inadvertently ignored.

Hyperhomocysteinemia (HHcy) is an elevation of serum homocysteine (Hcy) concentration due to the methionine

metabolic disorder [3]. Characterized by the atherogenic and thrombogenic effects, Hcy is recognized as the independent risk factor for the major adverse cardiovascular and cerebrovascular events (MACCEs) and mortality [4, 5]. Apparently, previous studies have focused on hemorrhagic stroke and unfavorable outcomes [5, 6]. Moreover, some studies suggested that Hcy disorders and hemorrhagic bAVMs shared similar underlying mechanisms in terms of hemodynamics [7–9] and molecular abnormalities [10–14]. However, the above-mentioned studies were based on other hemorrhagic subtypes and animal experiments; the clinical significance of Hcy in patients with bAVM has not been discussed yet.

The present study was investigated to take an exploratory look into the association between serum Hcy levels in

patients with bAVM and their impact on neurological outcome during hospitalization.

2. Materials and Methods

2.1. Study Design and Participants. We retrospectively reviewed patients diagnosed with bAVMs at the Department of Neurosurgery, Beijing Tiantan Hospital, from January 2019 to August 2020. The study was approved by the Institutional Review Board of our institution, and informed consent was waived considering the retrospective design of the study.

Among 402 patients with cerebral vascular malformations admitted to our hospital between January 2019 and August 2020, 332 patients were diagnosed with bAVMs using digital subtraction angiography (DSA) or magnetic resonance imaging (MRI). Patients with inadequate laboratory or DSA data were excluded. Finally, a total of 175 patients were included in the study (Figure 1). The enrolled patients were divided into two groups according to the neurological outcome at discharge (Group 1, modified Rankin Scale [mRS] ≤ 2 ; Group 2, mRS > 2).

2.2. Data Collection and Outcome Evaluation. Demographic data, medical and personal history, prior treatments, primary symptoms, bAVM radiographic characteristics, clinical features, laboratory results, and treatment modality were obtained. Medical and personal history including hypertension, diabetes mellitus, hyperlipidemia, cigarette smoking, and alcohol drinking were recorded. The treatment history included embolization, radiosurgery, and microsurgery. Primary symptoms were summarized as hemorrhage, seizure, and neurological dysfunction. Radiographic characteristics included volume of lesion, deep and eloquent location, venous drainage patterns, and associated aneurysms. The AVM volume was calculated by $(a \times b \times c)/2$. Spetzler-Martin (SM) grading scale was evaluated to stratify the bAVMs. The treatment modalities were dichotomized based on the involvement of microsurgery. The clinical status was determined by the mRS score at admission and discharge. Neurological disability (mRS > 2) was defined as the clinical outcome. The neurological assessment at discharge was considered a short-term outcome.

Heart rate and blood pressure were also obtained. Body mass index (BMI) was calculated as $\text{weight (kg)}/[\text{height (m)}]^2$. Fast venous blood samples were collected in the morning after admission for all bAVM patients. Levels of blood glucose, albumin (ALB), creatinine, uric acid (UA), total cholesterol (TC), triglyceride (TG), high-density lipoprotein cholesterol (HDL-C), low-density lipoprotein cholesterol (LDL-C), apolipoprotein A (ApoA), apolipoprotein B (ApoB), and Hcy were measured using enzymatic methods. Serum Hcy $\geq 15.0 \mu\text{mol/L}$ was defined as HHcy [15].

2.3. Statistical Analysis. Categorical variables were expressed as frequencies, and continuous variables were presented with a mean (standard deviation (SD)) or median (interquartile range (IQR)). A chi-square test or Fisher's exact test was performed to compare categorical variables between groups. Continuous variables were compared by two-tailed Student's

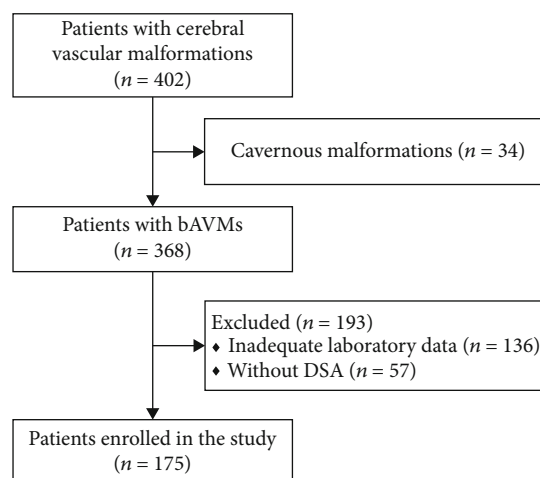


FIGURE 1: Flow diagram of the study participants. bAVMs: brain arteriovenous malformations; DSA: digital subtraction angiography.

t-test or Mann–Whitney *U* test. The association between variables and Hcy quartiles was analyzed using the Cochran–Armitage test for bivariate variables and Spearman's rank correlation test for continuous variables. Logistic regression analyses were conducted to identify the potential risk factors for short-term neurological outcome. Variables achieving $P < 0.10$ in univariate analysis were included in the multivariate analysis. P value < 0.05 was considered statistical significance. Statistical analyses were performed using SPSS 26.0 (IBM, New York, USA).

3. Results

Four hundred and two cerebral vascular malformation patients were identified. After excluding 34 cavernous malformations and 193 patients with incomplete data, a total of 175 bAVM patients were enrolled in our study (Figure 1).

3.1. Baseline Characteristics of bAVM Patients. The baseline characteristics of bAVM patients are shown in Table 1. The mean age at diagnosis was 29.6 years, with a male-to-female ratio of 1.3:1. Thirty-one cases (17.7%) were at cigarette smoking status, and 17 cases (9.7%) were current alcohol abused. Sixty cases (34.3%) had received prior treatments, including embolization in 43 (24.6%), radiosurgery in 12 (6.9%), and microsurgery in 5 (2.9%). Hemorrhage (56.6%) occurred as the most common primary symptom, followed by seizure (20.0%) and neurological dysfunction (17.7%). Poor neurological status (mRS > 2) was observed in 15.4% of cases ($n = 27$) on admission. Twenty-eight cases (16.0%) harbored SM grade IV–V lesions. The average volume of lesions was 8.6 cm^3 . Deep locations were found in 51 cases (29.1%), and eloquent areas were involved in 52.0% of cases ($n = 91$). 34.3% of cases ($n = 60$) had deep venous drainage, and 12.6% of cases ($n = 22$) had associated aneurysms. HHcy was identified in 32.6% of cases ($n = 57$). According to the treatment modalities, microsurgery was involved in 78 cases (44.6%). Compared with Group 1, patients in Group 2 more likely presented with hemorrhage ($P = 0.001$), and exhibited

TABLE 1: Baseline characteristics of bAVM patients between groups.

Variables	Total (n = 175)	Group 1 [#] (n = 139)	Group 2 [#] (n = 36)	P value
Age (y), mean (SD)	29.6 (14.7)	29.9 (14.6)	28.6 (15.1)	0.635
Sex, male (%)	100 (57.1)	78 (56.1)	22 (61.1)	0.589
Medical and personal history (%)				
Hypertension	14 (8.0)	9 (6.5)	5 (13.9)	0.264
Diabetes mellitus	5 (2.9)	3 (2.2)	2 (5.6)	0.597
Hyperlipidemia	1 (0.6)	1 (0.7)	0 (0)	>0.999
Cigarette smoking	31 (17.7)	25 (18.0)	6 (16.7)	0.853
Alcohol drinking	17 (9.7)	13 (9.4)	4 (11.1)	0.999
Prior treatments (%)				
Embolization	43 (24.6)	32 (23.0)	11 (30.6)	0.349
Radiosurgery	12 (6.9)	8 (5.8)	4 (11.1)	0.445
Microsurgery	5 (2.9)	5 (3.6)	0 (0)	0.585
Primary symptom (%)				
Hemorrhage	99 (56.6)	70 (50.4)	29 (80.6)	0.001*
Seizure	35 (20.0)	30 (21.6)	5 (13.9)	0.304
Neurological dysfunction	31 (17.7)	24 (17.3)	7 (19.4)	0.760
Admission mRS > 2 (%)	27 (15.4)	6 (4.3)	21 (58.3)	<0.001*
Radiographic characteristics				
Spetzler-Martin grade (%)				
I-II	91 (52.0)	79 (56.8)	12 (33.3)	0.012*
III	56 (32.0)	41 (29.5)	15 (41.7)	0.163
IV-V	28 (16.0)	19 (13.7)	9 (25.0)	0.098
Volume (cm ³), median (IQR)	8.6 (4.1-25.6)	8.5 (4.1-25.6)	8.7 (4.3-26.5)	0.388
Deep location (%)	51 (29.1)	35 (25.2)	16 (44.4)	0.023*
Eloquent location (%)	91 (52.0)	68 (48.9)	23 (63.9)	0.109
Deep venous drainage (%)	60 (34.3)	42 (30.2)	18 (50.0)	0.026*
Associated aneurysms (%)	22 (12.6)	14 (10.1)	8 (22.2)	0.093
Clinical features, mean (SD)				
Heart rate, bpm	80 (10)	80.3 (9.8)	77.0 (9.3)	0.312
SBP (mm Hg)	120 (19)	119.5 (17.1)	121.4 (25.7)	0.666
DBP (mm Hg)	77 (11)	76.8 (10.4)	80.1 (12.8)	0.162
BMI (kg/m ²)	22.5 (4.5)	22.6 (4.5)	22.2 (4.5)	0.654
Laboratory results, median (IQR)				
Glucose (mmol/L)	4.7 (4.4-5.1)	4.7 (4.4-5.1)	4.9 (4.3-5.2)	0.034*
Albumin (g/L)	43.9 (41.4-46.1)	44.3 (41.4-46.1)	42.5 (41.1-46.2)	0.019*
Creatinine (μmol/L)	58.5 (46.5-68.3)	58.6 (46.5-68.3)	55.7 (46.8-68.2)	0.591
UA (μmol/L)	309.7 (254.9-363.6)	314.0 (254.9-362.2)	302.2 (247.9-362.9)	0.269
TC (mmol/L)	4.2 (3.6-4.8)	4.3 (3.6-4.8)	4.1 (3.6-4.9)	0.072
TG (mmol/L)	1.0 (0.7-1.5)	1.0 (0.7-1.5)	1.0 (0.7-1.5)	0.622
HDL-C (mmol/L)	1.2 (1.0-1.5)	1.2 (1.0-1.5)	1.2 (1.0-1.5)	0.480
LDL-C (mmol/L)	2.6 (2.0-3.1)	2.6 (2.0-3.1)	2.4 (1.9-3.1)	0.191
ApoA (g/L)	1.3 (1.1-1.4)	1.3 (1.1-1.4)	1.2 (1.1-1.4)	0.690
ApoB (g/L)	0.8 (0.7-1.0)	0.8 (0.7-1.0)	0.8 (0.7-1.0)	0.203
Hcy (μmol/L)	12.5 (9.9-16.6)	13.0 (9.9-16.6)	10.2 (9.8-15.9)	0.023*
HHcy (%)	57 (32.6)	49 (35.3)	8 (22.2)	0.137
Treatment modality				0.137
Microsurgery involvement	78 (44.6)	58 (41.7)	20 (55.6)	
Nonmicrosurgery involvement	97 (55.4)	81 (58.3)	16 (44.4)	

bAVM: brain arteriovenous malformation; SD: standard deviation; mRS: modified Rankin Scale; IQR: interquartile range; SBP: systolic blood pressure; DBP: diastolic blood pressure; BMI: body mass index; UA: uric acid; TC: total cholesterol; TG: triglyceride; HDL-C: high-density lipoprotein cholesterol; LDL-C: low-density lipoprotein cholesterol; ApoA: apolipoprotein A; ApoB: apolipoprotein B; Hcy: homocysteine; HHcy: hyperhomocysteinemia. [#]Group 1, modified Rankin Scale [mRS] ≤ 2. Group 2, mRS > 2. *P < 0.05, significant difference.

poor neurological status (mRS > 2) ($P < 0.001$). In terms of the radiographic characteristics, the proportion of low SM grade (I-II) was found a significant difference between groups ($P = 0.012$). Patients with unfavorable outcomes were more located in deep areas ($P = 0.023$) and drained by deep veins ($P = 0.026$). In addition, higher level of glucose ($P = 0.034$), lower level of albumin ($P = 0.019$), and Hcy ($P = 0.023$) were found in Group 2.

3.2. Characteristics of bAVM Patients according to Hcy Quartiles. Clinical variables according to Hcy quartiles are summarized in Table 2. A linear association was observed between Hcy level and male sex ($P < 0.001$). Serum Hcy level was also related to age ($P = 0.011$), cigarette smoking ($P = 0.001$), and seizure manifestation ($P = 0.034$). Furthermore, Hcy was correlated with short-term neurological outcome ($P = 0.027$). Although the hemorrhagic risk was not a significant difference between Hcy quartiles ($P = 0.052$), a relatively lower incidence of rupture occurred in the groups of higher Hcy level (Q1: 61.4%; Q2, 59.1%; Q3, 58.1%; and Q4, 47.7%). Other variables were similar across groups ($P > 0.05$ for all).

3.3. Analysis of Neurological Outcomes. Neurological outcomes of bAVM patients were analyzed. Thirty-six patients (20.6%) were disabled (mRS > 2) at discharge, with no significant difference compared with admission ($P = 0.211$) (Figure 2). No in-hospital mortality occurred during hospitalization. According to the variation of mRS scores, most patients experienced an improved or unchanged neurological status in the short-term (81.7%, $n = 143$).

Risk factors for the neurological outcome of bAVM patients were identified (Table 3). Univariate analysis showed that hemorrhagic presentation, admission mRS score, AVM volume, deep location, deep venous drainage, associated aneurysms, glucose, albumin, TC, and Hcy were related to the neurological outcome. After additionally adjusting for age and male sex, hemorrhagic presentation (OR [odds ratios] 5.360, 95% CI [confidence intervals] 1.208-23.790; $P = 0.027$), admission mRS score (OR 2.225, 95% CI 1.402-3.530; $P = 0.001$), AVM volume (OR 1.024, 95% CI 1.004-1.046; $P = 0.021$), deep venous drainage (OR 8.813, 95% CI 1.965-39.534; $P = 0.004$), associated aneurysms (OR 5.711, 95% CI 1.389-23.488; $P = 0.016$), glucose (OR 1.897, 95% CI 1.115-3.229; $P = 0.018$), and Hcy (OR 0.838, 95% CI 0.720-0.976; $P = 0.023$) were shown to be significantly associated with short-term disability in the multivariate analysis.

4. Discussion

Our retrospective study demonstrated the potential for serum levels of Hcy to serve as an objective biomarker for prognosticating short-term neurological outcomes in patients with bAVMs. The lower serum Hcy level predicted a higher risk of an unfavorable outcome. Furthermore, we identified a positive correlation between HHcy and symptomatic seizures on admission.

Admittedly, previously verified factors, including hemorrhagic presentation, admission mRS score, AVM volume,

deep venous drainage, and associated aneurysms, have been broadly studied [1, 16]. Sometimes, the evaluation between such indicators and prognosis will be subjective. When the classic Spetzler-Martin (SM) grading system [17], supplementary scale [18], and even with evolving fMRI-based HDVL grading scale combined with lesion-to eloquence distance (LED) are added [19], the evaluation becomes accurate but tedious at the same time. And there are some objectively advanced biomarkers, such as S100B, matrix metalloproteinase-9 (MMP-9), interleukin-1 beta (IL-1 β), vascular endothelial growth factor (VEGF), and N6-methyladenosine methyltransferase 3 (METTL3) [12, 20–22], which were proposed to be the predictors for the in-hospital complications and neurological outcomes. However, these indicators were unable to directly provide guidance for clinical practice. The underlying diagnostic and predictable values of laboratory biomarkers routinely examined after admission are required to be further excavated. To our best knowledge, we first associated the serum Hcy level with the short-term neurological outcome. After being adjusted for other known factors, the predicted value would still be significant (OR 0.838, 95% CI 0.720-0.976; $P = 0.023$).

For decades, the abnormal Hcy level was acknowledged as the independent risk factors for the onset of ischemic stroke in several large scale multicenter trials [3, 5, 23, 24]. Afterward, the relationship between hemorrhagic stroke and HHcy has been subsequently studied but reached contrary conclusions. Li et al. found that elevated Hcy was correlated with hemorrhagic stroke by 1.94-fold compared to the controls [5]. Larger hematoma volume in patients with thalamoganglionic intracerebral hemorrhage (ICH) associated with the elevated Hcy level was identified by Hu et al. [25]. Furthermore, Zhang and his colleagues developed a model consisted of Hcy level to identify high-risk groups for predicting recurrent ICH, which can facilitate the pre-emptive clinical intervention [26]. Zhou et al. conducted a meta-analysis including 667 ICH patients and demonstrated that the Hcy level is positively associated with a high risk of ICH [6]. Nevertheless, two cohorts in China found that HHcy correlated with a lower risk of hemorrhagic stroke [27]. For other hemorrhagic subtypes, such as subarachnoid hemorrhage (SAH), researchers gained different findings. In 2001, McEvoy et al. revealed no association between the Hcy level and the etiology of SAH [28]. In favor of the upper conclusion, Grobelny et al. found no correlations between Hcy and delayed cerebral ischemia (DCI), while the gain-of-function polymorphisms of the cystathionine β -synthase (CBS) gene could reduce the risk of DCI after aneurysmal SAH and improve the outcome at discharge [29]. Moreover, the CARAS study showed that increased CBS activity may exert its neuroprotective effects in altering the Hcy level and then improve clinical outcomes [30]. Another gene polymorphism methylenetetrahydrofolate reductase (MTHFR) C677T might contribute to a higher Hcy level to impair the clinical outcomes in patients with SAH [31]. Unlike their predecessors, Dhandapani et al. explored a reverse epidemiology paradox, where the higher Hcy level appears to be a significant association with both survival and favorable neurological outcomes [32].

TABLE 2: Characteristics of bAVM patients according to Hcy quartiles.

Variables	Hcy quartiles ^a (μmol/L)					P trend
	All (n = 175)	Q1 (n = 44)	Q2 (n = 44)	Q3 (n = 43)	Q4 (n = 44)	
Age (y), mean (SD)	29.6 (14.7)	24.0 (15.7)	30.8 (14.2)	34.4 (13.4)	29.3 (13.8)	0.011*
Sex, male (%)	100 (57.1)	13 (29.5)	22 (50.0)	29 (67.4)	36 (81.8)	<0.001*
Medical history (%)						
Hypertension	14 (8.0)	2 (4.5)	2 (4.5)	6 (14.0)	4 (9.1)	0.210
Diabetes mellitus	5 (2.9)	1 (2.3)	1 (2.3)	1 (2.3)	2 (4.5)	0.540
Hyperlipidemia	1 (0.6)	0 (0)	0 (0)	1 (2.3)	0 (0)	0.653
Cigarette smoking	31 (17.7)	1 (2.3)	7 (15.9)	10 (23.3)	13 (29.5)	0.001*
Alcohol drinking	17 (9.7)	0 (0)	4 (9.1)	9 (20.9)	4 (9.1)	0.052
Primary symptom (%)						
Hemorrhage	99 (56.6)	27 (61.4)	26 (59.1)	25 (58.1)	21 (47.7)	0.210
Seizure	35 (20.0)	5 (11.4)	8 (18.2)	9 (20.9)	13 (29.5)	0.034*
Neurological dysfunction	31 (17.7)	9 (20.5)	8 (18.2)	8 (18.6)	6 (13.6)	0.416
Admission mRS > 2 (%)	27 (15.4)	13 (29.5)	3 (6.8)	6 (14.0)	5 (11.4)	0.052
AVM characteristics						
Spetzler-Martin grade (%)						0.885
I-II	91 (52.0)	19 (43.2)	27 (61.4)	23 (53.5)	22 (50.0)	
III	56 (32.0)	17 (38.6)	12 (27.3)	13 (30.2)	14 (31.8)	
IV-V	28 (16.0)	8 (18.2)	5 (11.4)	7 (16.3)	8 (18.2)	
Volume (cm ³), median (IQR)	8.6 (4.1-25.6)	11.4 (5.0-29.7)	7.3 (4.5-18.7)	8.6 (3.1-22.7)	11.5 (4.1-31.8)	0.596
Deep location (%)	51 (29.1)	13 (29.5)	11 (25.0)	12 (27.9)	15 (34.1)	0.338
Eloquent location (%)	91 (52.0)	26 (59.1)	21 (47.7)	23 (53.5)	21 (47.7)	0.400
Deep venous drainage (%)	60 (34.3)	15 (34.1)	13 (29.5)	16 (37.2)	16 (36.4)	0.687
Associated aneurysms (%)	22 (12.6)	6 (13.6)	5 (11.4)	6 (14.0)	5 (11.4)	0.849
Microsurgery involvement (%)	78 (44.5)	23 (52.3)	19 (43.2)	18 (41.9)	18 (40.9)	0.145
Postoperative stroke (%)	13 (7.4)	5 (11.4)	1 (2.3)	6 (14.0)	1 (2.3)	0.373
Short-term neurological disability (%)	36 (20.6)	17 (38.6)	4 (9.1)	9 (20.9)	6 (13.6)	0.027*

bAVM: brain arteriovenous malformation; Hcy: homocysteine; SD: standard deviation; mRS: modified Rankin Scale; IQR: interquartile range. *P < 0.05, significant difference. ^aSerum levels of Hcy in quartiles: Q1, <9.9 μmol/L; Q2, 9.9-12.7 μmol/L; Q3, 12.8-16.6 μmol/L; and Q4, ≥16.1 μmol/L.

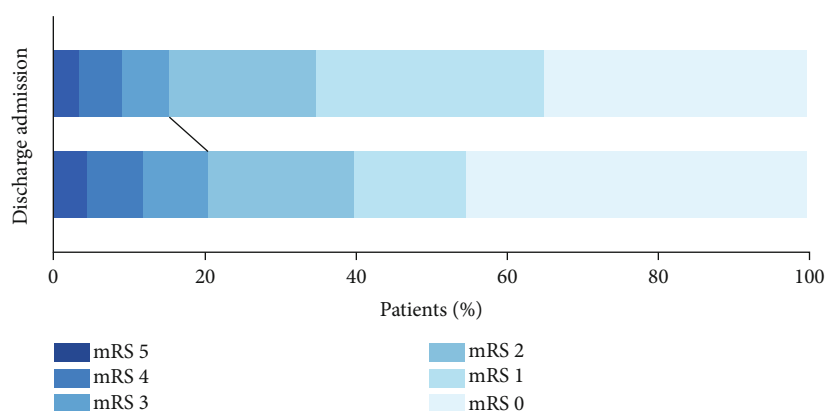


FIGURE 2: Comparison of mRS score in bAVM patients at admission and discharge. Thirty-six patients (20.6%) were disabled (mRS > 2) at discharge, with no significant difference compared with admission (P = 0.211). mRS: modified Rankin Scale.

In the present study, we reached a similar conclusion as SAH groups. Higher serum Hcy levels seemed to be a survival advantage in patients with bAVMs. We supposed that the lower serum Hcy level attributed to the activation in the cas-

cade usage of Hcy's endogenously thrombotic effect after the hemorrhagic bAVM. As an intermediate metabolic product in the circle involving folate and vitamins, Hcy could be modifiable [33]. Two randomized controlled trials showed

TABLE 3: Logistic regression analysis on the neurological outcome.

Variables	Univariate analysis			Multivariate analysis		
	OR	95% CI	P value	OR	95% CI	P value
Age	0.994	0.969-1.019	0.633	1.011	0.969-1.055	0.609
Male sex	1.229	0.581-2.599	0.590	2.528	0.659-9.698	0.177
Medical history						
Hypertension	2.330	0.729-7.441	0.153			
Diabetes mellitus	2.667	0.429-16.594	0.293			
Cigarette smoking	0.912	0.343-2.424	0.853			
Alcohol drinking	1.212	0.370-3.966	0.751			
Primary symptoms						
Hemorrhage	4.084	1.677-9.943	0.002	5.360	1.208-23.790	0.027*
Seizure	0.586	0.210-1.637	0.308			
Neurological dysfunction	1.157	0.454-2.947	0.760			
Admission mRS score	2.496	1.803-3.457	<0.001	2.225	1.402-3.530	0.001*
AVM characteristics						
Volume	1.018	1.005-1.032	0.007	1.024	1.004-1.046	0.021*
Deep location	2.377	1.111-5.087	0.026	0.927	0.238-3.613	0.913
Eloquent location	1.847	0.866-3.938	0.112			
Deep venous drainage	2.310	1.094-4.874	0.028	8.813	1.965-39.534	0.004*
Associated aneurysms	2.551	0.976-6.666	0.056	5.711	1.389-23.488	0.016*
Clinical features						
Heart rate	0.980	0.944-1.019	0.311			
SBP	1.004	0.985-1.025	0.664			
DBP	1.024	0.990-1.059	0.164			
BMI	0.980	0.899-1.069	0.652			
Laboratory results						
Glucose	1.579	1.151-2.166	0.005	1.897	1.115-3.229	0.018*
Albumin	0.900	0.816-0.993	0.035	0.968	0.820-1.142	0.697
Creatinine	0.995	0.972-1.018	0.667			
UA	1.001	0.999-1.002	0.325			
TC	0.643	0.421-0.983	0.042	0.194	0.033-1.129	0.068
TG	0.944	0.636-1.403	0.776			
HDL-C	1.639	0.870-3.088	0.126			
LDL-C	0.692	0.441-1.086	0.109			
ApoA	0.868	0.228-3.303	0.836			
ApoB	0.253	0.040-1.595	0.143			
Hcy	0.937	0.878-1.001	0.055	0.838	0.720-0.976	0.023*
Microsurgery involvement	1.746	0.834-3.654	0.139			

OR: odds ratio; CI: confidence intervals; AVM: arteriovenous malformation; SBP: systolic blood pressure; DBP: diastolic blood pressure; BMI: body mass index; UA: uric acid; TC: total cholesterol; TG: triglyceride; HDL-C: high-density lipoprotein cholesterol; LDL-C: low-density lipoprotein cholesterol; ApoA: apolipoprotein A; ApoB: apolipoprotein B; Hcy: homocysteine. * $P < 0.05$, significant difference.

that folic acid/vitamin B12 or vitamin B6 had no effect of treatment on total mortality [3, 4]. However, Wang et al. performed a meta-analysis showing effective reduction in patients with stroke in primary prevention [34]. The conflicts between these studies were an account of the baseline folate consumption. The management of oral nutritional supplements on Hcy in the bAVMs group needs further investigation.

Another independent prominent predictor for the unfavorable neurological outcome is the higher serum glucose

level (OR 1.897, 95% CI 1.115-3.229; $P = 0.018$). The same results were reached in the hemorrhagic subtypes, including ICH and SAH [35, 36].

Some clinical features of bAVMs determined by this study differed from those in previous reports. We demonstrated a statistical significance between Hcy quartiles and seizure manifestation ($P = 0.034$), which can induce unfavorable outcomes at discharge in the patients with bAVMs. The relationship between Hcy and seizure was first proposed in

an intrathecal chemotherapy-treated boy who suffered from leukemia [37]. And any transient elevation of Hcy may be related to the seizure risk [38, 39]. Although it is hard to determine whether the elevated Hcy is the cause or the result of a seizure, we offered neurosurgeons a new insight into the prophylactic and off-label utility of antiepileptic drugs.

There are some limitations that should be acknowledged. First, due to the nature of the respective study, we are aware of the fact that its design is one of the considerations which should be improved in the future. This study's small sample size is the second considerable limitation because larger samples are preferred for relevant studies. As such, findings should be interpreted with caution until further high-level prospective studies or larger data sets are available. Third, the baseline dietary and folate status of the patients were undocumented. Though the population was under established policies of population folate supplementation for the few decades nationwide, we enrolled patients before the policy was carried out, which could be a confounding variable. Fourth, the outcomes were only measured at the discharge point and were not conducted at the 3-month follow-up. This is our ongoing study of enrolled patients, and we expect to make some progress in the recent future. Further, longer follow-up studies should be conducted to demonstrate the clinical relevance between the serum Hcy level and long-term outcomes.

5. Conclusions

In conclusion, our results indicated that the lower serum Hcy level is strongly associated with in-hospital unfavorable outcomes. Further prospective studies of Hcy natural history and management in the bAVMs groups are needed, which would be valuable for evaluating the disease-modifying efficacy of oral nutritional supplements in bAVM patients.

Data Availability

The data used to support the findings of this study are available from the corresponding author upon reasonable request.

Conflicts of Interest

The authors declare that they have no conflicts of interest.

Authors' Contributions

Fa Lin, Chaofan Zeng, and Peicong Ge contributed equally to this work.

Acknowledgments

This study was supported by the National Key Technologies Research and Development Program of China (2016YFC1301800), Beijing Science and Technology Supporting Plan (D161100003816005), and Beijing Municipal Administration of Hospitals' Mission Plan (SML20150501).





References

- [1] R. M. Friedlander, "Arteriovenous malformations of the brain," *The New England Journal of Medicine*, vol. 356, no. 26, pp. 2704–2712, 2007.
- [2] S. I. Nikolaev, S. Vetiska, X. Bonilla et al., "Somatic Activating KRAS Mutations in arteriovenous malformations of the brain," *The New England Journal of Medicine*, vol. 378, no. 3, pp. 250–261, 2018.
- [3] M. V. Holmes, P. Newcombe, J. A. Hubacek et al., "Effect modification by population dietary folate on the association between *MTHFR* genotype, homocysteine, and stroke risk: a meta-analysis of genetic studies and randomised trials," *The Lancet*, vol. 378, no. 9791, pp. 584–594, 2011.
- [4] M. Ebbing, Ø. Bleie, P. M. Ueland et al., "Mortality and cardiovascular events in patients treated with homocysteine-lowering B vitamins after coronary angiography: a randomized controlled trial," *JAMA*, vol. 300, no. 7, pp. 795–804, 2008.
- [5] Z. Li, L. Sun, H. Zhang et al., "Elevated plasma homocysteine was associated with hemorrhagic and ischemic stroke, but methylenetetrahydrofolate reductase gene C677T polymorphism was a risk factor for thrombotic stroke: a multicenter case-control study in China," *Stroke*, vol. 34, no. 9, pp. 2085–2090, 2003.
- [6] Z. Zhou, Y. Liang, H. Qu et al., "Plasma homocysteine concentrations and risk of intracerebral hemorrhage: a systematic review and meta-analysis," *Scientific Reports*, vol. 8, no. 1, p. 2568, 2018.
- [7] V. V. Aleksandrin, A. V. Ivanov, E. D. Virus, P. O. Bulgakova, and A. A. Kubatiev, "Application of wavelet analysis to detect dysfunction in cerebral blood flow autoregulation during experimental hyperhomocysteinaemia," *Lasers in Medical Science*, vol. 33, no. 6, pp. 1327–1333, 2018.
- [8] M. Hatefi, S. Behzadi, M. M. Dastjerdi et al., "Correlation of homocysteine with cerebral hemodynamic abnormality, endothelial dysfunction markers, and cognition impairment in patients with traumatic brain injury," *World Neurosurgery*, vol. 97, pp. 70–79, 2017.
- [9] M.-H. Lim, Y. I. Cho, and S.-K. Jeong, "Homocysteine and pulsatility index of cerebral arteries," *Stroke*, vol. 40, no. 10, pp. 3216–3220, 2009.
- [10] T. Hashimoto, G. Wen, M. T. Lawton et al., "Abnormal expression of matrix metalloproteinases and tissue inhibitors of metalloproteinases in brain arteriovenous malformations," *Stroke*, vol. 34, no. 4, pp. 925–931, 2003.
- [11] H. Min, J. Hong, I.-H. Cho et al., "TLR2-induced astrocyte MMP9 activation compromises the blood brain barrier and exacerbates intracerebral hemorrhage in animal models," *Molecular Brain*, vol. 8, no. 1, p. 23, 2015.
- [12] E. Shotar, C. Amouyal, A. Jacquens et al., "S100B serum elevation predicts in-hospital mortality after brain arteriovenous malformation rupture," *Stroke*, vol. 50, no. 5, pp. 1250–1253, 2019.
- [13] N. Tyagi, W. Gillespie, J. C. Vacek, U. Sen, S. C. Tyagi, and D. Lominadze, "Activation of GABA-A receptor ameliorates homocysteine-induced MMP-9 activation by ERK pathway," *Journal of Cellular Physiology*, vol. 220, no. 1, pp. 257–266, 2009.
- [14] I. Wiernicki, B. Millo, K. Safranow, B. Gorecka-Szyld, and P. Gutowski, "MMP-9, homocysteine and CRP circulating levels are associated with intraluminal thrombus thickness of

- abdominal aortic aneurysms—new implication of the old biomarkers,” *Disease Markers*, vol. 31, no. 2, pp. 67–74, 2011.
- [15] Q. Wang, J. Zhang, K. Zhao, and B. Xu, “Hyperhomocysteinemia is an independent risk factor for intracranial aneurysms: a case-control study in a Chinese Han population,” *Neurosurgical Review*, vol. 43, no. 4, pp. 1127–1134, 2020.
- [16] C. S. Ogilvy, P. E. Stieg, I. Awad et al., “Recommendations for the management of intracranial arteriovenous malformations: a statement for healthcare professionals from a special writing group of the Stroke Council, American Stroke Association,” *Circulation*, vol. 103, no. 21, pp. 2644–2657, 2001.
- [17] R. F. Spetzler and N. A. Martin, “A proposed grading system for arteriovenous malformations,” *Journal of Neurosurgery*, vol. 65, no. 4, pp. 476–483, 1986.
- [18] M. T. Lawton, H. Kim, C. E. McCulloch, B. Mikhak, and W. L. Young, “A supplementary grading scale for selecting patients with brain arteriovenous malformations for surgery,” *Neurosurgery*, vol. 66, no. 4, pp. 702–713, 2010.
- [19] Y. Jiao, F. Lin, J. Wu et al., “A supplementary grading scale combining lesion-to-eloquence distance for predicting surgical outcomes of patients with brain arteriovenous malformations,” *Journal of Neurosurgery*, vol. 128, no. 2, pp. 530–540, 2018.
- [20] H. Kim, L. Pawlikowska, Y. Chen, H. Su, G. Y. Yang, and W. L. Young, “Brain arteriovenous malformation biology relevant to hemorrhage and implication for therapeutic development,” *Stroke*, vol. 40, no. 3, Supplement 1, pp. S95–S97, 2009.
- [21] L. J. Wang, Y. Xue, R. Huo et al., “N6-methyladenosine methyltransferase METTL3 affects the phenotype of cerebral arteriovenous malformation via modulating Notch signaling pathway,” *Journal of Biomedical Science*, vol. 27, no. 1, p. 62, 2020.
- [22] M. Xu, X. Liu, G. Mei, J. Zhang, W. Wang, and H. Xu, “Radio-surgery reduces plasma levels of angiogenic factors in brain arteriovenous malformation patients,” *Brain Research Bulletin*, vol. 140, pp. 220–225, 2018.
- [23] G. Boysen, T. Brander, H. Christensen, R. Gideon, and T. Truelsen, “Homocysteine and risk of recurrent stroke,” *Stroke*, vol. 34, no. 5, pp. 1258–1261, 2003.
- [24] H. Iso, Y. Moriyama, S. Sato et al., “Serum total homocysteine concentrations and risk of stroke and its subtypes in Japanese,” *Circulation*, vol. 109, no. 22, pp. 2766–2772, 2004.
- [25] F. Zhou, B. Chen, C. Chen et al., “Elevated homocysteine levels contribute to larger hematoma volume in patients with intracerebral hemorrhage,” *Journal of Stroke and Cerebrovascular Diseases*, vol. 24, no. 4, pp. 784–788, 2015.
- [26] S. Zhang, X. Zhang, Y. Ling, and A. Li, “Predicting recurrent hypertensive intracerebral hemorrhage: derivation and validation of a risk-scoring model based on clinical characteristics,” *World Neurosurgery*, vol. 127, pp. e162–e171, 2019.
- [27] T. H. T. Chiu, H.-R. Chang, L.-Y. Wang, C.-C. Chang, M.-N. Lin, and C.-L. Lin, “Vegetarian diet and incidence of total, ischemic, and hemorrhagic stroke in 2 cohorts in Taiwan,” *Neurology*, vol. 94, no. 11, pp. e1112–e1121, 2020.
- [28] A. W. McEvoy, C. Marras, N. D. Kitchen, and A. Briddon, “Plasma total homocysteine and subarachnoid haemorrhage in a co-factor replete population,” *Amino Acids*, vol. 21, no. 3, pp. 237–241, 2001.
- [29] B. T. Grobelny, A. F. Ducruet, P. A. DeRosa et al., “Gain-of-function polymorphisms of cystathionine β -synthase and delayed cerebral ischemia following aneurysmal subarachnoid hemorrhage,” *Journal of Neurosurgery*, vol. 115, no. 1, pp. 101–107, 2011.
- [30] P. Hendrix, P. M. Foreman, M. R. Harrigan et al., “Association of cystathionine beta-synthase polymorphisms and aneurysmal subarachnoid hemorrhage,” *Journal of Neurosurgery*, vol. 128, no. 6, pp. 1771–1777, 2018.
- [31] M. Kumar, S. Goudihalli, K. Mukherjee, S. Dhandapani, and R. Sandhir, “Methylenetetrahydrofolate reductase C677T variant and hyperhomocysteinemia in subarachnoid hemorrhage patients from India,” *Metabolic Brain Disease*, vol. 33, no. 5, pp. 1617–1624, 2018.
- [32] S. Dhandapani, S. Goudihalli, K. K. Mukherjee et al., “Prospective study of the correlation between admission plasma homocysteine levels and neurological outcome following subarachnoid hemorrhage: a case for the reverse epidemiology paradox?,” *Acta Neurochirurgica*, vol. 157, no. 3, pp. 399–407, 2015.
- [33] P. Ge, Q. Zhang, X. Ye et al., “Modifiable risk factors associated with Moyamoya disease,” *Stroke*, vol. 51, no. 8, pp. 2472–2479, 2020.
- [34] X. Wang, X. Qin, H. Demirtas et al., “Efficacy of folic acid supplementation in stroke prevention: a meta-analysis,” *The Lancet*, vol. 369, no. 9576, pp. 1876–1882, 2007.
- [35] S. Hafez, M. Abdelsaid, S. El-Shafey, M. H. Johnson, S. C. Fagan, and A. Ergul, “Matrix metalloproteinase 3 exacerbates hemorrhagic transformation and worsens functional outcomes in hyperglycemic stroke,” *Stroke*, vol. 47, no. 3, pp. 843–851, 2016.
- [36] F. Schlenk, A. Nagel, D. Graetz, and A. S. Sarrafzadeh, “Hyperglycemia and cerebral glucose in aneurysmal subarachnoid hemorrhage,” *Intensive Care Medicine*, vol. 34, no. 7, pp. 1200–1207, 2008.
- [37] C. T. Quinn, J. C. Griener, T. Bottiglieri, and B. A. Kamen, “Methotrexate, homocysteine, and seizures,” *Journal of Clinical Oncology*, vol. 16, no. 1, pp. 393–394, 1998.
- [38] R. He, R. Mo, M. Shen et al., “Variable phenotypes and outcomes associated with the MMACHC c.609G>A homologous mutation: long term follow-up in a large cohort of cases,” *Orphanet Journal of Rare Diseases*, vol. 15, no. 1, p. 200, 2020.
- [39] S. Kishi, J. Griener, C. Cheng et al., “Homocysteine, pharmacogenetics, and neurotoxicity in children with leukemia,” *Journal of Clinical Oncology*, vol. 21, no. 16, pp. 3084–3091, 2003.

Research Article

FAM225B Is a Prognostic lncRNA for Patients with Recurrent Glioblastoma

Junsheng Li ^{1,2,3,4,5}, Qian Zhang,^{1,2,3,4,5} Peicong Ge,^{1,2,3,4,5} Chaofan Zeng ^{1,2,3,4,5},
Fa Lin,^{1,2,3,4,5} Wen Wang ^{1,2,3,4,5} and Jizong Zhao ^{1,2,3,4,5,6}

¹Department of Neurosurgery, Beijing Tiantan Hospital, Capital Medical University, China

²China National Clinical Research Center for Neurological Diseases, China

³Center of Stroke, Beijing Institute for Brain Disorders, China

⁴Beijing Key Laboratory of Translational Medicine for Cerebrovascular Disease, China

⁵Beijing Translational Engineering Center for 3D Printer in Clinical Neuroscience, China

⁶Savaid Medical School, University of the Chinese Academy of Sciences, China

Correspondence should be addressed to Wen Wang; wangwentty@126.com and Jizong Zhao; zhaojz205@163.com

Received 26 September 2020; Revised 22 October 2020; Accepted 29 October 2020; Published 23 November 2020

Academic Editor: Wen-Jun Tu

Copyright © 2020 Junsheng Li et al. This is an open access article distributed under the Creative Commons Attribution License, which permits unrestricted use, distribution, and reproduction in any medium, provided the original work is properly cited.

Objective. The overall survival of patients with recurrent glioblastoma (rGBM) is quite different, so clinical outcome prediction is necessary to guide personalized clinical treatment for patients with rGBM. The expression level of lncRNA *FAM225B* was analyzed to determine its prognostic value in rGBMs. **Methods.** We collected 109 samples of Chinese Glioma Genome Atlas (CGGA) RNA sequencing dataset and divided into training set and validation set. Then, we analyzed the expression of *FAM225B*, clinical characteristics, and overall survival (OS) information. Kaplan-Meier survival analysis was used to estimate the OS distributions. The prognostic value of *FAM225B* in rGBMs was tested by univariate and multivariate Cox regression analyses. Moreover, we analyzed the biological processes and signaling pathways of *FAM225B*. **Results.** We found that *FAM225B* was upregulated in rGBMs ($P = 0.0009$). The expression of *FAM225B* increased with the grades of gliomas ($P < 0.0001$). The OS of rGBMs in the low-expression group was significantly longer than that in the high-expression group ($P = 0.0041$). Similar result was found in the training set ($P = 0.0340$) and verified in the validation set ($P = 0.0292$). In multivariate Cox regression analysis, *FAM225B* was identified to be an independent prognostic factor for rGBMs ($P = 0.003$). Biological process and KEGG pathway analyses implied *FAM225B* mainly played a functional role on transcription, regulation of transcription, cell migration, focal adhesion, etc. **Conclusions.** *FAM225B* is expected to be as a new prognostic biomarker for the identification of rGBM patients with poor outcome. And our study provided a potential therapeutic target for rGBMs.

1. Introduction

As the most common intracranial malignant tumor in adults [1, 2], glioblastoma (GBM) has a median overall survival (OS) of only 14.6 months [3]. Most GBMs will relapse after standard treatment such as surgical resection, radiotherapy, and chemotherapy [4–6]. In recurrent glioblastoma (rGBM) cases, the patients may lose the opportunity for surgery because of the invasion to the functional area by tumors [7]. And rGBMs are less sensitive to chemotherapy or radiotherapy than primary ones as well [8–10]. So progress in prognostic biomarker identification is required for person-

alized treatment of patients with rGBM [11]. Further understanding the molecular factors of rGBMs will provide novel insights for the potential biological characteristics and elucidate the possible therapeutic targets.

Long noncoding RNAs (lncRNAs) refer to noncoding RNAs more than 200 nucleotides in length [12, 13] and are associated with a series of cellular process [14–16], such as epigenetic regulation and transcriptional regulation. The dysregulated lncRNAs can be used as prognostic factors for patients [17–20].

In this study, we collected 109 rGBM samples from the Chinese Glioma Genome Atlas (CGGA, <http://www.cgga>

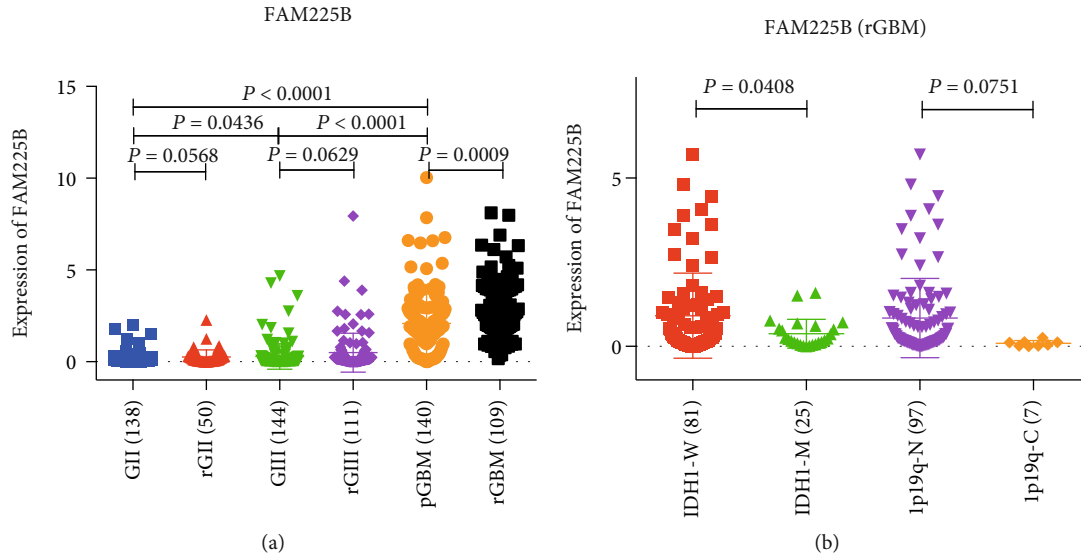


FIGURE 1: The expression pattern of *FAM225B* in gliomas: (a) *FAM225B* expression in different grades (grade II to grade IV) and types (primary or recurrent); (b) *FAM225B* expression in different IDH1 status and 1p/19q status.

.org.cn/) RNA sequencing dataset. We identified a new prognostic lncRNA *FAM225B* in rGBMs. We investigated the expression patterns of *FAM225B* and evaluated its prognostic value. The expression of *FAM225B* increased with the glioma grades, and it indicated the poor prognosis in rGBM patients. Therefore, *FAM225B* could be a prognostic indicator and a potential therapeutic target for rGBMs.

2. Materials and Methods

2.1. Patients and Datasets. Our study obtained 109 rGBM samples from the CGGA RNA sequencing dataset with expression data and clinical information [21, 22]. All samples were initially diagnosed with primary glioblastoma (pGBM) and relapsed after standard treatment. The cases were randomly divided into training set and validation set without bias [23]. And the median relative expression of *FAM225B* was used as the cut-off value to divide the samples into a low-expression group and high-expression group. All these samples were diagnosed histologically by 2 neuropathologists according to the 2016 WHO classification guideline of nervous system tumors. Our study was approved by the Ethics Committee of Beijing Tiantan Hospital.

2.2. Statistical and Bioinformatic Analysis. SPSS software (version 22; SPSS Inc., Chicago, IL, USA) and R programming language (version 3.2.3) were used for statistical analyses. Survival distributions were estimated by using Kaplan-Meier survival analysis (GraphPad Software Inc., La Jolla, CA, USA). Univariate and multivariate Cox regression analyses evaluated the hazard ratios (HRs) of different prognostic factors and were used to identify the independent prognostic factor. A two-sided *P* value less than 0.05 was set to be statistically significant. Biological process and Kyoto Encyclopedia of Genes and Genomes (KEGG) analysis were conducted by using DAVID (the Database for Annotation,

Visualization and Integrated Discovery, <https://david-d.ncifcrf.gov/home.jsp>) [24, 25].

3. Results

3.1. *FAM225B* Was Dysregulated in rGBMs. We first investigated the expression pattern of *FAM225B*. The expression of *FAM225B* showed significant difference between the pGBMs and rGBMs ($P = 0.0009$, Figure 1(a)). Moreover, the expression of *FAM225B* increased with grades of gliomas ($P = 0.0436$; $P < 0.0001$; $P < 0.0001$, Figure 1(a)). Then, we compared the *FAM225B* expression level in primary and recurrent gliomas of grade II ($P = 0.0568$) and grade III ($P = 0.0629$, Figure 1(a)).

The IDH1 and 1p/19q status is related to the prognosis of gliomas [26–29]. Therefore, we explored the expression pattern of *FAM225B* in the subtypes of rGBMs. The result showed that the expression of *FAM225B* enhanced in the IDH1-wild-type subtype ($P = 0.0408$, Figure 1(b)). However, no statistically significant differences were observed in the expression of *FAM225B* in rGBM patients with 1p/19q-codeletion or 1p/19q-noncodeletion ($P = 0.0751$, Figure 1(b)).

3.2. *FAM225B* Predicted Poorer Overall Survival in rGBMs. All 109 rGBM samples were randomly divided into training set and validation set with no significant data bias. By using the median relative expression of *FAM225B* as the cut-off value, samples were divided into two categories including the low-expression group and high-expression group. Kaplan-Meier analysis was used to investigate the correlation between *FAM225B* expression and OS of rGBM patients.

We found that the OS of patients in the low-expression group were significantly longer ($P = 0.0041$, Figure 2(a)). In the training group, the OS of patients in the high-expression group were shorter than those in the low-expression group ($P = 0.0340$, Figure 2(b)). And similar

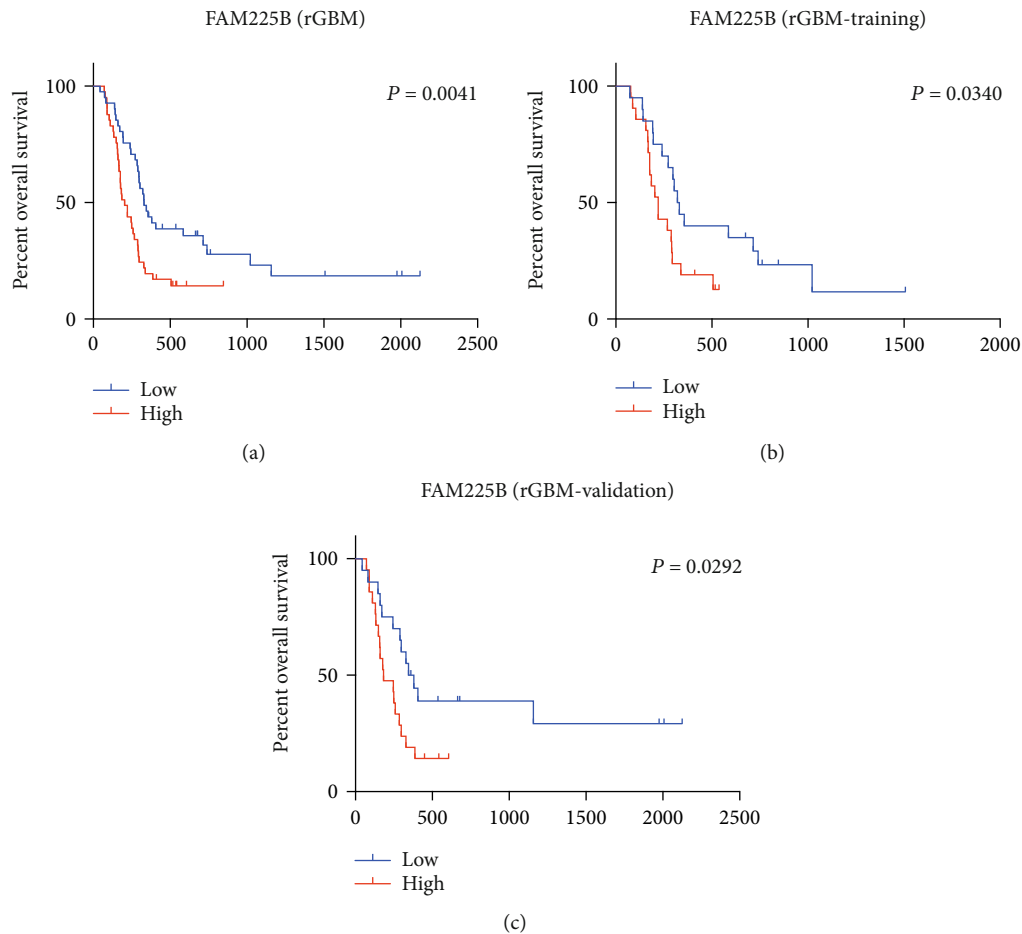


FIGURE 2: Kaplan-Meier curves of OS among rGBM patients from different groups stratified by the expression of *FAM225B*: (a) Kaplan-Meier curves of OS among rGBMs with different *FAM225B*-expressing levels (high-expression group and low-expression group); (b) Kaplan-Meier curves of OS among rGBMs with different *FAM225B*-expressing levels in the training set (high-expression group and low-expression group); (c). Kaplan-Meier curves of OS among rGBMs with different *FAM225B*-expressing levels in the validation set (high-expression group and low-expression group).

result was observed in the validation set ($P = 0.0292$, Figure 2(c)).

3.3. Associations between *FAM225B* and Clinicopathologic Features. We analyzed the relationship between *FAM225B* expression and clinicopathologic features (Figure 3). The results were obtained by the univariate and multivariate Cox regression analyses (Table 1). The univariate Cox regression analysis found that chemotherapy ($P = 0.003$) and *FAM225B* ($P = 0.007$) were potential survival predictors. On the multivariate Cox regression analysis, it showed that *FAM225B* ($P = 0.003$) was an independent prognostic factor. *FAM225B* was significantly related to the prognosis of rGBMs.

3.4. Functional Annotation of *FAM225B*. To explain the different prognoses of rGBMs divided by *FAM225B*, we extracted 902 related genes using Pearson correlation analysis (correlation value 0.4; $P < 0.001$). The biological process and KEGG pathway analyses of *FAM225B* were performed using DAVID. It showed that major biological processes were enriched in transcription, regulation of transcription,

cell division, positive regulation of migration, cell migration, etc. (Figure 4(a)). KEGG pathway analysis showed that selected genes were enriched in ubiquitin-mediated proteolysis, Wnt signaling pathway, cell cycle, focal adhesion, regulation of actin cytoskeleton, etc. (Figure 4(b)).

4. Discussion

Despite great efforts on the multimodal diagnosis and treatment of rGBMs, the clinical prognosis for patients remains poor due to the proliferation potential and antiapoptosis characteristics of this malignant tumor [30–32]. Therefore, understanding the expression of key factors may significantly influence the development and clinical outcome of rGBM patients. Recent studies have found that the dysregulated lncRNAs can provide insights for glioma diagnosis, prognosis, and treatment strategy [33–37].

In this study, we established a dataset of 109 rGBMs collected from the CGGA RNA sequencing dataset to explore the effect of lncRNAs on the prognosis of rGBM patients. By comparing the expression level of *FAM225B* between pGBMs and rGBMs, we found that *FAM225B* expression

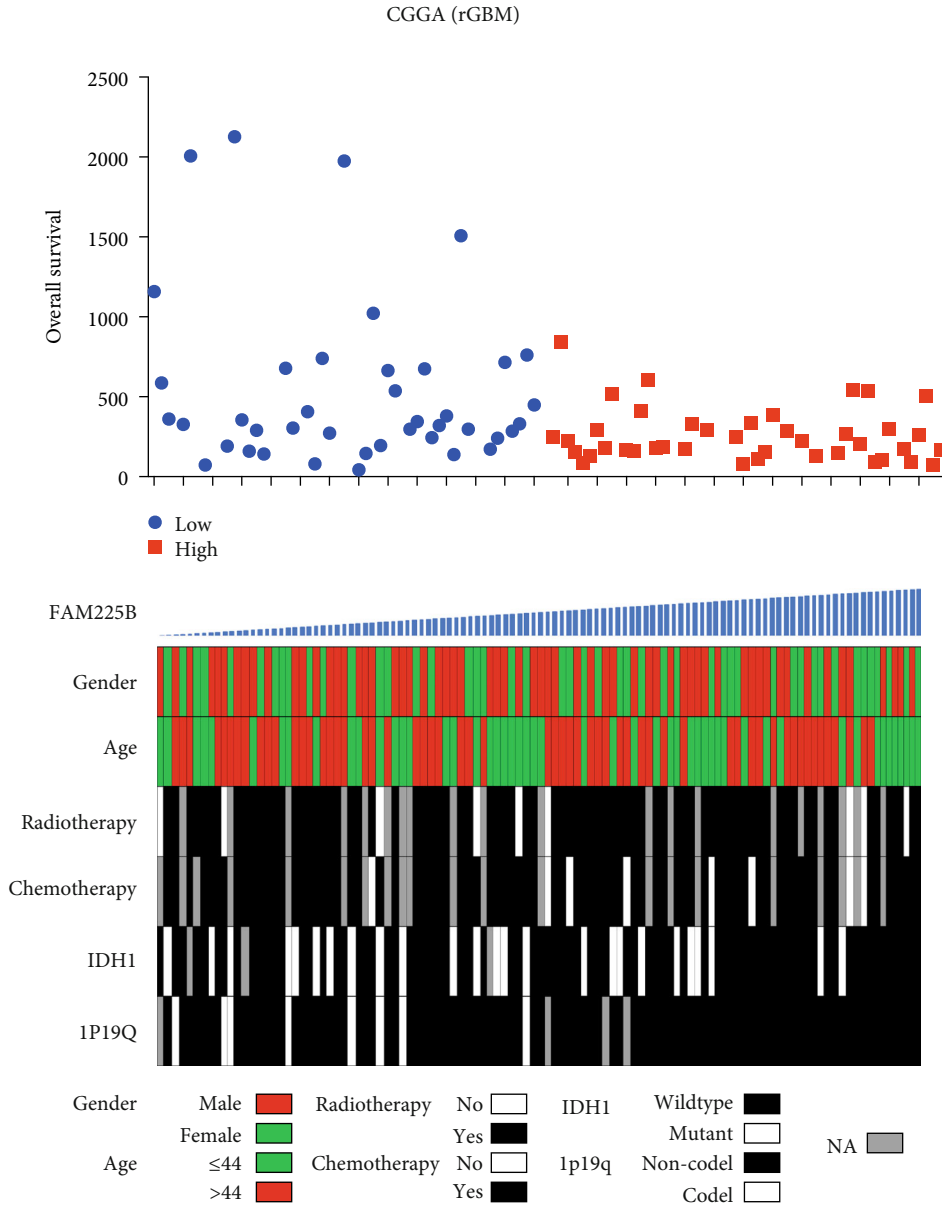


FIGURE 3: Distribution of clinicopathologic features according to the expression of *FAM225B*. Rows represent corresponding genes, while columns indicate corresponding patients.

TABLE 1: Univariate and multivariate Cox regression analysis of survival in rGBMs.

Items	Univariate Cox <i>p</i> value	Univariate Cox HR	Multivariate Cox <i>p</i> value	Multivariate Cox HR
Gender	0.415	0.811		
Age	0.286	1.010		
IDH1	0.083	0.645		
1p/19q	0.100	0.375		
Radiotherapy	0.102	1.805		
Chemotherapy	0.003	0.256	0.003	0.257
<i>FAM225B</i>	0.007	1.279	0.003	1.313

Gender: male, female; IDH1 status: wild type, mutant; 1p/19q status: noncodeletion, codeletion; radiotherapy: no, yes; chemotherapy: no, yes.

enhanced in rGBMs ($P = 0.0009$). It indicated that *FAM225B* may play a key role in the recurrence process of GBMs. Then, we analyzed the expression of *FAM225B* in different grades of glioma, including grade II, grade III, and GBM ($P < 0.0001$). The result showed that the expression of *FAM225B* was positively correlated with the grade of gliomas. This indicated that *FAM225B* was associated with glioma malignancy and may serve as a potential indicator for glioma grade. In addition, we explored that the expression of *FAM225B* enhanced in IDH1-wild type ($P = 0.0408$). Based on the data analysis above, we inferred that *FAM225B* can be used as a specific diagnostic marker for GBM recurrence.

We explored the correlation between *FAM225B* expression and survival distribution of rGBM patients. It showed

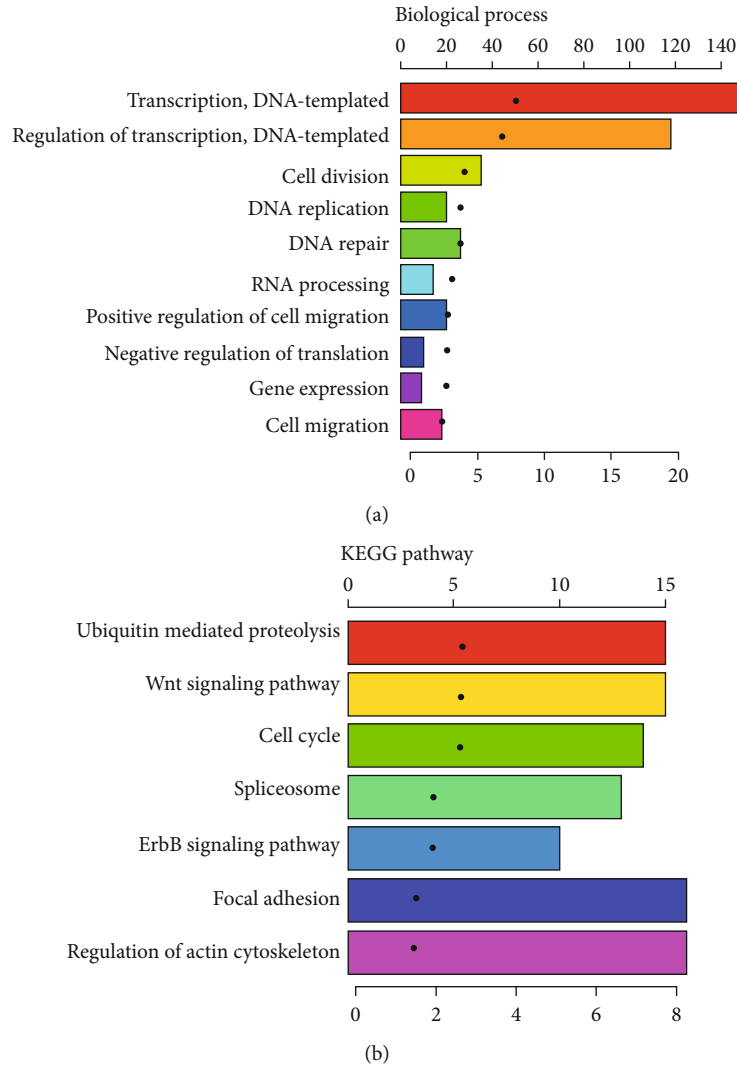


FIGURE 4: Functional annotation of *FAM225B* in rGBM patients: (a) biological process analysis of the related genes; (b) KEGG pathway analysis of the related genes.

that the OS decreased with the enhancement of *FAM225B* expression ($P = 0.0041$). *FAM225B* enhancement may predict the poor prognosis in rGBMs. We analyzed the relationship between *FAM225B* expression and clinicopathologic features. It indicated that *FAM225B* expression could be a significantly independent prognostic maker in rGBMs.

In our studies, functional annotation analysis showed a strong correlation between *FAM225B* and transcription. It suggested that *FAM225B* may play an important role in rGBM through transcription and its regulation. By using the starBase website (<https://starbase.sysu.edu.cn/>), we found the candidate miRNAs (miR-1-3p, miR-206, and miR-205-5p) which may be correlated to *FAM225B*. *FAM225B* could competitively bind with miR-1-3p and miR-206, inducing the upregulation of AXL. It may lead to the enhancement of drug resistance and cell proliferation in glioma [38]. Furthermore, it has reported that miR-205-5p is involved in Wnt signaling, cell cycle, and focal adhesion [39], which is consistent with our KEGG

findings. These processes may be associated with the recurrence of GBM. However, there are a few limitations in our study. The sample size of our dataset is still limited. Moreover, this is a retrospective study, and different treatments may have an impact on patient survival outcomes. And these findings were based on bioinformatic analysis. Prospective study is needed to clarify the mechanism of *FAM225B* and to further validate the clinical application in patients with rGBMs.

5. Conclusion

Our study found that *FAM225B* enhanced in rGBMs and its upregulation was related to the poor prognosis of rGBM patients. Therefore, our study provides a new perspective for *FAM225B*, as a prognosis biomarker and a potential therapeutic target for rGBMs. Further study will investigate the mechanisms of *FAM225B* in rGBMs.

Data Availability

All CGGA data used in this study was available from the CGGA website (<http://www.cgga.org.cn>).

Ethical Approval

This study was approved by the Ethics Committee in Beijing Tiantan Hospital.

Consent

Patient informed consents were waived due to the retrospective nature of the study.

Conflicts of Interest

The authors have declared that no competing interests exist.

Authors' Contributions

Junsheng Li analyzed the results and wrote the manuscript. Qian Zhang and Peicong Ge made the statistical comparison. Chaofan Zeng and Fa Lin revised the manuscript. Wen Wang performed the gene analysis and the functional annotation analysis. Jizong Zhao designed the study. All authors have read and approved the final manuscript.

Acknowledgments

This work was supported by grants from Beijing Municipal Administration of Hospitals' Mission Plan (SML20150501); "13th Five-Year Plan" National Science and Technology supporting plan (2015BAI09B04); and Foundation of Beijing Tiantan Hospital (No. 2018-YQN-6).

References

- [1] T. Zeng, L. Li, Y. Zhou, and L. Gao, "Exploring Long noncoding RNAs in glioblastoma: regulatory mechanisms and clinical potentials," *International journal of genomics*, vol. 2018, Article ID 2895958, 13 pages, 2018.
- [2] L. Geraldo, C. Garcia, A. da Fonseca et al., "Glioblastoma therapy in the age of molecular medicine," *Trends in cancer*, vol. 5, no. 1, pp. 46–65, 2019.
- [3] P. Tully, A. Gogos, C. Love, D. Liew, K. Drummond, and A. Morokoff, "Reoperation for recurrent glioblastoma and its association with survival benefit," *Neurosurgery*, vol. 79, no. 5, pp. 678–689, 2016.
- [4] R. Steffens, S. Semrau, G. Lahmer et al., "Recurrent glioblastoma: who receives tumor specific treatment and how often?," *Journal of Neuro-Oncology*, vol. 128, no. 1, pp. 85–92, 2016.
- [5] A. Krivoshapkin, A. Gaytan, N. Salim et al., "Repeat resection and intraoperative radiotherapy for malignant gliomas of the brain: a history and review of current techniques," *World Neurosurgery*, vol. 132, pp. 356–362, 2019.
- [6] M. Weller, E. le Rhun, M. Preusser, J. Tonn, and P. Roth, "How we treat glioblastoma," *ESMO open*, vol. 4, article e000520, Suppl 2, 2020.
- [7] D. Botros, H. Dux, C. Price, A. Khalafallah, and D. Mukherjee, "Assessing the efficacy of repeat resections in recurrent glioblastoma: a systematic review," *Neurosurgical Review*, 2020.
- [8] J. Huang, R. Chaudhary, A. L. Cohen et al., "A multicenter phase II study of temozolomide plus disulfiram and copper for recurrent temozolomide-resistant glioblastoma," *Journal of Neuro-Oncology*, vol. 142, no. 3, pp. 537–544, 2019.
- [9] F. Kazmi, Y. Y. Soon, Y. H. Leong, W. Y. Koh, and B. Vellayappan, "Re-irradiation for recurrent glioblastoma (GBM): a systematic review and meta-analysis," *Journal of Neuro-Oncology*, vol. 142, no. 1, pp. 79–90, 2019.
- [10] B. Campos, L. R. Olsen, T. Urup, and H. S. Poulsen, "A comprehensive profile of recurrent glioblastoma," *Oncogene*, vol. 35, no. 45, pp. 5819–5825, 2016.
- [11] A. O. Sasmita, Y. P. Wong, and A. P. K. Ling, "Biomarkers and therapeutic advances in glioblastoma multiforme," *Asia-Pacific Journal of Clinical Oncology*, vol. 14, no. 1, pp. 40–51, 2018.
- [12] I. Ulitsky and D. P. Bartel, "lincRNAs: genomics, evolution, and mechanisms," *Cell*, vol. 154, no. 1, pp. 26–46, 2013.
- [13] J. Li, H. Meng, Y. Bai, and K. Wang, "Regulation of lincRNA and its role in cancer metastasis," *Oncology Research*, vol. 23, no. 5, pp. 205–217, 2016.
- [14] P. J. Batista and H. Y. Chang, "Long noncoding RNAs: cellular address codes in development and disease," *Cell*, vol. 152, no. 6, pp. 1298–1307, 2013.
- [15] J. H. Noh, K. M. Kim, W. G. McClusky, K. Abdelmohsen, and M. Gorospe, "Cytoplasmic functions of long noncoding RNAs," *Wiley interdisciplinary reviews RNA*, vol. 9, no. 3, article e1471, 2018.
- [16] S. U. Schmitz, P. Grote, and B. G. Herrmann, "Mechanisms of long noncoding RNA function in development and disease," *Cellular and molecular life sciences*, vol. 73, no. 13, pp. 2491–2509, 2016.
- [17] M. Zhou, Z. Zhang, H. Zhao, S. Bao, L. Cheng, and J. Sun, "An immune-related six-lincRNA signature to improve prognosis prediction of glioblastoma multiforme," *Molecular Neurobiology*, vol. 55, no. 5, pp. 3684–3697, 2017.
- [18] S. Liu, R. Mitra, M. M. Zhao et al., "The potential roles of long noncoding RNAs (lincRNA) in glioblastoma development," *Molecular Cancer Therapeutics*, vol. 15, no. 12, pp. 2977–2986, 2016.
- [19] M. Li, S. Long, J. Hu, Z. Wang, C. Geng, and S. Ou, "Systematic identification of lincRNA-based prognostic biomarkers for glioblastoma," *Aging*, vol. 11, no. 21, pp. 9405–9423, 2019.
- [20] W. X. Peng, P. Koirala, and Y. Y. Mo, "lincRNA-mediated regulation of cell signaling in cancer," *Oncogene*, vol. 36, no. 41, pp. 5661–5667, 2017.
- [21] W. Cheng, X. Ren, C. Zhang et al., "Bioinformatic profiling identifies an immune-related risk signature for glioblastoma," *Neurology*, vol. 86, no. 24, pp. 2226–2234, 2016.
- [22] W. Wang, Z. Zhao, F. Wu et al., "Bioinformatic analysis of gene expression and methylation regulation in glioblastoma," *Journal of Neuro-Oncology*, vol. 136, no. 3, pp. 495–503, 2018.
- [23] J. X. Zhang, L. Han, Z. S. Bao et al., "HOTAIR, a cell cycle-associated long noncoding RNA and a strong predictor of survival, is preferentially expressed in classical and mesenchymal glioma," *Neuro-Oncology*, vol. 15, no. 12, pp. 1595–1603, 2013.
- [24] L. Chen, Y. H. Zhang, G. Lu, T. Huang, and Y. D. Cai, "Analysis of cancer-related lincRNAs using gene ontology and

- KEGG pathways,” *Artificial Intelligence in Medicine*, vol. 76, pp. 27–36, 2017.
- [25] L. Chen, Y. H. Zhang, S. Wang, Y. Zhang, T. Huang, and Y. D. Cai, “Prediction and analysis of essential genes using the enrichments of gene ontology and KEGG pathways,” *PLoS One*, vol. 12, no. 9, article e0184129, 2017.
- [26] W. Szopa, T. A. Burley, G. Kramer-Marek, and W. Kaspera, “Diagnostic and therapeutic biomarkers in glioblastoma: current status and future perspectives,” *BioMed Research International*, vol. 2017, Article ID 8013575, 13 pages, 2017.
- [27] K. Ludwig and H. I. Kornblum, “Molecular markers in glioma,” *Journal of Neuro-Oncology*, vol. 134, no. 3, pp. 505–512, 2017.
- [28] M. Rahman, J. Kresak, C. Yang et al., “Analysis of immunobiologic markers in primary and recurrent glioblastoma,” *Journal of Neuro-Oncology*, vol. 137, no. 2, pp. 249–257, 2018.
- [29] K. Aldape, G. Zadeh, S. Mansouri, G. Reifenberger, and A. von Deimling, “Glioblastoma: pathology, molecular mechanisms and markers,” *Acta Neuropathologica*, vol. 129, no. 6, pp. 829–848, 2015.
- [30] K. Seystahl, W. Wick, and M. Weller, “Therapeutic options in recurrent glioblastoma—an update,” *Critical Reviews in Oncology/Hematology*, vol. 99, pp. 389–408, 2016.
- [31] J. L. Shah, G. Li, J. L. Shaffer et al., “Stereotactic radiosurgery and hypofractionated radiotherapy for glioblastoma,” *Neurosurgery*, vol. 82, no. 1, pp. 24–34, 2018.
- [32] J. M. Frischer, C. Marosi, A. Woehrer et al., “Gamma knife radiosurgery in recurrent glioblastoma,” *Stereotactic and Functional Neurosurgery*, vol. 94, no. 4, pp. 265–272, 2016.
- [33] F. Wu, C. Zhang, J. Cai et al., “Upregulation of long noncoding RNA HOXA-AS3 promotes tumor progression and predicts poor prognosis in glioma,” *Oncotarget*, vol. 8, no. 32, pp. 53110–53123, 2017.
- [34] W. Zhao, C. Sun, and Z. Cui, “A long noncoding RNA UCA1 promotes proliferation and predicts poor prognosis in glioma,” *Clinical and Translational Oncology*, vol. 19, no. 6, pp. 735–741, 2017.
- [35] C. Y. Dong, J. Cui, D. H. Li, Q. Li, and X. Y. Hong, “HOXA10-AS: a novel oncogenic long non-coding RNA in glioma,” *Oncology Reports*, vol. 40, no. 5, pp. 2573–2583, 2018.
- [36] H. Xiao, N. Ding, H. Liao et al., “Prediction of relapse and prognosis by expression levels of long noncoding RNA PEG10 in glioma patients,” *Medicine*, vol. 98, no. 45, article e17583, 2019.
- [37] K. X. Ma, H. J. Wang, X. R. Li et al., “Long noncoding RNA MALAT1 associates with the malignant status and poor prognosis in glioma,” *Tumor Biology*, vol. 36, no. 5, pp. 3355–3359, 2015.
- [38] Y. Ma, G. Zhou, M. Li et al., “Long noncoding RNA DANCR mediates cisplatin resistance in glioma cells via activating AXL/PI3K/Akt/NF- κ B signaling pathway,” *Neurochemistry International*, vol. 118, pp. 233–241, 2018.
- [39] B. L. Zhang, F. L. Dong, T. W. Guo, X. H. Gu, L. Y. Huang, and D. S. Gao, “MiRNAs mediate GDNF-induced proliferation and migration of glioma cells,” *Cellular Physiology and Biochemistry*, vol. 44, no. 5, pp. 1923–1938, 2018.

Research Article

Analysis of Long Noncoding RNA ZNF667-AS1 as a Potential Biomarker for Diagnosis and Prognosis of Glioma Patients

Qin Yuan,¹ Chao Gao,² Xiao-dong Lai,³ Liang-yi Chen ,⁴ and Tian-bao Lai ⁴

¹Department of Oncology and Hematology, Hubei Provincial Hospital of Integrated Chinese and Western Medicine, Wuhan, 430015 Hubei, China

²Department of Oncology, First People's Hospital of Zaoyang, Zaoyang, 441200 Hubei, China

³Fuzhou Medical College of Nanchang University, Fuzhou, 344000 Nanchang, China

⁴Department of Neurology, Zhongshan Hospital Affiliated to Xiamen University, Xiamen, 361004 Fujian, China

Correspondence should be addressed to Liang-yi Chen; chenliangyix@163.com and Tian-bao Lai; dr.laitianbao@qq.com

Received 31 August 2020; Revised 15 September 2020; Accepted 19 October 2020; Published 17 November 2020

Academic Editor: Wen-Jun Tu

Copyright © 2020 Qin Yuan et al. This is an open access article distributed under the Creative Commons Attribution License, which permits unrestricted use, distribution, and reproduction in any medium, provided the original work is properly cited.

Objective. Long noncoding RNAs (lncRNAs) have been strongly associated with various types of cancer. The present study aimed at exploring the diagnostic and prognostic value of lncRNA Zinc finger protein 667-antisense RNA 1 (ZNF667-AS1) in glioma patients. **Patients and Methods.** The expressions of ZNF667-AS1 were detected in 155 glioma tissues and matched normal brain tissue samples by qRT-PCR. The receiver operating characteristic (ROC) curve was performed to estimate the diagnostic value of ZNF667-AS1. The association between the ZNF667-AS1 expression and clinicopathological characteristics was analyzed by the chi-square test. The Kaplan-Meier method was performed to determine the influence of the ZNF667-AS1 expression on the overall survival and disease-free survival of glioma patients. The Cox regression analysis was used to evaluate the effect of independent prognostic factors on survival outcome. Cell proliferation was measured by the respective cell counting Kit-8 (CCK-8) assays. **Results.** We observed that ZNF667-AS1 was significantly upregulated in glioma tissues compared to normal tissue samples ($p < 0.01$). Higher levels of ZNF667-AS1 were positively associated with the WHO grade ($p = 0.018$) and KPS score ($p = 0.008$). ROC assays revealed that the high ZNF667-AS1 expression had an AUC value of 0.8541 (95% CI: 0.8148 to 0.8934) for glioma. Survival data revealed that glioma patients in the high ZNF667-AS1 expression group had significantly shorter 5-year overall survival ($p = 0.0026$) and disease-free survival ($p = 0.0005$) time than those in the low ZNF667-AS1 expression group. Moreover, multivariate analyses confirmed that the ZNF667-AS1 expression was an independent predictor of the overall survival and disease-free survival for glioma patients. Functionally, we found that knockdown of ZNF667-AS1 suppressed the proliferation of glioma cells. **Conclusions.** Our results suggest that ZNF667-AS1 could be used as a potential diagnostic and prognostic biomarker in glioma.

1. Introduction

Human gliomas refer to the commonest malignant tumors of the core nervous mechanism, achieving ~6/100,000 incidence each year globally [1]. Malignant glioma exhibits aggressiveness, high infiltration, and resistance to normal therapies [2]. It is noteworthy that glioblastoma multiform (GBM), a particular glioma kind, exhibits the highest aggressiveness for the rapid growing process and frequent spread to close brain-related tissues [3]. Though the overall treating condition of brain gliomas continues to progress, such malig-

nancy outcome is not optimized significantly [4, 5]. Thus, emerging molecular markers should be developed for improving gliomas classifying process, patient prognosis, and treating plans.

Over the past few years, according to research with various overall genome methods, e.g., the ENCODE program, most mammalian genome receives transcription, whereas only 1.2% of the mentioned transcripts suggest the genes coding protein [6, 7]. Long noncoding RNAs (lncRNAs) refer to a sequence of transcripts with over 200 nt exhibiting slight or no ability to the code protein and critically impact a

wide range of cellular processes, e.g., splicing, X chromosome inactivation, epigenetic controls, and gene transcription regulation [8, 9]. Numerous lncRNAs suggested aberrant expression in various cancer types, and several lncRNAs with dysregulation become oncogenes or tumor-suppressing elements under special cases [10, 11]. For instance, lncRNA NFIA-AS2 was shown to be highly expressed in glioma and promoted the proliferation and migration of glioma cells via modulating the miRNA-655-3p/ZFX axis [12]. lncRNA RNCR3 was shown to promote the proliferation and metastasis of glioma cells via regulating the Akt/GSK-3 β pathway [13]. In addition, more and more lncRNAs were identified to be potential diagnostic and prognostic biomarkers for various tumor patients, including glioma [14–17]. Although several studies have investigated lncRNAs in glioma, their completely biological roles and clinical significance are still obscure.

lncRNA Zinc finger protein 667-antisense RNA 1 (ZNF667-AS1) in chromosome 19q13.43 of human was recently identified as tumor-related lncRNA. Previously, several studies have reported that ZNF667-AS1 was abnormally expressed in several tumor specimens and cells by the use of RT-PCR and high-throughput sequencing [18–20]. In addition, its tumor-related functions acting as tumor promoters or antioncogenes have been reported in nasopharyngeal carcinoma, esophageal squamous cell carcinoma, and cervical cancer [21–23]. However, whether ZNF667-AS1 also displayed an abnormal expression in glioma had not been investigated. Here, its expressing pattern and clinical significance in glioma patients are to be primarily explored.

2. Patients and Methods

2.1. Patient Data and Tissue Samples. Patients with glioma admitted to the oncology from June 2012 to August 2015 were drawn from the hospital tumor registry. The 155 enrolled patients were aged from 29 to 65 years, with a median age of 42 years. Histological diagnoses were made according to the 2007 WHO classification. 141 glioma patients completed follow-up, and the rate of loss to follow-up was 9%. All the patients did not receive prior anticancer treatment.

The flow chart in the section of study patients was shown in Figure 1. This study proved overall samples by pathology-related tests and incubated them in liquid nitrogen to achieve the subsequent overall RNA extracting process. The clinical and pathological data for the patients are reported in Table 1. The present study was ethically approved by the Research Ethics Committee of the Hubei Provincial Hospital of Integrated Chinese and Western Medicine (number: 20180056), and written informed consent was acquired from patient.

2.2. Cell Culture and siRNA Transfection. Human glioma cell lines, LN118, SHG44, U87, U251, and A172, were obtained from Cell Bank of Chinese Academy of Sciences (Pudong, Shanghai, China). The cells were grown in the Roswell Park Memorial Institute (RPMI) 1640 medium, supplemented with 10% fetal bovine serum (FBS) (Yunshan Technology, Haidian, Beijing, China), 100 U/ml penicillin G (Yunshan Technology, Haidian, Beijing, China), and 100 μ g/ml strepto-

mycin (Sigma, Suzhou, Jiangsu, China). Normal human astrocytes (NHA) were obtained from Weihui Biot (Hangzhou, Zhejiang, China) and were grown in Dulbecco's Modified Eagle's Medium with high glucose and sodium pyruvate.

The siRNAs used to knockdown ZNF667-AS1 were purchased from GEMA GENE (Pudong, Shanghai, China). The siRNA sequences were as follows: si-ZNF667-AS1: CTAC CACAGCTTCCATG; si-ZNF667-AS1-2: GCCCACTGTAT TCAACA. Cell transfection was conducted by using the LipofectamineTM 2000 transfection reagent (Invitrogen, Guangzhou, Guangdong, China) according to the manufacturer's instructions. After transfection for 24 h, the knockdown efficiency was evaluated by RT-PCR.

2.3. Reverse Transcription and qPCR Analyses. Total RNA from glioma specimens and nontumor specimens was extracted with the Trizol reagent (Takara, Kunshan, Jiangsu, China) by complying with the plan of the producer. RNA concentration was ascertained; this study adopted 100 μ g of RNA during reverse transcription. Based on an ABI 7900 Real-Time PCR System, this study conducted qPCR with the plan below: 95°C for 3 min., 40 cycles of 95°C for 15 sec., 60°C for 15 sec., and 72°C for 30 sec. The comparative expressing level of ZNF667-AS1 underwent the normalization to GAPDH. The primers included ZNF667-AS1 forward, 5'-GGTCCACTTCACGCACTTGC-3'; ZNF667-AS1 reverse, 5'-ACCATTCGAACTTGGCTACA-3'; GAPDH forward, 5'-GTCAACGGATTTGGTCTGTA-3'; GAPDH reverse, 5'-AGTCTTCTGGGTGGCAGTG-3'. Using the $2^{-\Delta\Delta Ct}$ approach, the relative expression conditions of the gene of interest were obtained. qRT-PCR reaction processes were overall performed 3 times.

2.4. Cell Proliferation Assays. For the cell proliferation analysis, 300 living cells (A172 and LN118 cells) were transfected with either si-ZNF667-AS1-1, ZNF667-AS1-2, or a scrambled control and plated onto 96-well plates. Every 24 h, the CCK-8 solution (10 μ l) was added to three randomly selected wells, and the cultures were incubated at 37°C for 90 min. The absorbance was measured at 450 nm using a microplate reader.

2.5. Statistical Analysis. Statistical analysis was conducted with SPSS version 13.0 software (SPSS Inc, Chicago, IL, USA). With the Student's *t*-test, the diversifications of two cohorts were discussed. The relationship between the ZNF667-AS1-expressing level and clinical-pathological characteristics was analyzed with the chi-square test. Based on the Kaplan-Meier approach, the overall survival (OS) and disease-free survival (DFS) ratios were obtained with the log-rank experiment adopted to draw the comparing process. Multivariate Cox regression analyses were carried out for analyzing the survival information. A *p* value <0.05 was suggested to exhibit statistical significance.

3. Results

3.1. ZNF667-AS1 Was Upregulated in Glioma. To determine the possible functions of ZNF667-AS1 in glioma, we enrolled

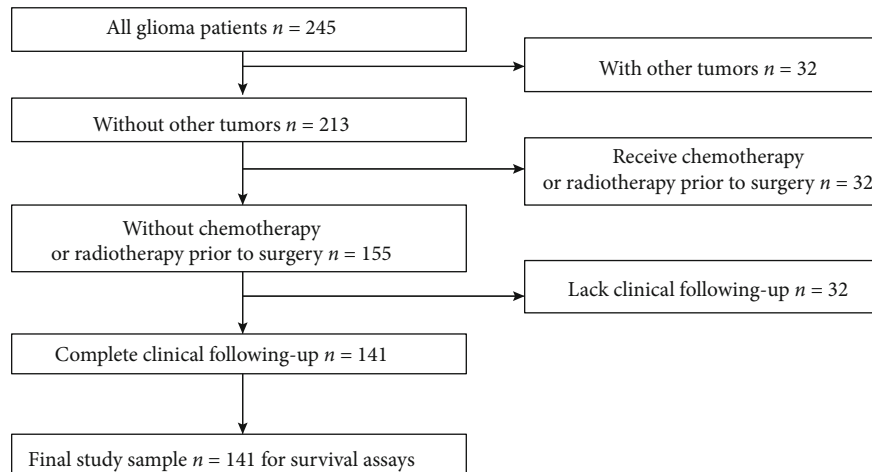


FIGURE 1: Flow chart in the selection of study patients.

TABLE 1: The association between the ZNF667-AS1 expression and different clinicopathological features of 155 human gliomas.

Parameter	No. of cases	ZNF667-AS1 expression		<i>p</i> value
		High	Low	
Age				0.369
<50	82	39	43	
≥50	73	40	33	
Gender				0.394
Male	93	50	43	
Female	62	29	33	
WHO grade				0.005
I-II	108	47	61	
III-IV	47	32	15	
KPS score				0.008
<80	57	37	20	
≥80	98	42	56	
Tumor size				0.145
<3 cm	95	44	51	
≥3 cm	60	35	25	

155 glioma patients and performed RT-PCR to examine the expression of ZNF667-AS1 in a total of 155 paired glioma tissues and corresponding nontumor tissues. As shown in Figure 2(a), we observed that the ZNF667-AS1 expression was distinctly increased in glioma specimens compared to matched nontumor specimens ($p < 0.01$). Besides, we also observed that glioma specimens with advanced stages exhibited a higher level of ZNF667-AS1 than those with early stages ($p < 0.01$, Figure 2(b)). Overall, our findings suggested ZNF667-AS1 as a functional regulator in glioma progression.

3.2. The Diagnostic Significance of the Overexpression of ZNF667-AS1 in Glioma. Previous studies have revealed several functional lncRNA that displayed a diagnostic value in glioma patients. Then, we performed ROC assays which

showed that the high ZNF667-AS1 expression had an AUC value of 0.8541 (95% CI: 0.8148 to 0.8934) for glioma (Figure 3(a)). The sensitivity and specificity of ZNF667-AS1 expressions for distinguishing glioma samples from normal samples were 68.22%/84.57%. In addition, we also observed that ZNF667-AS1 could be used as a molecular marker for distinguishing glioma specimens with advanced stages from glioma specimens with early stages with an AUC of 0.7742 (95% CI: 0.6990-0.8494; $p < 0.01$, Figure 3(b)). Our findings suggested ZNF667-AS1 as an early diagnosis indicator for glioma patients.

3.3. Correlations between ZNF667-AS1 and Clinical Features of Glioma. For better understanding of the clinical relevance of the ZNF667-AS1 expression in glioma, the 155 glioma patients were split as a high expression cohort ($n = 79$) and a low expression cohort ($n = 76$), complying with the median expressing condition of ZNF667-AS1 (5.62) in all glioma samples. Then, our group determined the possible association between ZNF667-AS1 levels and several clinical factors using the chi-square test which suggested that the high ZNF667-AS1 expression was associated with the WHO grade ($p = 0.005$) and KPS score ($p = 0.008$, Table 1). However, there were no significant correlations of the ZNF667-AS1 expression with other clinical features ($p > 0.05$).

3.4. The Possible Prognostic Values of the ZNF667-AS1 Expression in Glioma. To further explore whether ZNF667-AS1 may display a positive influence on the survivals of glioma patients, we collected the survival data of all 141 patients who completed five-year follow-up, which were analyzed using the Kaplan-Meier survival curves. Interestingly, our results revealed that patients with the high expression of ZNF667-AS1 had shorter OS ($p < 0.0026$; Figure 4(a)) and DFS ($p < 0.005$; Figure 4(b)) as compared with the ZNF667-AS1 low group. More importantly, in a multivariate Cox model, we demonstrated that the ZNF667-AS1 expression was an independent poor prognostic factor for both 5-year OS (HR = 2.897, 95% CI: 1.365-

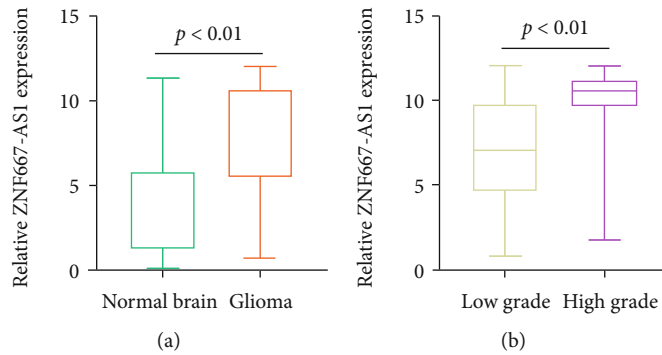


FIGURE 2: The ZNF667-AS1 expression is increased in glioma tissues. (a) The relative expression of ZNF667-AS1 in paired tumor and nontumor tissues ($n = 155$) by RT-PCR. The expression of ZNF667-AS1 in different tumor grades.

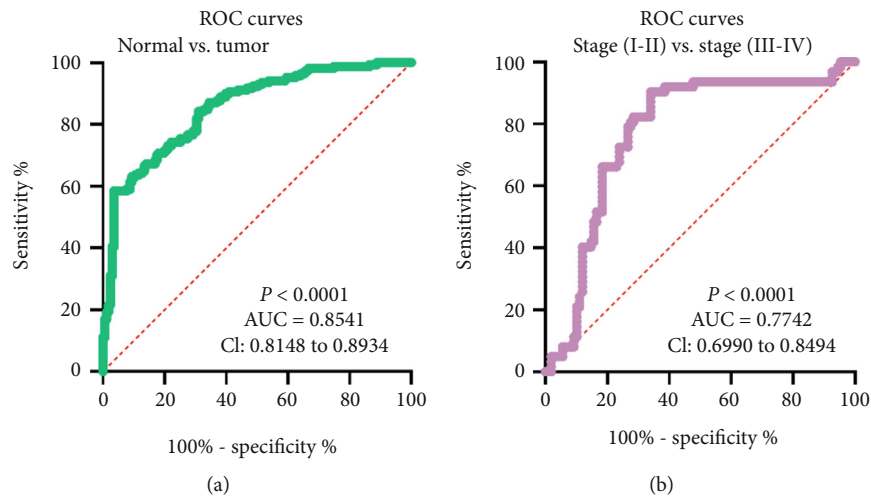


FIGURE 3: ZNF667-AS1 may be a potential diagnostic biomarker for glioma patients. (a) The ROC curve for the diagnostic value of ZNF667-AS1 in distinguishing glioma specimens from nontumor brain specimens. (b) The ROC curve for the diagnostic value of ZNF667-AS1 in distinguishing glioma specimens with stages (I-II) from glioma specimens with stages (III-IV).

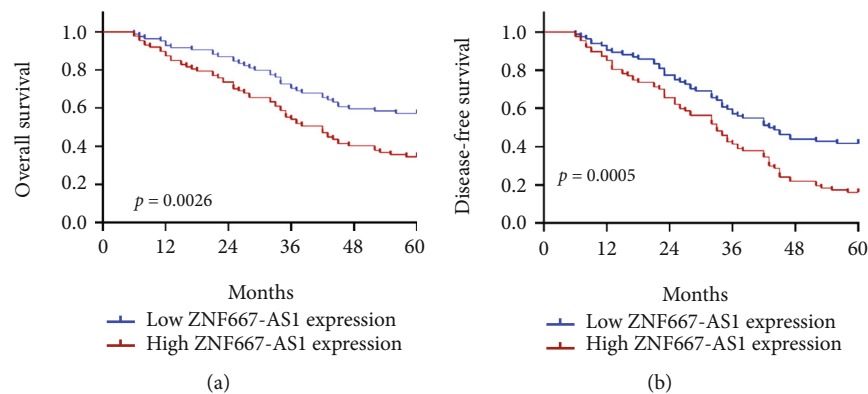


FIGURE 4: Kaplan-Meier curves of the overall survival (a) and disease-free survival (b) of 155 glioma patients.

4.784, $p = 0.008$) and 5-year DFS (HR = 3.019, CI=1.414-4.899, $p = 0.005$) in glioma (Table 2).

3.5. Effects of ZNF667-AS1 on Proliferation of Glioma Cells. To analyze the possible function of ZNF667-AS1 on the proliferation of glioma cell, we firstly examine the expression of ZNF667-AS1 in five glioma cells, finding that ZNF667-AS1

was highly expressed in five glioma cells compared to NHA (Figure 5(a)). Because A172 and LN118 cells exhibited a higher level of ZNF667-AS1, we chose them for the following experiments. Real-time PCR was performed to confirm the successful knockdown of ZNF667-AS1 in A172 and LN118 cells after the transfection of si-ZNF667-AS1-1 and si-ZNF667-AS1-2 (Figure 5(b)). CCK-8 assays revealed that

TABLE 2: Multivariate analysis of the overall survival and disease-free survival in glioma patients.

Variables	Overall survival			Disease free survival		
	HR	95% CI	<i>p</i> value	HR	95% CI	<i>p</i> value
Age	0.882	0.452-1.342	0.233	1.113	0.673-1.732	0.143
Gender	1.442	0.642-2.104	0.342	1.632	0.773-2.341	0.219
WHO grade	2.893	1.324-4.872	0.009	3.014	1.432-5.118	0.005
KPS score	2.782	1.423-4.563	0.013	2.964	1.395-4.895	0.007
Tumor size	1.237	0.672-1.897	0.213	1.427	0.875-2.137	0.136
ZNF667-AS1 expression	2.897	1.365-4.784	0.008	3.019	1.414-4.899	0.005

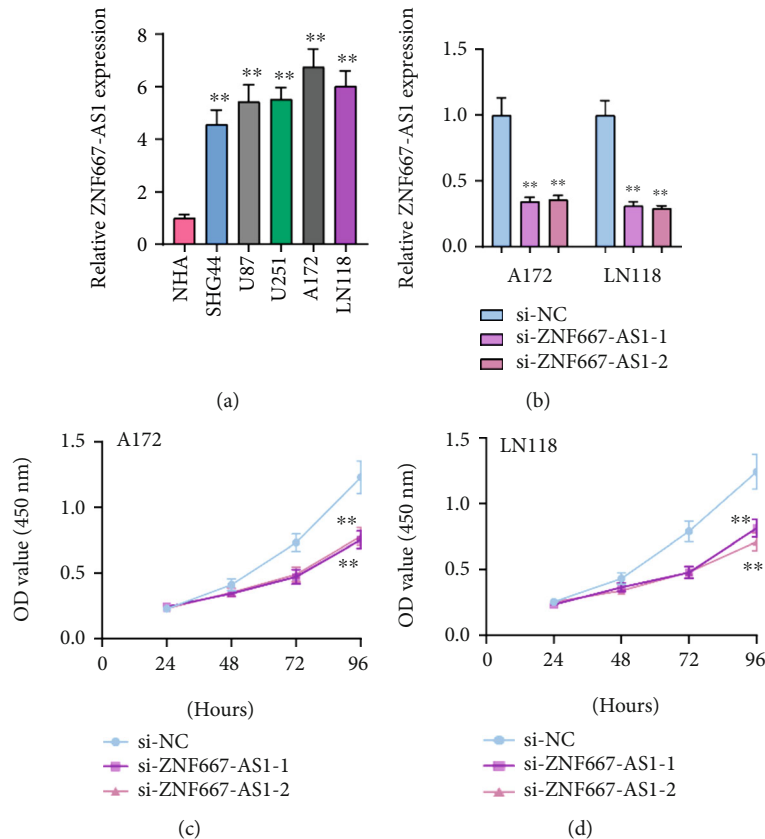


FIGURE 5: Knockdown of ZNF667-AS1 silencing inhibits the proliferation of A172 and LN118 cells. (a) RT-PCR for the demonstration of the ZNF667-AS1 expression in five glioma cells and NHA. (b) qPCR analyses of ZNF667-AS1 levels following treatment of A172 and LN118 cells with si-ZNF667-AS1-1, ZNF667-AS1-2, or si-NC. (c, d) The MTT assay was performed to determine the proliferation of A172 and LN118. $**p < 0.05$.

knockdown of ZNF667-AS1 significantly suppressed cell proliferation in A172 and LN118 cells (Figures 5(c) and 5(d)). Overall, our findings suggested that ZNF667-AS1 served as a tumor promotor in glioma.

4. Discussion

Glioma is the most common intracranial malignant tumor in humans [1, 24]. Highly glioma presents unique challenges due to its tendency to proliferate and invade tissues. Malignant gliomas, including glioblastomas, with radiotherapy and temozolomide have only a small survival benefit [25, 26]. The sensitive biomarkers were very important for the

treatments of tumor patients [27, 28]. However, none of the currently identified biomarkers are sensitive or specific enough for reliable glioma screening in clinical settings. In recent years, growing studies have indicated that some functional lncRNAs could be used as novel biomarkers for prognosis, survival, and responses to the treating process that paved a novel wave of research into molecular markers of glioma [29, 30]. In this study, we forced on a novel glioma-related lncRNA ZNF667-AS1.

In recent years, several studies have reported the dysregulated expression of ZNF667-AS1 and its possible effects in several tumors. For instance, Chen et al. [21] reported that the expression of ZNF667-AS1 was distinctly decreased in

nasopharyngeal carcinoma specimens and cell lines. Functionally, the overexpression of ZNF667-AS1 was shown to suppress the proliferation of nasopharyngeal carcinoma cells via increasing the ABLIM1 expression via adsorbing miR-1290. Li et al. [23] showed that ZNF667-AS1 was significantly highly expressed in cervical cancer, and its low levels suggested a poor prognosis of cervical cancer patients. In vitro and in vivo assays indicated that the forced expression of ZNF667-AS1 inhibited the proliferation and metastasis through counteracting the miR-93-3p-dependent PEG3 suppression. Moreover, ZNF667-AS1 was also shown to suppress the inflammatory response, promoting the recovery of spinal cord injury via suppressing the JAK-STAT pathway [31]. The negatively regulatory association between ZNF667-AS1 and JAK-STAT pathway highlighted its potential effects acting as tumor suppressors in tumors due to the important effects of the JAK-STAT pathway in tumor progression. All previous findings suggested ZNF667-AS1 may be a critical regulator in several tumor kinds. However, the expressing and clinical value of ZNF667-AS1 in glioma remained unclear.

Here, the expressing condition of ZNF667-AS1 in 155 glioma patients was first examined, confirming that the ZNF667-AS1 expression was distinctly upregulated in glioma specimens in comparison with matched nontumor brain tissues, which was inconsistent with its expression trend in other several tumors. Then, we determined the diagnostic value in glioma patients and found that ZNF667-AS1 in tissues effectively differentiated glioma tissues from nontumor specimens with an area under the ROC curves (AUC) of 0.8541. The diagnostic value of the ZNF667-AS1 expression was also confirmed in patients with different stages. Then, we analyzed the clinical significance of the ZNF667-AS1 expression, finding that the high ZNF667-AS1 expression was associated with the KPS score and advanced WHO grade, suggesting it that acted as a tumor promotor in clinical progression of glioma. Moreover, after analyzing the survival data with five-year following-up, we confirmed that patients with high ZNF667-AS1 expressions exhibited a longer OS and DFS than those with low ZNF667-AS1 expressions. Finally, the results of the multivariate study verified ZNF667-AS1 a single predictor for OS and DFS in glioma patients. On the other hand, we also performed CCK-8 assays to explore the tumor-related effects of ZNF667-AS1 on glioma cells, confirming that knockdown of ZNF667-AS1 suppressed the proliferation of glioma cells. Our findings suggested ZNF667-AS1 as a tumor promotor in glioma progression.

Some limitations of this study should be noted. First, because of the small number of patients analyzed in our research, more patients for clinical experiments are required to confirm our findings. Second, we fail to determine whether the serum ZNF667-AS1 expression was dysregulated in glioma patients. The serum biomarkers are very important for the monitor of the therapy response in real-time. Third, the potential effects of ZNF667-AS1 on the metastasis ability and in vivo assays are not performed. In the future, we plan to more fully describe the mechanisms and relationships with lncRNAs related to glioma biomarkers.

5. Conclusions

The results revealed initially that ZNF667-AS1 may represent a valuable independent prognostic indicator for glioma. Further study to discover the molecular mechanism of ZNF667-AS1 about tumor migration and invasion is currently in progress.

Data Availability

The data used to support the findings of this study are available from the corresponding author upon request.

Conflicts of Interest

The authors declare no conflicts of interest.

Authors' Contributions

Qin Yuan and Chao Gao are co-first authors.

Acknowledgments

This study was supported by the Fujian Provincial Health and Family Planning Youth Scientific Research Project (No. 2016-2-66).

References

- [1] Q. T. Ostrom, L. Bauchet, F. G. Davis et al., "The epidemiology of glioma in adults: a "state of the science" review," *Neuro-Oncology*, vol. 16, no. 7, pp. 896–913, 2014.
- [2] S. A. Grimm and M. C. Chamberlain, "Brainstem glioma: a review," *Current Neurology and Neuroscience Reports*, vol. 13, no. 5, 2013.
- [3] R. Chen, M. Smith-Cohn, A. L. Cohen, and H. Colman, "Glioma subclassifications and their clinical significance," *Neurotherapeutics*, vol. 14, no. 2, pp. 284–297, 2017.
- [4] N. A. Bush, S. M. Chang, and M. S. Berger, "Current and future strategies for treatment of glioma," *Neurosurgical Review*, vol. 40, no. 1, pp. 1–14, 2017.
- [5] S. L. Hervey-Jumper and M. S. Berger, "Insular glioma surgery: an evolution of thought and practice," *Journal of Neurosurgery*, vol. 130, no. 1, pp. 9–16, 2019.
- [6] L. Liu, Q. Wang, Z. Qiu et al., "Noncoding RNAs: the shot callers in tumor immune escape," *Signal Transduction and Targeted Therapy*, vol. 5, no. 1, 2020.
- [7] M. Matsui and D. R. Corey, "Non-coding RNAs as drug targets," *Nature Reviews Drug Discovery*, vol. 16, no. 3, pp. 167–179, 2017.
- [8] S. Jathar, V. Kumar, J. Srivastava, and V. Tripathi, "Technological developments in lncRNA biology," *Advances in Experimental Medicine and Biology*, vol. 1008, pp. 283–323, 2017.
- [9] M. M. Kumar and R. Goyal, "LncRNA as a therapeutic target for angiogenesis," *Current Topics in Medicinal Chemistry*, vol. 17, no. 15, pp. 1750–1757, 2017.
- [10] G. Romano, M. Saviana, P. Le et al., "Non-coding RNA editing in cancer pathogenesis," *Cancers*, vol. 12, no. 7, article 1845, 2020.

- [11] F. Ferrè, A. Colantoni, and M. Helmer-Citterich, "Revealing protein-lncRNA interaction." *Briefings in Bioinformatics*, vol. 17, no. 1, pp. 106–116, 2016.
- [12] J. Xin, Y. H. Zhao, X. Y. Zhang, and L. Q. Tian, "LncRNA NFIA-AS2 promotes glioma progression through modulating the miR-655-3p/ZFX axis," *Human Cell*, vol. 33, no. 4, pp. 1273–1280, 2020.
- [13] B. Zhu, S. Zhang, N. Meng, H. Zhang, S. Yuan, and J. Zhang, "Long non-coding RNA RNCR3 promotes glioma progression involving the Akt/GSK-3 β pathway," *Oncology Letters*, vol. 18, no. 6, pp. 6315–6322, 2019.
- [14] A. M. Schmitt and H. Y. Chang, "Long noncoding RNAs in cancer pathways," *Cancer Cell*, vol. 29, no. 4, pp. 452–463, 2016.
- [15] J. Li, Z. Li, W. Zheng et al., "LncRNA-ATB: an indispensable cancer-related long noncoding RNA," *Cell proliferation*, vol. 50, no. 6, article e12381, 2017.
- [16] J. Song, X. Chen, Q. Tian et al., "The value of lncRNA GHET1 as a prognostic factor for survival of Chinese cancer outcome: a meta-analysis," *Disease Markers*, vol. 2019, Article ID 5824190, 7 pages, 2019.
- [17] J. Huang, Y. Zheng, X. Xiao et al., "A circulating long noncoding RNA panel serves as a diagnostic marker for hepatocellular carcinoma," *Disease Markers*, vol. 2020, Article ID 5417598, 12 pages, 2020.
- [18] L. Vrba and B. W. Futscher, "Epigenetic silencing of lncRNA MORT in 16 TCGA cancer types," *F1000Research*, vol. 7, 2018.
- [19] L. Vrba and B. W. Futscher, "Epigenetic silencing of MORT is an early event in cancer and is associated with luminal, receptor positive breast tumor subtypes," *Journal of breast cancer*, vol. 20, no. 2, pp. 198–202, 2017.
- [20] L. Vrba, J. C. Garbe, M. R. Stampfer, and B. W. Futscher, "A lincRNA connected to cell mortality and epigenetically-silenced in most common human cancers," *Epigenetics*, vol. 10, no. 11, pp. 1074–1083, 2015.
- [21] X. Chen, Y. Huang, D. Shi et al., "LncRNA ZNF667-AS1 Promotes ABLIM1 Expression by Adsorbing microRNA-1290 to Suppress Nasopharyngeal Carcinoma Cell Progression," *OncoTargets and Therapy*, vol. 13, pp. 4397–4409, 2020.
- [22] Z. Dong, S. Li, X. Wu et al., "Aberrant hypermethylation-mediated downregulation of antisense lncRNA ZNF667-AS1 and its sense gene ZNF667 correlate with progression and prognosis of esophageal squamous cell carcinoma," *Cell Death & Disease*, vol. 10, no. 12, 2019.
- [23] Y. J. Li, Z. Yang, Y. Y. Wang, and Y. Wang, "Long noncoding RNA ZNF667-AS1 reduces tumor invasion and metastasis in cervical cancer by counteracting microRNA-93-3p-dependent PEG3 downregulation," *Molecular oncology*, vol. 13, no. 11, pp. 2375–2392, 2019.
- [24] Z. Zhao, K. N. Zhang, R. C. Chai et al., "ADAMTSL4, a secreted glycoprotein is a novel immune-related biomarker for primary glioblastoma multiforme," *Disease markers*, vol. 2019, Article ID 1802620, 12 pages, 2019.
- [25] S. Lapointe, A. Perry, and N. A. Butowski, "Primary brain tumours in adults," *Lancet (London, England)*, vol. 392, no. 10145, pp. 432–446, 2018.
- [26] D. Bready and D. G. Placantonakis, "Molecular pathogenesis of low-grade glioma," *Neurosurgery Clinics of North America*, vol. 30, no. 1, pp. 17–25, 2019.
- [27] R. X. Geng, N. Li, Y. Xu et al., "Identification of core biomarkers associated with outcome in glioma: evidence from bioinformatics analysis," *Disease markers*, vol. 2018, Article ID 3215958, 16 pages, 2018.
- [28] F. Yuan, L. Yi, L. Hai et al., "Identification of key pathways and genes in the Orai2 mediated classical and mesenchymal subtype of glioblastoma by bioinformatic analyses," *Disease markers*, vol. 2019, Article ID 7049294, 13 pages, 2019.
- [29] M. Velázquez-Flores, J. M. Rodríguez-Corona, J. E. López-Aguilar et al., "Noncoding RNAs as potential biomarkers for DIPG diagnosis and prognosis: XIST and XIST-210 involvement," *Clinical and Translational Oncology*, vol. 22, 2020.
- [30] A. Zottel, N. Šamec, A. Videtič Paska, and I. Jovčevska, "Coding of glioblastoma progression and therapy resistance through long noncoding RNAs," *Cancers*, vol. 12, no. 7, article 1842, 2020.
- [31] J. W. Li, Y. Kuang, L. Chen, and J. F. Wang, "LncRNA ZNF667-AS1 inhibits inflammatory response and promotes recovery of spinal cord injury via suppressing JAK-STAT pathway," *European review for medical and pharmacological sciences*, vol. 22, no. 22, pp. 7614–7620, 2018.

Review Article

Explicating the Pivotal Pathogenic, Diagnostic, and Therapeutic Biomarker Potentials of Myeloid-Derived Suppressor Cells in Glioblastoma

Seidu A. Richard 

Department of Medicine, Princefield University, P. O. Box MA 128, Ho, Ghana

Correspondence should be addressed to Seidu A. Richard; gbepoo@gmail.com

Received 3 September 2020; Revised 19 October 2020; Accepted 24 October 2020; Published 4 November 2020

Academic Editor: Wen-Jun Tu

Copyright © 2020 Seidu A. Richard. This is an open access article distributed under the Creative Commons Attribution License, which permits unrestricted use, distribution, and reproduction in any medium, provided the original work is properly cited.

Glioblastoma (GBM) is a malignant and aggressive central nervous tumor that originates from astrocytes. These pathogenic astrocytes divide rapidly and are sustained by enormous network of blood vessels via which they receive requisite nutrients. It well proven that GBM microenvironment is extremely infiltrated by myeloid-derived suppressor cells (MDSCs). MDSCs are a heterogeneous cluster of immature myeloid progenitors. They are key mediates in immune suppression as well as sustenance glioma growth, invasion, vascularization, and upsurge of regulatory T cells via different molecules. MDSCs are often elevated in the peripheral blood of patients with GBM. MDSCs in the peripheral blood as well as those infiltrating the GBM microenvironment correlated with poor prognosis. Also, an upsurge in circulating MDSCs in the peripheral blood of patients with GBM was observed compared to benign and grade I/II glioma patients. GBM patients with good prognosis presented with reduced MDSCs as well as augmented dendritic cells. Almost all chemotherapeutic medication for GBM has shown no obvious improvement in overall survival in patients. Nevertheless, low-dose chemotherapies were capable of suppressing the levels of MDSCs in GBM as well as multiple tumor models with metastatic to the brain. Thus, MDSCs are potential diagnostic as well as therapeutic biomarkers for GBM patients.

1. Introduction

Glioblastoma (GBM) is a malignant and aggressive central nervous tumor that originates from astrocytes [1, 2]. Astrocytes are star-shaped cells and are recognized to maintain brain tissue [1]. In GBM, pathogenic astrocytes divide rapidly and are sustained by enormous network of blood vessels via which they receive requisite nutrients [1, 2]. Currently, standard management for patient with GBM comprises of maximal safe surgical resection, subsequent to concurrent radiation therapy as well as chemotherapy [3, 4]. The current chemotherapeutic medication includes temozolomide, lomustine, bevacizumab, and carmustine wafers [3, 5]. Nevertheless, none of these medications have shown obvious improvement in overall survival [3, 5]. The GBM microenvironment is extremely infiltrated by myeloid-derived suppressor cells (MDSCs) [1, 6–8].

MDSCs are a heterogeneous cluster of immature myeloid progenitors [9]. They are key mediates in immune suppres-

sion as well as sustenance glioma growth, invasion, vascularization, and upsurge of regulatory T cells via different molecules [9]. MDSCs are derived from monocytes and attain immunosuppressive ability during certain disease circumstances most especial cancer [10–12]. Human MDSCs are often depicted with pan-myeloid marker CD33, with monocytic CD14⁺ as well as granulocytic CD15⁺ subsets [10]. Interestingly, GBM microenvironment is usually depicted with the elevation of MDSC levels [10, 13]. Several studies have demonstrated that MDSCs are capable of blocking T cell as well as natural killer (NK) cell functions [14–16]. These blockades resulted in immunocompromise as well as a tumor-facilitatory microenvironment [14, 17, 18].

Studies have demonstrated that MDSCs via different mechanisms are capable of blocking T cell stimulation as well as expansion [11, 19, 20]. These mechanisms involve the generation of arginase and inducible nitric oxide synthase (iNOS), reactive oxygen species and/or reactive nitrogen species (ROS

and/or RNS), secretion of interleukin- (IL-) 10, and upsurge in regulatory T cells (Tregs), as well as blockade of T cell migration [11, 19–21]. Furthermore, MDSCs were capable of facilitating immunosuppression as well as tumor succession [11, 19, 20]. In view of lack of concrete biomarkers for GBM, this review explores the fundamental pathogenic and diagnostic as well as therapeutic biomarker potentials of MDSCs in GBM. The “boolean logic” was utilized to search for article on the subject matter. Most of the articles were indexed in PubMed and PubMed Central with strict inclusion criteria being *in vitro* and *in vivo* up or downregulation as well as therapeutic potentials of MDSCs in GBM.

2. MDSC Types and Subtypes in Glioma

Granulocytic/polymorphonuclear (G-MDSCs/PMN-MDSCs) and monocytic (M-MDSCs) are two groups of MDSCs [22, 23]. These two groups of MDSCs are phenotypically as well as morphologically analogous to neutrophils and monocytes, correspondingly [22, 23]. Elevated levels of both groups have been detected in the blood of patients with GBM [24]. Nevertheless, elevated levels of M-MDSCs correlated with tumor grade [24]. Dubinski et al. observed a downregulation of CD16 and upregulation of HLA-DR in both G-MDSCs and M-MDSCs at the tumor microenvironment of GBM tissues [22]. Nevertheless, the downregulation of CD16 and upregulation of HLA-DR were more prominent in M-MDSCs compared to G-MDSCs [22]. On the other hand, while eosinophilic MDSCs showed a robust upregulation of HLA-DR, neutrophilic MDSCs exhibited a dissimilar HLA-DR secretory pattern [22].

MDSCs are further subgrouped into CD11b⁺CD45^{low} and CD11b⁺CD45^{high} based on CD45 secretory levels in both rodent and human GBM [14]. Furthermore, CD11b⁺CD45^{low} cells are believed to be microglia while CD11b⁺CD45^{high} cells are believed to be peripheral macrophages [14, 25]. Nevertheless, the CD11b⁺CD45^{high} cells comprise of both macrophages and microglia [14, 26]. Also, in rodent GBM models, CD11b⁺CD45^{high} cell fraction was the predominantly expressed when the samples were stimulated with proinflammatory and immunosuppressing molecules [14]. Therefore, the CD11b⁺CD45^{high} cells appear to be the most reactive cells in GBM microenvironment influencing tumor progression [14].

In GBM microenvironment, the CD11b⁺CD45^{high} cell fraction, comprising microglia as well as macrophages, increased in a time-dependent manner, and naïve microglia triggered upregulate of CD45 [14, 26]. Comparatively, the stimulation of molecules like major histocompatibility complex (MHC) classes I and II, GR1, CD80, and CD86, as well as IL-10 showed observable effects in CD11b⁺CD45^{high} cells, while in CD11b⁺CD45^{low} fraction, no observable effects were visible [14]. Severe studies have also implicated CD11b⁺GR1⁺ cells as MDSC subtypes in GBM [14, 27, 28]. This subtype was capable of blocking antitumor responses as well as accelerated tumor progression [14, 27, 28]. Brandenburg et al. observed a robust upregulation of GR1 in MDSCs obtained from glioma samples which was limited to only the CD11b⁺CD45^{high} population [14]. They indi-

cated that the high secretion of GR1 in CD11b⁺CD45^{high} cells as well as their potential suppressive phenotype could inhibit some proinflammatory factors [14].

Studies have shown that tumor-bearing mice depleted of CD11b⁺Gr1⁺ cells survive longer compared to those treated with control isotype IgG [17, 29]. This means that this immune group actively participated in the pathogenesis as well as prognosis of gliomas [29]. CD11b⁺Gr1^{+/high} cells were the most predominate BIL population in the brain. CD11b⁺Gr1^{low} cell secretion resulted in an upregulation of IL-4R α in the tumor microenvironment as compared to healthy brain cells [29, 30]. MDSCs constituted about 5% of the cells within GBM tumor masses and were depicted with obvious CD33⁺/CD15⁻/CD14⁻/HLA-DR⁻ negative lineage subsequent to CD33⁺/CD15⁺/CD14⁻/HLA-DR⁻ neutrophilic as well as CD33⁺/CD15⁻/CD14⁺/HLA-DR⁻ monocytic subtypes [29–31].

3. MDSCs at the Glioblastoma Microenvironment

Several studies have demonstrated that MDSCs amass in the tumor and spleen, as well as the peripheral blood of patients with GBM [11, 13, 22, 28, 31–33]. They are capable of eliciting immune blockade via dampening the function of NK cells and cytotoxic T lymphocytes (CTLs) in these tissues [11, 13, 22, 28, 31–33]. Several studies have further demonstrated that MDSCs infiltrate the glioma microenvironment and function as drivers of immune-inhibitory phenotype distinctive to these lesions [10, 34, 35]. Suppression of MDSCs within glioma microenvironment facilitated survival as a result of concurrent upsurge of MDSCs within bone marrow, as well as an upsurge in functional tumor-infiltrating lymphocytes [34].

In the GBM microenvironment, angiogenin, insulin-like growth factor binding protein (IGFBP 2&3), IL-6, IL-8, monocyte chemoattractant protein-1 (MCP-1/CCL2), macrophage migration inhibitory factor (MIF), and osteopontin, as well as tissue inhibitor of metalloproteinases (TIMP 1&2) were significantly elevated [36]. Several studies have demonstrated that chemokine receptors particularly chemokine receptor 2 (CCR2) were capable of activating the collection of MDSCs at the GBM microenvironment [10, 34, 37]. Also, studies have demonstrated that GBM was capable of secreting IL-8 which in turn triggered the trafficking of MDSCs into the tumor environment via the CXCR2 receptor which functions as MIF receptors [36, 38]. Studies have further demonstrated that higher levels of MCP-1/CCL-2 are secreted GBMs as well as other glioma variants [36, 39, 40]. MCP-1/CCL-2 secreted by GBMs is capable of trafficking MDSCs into the tumor microenvironment and felicitated tumor growth via MDSCs [36, 39, 40].

In GBMs, monocytic Ly6C-secreting MDSCs are the principal constituent of the GBM microenvironment and represent about 40% of the total tumor mass [34, 37]. Ly6C^{high} inflammatory monocytes principally secrete CCR2 [34, 37]. Flores-Toro et al. observed a reduction in CD11b⁺/Ly6C^{high}/PD-L1⁺ MDSCs in GBMs which was associated with an upsurge in overall CCR2⁺ cells as well as MDSCs

within bone marrow of CCR2-deficient mice [34]. They further established that CCR2 antagonist CCX872 prolonged median survival as a monotherapy in KR158 glioma-bearing animals [34]. Furthermore, it also prolonged median as well as overall survival when combined with anti-PD-1 [34]. Nevertheless, a combination of CCX872 and anti-PD-1 lengthened median survival time in 005 GSC GBM-bearing mice [34]. Also, in both models, CCX872 reduced tumor-related MDSCs as well as augmented these cells within the bone marrow [34].

NF- κ B signaling demonstrated to be capable of mediation in MDSC expansion in an aging brain model [41, 42]. Tumor-associated myeloid cells deficient in NF- κ B signaling exhibit anti-inflammatory properties, which was seen as augmentation in inflammatory mediators subsequent to restricted deletion of p65 in myeloid cells in GBM models [41]. On the other hand, Janus Kinase (JAK)/Signal Transducer and Activator of Transcription (STAT) pathway is often stimulated during inflammatory and immune responses [41–43]. This pathway has demonstrated to be capable of influencing MDSC reaction in response to several stimuli [41, 43].

NF- κ B was capable of triggering STAT3 resulting in the induction of indoleamine 2,3-dioxygenase (IDO) enzyme upregulation which functions as an immune suppressive mediator in MDSCs [41, 43]. Also, stimulation of the IDO enzyme in dendritic cells (DCs) resulted in GBM immune evasion [44, 45]. Furthermore, tryptophan was extremely metabolized in tumor microenvironment [44]. Also, tryptophan metabolites which were initially observed in peripheral tolerance and maternal tolerance of fetus as well as stimulation of autoimmune disease were associated with MDSC immunosuppressive mechanisms [44, 45]. Also, IL-6 is an effective stimulator of STAT3 which has demonstrated to regulate MDSC-facilitated immunosuppression [36, 46].

MDSCs are capable of blocking adaptive immunity of the body via the triggering of Treg cells [1, 47]. Treg cells are CD4⁺ T cells with associated prominent FOXP3 and are recognized to be capable of inhibiting innate immune responses [1, 48]. Arginase-1 (Arg-1) was capable of triggering MDSC immunosuppression via the depletion L-arginine fundamental for growth as well as differentiation of T cells, leading to T cell dysfunction [9, 49]. Huang et al. demonstrated that MDSCs were capable of stimulating the development of Treg cells both *in vitro* and *in vivo*, via the stimulation of TGF- β and IL-10 as well as cell-cell communication [50]. MDSC modifications resulted in a reduction in TCR binding to MHC I-peptide complexes in CD8⁺ T cells as well as decreased the ability of these cells to respond to antigen peptides [44].

MDSCs generated excessive ROS as well as RNS which were capable of inhibiting the maturation of DC which in turn resulted in the accumulation of MDSCs [44]. Also, ROS and RNS have been implicated in T cell inactivation. Furthermore, peroxy-nitrite generation resulted in posttranslation protein alterations via the nitration of tyrosine, cysteine, and methionine as well as tryptophan [44]. MDSCs are capable of inhibiting the production and storage of T cells in lymph nodes [44]. Naive T cells infiltrate secondary lymph nodes via the secretion of L-selectin and become stimulated

via antigen peptides originating from tumor sites through lymphatic vessels [44, 51]. MDSCs are capable of downregulating L-selectin secretion on naive T cell surface via the release of ADAM metallopeptidase domain 17 (ADAM17, 44, and 51). ADAM17 is associated with the proteolytic cleavage and shedding of the L-selectin ectodomain [44, 51].

Freshly isolated blood-derived neutrophilic and less efficiently eosinophilic MDSCs were capable of inhibiting autologous nonspecific T cell proliferation and IFN- γ secretion *in vitro* and not monocytic MDSCs [22]. Studies have shown that peripheral cellular immunosuppression in patients with GBM was mediated by degranulated neutrophils or CD33⁺HLA-DR⁺CD15⁺ cells [13, 22, 52]. Tumor-related MDSCs secreted higher levels of MHC-II compared to microglia and macrophages in patients with GBM [53]. Contrary, MDSCs were characterized by deficiency of MHC-II secretion and the existence of the myeloid marker CD33 in blood or CD11b in tumor tissue [33].

Kohanbash et al. demonstrated that IL-4R α was upregulated in myeloid cells precisely at the tumor microenvironment but not in the periphery in patients with GBM and *de novo* murine glioma models [30]. They further revealed that GM-CSF, which is distinctively upregulated in the glioma microenvironment, triggered the secretion of IL-4R α in myeloid cells resulting in the promotion of IL-13-stimulated Arg-1 secretion as well as T cell suppression *in vitro* cultured cells as well as cells isolated from glioma-bearing hosts [30]. Future studies should focus on the functional role of MDSCs in gliomagenesis as well as malignant degeneration.

4. TAM and Glioblastoma

In GBMs, tumor-associated macrophages (TAMs) constitute about 20-30% of the cells in the entire tumor [54, 55]. TAMs are capable of secreting soluble factors as well as surface molecules that inhibit immune surveillance via endogenous T cells and NK cells resulting in the blockade of crosstalk between the adaptive and innate immune systems [54, 56, 57]. TAMs are classified into M1 macrophages and M2 macrophages [54, 55]. Several studies have demonstrated that GBMs are depicted cardinaly with the infiltration of TAM which influences the tumor progression, with both resident microglia and bone marrow-derived infiltrating monocytes capable of eliciting tumor growth-facilitatory activities [1, 6–8]. In GBM, fraction of TAM infiltration of the tumor correlated positively with the tumor grade [9, 58].

Classically stimulated M1 macrophages trigger antitumor response via generation of proinflammatory cytokines, presenting antigens to adaptive immune cells as well as phagocytosing tumor cells [9]. MDSCs are capable of secreting markers for proinflammatory M1 cells like iNOS, IL-1 β , and TNF- α , as well as CXCL10 [29]. Also, MDSCs are capable of secreting tumor-supportive M2-polarized macrophages like Arg-1, CCL17, and CD206, as well as CD36 [29]. Thus, MDSCs are pleiotropic nature [29]. Conventionally, studies have demonstrated that the alternatively secreted M2 macrophages secrete immunosuppressive cytokines like STAT3 as well as scavenger receptors like CD163, CD204,

and CD206 and facilitate tumor supportive CD4⁺ regulatory T cells [9, 59].

Studies have demonstrated that TAMs and MDSCs often form a sizeable percentage of tumor-infiltrating immune cells in the GBM tumor microenvironment [23, 60–62]. They range from 30–90% in human GBM samples, with CD11b⁺ MDSCs constituting the majority of infiltrating inflammatory cells in human gliomas [23, 61, 62]. Microglial TAMs were enhanced in the principal edge of the tumor as well as surrounding white matter in a study involving single-cell RNA sequencing of gliomas while blood-derived TAMs were more often seen within regions of microvascular proliferation as well as perinecrotic regions within the core of the tumor [23]. This is correlated with intense secretion of proinflammatory factors in the periphery as well as anti-inflammatory factors in the core [23, 63].

Also, TAMs that arose from the blood and migrate to brain tumors, where they assume an additional tissue-specific phenotype, proved to have a different metabolism and augmented secretion of immunosuppressive markers compared to microglia [23, 64]. Moreover, as glioma grade ascended, the proportion of blood-derived TAMs to microglia simultaneously ascended too [23, 65]. Nevertheless, notwithstanding the augmented affinity of microglia toward a proinflammatory phenotype, both cell categories have the possibility of triggering tumor-based microenvironment toward MDSCs and therefore are potential targets for myeloid therapy [23, 66].

5. MDSCs and Macrophage Migration Inhibitory Factor

Macrophage migration inhibitory factor (MIF) is derived from GBM cells, precisely medicinally resistant cancer stem cells, and it is obligatory for MDSC survival and function [32, 67]. Downregulation of MIF levels in GBM cells was incapable of modifying their proliferation [32, 67]. Nevertheless, an augmented host survival and an upsurge in the quantity of CD8⁺ T cells in the tumor microenvironment were observed when they were transplanted into an immune-proficient orthotopic model [32, 67, 68]. Also, MDSCs are capable of influencing macrophages resulting in inflammation as well as immunosuppressive effects in the tumor microenvironment [1, 69].

GBM tumors are often depicted with immunosuppressive milieu as well as participate in numerous pathways leading evasion of innate immune surveillance [1]. Most importantly, macrophage subtypes, principally M1 and M2, are the main origins of inflammatory cytokines [1]. M1 macrophages express IL-12 that facilitates the production of T helper 1 (Th1) adaptive immunity resulting in the triggering of cytotoxic effects in tumor cells [1, 70]. On the other hand, M2 macrophages are immune suppressive cells which are capable of facilitating matrix remodeling leading to tumor progression [1, 71]. M1 macrophages are depicted with elevated secretion of CD86 as well as IL-12 [1, 72].

A crosstalk between MDSCs and GBM tumor stem cells via MIF resulted in an augmented MDSC function as well as an upsurge in cytotoxic T cell infiltration, which may be

a potential target for inhibiting GBM progression [35, 67]. Kumar et al. established that MIF was prominent across all three of their glioma prepared samples [36]. Studies have shown that MIF was significantly secreted by GBM cells resulting GBM-mediated immunosuppression [36, 73, 74]. The most crucial MIF inhibitor is the 4-iodo-6 phenylpyrimidine (4-IPP) which has also demonstrated to be capable of inhibiting MDSC development [36, 75, 76].

6. MDSCs and Glioblastoma Hypoxia

Hypoxia is very fundamental in the progression as well as immunosuppressive function of GBMs. Hypoxia-triggered glioma culture medium was capable of differentiating tumor-associated macrophages to immunosuppressive M2 subtype [77, 78]. In hypoxic milieu, GBM cells are induced to express distinctive kinds of exosomes that are transported to normoxic zones of the tumor to facilitate the tumor progression [77, 79]. Exosomes are tiny vesicles of about 50–150 nm in diameter present in all bodily fluids and are expressed by both normal and malignant cells [77, 80]. Several studies have demonstrated that tumor exosomes transport genetic materials as well as proteins efficient in inhibiting the functions of immune cells as well as stimulating the triggering and expansion of MDSCs *in vitro* and *in vivo* [77, 81].

Several studies have demonstrated that hypoxia was capable of influencing the secretion and quantities of miRNA by exosomes which resulted in MDSC differentiation and accumulation [77, 79, 82]. Studies have further shown that GBM-derived exosomes (GDEs) are able to modify the mRNA secretory profiles of their fibroblasts as well as TAMs [77, 83, 84]. Guo et al. demonstrated that hypoxia facilitated the secretion of exosomes via GBM and that normoxia-stimulated GDEs (N-GDEs) as well as hypoxia-stimulated (H-GDEs) were taken up by MDSCs in mice [77]. They indicated that H-GDEs were more capable of triggering the expansion as well as immunosuppressive activities of MDSCs *in vivo* and *in vitro* [77]. Furthermore, miR-10a and miR-21 were upregulated in H-GDEs and had the most robust MDSC stimulatory influence amongst the 20 highest secretory GDE miRNAs [77].

Hypoxia-stimulatory miR-10a as well as miR-21 secretion in GDEs augmented the expansion as well as suppressive actions of MDSCs [78]. Thus, miRNAs are capable of being transferred from tumor cells to MDSCs via GDE crosstalk [77]. Extracellular transfer of hypoxia-stimulatory miR-10a as well as miR-21 in GDEs led to MDSC stimulation and downregulation of miR-10a as well as miR-21 target proteins [77, 78]. Hypoxia facilitated the expression as well as upregulation of miR-10a and miR-21 levels in GDEs [77]. Furthermore, H-GDEs miR-10a and miR-21 facilitated MDSC stimulation via the Rora/IκBα/NF-κB and Pten/PI3K/AKT pathways [77, 78]. Also, reduced MDSCs were detected in the spleens of mice bearing miR-10a or miR-21 knockout glioma cells compared to those bearing normal glioma cells [77]. Studies have proven that hypoxia-stimulated upregulation of miR-155 and miR-584 and the downregulation of miR-244 were associated with glioma progression [77, 85–87].

7. MDSC and T Cells

GBMs are highly immunosuppressive brain tumors that are well recognized for their T cell paucity [88]. GBMs are capable of escaping immunosurveillance via the trapping of T cells in the bone marrow via the loss of sphingosine-1-phosphate (S1P) receptor on the T cell surface [88]. Thus, GBMs were capable of escaping immunosurveillance via the locking away T cells in the bone marrow [88]. Bone marrow aspirates from treatment-naïve GBM patients as well as GBM-bearing mice showed extreme T cells in the bone marrow compared to the blood, while controls had matching T cell quantities in both bone marrow and blood [88]. Also, T cells were also scanty in the spleen, resulting in splenic shrinkage which implied that T cell generation in the bone marrow may be shrunken [88].

Domenis et al. observed a blockade of CD4⁺ T cell effector activities in unfractionated peripheral blood mononuclear cells (PBMCs) [89]. They explained that this blockade effect was as a result of the stimulation of monocytes, which required the skewing of immature immunophenotype towards the expansion of M-MDSCs and not as a result of direct delivery of exosomes to T cells [89]. They further indicated that GDEs were associated with the conversion of monocytes to Arg-1- and IL-10-generating M-MDSC cells that resulted in T cell immunosuppression without obligatory direct contact between monocytes and GBM cells [89].

MDSCs were capable of suppressing T cell activities via numerous mechanisms, including the generation as well as expression of nitric oxide (NO), Arg-1, and ROS most especially H₂O₂ [22, 33, 90]. Also, MDSCs' ability to suppress T cell responses resulted in the depletion of specific amino acids like L-arginine which are fundamental for T cell function. Arg-1 and nitric oxide synthase 2 (NOS2) are the two main catabolic enzymes via which MDSCs metabolize L-arginine [11, 22]. Patients with freshly detected GBM had an augmented quantity of circulating CD33⁺ HLA-DR2 MDSCs in their blood which comprises of neutrophilic (CD15⁺) and immature (CD152 and CD142), as well as monocytic (CD14⁺) subsets [22].

On the other hand, knockout of MDSCs from PBMCs with anti-CD33/CD15-coated beads *in vitro* partly restored T cell generation of IFN- γ after induction with anti-CD3/anti-CD28 antibodies [22]. Moreover, MDSC was not restricted to only the suppressing of CD4⁺ and CD8⁺ T cells, but also suppressing of cytotoxic activities of NK and NK T cells [91]. Thus, during cell cycle, MDSC uses numerous mechanisms to suppress immune responses. These suppressive mechanisms include arresting T cells in the G0-G1 phase, interfering with T cell trafficking such as CD8⁺ T cells unresponsive to antigen-specific activation and stimulation as well as expansion of Treg cells, and stimulating energy generation in NK cells, suppressing NK cell cytotoxicity as well as potential stimulation of NK T cells [91].

8. MDSCs and B Cells

B cells are produced from lymphoid precursors in the bone marrow in a strictly regulated process, with stepwise recom-

bination of V, (D) and J gene fragments coding for the variable (V) region of the immunoglobulin (Ig) heavy as well as the light chains [92, 93]. B cells are capable of producing functional, nonautoreactive B cell receptor (BCR) which differentiates into mature, naïve B cells [92]. B cells are capable of proliferating as well as differentiating into plasma cells without the support of T cells when B cell receptors are stimulated [92]. B cells are stimulated in the periphery before they migrate into secondary lymphoid tissues [92]. Furthermore, another route which B cells are stimulated locally via floating antigen or immune complexes was presented by DCs [92].

B cells have demonstrated to be fundamental in the GBM immune landscape [94, 95]. Lee-Chang et al. demonstrated that human as well as murine GBM-associated B cells exhibit an immunosuppressive phenotype depicted with the presence of inhibitory molecules such as PD-L1 and CD155 as well as the production of immunoregulatory cytokines like TGF- β and IL-10 [94]. They observed that regulatory B cells (Bregs) constituted about 10% of bone marrow-derived infiltrating immune cells in GL261 and CT2A orthotopic brain tumor models, and 40% of GBM patients were positive for B cell tumor infiltration during screening [94].

GBM-associated B cells exhibited immunosuppressive activities toward stimulated CD8⁺ T cells, and their pathophysiological significance was underlined by prolonged animal survival after local administration of B cell-depleting immunotherapy [94]. At the tumor microenvironment, MDSCs were capable of facilitating immunosuppression of B cells [94]. Also, MDSCs facilitated the transfer of membrane-bound PD-L1 to B cells, leading to the facilitation of B cell-associated immunosuppression [94]. Lee-Chang et al. detected that local intratumoral depletion of B cells correlated well with the enhancement of animal survival [94].

Moreover, the therapeutic efficiency of depleted of B cells was associated with augmented intratumor GzmB⁺ CD8⁺ T cells [96, 97]. This means that depletion of GBM-associated Bregs promoted CD8⁺ T cell stimulation and facilitated their effector function [96, 97]. On the other hand, *ex vivo* tumor-infiltrating B cells from GBM tumor samples demonstrated immunosuppressive activities toward CD8⁺ T cell stimulation [96, 97]. Also, adoptive transfer of naïve B cells not only salvaged the survival phenotype but also demonstrated that only tumor-infiltrating B cells exhibit elevated PD-L1 and CD155 [94]. Thus, dynamic process most likely occurred in the tumor microenvironment that switches naïve B cells into GBM-associated Bregs [94].

9. MDSCs and Interferons

Interferons (IFNs) are effective and extensively active cytokines that are capable of triggering cellular responses to nucleic acids of abnormal structure or location [98, 99]. Interferons have been detected in normal as well as malignant cells of all lineages in response to pathogenic molecular stimuli [98]. Interferons were capable of triggering transcription of numerous genes resulting in protein synthesis in both cellular and viral, autophagy, apoptosis, and angiogenesis as well as innate and adaptive immunity [98, 99].

MDSCs are able to illicit their immunosuppressive functions via feedback reaction to IFN- γ release by stimulated T cells, which in turn triggers the expression of IL-10 and TGF- β [50, 100]. The suppressive functions of MDSC was associated with IFN- γ secretion because MDSCs from IFN- $\gamma^{-/-}$ mice did not have the above capabilities [100, 101]. The presence of antibodies against mouse IFN- γ did not result in the elevation of lytic response in normal allo-cultures lacking MDSCs, while it does restore entirely immune responsiveness in cultures containing MDSCs [101]. Furthermore, exogenous IFN- γ was capable of replacing cytokines generated by either T lymphocytes or MDSCs derived from either the spleen or tumor infiltrate in supporting T lymphocyte blockade [101].

Pituch et al. demonstrated that, analogous to human chimeric antigen receptor (CAR) T cells, murine CAR T cells were associated with IL13R α 2-secreting glioma cells [102]. This was observed via their cytolytic actions as well as the production of IFN- γ and TNF- α in the presence of IL13R α 2-positive glioma cells [102]. They indicated that IL13R α 2-CAR T cells had antiglioma actions in two syngeneic glioma models and produced a proinflammatory tumor microenvironment in their *in vivo* experiments [102]. IL13R α 2-CAR.CD28. ζ T cell proliferation resulted in the production of IFN- γ and TNF- α as well as facilitated phenotypically proinflammatory glioma microenvironment by triggering elevated levels CD4 $^{+}$ and CD8 $^{+}$ T cells and CD8 α^{+} DCs as well as a reduction in Ly6G $^{+}$ MDSC levels [102].

IFN- γ was capable of binding with receptors that resulted in the stimulation JAK/STAT signaling pathway, which in turn resulted in the downregulatory secretion and stimulation of IRF-1, leading to secretion of PD-L1 by tumor cells [103, 104]. Studies have shown that, PD-1/PD-L1 was capable of reversing the immune evasion of glioma [103, 105]. Nduom et al. observed that PD-L1 was a negative prognostic indicator for GBM during their study involving 94 GBM patients [106].

Qian et al. found that the distribution of PD-L1 in glioma corresponded with morphologically apoptotic T cells [103]. They further observed that IFN- γ triggered PD-L1 release in primary cultured microglia and bone marrow-derived macrophages as well as GL261 tumor cells [103]. They concluded that IFN- γ derived from tumor-infiltrating T cells was capable of triggering PD-L1 secretion in the tumor microenvironment [103]. Studies on IFN- γ /PD-L1/MDSC axis are warranted.

10. MDSCs in Glioblastoma Therapy

GBMs which are exceedingly heterogeneous, comprising of tumor cells, tumor-activating cells, infiltrating immune cells, and endothelial cells as well as other tumor-related stromal cells are often observe at cellular level which makes developing targeted therapies very difficult [1, 6–8]. Studies have demonstrated that MDSCs may contribute to the failure of immune therapies for GBM because they are capable of potentiating immune suppression in GBM patients [10, 34, 37]. Ranjan et al. demonstrated that oral administration of 10 mg/kg penfluridol daily suppressed the growth of GBM

tumors in a subcutaneous as well as intracranial model [1, 107]. They indicated that oral administration of 10 mg/kg penfluridol daily for 48 days also reduced mouse MDSCs by 72% (Figure 1(a)) [1]. They further demonstrated that penfluridol treatment drastically suppressed the growth of metastatic breast tumors in brain [1, 108].

Several studies established that low-dose chemotherapies were capable of suppressing the levels of MDSCs in multiple tumor models [3, 109, 110]. Peereboom et al. demonstrated that 5-fluorouracil (5-FU) was capable of suppressing MDSCs in preclinical GBM mouse models (Figure 1(a)) [3]. 5-FU is an antimetabolite drug that enters both RNA and DNA via the blockade of thymidylate synthase resulting in decrease dTTP concentrations [3]. It was established that dUTP and FdUTP have less competition and are thus more likely to enter DNA [3, 67, 111]. Metronomic low-dose 5-FU was capable of suppressing circulating MDSCs and augmented intratumoral-stimulated T cells as well as prolonged survival (Figure 1(a)) [3, 67].

Current treatment of GBM involves the use of corticosteroids prior to surgery [35]. A new trend points to the fact that steroids are capable of modifying MDSC subtypes in GBM patients toward the augmentation of immune suppression [35]. This strengthens the idea of targeting MDSCs in GBM patients, because all receive steroids therapy at the time of surgery [35]. Alban et al. also observed immunosuppression intratumorally, where MDSCs correlated with good prognosis of patients with GBM (Figure 1(b)) [35]. They used matched primary as well as recurrent tumor-resection samples to arrive at the above [35]. They further observed elevated levels of CD33 $^{+}$ MDSC levels at recurrence correlated with overall survival, whereas infiltration of MDSCs into the tumor microenvironment correlated with poor prognosis (Figure 1(b)) [35].

Nevertheless, some patients may receive dexamethasone for several days to weeks before surgery because of symptoms resulting from extensive edema [24, 112]. Studies demonstrated that the extent of dexamethasone therapy correlated with an upsurge in MDSCs in blood of glioma patients, as well as in experimental glioma mice models (Figure 1(a)) [24, 113]. Gielen et al. did not observe any correlation between dexamethasone and upsurge of MDSC within tumor tissues (Figure 1(a)) [24]. Also, a similar study did not find an effect of the duration of dexamethasone therapy on S100A8/9 or arginase secretion [24]. Further studies on the effects of dexamethasone on MDSCs in GBM patients are needed because the current evidences are conflicting.

Several studies observed a spike upsurge in MDSC levels in peripheral blood immediately after their surgical resections in primary GBM patients as well as recurrent GBM patients put on trial chemotherapeutic agents (Figure 1(a)) [3, 35, 114]. Also, elevated levels of MDSCs in the peripheral blood after surgery in GBM patients were observed after surgical intervention in multiple cancer types as well as in untreated GBM patients [3, 115–117]. Peereboom et al. indicated that their tumor immune profiles were analyzed on surgical samples obtained before bevacizumab therapy although all the patients on their trial received both capecitabine and bevacizumab [3]. Thus, the observed intratumoral

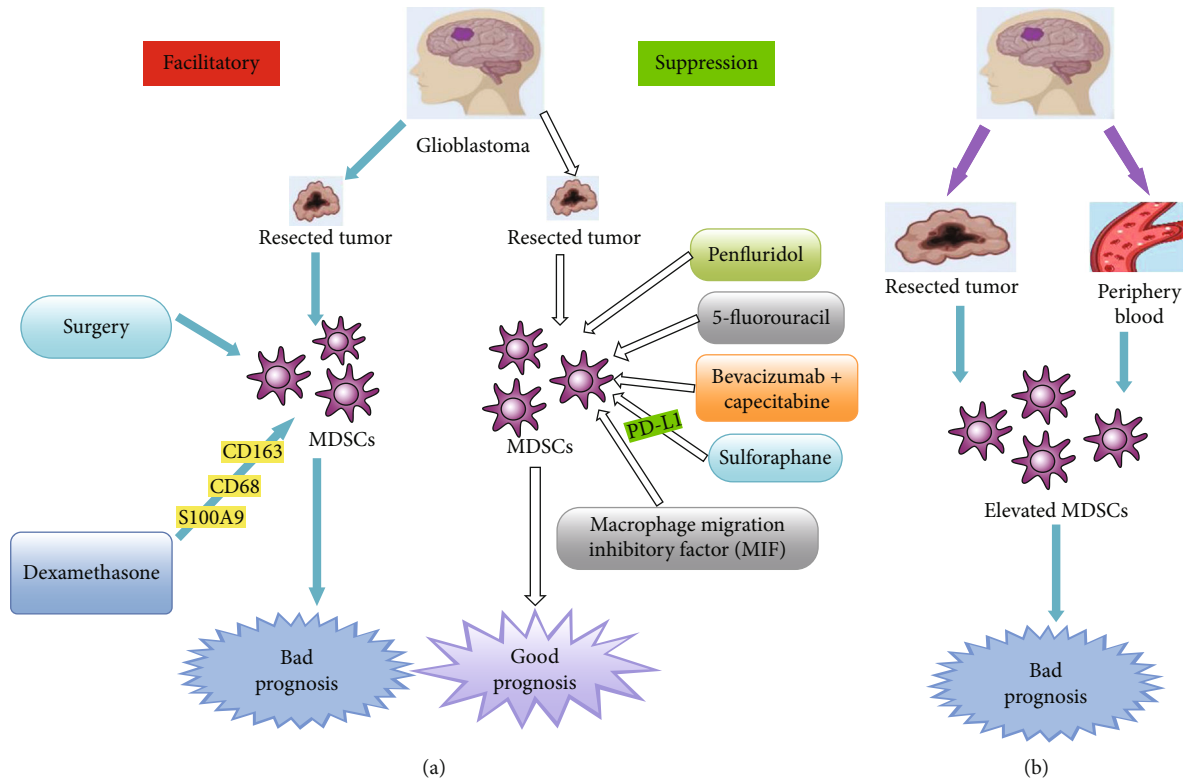


FIGURE 1: Diagnostic and therapeutic biomarker potentials of myeloid-derived suppressor cells in glioblastoma. (a) Shows therapeutic biomarker potential of MDSCs after various chemotherapeutic agents as well as surgical outcomes. Facilitation of MDSC secretion leads to bad prognosis while suppression of MDSCs leads to good prognosis. (b) Shows the diagnostic biomarker potentials of MDSCs. MDSCs are elevated in both glioblastoma tumor and the periphery blood indicating bad prognosis.

consequences of capecitabine were not triggered by bevacizumab therapy [3].

Moreover, MDSC modifications began to appear before the beginning of bevacizumab although circulating MDSC levels were analyzed while patients were on bevacizumab and capecitabine (Figure 1(a)) [3]. The diminishing MDSC levels also happened in a capecitabine dose-dependent manner (Figure 1(a)), making it unlikely that bevacizumab played a substantial role [3]. Nevertheless, the potential adjuvant properties of bevacizumab on circulating immune types could not be deduced from their results [3].

Moyes et al. evaluated the incidence of usual myeloid markers like CD163, CD68, and CD33, as well as S100A9 using quantitatively analyzed tissue microarrays made of samples taken from grades I-III astrocytoma's and GBM [54]. They found that CD163 and CD68, as well as S100A9 rates were elevated in dexamethasone-treated grade I astrocytoma and GBM compared to normal brain tissue and grades II and III tumors [54]. Dexamethasone is a resilient glucocorticosteroid drug with anti-inflammatory as well as immunosuppressant properties [54]. It is administered to brain-tumor patients with edema one day prior to surgery in order to decrease the edema before surgery and after surgery, and its usage is rapidly tapered [24, 112].

MIF has demonstrated to be an appealing therapeutic target to reverse glioma-mediated MDSC buildup (Figure 1(a)) [32, 36]. Kumar et al. observed that administration of anti-MIF-inhibiting antibody inhibited the production of CD14⁺/-

HLA-DR-MDSCs stimulated by glioma-conditioned media (GCM) in their experimental models [36]. Furthermore, GCM had intrinsic tautomerase function compatible with the presence of MIF that was suppressed by the administration of sulforaphane (SFN) [36]. SFN is nontoxic to leukocytes at moderate to high doses but exhibits some intrinsic antiglioma activities at lower doses [36]. Moreover, SFN at reasonably low doses decreased MDSC production in GCM [36].

GBM expressed relatively high levels of PD-L1 in M-MDSCs which was reduced upon administration of SFN [36]. Furthermore, SFN facilitated the development of proinflammatory DCs from monocytes cultured in both fresh media and GCM in addition to its effects in reducing MDSC levels [36]. Nevertheless, only mature DCs (CD83⁺) were observed in the presence of GCM [36]. Moreover, in addition to its proinflammatory properties, SFN was also directly toxic to glioma cells signifying that it might have extra therapeutic benefits in patients with GBM [36].

11. MDSCs as Biomarkers for Glioblastoma

In a study involving 481 lower-grade glioma patients, Jacobs et al. observed that rs147960238, which was situated in the tenth intron of CD163, and rs17138945, which was situated in the second intron of MET, were considerably correlated with survival [118]. Several studies have demonstrated that CD163 is a hemoglobin/haptoglobin complex receptor that is secreted by macrophages and microglia. It was established

that CD163 was capable of influencing inflammation via macrophages [118–120]. On the other hand, MET is a receptor tyrosine kinase as well as a protooncogene that is often associated with the expansion of MDSCs [118, 121]. Studies have proven that MDSCs are often elevated in the peripheral blood of patients with GBM (Figure 1(b)) [34, 35]. Studies have further shown that MDSCs in the peripheral blood as well as those infiltrating the GBM microenvironment correlated with poor prognosis (Figure 1(b)) [24, 32, 35].

Several studies have demonstrated elevation of CD33+/HLA-DR-MDSCs in the peripheral blood of patients with GBM compared to normal controls (Figure 1(b)) [13, 29, 100]. The MDSCs observed in the blood of patients with GBM consisted mainly of CD33⁺/CD15⁺/CD14⁻/HLA-DR⁻ neutrophilic subset with very few CD33⁺/CD15⁻/CD14⁻/HLA-DR⁻ negative lineage as well as CD33⁺/CD15⁻/CD14⁺/HLA-DR⁻ monocytic subtypes [13, 29]. Moreover, studies identified an upsurge in circulating M-MDSCs in the peripheral blood of patients with GBM compared to benign and grade I/II glioma patients (Figure 1(b)) [10, 24, 32]. Furthermore, there was a correlation between the secretory levels of intracellular S100A8/9 and upsurge in M-MDSCs in low-grade glioma patients [24]. Also, serum levels of S100A8/9 correlated with the function of arginase [24]. However, the values observed in this study were not predictable for the percentage of intratumoral MDSCs [24].

Studies have shown that elevation of peripheral MDSC levels correlated well with their immunosuppressive phenotypes, as well as with tumors that were refractory to immune-stimulating therapies like immune checkpoint blockers in multiple solid-tumor models as well as clinical trials (Figure 1(b)) [3, 122, 123]. Alban et al. demonstrated that GBM patients with good prognosis presented with reduced MDSCs as well as augmented DCs [35]. Thus, MDSC differentiation may be linked to an upsurge in immune stimulation leading to a decrease in GBM growth [35]. They found that immunosuppressive MDSC levels were high in high-grade glial malignancies as well as in nonglial malignancies with brain metastases, whereas suppressive T cell subtypes were not augmented, as initially described [33, 35, 124, 125]. They also found that steroid use inclines toward being a substantial predictor of MDSC levels in a univariable linear model [35].

Chae et al. demonstrated that mice receiving tumor cells and monocytes concurrently had augmented intratumoral MDSCs at sacrifice contrary to mice receiving tumor cells alone [28]. They indicated that mice receiving tumor cells mixed with monocytes had twice fold the quantity of splenic as well as bone marrow MDSCs contrary to mice receiving only tumor cells or only monocytes or control mice deprived of intracranial injection [28]. Their study concluded that augmenting glioma-associated monocytes led to an upsurge in intratumoral as well as systemic MDSCs in their experimental model (Figure 1(b)) [28]. In another study, they observed that normal human monocytes developed MDSC-like phenotype upon interaction with glioma cells which means that augmented glioma-associated monocytes/macrophages were capable of augmenting systemic MDSCs in patients with GBM as well [100].

Dubinski et al. observed that in peripheral blood, both the fraction of CD14^{high}CD15^{pos} M-MDSCs and CD14^{low}CD15^{pos} G-MDSCs were elevated compared with healthy controls (Figure 1(b)) [22]. They further observed that majority of G-MDSCs comprised of CD14^{low}CD15^{pos} neutrophilic MDSCs [22]. Nevertheless, at the tumor side, they observed that a large percentage of CD14^{low}CD15^{pos} G-MDSCs did not only compose of neutrophilic CD14^{low}CD15^{high} MDSCs but also elevated levels of CD14^{high}CD15^{pos} M-MDSCs [22]. Raychaudhuri et al. also observed elevated levels of CD15⁺CD14⁻ G-MDSCs over CD15⁺CD14⁺ M-MDSCs in tumor specimens of GBM patients (Figure 1(b)) [31].

Gielen et al. practically entirely observed CD15⁺CD14⁻ MDSCs within GBM tissue located both in viable and necrotic tumor zones (Figure 1(b)) [33]. Soler et al. designed a novel differential diagnostic approach merging analysis of secretion of two MDSC biomarkers; traditional HLA-DR as well as novel vascular noninflammatory molecule 2 (VNN2⁺) secretion on CD14⁺ monocytes was obtained from PBMC of GBM and/or radiation necrosis (RN) patients [126]. They indicated that this novel liquid biopsy could eliminate the necessity for biopsy to differentiate GBM from RN utilizing a minimally invasive and cheap as well as safe technique [126].

12. Conclusion

MDSCs are often elevated in the peripheral blood of patients with GBM. MDSCs in the peripheral blood as well as those infiltrating the GBM microenvironment correlated with poor prognosis. CD33+/HLA-DR-MDSCs were elevated in the peripheral blood of patients with GBM compared to normal controls. Also, an upsurge in circulating M-MDSCs in the peripheral blood of patients with GBM was observed compared to benign and grade I/II glioma patients. Furthermore, there was a correlation between the secretory levels of intracellular S100A8/9 as well as an upsurge in M-MDSCs in low-grade glioma patients. Also, serum levels of S100A8/9 correlated with the function of arginase. GBM patients with good prognosis presented with reduced MDSCs as well as augmented DCs. Nevertheless, augmenting glioma-associated monocytes led to an upsurge in intratumoral as well as systemic MDSCs in experimental model. MDSCs may contribute to the failure of immune therapies for GBM because they are capable of potentiating immune suppression in GBM patients. Low-dose chemotherapies were capable of suppressing the levels of MDSCs in multiple tumor models. These observations point to the fact that MDSCs are potential diagnostic as well as therapeutic biomarkers for GBM patients.

Abbreviations

Arg-1:	Arginase-1
ADAM17:	ADAM metalloproteinase domain 17
BCR:	B cell receptor
CTLs:	Cytotoxic T lymphocytes
CCR:	Chemokine receptor
DCs:	Dendritic cells
GBM:	Glioblastoma
GDEs:	GBM-derived exosomes

N-GDEs:	Normoxia-stimulated GDEs
H-GDEs:	Hypoxia-stimulated
G-MDSCs:	Granulocytic MDSCs
GCM:	Glioma-conditioned media
iNOS:	Inducible nitric oxide synthase
IL:	Interleukin
IGFBP:	Insulin-like growth factor binding protein
IDO:	Indoleamine 2,3-dioxygenase
IFNs:	Interferons
JAK:	Janus kinase
MDSCs:	Myeloid-derived suppressor cells
M-MDSCs:	Monocytic MDSCs
MCP-1:	Monocyte chemoattractant protein-1
MIF:	Macrophage migration inhibitory factor
NK:	Natural killer
NO:	Nitric oxide
NOS2:	Nitric oxide synthase 2
PMN-MDSCs:	Polymorphonuclear MDSCs
PBMCs:	Peripheral blood mononuclear cells
ROS:	Reactive oxygen species
RNS:	Reactive nitrogen species
Tregs:	Regulatory T cells
RN:	Radiation necrosis
Bregs:	Regulatory B cells
TIMP:	Tissue inhibitor of metalloproteinases
TAMs:	Tumor-associated macrophages
Th1:	T helper 1
STAT:	Signal transducer and activator of transcription
SFN:	Sulforaphane
VNN2 ⁺ :	Vascular noninflammatory molecule 2
4-IPP:	4-Iodo-6 phenylpyrimidine
5-FU:	5-Fluorouracil.

Conflicts of Interest

The author declares that he has no conflicts of interest.

References

- [1] A. Ranjan, S. Wright, and S. K. Srivastava, "Immune consequences of penfluridol treatment associated with inhibition of glioblastoma tumor growth," *Oncotarget*, vol. 8, no. 29, pp. 47632–47641, 2017.
- [2] H. Zong, R. G. Verhaak, and P. Canoll, "The cellular origin for malignant glioma and prospects for clinical advancements," *Expert review of molecular diagnostics*, vol. 12, no. 4, pp. 383–394, 2012.
- [3] D. M. Peereboom, T. J. Alban, M. M. Grabowski et al., "Metronomic capecitabine as an immune modulator in glioblastoma patients reduces myeloid-derived suppressor cells," *JCI insight*, vol. 4, no. 22, 2019.
- [4] R. Stupp, M. E. Hegi, W. P. Mason et al., "Effects of radiotherapy with concomitant and adjuvant temozolomide versus radiotherapy alone on survival in glioblastoma in a randomised phase III study: 5-year analysis of the EORTC-NCIC trial," *The lancet oncology*, vol. 10, no. 5, pp. 459–466, 2009.
- [5] U. Herrlinger, T. Tzaridis, F. Mack et al., "Lomustine-temozolomide combination therapy versus standard temozolomide therapy in patients with newly diagnosed glioblastoma with methylated MGMT promoter (CeTeG/NOA-09): a randomised, open-label, phase 3 trial," *The Lancet*, vol. 393, no. 10172, pp. 678–688, 2019.
- [6] X.-Y. Ji, J.-W. Ma, and J. Dong, "Myeloid-derived suppressor cells and nonresolving inflammatory cells in glioma microenvironment: Molecular mechanisms and therapeutic strategies," *Glioma*, vol. 1, no. 1, p. 2, 2018.
- [7] L. Pinton, S. Magri, E. Masetto et al., "Targeting of immunosuppressive myeloid cells from glioblastoma patients by modulation of size and surface charge of lipid nanocapsules," *Journal of Nanobiotechnology*, vol. 18, no. 1, 2020.
- [8] W.-J. Won, J. S. Deshane, J. W. Leavenworth, C. R. Oliva, and C. E. Griguer, "Metabolic and functional reprogramming of myeloid-derived suppressor cells and their therapeutic control in glioblastoma," *Cell stress*, vol. 3, no. 2, pp. 47–65, 2019.
- [9] I. A. Ho and W. S. Shim, "Contribution of the microenvironmental niche to glioblastoma heterogeneity," *BioMed Research International*, vol. 2017, Article ID 9634172, 13 pages, 2017.
- [10] A. L. Chang, J. Miska, D. A. Wainwright et al., "CCL2 produced by the glioma microenvironment is essential for the recruitment of regulatory T cells and myeloid-derived suppressor cells," *Cancer research*, vol. 76, no. 19, pp. 5671–5682, 2016.
- [11] D. I. Gabrilovich and S. Nagaraj, "Myeloid-derived suppressor cells as regulators of the immune system," *Nature Reviews Immunology*, vol. 9, no. 3, pp. 162–174, 2009.
- [12] Y. S. Khaled, B. J. Ammori, and E. Elkord, "Myeloid-derived suppressor cells in cancer: recent progress and prospects," *Immunology & Cell Biology*, vol. 91, no. 8, pp. 493–502, 2013.
- [13] B. Raychaudhuri, P. Rayman, J. Ireland et al., "Myeloid-derived suppressor cell accumulation and function in patients with newly diagnosed glioblastoma," *Neuro-Oncology*, vol. 13, no. 6, pp. 591–599, 2011.
- [14] S. Brandenburg, K. Turkowski, A. Mueller, Y. T. Radev, S. Seidlitz, and P. Vajkoczy, "Myeloid cells expressing high level of CD45 are associated with a distinct activated phenotype in glioma," *Immunologic research*, vol. 65, no. 3, pp. 757–768, 2017.
- [15] T. Condamine and D. I. Gabrilovich, "Molecular mechanisms regulating myeloid-derived suppressor cell differentiation and function," *Trends in immunology*, vol. 32, no. 1, pp. 19–25, 2011.
- [16] B. Hoehchst, T. Voigtlaender, L. Ormandy et al., "Myeloid derived suppressor cells inhibit natural killer cells in patients with hepatocellular carcinoma via the NKp30 receptor," *Hepatology*, vol. 50, no. 3, pp. 799–807, 2009.
- [17] M. Fujita, G. Kohanbash, W. Fellows-Mayle et al., "COX-2 blockade suppresses gliomagenesis by inhibiting myeloid-derived suppressor cells," *Cancer research*, vol. 71, no. 7, pp. 2664–2674, 2011.
- [18] L. Yang, L. M. DeBusk, K. Fukuda et al., "Expansion of myeloid immune suppressor Gr⁺ CD11b⁺ cells in tumor-bearing host directly promotes tumor angiogenesis," *Cancer cell*, vol. 6, no. 4, pp. 409–421, 2004.
- [19] N. Kamran, P. Kadiyala, M. Saxena et al., "Immunosuppressive myeloid cells' blockade in the glioma microenvironment enhances the efficacy of immune-stimulatory gene therapy," *Molecular Therapy*, vol. 25, no. 1, pp. 232–248, 2017.
- [20] E. M. Hanson, V. K. Clements, P. Sinha, D. Ilkovitch, and S. Ostrand-Rosenberg, "Myeloid-derived suppressor cells

- down-regulate L-selectin expression on CD4+ and CD8+ T cells," *The Journal of Immunology*, vol. 183, no. 2, pp. 937–944, 2009.
- [21] D. Marvel and D. I. Gabrilovich, "Myeloid-derived suppressor cells in the tumor microenvironment: expect the unexpected," *The Journal of clinical investigation*, vol. 125, no. 9, pp. 3356–3364, 2015.
- [22] D. Dubinski, J. Wölfer, M. Hasselblatt et al., "CD4+ T effector memory cell dysfunction is associated with the accumulation of granulocytic myeloid-derived suppressor cells in glioblastoma patients," *Neuro-oncology*, vol. 18, no. 6, pp. 807–818, 2016.
- [23] A. Ding, D. Routkevitch, C. Jackson, and M. Lim, "Targeting myeloid cells in combination treatments for glioma and other tumors," *Frontiers in immunology*, vol. 10, 2019.
- [24] P. R. Gielen, B. M. Schulte, E. D. Kers-Rebel et al., "Elevated levels of polymorphonuclear myeloid-derived suppressor cells in patients with glioblastoma highly express S100A8/9 and arginase and suppress T cell function," *Neuro-Oncology*, vol. 18, no. 9, pp. 1253–1264, 2016.
- [25] B. Badie and J. M. Schartner, "Flow cytometric characterization of tumor-associated macrophages in experimental gliomas," *Neurosurgery*, vol. 46, no. 4, pp. 957–962, 2000.
- [26] A. Müller, S. Brandenburg, K. Turkowski, S. Müller, and P. Vajkoczy, "Resident microglia, and not peripheral macrophages, are the main source of brain tumor mononuclear cells," *International journal of cancer*, vol. 137, no. 2, pp. 278–288, 2015.
- [27] X. Zhu, M. Fujita, L. A. Snyder, and H. Okada, "Systemic delivery of neutralizing antibody targeting CCL2 for glioma therapy," *Journal of neuro-oncology*, vol. 104, no. 1, pp. 83–92, 2011.
- [28] M. Chae, T. E. Peterson, A. Balgeman et al., "Increasing glioma-associated monocytes leads to increased intratumoral and systemic myeloid-derived suppressor cells in a murine model," *Neuro-Oncology*, vol. 17, no. 7, pp. 978–991, 2015.
- [29] K. Gabrusiewicz, N. Colwell, and A. Heimberger, "The role of myeloid-derived suppressor cells in immunosuppression in brain tumors," in *Translational Immunotherapy of Brain Tumors*, pp. 63–82, Elsevier, 2017.
- [30] G. Kohanbash, K. McKaveney, M. Sakaki et al., "GM-CSF promotes the immunosuppressive activity of glioma-infiltrating myeloid cells through interleukin-4 receptor-," *Cancer research*, vol. 73, no. 21, pp. 6413–6423, 2013.
- [31] B. Raychaudhuri, P. Rayman, P. Huang et al., "Myeloid derived suppressor cell infiltration of murine and human gliomas is associated with reduction of tumor infiltrating lymphocytes," *Journal of neuro-oncology*, vol. 122, no. 2, pp. 293–301, 2015.
- [32] T. J. Alban, D. Bayik, B. Otvos et al., "Glioblastoma myeloid-derived suppressor cell subsets express differential macrophage migration inhibitory factor receptor profiles that can be targeted to reduce immune suppression," *Frontiers in immunology*, vol. 11, 2020.
- [33] P. R. Gielen, B. M. Schulte, E. D. Kers-Rebel et al., "Increase in both CD14-positive and CD15-positive myeloid-derived suppressor cell subpopulations in the blood of patients with glioma but predominance of CD15-positive myeloid-derived suppressor cells in glioma tissue," *Journal of Neuropathology & Experimental Neurology*, vol. 74, no. 5, pp. 390–400, 2015.
- [34] J. A. Flores-Toro, D. Luo, A. Gopinath et al., "CCR2 inhibition reduces tumor myeloid cells and unmasks a checkpoint inhibitor effect to slow progression of resistant murine gliomas," *Proceedings of the National Academy of Sciences*, vol. 117, no. 2, pp. 1129–1138, 2020.
- [35] T. J. Alban, A. G. Alvarado, M. D. Sorensen et al., "Global immune fingerprinting in glioblastoma patient peripheral blood reveals immune-suppression signatures associated with prognosis," *JCI insight*, vol. 3, no. 21, 2018.
- [36] R. Kumar, T. De Mooij, T. E. Peterson et al., "Modulating glioma-mediated myeloid-derived suppressor cell development with sulforaphane," *PLoS One*, vol. 12, no. 6, article e0179012, 2017.
- [37] X. Feng, F. Szulzewsky, A. Yerevanian et al., "Loss of CX3CR1 increases accumulation of inflammatory monocytes and promotes gliomagenesis," *Oncotarget*, vol. 6, no. 17, pp. 15077–15094, 2015.
- [38] S. L. Highfill, Y. Cui, A. J. Giles et al., "Disruption of CXCR2-mediated MDSC tumor trafficking enhances anti-PD1 efficacy," *Science Translational Medicine*, vol. 6, no. 237, 2014.
- [39] M. P. Gustafson, Y. Lin, K. C. New et al., "Systemic immune suppression in glioblastoma: the interplay between CD14+ HLA-DRlo/neg monocytes, tumor factors, and dexamethasone," *Neuro-oncology*, vol. 12, no. 7, pp. 631–644, 2010.
- [40] B. Huang, Z. Lei, J. Zhao et al., "CCL2/CCR2 pathway mediates recruitment of myeloid suppressor cells to cancers," *Cancer Letters*, vol. 252, no. 1, pp. 86–92, 2007.
- [41] B. R. Achyut, K. Angara, M. Jain et al., "Canonical NFκB signaling in myeloid cells is required for the glioblastoma growth," *Scientific Reports*, vol. 7, no. 1, 2017.
- [42] R. R. Flores, C. L. Clauson, J. Cho et al., "Expansion of myeloid-derived suppressor cells with aging in the bone marrow of mice through a NF-κB-dependent mechanism," *Aging cell*, vol. 16, no. 3, pp. 480–487, 2017.
- [43] J. Yu, Y. Wang, F. Yan et al., "Noncanonical NF-κB activation mediates STAT3-stimulated IDO upregulation in myeloid-derived suppressor cells in breast cancer," *The Journal of Immunology*, vol. 193, no. 5, pp. 2574–2586, 2014.
- [44] C. Arcuri, B. Fioretti, R. Bianchi et al., "Microglia-glioma cross-talk: a two way approach to new strategies against glioma," *Frontiers in Bioscience*, vol. 22, no. 2, pp. 268–309, 2017.
- [45] N. R. Monu and A. B. Frey, "Myeloid-derived suppressor cells and anti-tumor T cells: a complex relationship," *Immunological investigations*, vol. 41, no. 6-7, pp. 595–613, 2012.
- [46] L. Wu, H. Du, Y. Li, P. Qu, and C. Yan, "Signal transducer and activator of transcription 3 (Stat3C) promotes myeloid-derived suppressor cell expansion and immune suppression during lung tumorigenesis," *The American journal of pathology*, vol. 179, no. 4, pp. 2131–2141, 2011.
- [47] S. Ostrand-Rosenberg and P. Sinha, "Myeloid-derived suppressor cells: linking inflammation and cancer," *The Journal of Immunology*, vol. 182, no. 8, pp. 4499–4506, 2009.
- [48] M. A. Curotto de Lafaille and J. J. Lafaille, "Natural and adaptive foxp3+ regulatory T cells: more of the same or a division of labor?," *Immunity*, vol. 30, no. 5, pp. 626–635, 2009.
- [49] P. C. Rodríguez and A. C. Ochoa, "Arginine regulation by myeloid derived suppressor cells and tolerance in cancer: mechanisms and therapeutic perspectives," *Immunological Reviews*, vol. 222, no. 1, pp. 180–191, 2008.
- [50] B. Huang, P. Y. Pan, Q. Li et al., "Gr-1+ CD115+ immature myeloid suppressor cells mediate the development of tumor-induced T regulatory cells and T-cell anergy in

- tumor-bearing host,” *Cancer research*, vol. 66, no. 2, pp. 1123–1131, 2006.
- [51] Y. Li, J. Brazzell, A. Herrera, and B. Walcheck, “ADAM17 deficiency by mature neutrophils has differential effects on L-selectin shedding,” *Blood*, vol. 108, no. 7, pp. 2275–2279, 2006.
- [52] T. R. Sippel, J. White, K. Nag et al., “Neutrophil degranulation and immunosuppression in patients with GBM: restoration of cellular immune function by targeting arginase I,” *Clinical Cancer Research*, vol. 17, no. 22, pp. 6992–7002, 2011.
- [53] K. Gabrusiewicz, B. Rodriguez, J. Wei et al., “Glioblastoma-infiltrated innate immune cells resemble M0 macrophage phenotype,” *JCI insight*, vol. 1, no. 2, 2016.
- [54] K. W. Moyes, A. Davis, V. Hoglund et al., “Effects of tumor grade and dexamethasone on myeloid cells in patients with glioma,” *Oncoimmunology*, vol. 7, no. 11, article e1507668, 2018.
- [55] R. Glass and M. Synowitz, “CNS macrophages and peripheral myeloid cells in brain tumours,” *Acta Neuropathologica*, vol. 128, no. 3, pp. 347–362, 2014.
- [56] C. A. Crane, B. J. Ahn, S. J. Han, and A. T. Parsa, “Soluble factors secreted by glioblastoma cell lines facilitate recruitment, survival, and expansion of regulatory T cells: implications for immunotherapy,” *Neuro-Oncology*, vol. 14, no. 5, pp. 584–595, 2012.
- [57] C. A. Crane, K. Austgen, K. Haberthur et al., “Immune evasion mediated by tumor-derived lactate dehydrogenase induction of NKG2D ligands on myeloid cells in glioblastoma patients,” *Proceedings of the National Academy of Sciences*, vol. 111, no. 35, pp. 12823–12828, 2014.
- [58] Y. Komohara, K. Ohnishi, J. Kuratsu, and M. Takeya, “Possible involvement of the M2 anti-inflammatory macrophage phenotype in growth of human gliomas,” *The Journal of Pathology*, vol. 216, no. 1, pp. 15–24, 2008.
- [59] W. Jia, C. Jackson-Cook, and M. R. Graf, “Tumor-infiltrating, myeloid-derived suppressor cells inhibit T cell activity by nitric oxide production in an intracranial rat glioma+ vaccination model,” *Journal of Neuroimmunology*, vol. 223, no. 1-2, pp. 20–30, 2010.
- [60] S. F. Hussain, D. Yang, D. Suki, K. Aldape, E. Grimm, and A. B. Heimberger, “The role of human glioma-infiltrating microglia/macrophages in mediating antitumor immune responses,” *Neuro-Oncology*, vol. 8, no. 3, pp. 261–279, 2006.
- [61] N. Leffers, M. J. Gooden, R. A. de Jong et al., “Prognostic significance of tumor-infiltrating T-lymphocytes in primary and metastatic lesions of advanced stage ovarian cancer,” *Cancer Immunology, Immunotherapy*, vol. 58, no. 3, pp. 449–459, 2009.
- [62] I. F. Parney, J. S. Waldron, and A. T. Parsa, “Flow cytometry and in vitro analysis of human glioma-associated macrophages. Laboratory investigation,” *Journal of Neurosurgery*, vol. 110, no. 3, pp. 572–582, 2009.
- [63] S. Darmanis, S. A. Sloan, D. Croote et al., “Single-cell RNA-seq analysis of infiltrating neoplastic cells at the migrating front of human glioblastoma,” *Cell Reports*, vol. 21, no. 5, pp. 1399–1410, 2017.
- [64] S. Müller, G. Kohanbash, S. J. Liu et al., “Single-cell profiling of human gliomas reveals macrophage ontogeny as a basis for regional differences in macrophage activation in the tumor microenvironment,” *Genome biology*, vol. 18, no. 1, 2017.
- [65] A. S. Venteicher, I. Tirosh, C. Hebert et al., “Decoupling genetics, lineages, and microenvironment in IDH-mutant gliomas by single-cell RNA-seq,” *Science*, vol. 355, no. 6332, article eaai8478, 2017.
- [66] A. Wu, J. Wei, L. Y. Kong et al., “Glioma cancer stem cells induce immunosuppressive macrophages/microglia,” *Neuro-Oncology*, vol. 12, no. 11, pp. 1113–1125, 2010.
- [67] B. Otvos, D. J. Silver, E. E. Mulkearns-Hubert et al., “Cancer stem cell-secreted macrophage migration inhibitory factor stimulates myeloid derived suppressor cell function and facilitates glioblastoma immune evasion,” *Stem Cells*, vol. 34, no. 8, pp. 2026–2039, 2016.
- [68] K. D. Simpson, D. J. Templeton, and J. V. Cross, “Macrophage migration inhibitory factor promotes tumor growth and metastasis by inducing myeloid-derived suppressor cells in the tumor microenvironment,” *The Journal of Immunology*, vol. 189, no. 12, pp. 5533–5540, 2012.
- [69] D. W. Beury, K. H. Parker, M. Nyandjo, P. Sinha, K. A. Carter, and S. Ostrand-Rosenberg, “Cross-talk among myeloid-derived suppressor cells, macrophages, and tumor cells impacts the inflammatory milieu of solid tumors,” *Journal of leukocyte biology*, vol. 96, no. 6, pp. 1109–1118, 2014.
- [70] A. Sica, P. Larghi, A. Mancino et al., “Macrophage polarization in tumour progression,” *Seminars in Cancer Biology*, vol. 18, no. 5, pp. 349–355, 2008.
- [71] S. Sousa, R. Brion, M. Lintunen et al., “Human breast cancer cells educate macrophages toward the M2 activation status,” *Breast Cancer Research*, vol. 17, no. 1, 2015.
- [72] A. Kadl, A. K. Meher, P. R. Sharma et al., “Identification of a novel macrophage phenotype that develops in response to atherogenic phospholipids via Nrf2,” *Circulation Research*, vol. 107, no. 6, pp. 737–746, 2010.
- [73] C. Munaut, J. Boniver, J. M. Foidart, and M. Deprez, “Macrophage migration inhibitory factor (MIF) expression in human glioblastomas correlates with vascular endothelial growth factor (VEGF) expression,” *Neuropathology and Applied Neurobiology*, vol. 28, no. 6, pp. 452–460, 2002.
- [74] M. Mittelbronn, M. Platten, P. Zeiner et al., “Macrophage migration inhibitory factor (MIF) expression in human malignant gliomas contributes to immune escape and tumour progression,” *Acta neuropathologica*, vol. 122, no. 3, pp. 353–365, 2011.
- [75] S. Waigel, B. E. Rendon, G. Lamont, J. Richie, R. A. Mitchell, and K. Yaddanapudi, “MIF inhibition reverts the gene expression profile of human melanoma cell line-induced MDSCs to normal monocytes,” *Genomics Data*, vol. 7, pp. 240–242, 2016.
- [76] M. Winner, J. Meier, S. Zierow et al., “A novel, macrophage migration inhibitory factor suicide substrate inhibits motility and growth of lung cancer cells,” *Cancer research*, vol. 68, no. 18, pp. 7253–7257, 2008.
- [77] X. Guo, W. Qiu, Q. Liu et al., “Immunosuppressive effects of hypoxia-induced glioma exosomes through myeloid-derived suppressor cells via the miR-10a/Rora and miR-21/Pten pathways,” *Oncogene*, vol. 37, no. 31, pp. 4239–4259, 2018.
- [78] X. Guo, H. Xue, Q. Shao et al., “Hypoxia promotes glioma-associated macrophage infiltration via periostin and subsequent M2 polarization by upregulating TGF-beta and MCSFR,” *Oncotarget*, vol. 7, no. 49, pp. 80521–80542, 2016.
- [79] L. Li, C. Li, S. Wang et al., “Exosomes derived from hypoxic oral squamous cell carcinoma cells deliver miR-21 to

- normoxic cells to elicit a prometastatic phenotype,” *Cancer Research*, vol. 76, no. 7, pp. 1770–1780, 2016.
- [80] G. Raposo and W. Stoorvogel, “Extracellular vesicles: exosomes, microvesicles, and friends,” *Journal of Cell Biology*, vol. 200, no. 4, pp. 373–383, 2013.
- [81] T. L. Whiteside, “Immune modulation of T-cell and NK (natural killer) cell activities by TEXs (tumour-derived exosomes),” *Biochemical Society Transactions*, vol. 41, no. 1, pp. 245–251, 2013.
- [82] M. Z. Noman, B. Janji, S. Hu et al., “Tumor-promoting effects of myeloid-derived suppressor cells are potentiated by hypoxia-induced expression of miR-210,” *Cancer Research*, vol. 75, no. 18, pp. 3771–3787, 2015.
- [83] J. Skog, T. Würdinger, S. van Rijn et al., “Glioblastoma microvesicles transport RNA and proteins that promote tumour growth and provide diagnostic biomarkers,” *Nature cell Biology*, vol. 10, no. 12, pp. 1470–1476, 2008.
- [84] K. E. van der Vos, E. R. Abels, X. Zhang et al., “Directly visualized glioblastoma-derived extracellular vesicles transfer RNA to microglia/macrophages in the brain,” *Neuro-Oncology*, vol. 18, no. 1, pp. 58–69, 2016.
- [85] L. Li, J. Zhang, W. Diao et al., “MicroRNA-155 and MicroRNA-21 promote the expansion of functional myeloid-derived suppressor cells,” *The Journal of Immunology*, vol. 192, no. 3, pp. 1034–1043, 2014.
- [86] X. Guo, H. Xue, X. Guo et al., “MiR224-3p inhibits hypoxia-induced autophagy by targeting autophagy-related genes in human glioblastoma cells,” *Oncotarget*, vol. 6, no. 39, pp. 41620–41637, 2015.
- [87] H. Xue, X. Guo, X. Han et al., “MicroRNA-584-3p, a novel tumor suppressor and prognostic marker, reduces the migration and invasion of human glioma cells by targeting hypoxia-induced ROCK1,” *Oncotarget*, vol. 7, no. 4, pp. 4785–4805, 2016.
- [88] G. Vella and G. Bergers, “Where have all the T cells gone?,” *Immunity*, vol. 49, no. 4, pp. 592–594, 2018.
- [89] R. Domenis, D. Cesselli, B. Toffoletto et al., “Systemic T cells immunosuppression of glioma stem cell-derived exosomes is mediated by monocytic myeloid-derived suppressor cells,” *PLoS One*, vol. 12, no. 1, article e0169932, 2017.
- [90] D. Lindau, P. Gielen, M. Kroesen, P. Wesseling, and G. J. Adema, “The immunosuppressive tumour network: myeloid-derived suppressor cells, regulatory T cells and natural killer T cells,” *Immunology*, vol. 138, no. 2, pp. 105–115, 2013.
- [91] M. Mirghorbani, S. Van Gool, and N. Rezaei, “Myeloid-derived suppressor cells in glioma,” *Expert review of Neurotherapeutics*, vol. 13, no. 12, pp. 1395–1406, 2013.
- [92] M. Seifert and R. Küppers, “Human memory B cells,” *Leukemia*, vol. 30, no. 12, pp. 2283–2292, 2016.
- [93] K. Rajewsky, “Clonal selection and learning in the antibody system,” *Nature*, vol. 381, no. 6585, pp. 751–758, 1996.
- [94] C. Lee-Chang, A. Rashidi, J. Miska et al., “Myeloid-derived suppressive cells promote B cell-mediated immunosuppression via transfer of PD-L1 in glioblastoma,” *Cancer Immunology Research*, vol. 7, no. 12, pp. 1928–1943, 2019.
- [95] P. Domingues, M. González-Tablas, Á. Otero et al., “Tumor infiltrating immune cells in gliomas and meningiomas,” *Brain, Behavior, and Immunity*, vol. 53, pp. 1–15, 2016.
- [96] Z.-p. Ye, H.-y. He, H. Wang et al., “Glioma-derived ADAM10 induces regulatory B cells to suppress CD8+ T cells,” *PLoS One*, vol. 9, no. 8, article e105350, 2014.
- [97] S. Han, S. Feng, M. Ren et al., “Glioma cell-derived placental growth factor induces regulatory B cells,” *The International Journal of Biochemistry & Cell Biology*, vol. 57, pp. 63–68, 2014.
- [98] E. C. Borden, “Interferons α and β in cancer: therapeutic opportunities from new insights,” *Nature Reviews Drug Discovery*, vol. 18, no. 3, pp. 219–234, 2019.
- [99] E. C. Borden, G. C. Sen, G. Uze et al., “Interferons at age 50: past, current and future impact on biomedicine,” *Nature Reviews Drug Discovery*, vol. 6, no. 12, pp. 975–990, 2007.
- [100] J. C. Rodrigues, G. C. Gonzalez, L. Zhang et al., “Normal human monocytes exposed to glioma cells acquire myeloid-derived suppressor cell-like properties,” *Neuro-Oncology*, vol. 12, no. 4, pp. 351–365, 2010.
- [101] G. Gallina, L. Dolcetti, P. Serafini et al., “Tumors induce a subset of inflammatory monocytes with immunosuppressive activity on CD8+ T cells,” *The Journal of Clinical Investigation*, vol. 116, no. 10, pp. 2777–2790, 2006.
- [102] K. C. Pituch, J. Miska, G. Krenciute et al., “Adoptive transfer of IL13Ra2-specific chimeric antigen receptor T cells creates a pro-inflammatory environment in glioblastoma,” *Molecular Therapy*, vol. 26, no. 4, pp. 986–995, 2018.
- [103] J. Qian, C. Wang, B. Wang et al., “The IFN- γ /PD-L1 axis between T cells and tumor microenvironment: hints for glioma anti-PD-1/PD-L1 therapy,” *Journal of neuroinflammation*, vol. 15, no. 1, p. 290, 2018.
- [104] A. Garcia-Diaz, D. S. Shin, B. H. Moreno et al., “Interferon receptor signaling pathways regulating PD-L1 and PD-L2 expression,” *Cell Reports*, vol. 19, no. 6, pp. 1189–1201, 2017.
- [105] S. Xue, M. Hu, V. Iyer, and J. Yu, “Blocking the PD-1/PD-L1 pathway in glioma: a potential new treatment strategy,” *Journal of hematology & oncology*, vol. 10, no. 1, p. 81, 2017.
- [106] E. K. Nduom, J. Wei, N. K. Yaghi et al., “PD-L1 expression and prognostic impact in glioblastoma,” *Neuro-Oncology*, vol. 18, no. 2, pp. 195–205, 2016.
- [107] A. Ranjan and S. K. Srivastava, “Penfluridol suppresses glioblastoma tumor growth by Akt-mediated inhibition of GLI1,” *Oncotarget*, vol. 8, no. 20, pp. 32960–32976, 2017.
- [108] A. Ranjan, P. Gupta, and S. K. Srivastava, “Penfluridol: an antipsychotic agent suppresses metastatic tumor growth in triple-negative breast cancer by inhibiting integrin signaling axis,” *Cancer Research*, vol. 76, no. 4, pp. 877–890, 2016.
- [109] M. S. Nars and R. Kaneno, “Immunomodulatory effects of low dose chemotherapy and perspectives of its combination with immunotherapy,” *International Journal of Cancer*, vol. 132, no. 11, pp. 2471–2478, 2016.
- [110] J. Vincent, G. Mignot, F. Chalmin et al., “5-Fluorouracil selectively kills tumor-associated myeloid-derived suppressor cells resulting in enhanced T cell-dependent antitumor immunity,” *Cancer Research*, vol. 70, no. 8, pp. 3052–3061, 2010.
- [111] L. S. Li, J. C. Morales, M. Veigl et al., “DNA mismatch repair (MMR)-dependent 5-fluorouracil cytotoxicity and the potential for new therapeutic targets,” *British Journal of Pharmacology*, vol. 158, no. 3, pp. 679–692, 2009.
- [112] J. Dietrich, K. Rao, S. Pastorino, and S. Kesari, “Corticosteroids in brain cancer patients: benefits and pitfalls,” *Expert Review of Clinical Pharmacology*, vol. 4, no. 2, pp. 233–242, 2011.
- [113] G. Varga, J. Ehrchen, A. Tsianakas et al., “Glucocorticoids induce an activated, anti-inflammatory monocyte subset in mice that resembles myeloid-derived suppressor cells,” *Journal of Leukocyte biology*, vol. 84, no. 3, pp. 644–650, 2008.

- [114] J. Wang, L. Yang, L. Yu et al., "Surgery-induced monocytic myeloid-derived suppressor cells expand regulatory T cells in lung cancer," *Oncotarget*, vol. 8, no. 10, pp. 17050–17058, 2017.
- [115] Y. G. Najjar and J. H. Finke, "Clinical perspectives on targeting of myeloid derived suppressor cells in the treatment of cancer," *Frontiers in Oncology*, vol. 3, 2013.
- [116] V. Kumar, S. Patel, E. Tcyganov, and D. I. Gabrilovich, "The nature of myeloid-derived suppressor cells in the tumor microenvironment," *Trends Immunology*, vol. 37, no. 3, pp. 208–220, 2016.
- [117] A. J. Montero, C. M. Diaz-Montero, C. E. Kyriakopoulos, V. Bronte, and S. Mandruzzato, "Myeloid-derived suppressor cells in cancer patients: a clinical perspective," *Journal of Immunotherapy*, vol. 35, no. 2, pp. 107–115, 2012.
- [118] D. I. Jacobs, Y. Liu, K. Gabrusiewicz et al., "Germline polymorphisms in myeloid-associated genes are not associated with survival in glioma patients," *Journal of Neuro-Oncology*, vol. 136, no. 1, pp. 33–39, 2018.
- [119] D. J. Schaer, A. I. Alayash, and P. W. Buehler, "Gating the radical hemoglobin to macrophages: the anti-inflammatory role of CD163, a scavenger receptor," *Antioxidants & Redox Signaling*, vol. 9, no. 7, pp. 991–999, 2007.
- [120] J. T. Borda, X. Alvarez, M. Mohan et al., "CD163, a marker of perivascular macrophages, is up-regulated by microglia in simian immunodeficiency virus encephalitis after haptoglobin-hemoglobin complex stimulation and is suggestive of breakdown of the blood-brain barrier," *The American journal of pathology*, vol. 172, no. 3, pp. 725–737, 2008.
- [121] B. L. Yen, M.-L. Yen, P.-J. Hsu et al., "Multipotent human mesenchymal stromal cells mediate expansion of myeloid-derived suppressor cells via hepatocyte growth factor/c-met and STAT3," *Stem Cell Reports*, vol. 1, no. 2, pp. 139–151, 2013.
- [122] J. Larkin, V. Chiarion-Sileni, R. Gonzalez et al., "Combined Nivolumab and Ipilimumab or Monotherapy in Untreated Melanoma," *New England Journal of Medicine*, vol. 373, no. 1, pp. 23–34, 2015.
- [123] S. Kitano, M. A. Postow, C. Cortez et al., "Myeloid-derived suppressor cell quantity prior to treatment with ipilimumab at 10mg/kg to predict for overall survival in patients with metastatic melanoma," *American Society of Clinical Oncology*, vol. 30, Supplement 15, 2012.
- [124] J. F. Jacobs, A. J. Idema, K. F. Bol et al., "Regulatory T cells and the PD-L1/PD-1 pathway mediate immune suppression in malignant human brain tumors," *Neuro-Oncology*, vol. 11, no. 4, pp. 394–402, 2009.
- [125] J. F. Jacobs, A. J. Idema, K. F. Bol et al., "Prognostic significance and mechanism of Treg infiltration in human brain tumors," *Journal of Neuroimmunology*, vol. 225, no. 1-2, pp. 195–199, 2010.
- [126] D. C. Soler, A. B. Young, K. D. Cooper et al., "The ratio of HLA-DR and VNN2⁺ expression on CD14⁺ myeloid derived suppressor cells can distinguish glioblastoma from radiation necrosis patients," *Journal of neuro-oncology*, vol. 134, no. 1, pp. 189–196, 2017.

Research Article

Elevated Levels of Serum Neurofilament Light Chain Associated with Cognitive Impairment in Vascular Dementia

Weibin Ma, Jingjing Zhang, Jialei Xu , Depeng Feng, Xiaoling Wang, and Fengyu Zhang

Department of Neurology, Liaocheng People's Hospital, Liaocheng, Shandong, China 252000

Correspondence should be addressed to Jialei Xu; jialei621@163.com

Received 10 October 2020; Revised 20 October 2020; Accepted 22 October 2020; Published 2 November 2020

Academic Editor: Wen-Jun Tu

Copyright © 2020 Weibin Ma et al. This is an open access article distributed under the Creative Commons Attribution License, which permits unrestricted use, distribution, and reproduction in any medium, provided the original work is properly cited.

Objective. Vascular dementia (VaD) is a progressive neurodegenerative disease with cognitive decline caused by cerebrovascular factors. Despite the great progress made in the past decade, VaD still lacks effective treatments and peripheral blood biomarkers. In this study, we tested the level of peripheral blood neurofilament light chain (NfL) in VaD patients and explored its relationship with cognitive impairment. **Method.** A total of 176 study subjects including 80 normal controls (NC) and 96 VaD patients were included in our study. Upon admission, we collected clinical and biochemical characteristics of all research subjects. We also evaluate the Montreal cognitive assessment scale (MoCA) scores of all subjects. The serum NfL level was measured by the single-molecule array (Simoa) method. **Results.** The years of education in the NC group and VaD group were (11.65 ± 3.04) years and (10.53 ± 3.87) years, respectively. Compared with VaD patients, the NC group has a higher level of education ($p = 0.037$). Furthermore, the results of Simoa indicated that VaD subjects had higher serum NfL levels compared with the NC group [(8.49 ± 2.37) pg/ml vs. (19.26 ± 4.71) pg/ml, $p < 0.001$]. In terms of other clinical and biochemical characteristics, there was no significant difference between VaD and NC. The Spearman correlation analysis indicated that educational years have a significant positive correlation with MoCA scores ($r = 0.238$, $p = 0.041$), while age and serum NfL levels have a significantly negative correlation with MoCA scores (age: $r = -0.213$, $p = 0.040$; NfL: $r = -0.395$, $p = 0.027$). However, further multiple regression analysis showed that only serum NfL level might serve as an independent risk factor for cognitive decline in VaD ($\beta = 0.317$, $p = 0.021$). **Conclusion.** The serum NfL levels in VaD subjects are significantly elevated, which may be used as a potential peripheral blood marker for predicting cognitive impairment in patients with VaD.

1. Introduction

Vascular dementia (VaD) can be defined as a neurodegenerative disease related to vascular brain injury, which is mainly manifested as cognitive decline and memory loss [1, 2]. With the advent of a graying society, the number of people suffering from dementia has increased substantially. According to reports, the number of people diagnosed with dementia will double every 20 years [3]. Therefore, the number of dementia patients will reach 66 million in 2030 and 120 million in 2050 [4, 5]. VaD accounts for about 15%-20% of all dementias, and its incidence is second only to Alzheimer's disease (AD) [6]. Unlike AD, there is no licensed treatment for vascular dementia. In addition, VaD also lacks effective therapeutic targets [7, 8]. Therefore, it is becoming imminent to find reliable molecular biomarkers to assess the potential risk of VaD.

Neurofilaments (Nf) is a cytoskeletal protein mainly expressed in neurons, which belongs to Type IV intermediate filament family having structural similarity with some protein molecules such as nestin, peripherin, and a-internexin [9]. According to their molecular weight, Nf is biologically divided into three subunits: 68 kDa Nf light (NfL), 160 kDa Nf medium (NfM), and 205 kDa Nf heavy (NfH) chains [10]. Recently, Nf is considered as a biomarker of neuroaxonal damage. When brain parenchyma is damaged, Nf is released into cerebrospinal fluid (CSF) and peripheral blood circulation [11, 12]. The traditional enzyme-linked immunosorbent assay can only detect Nf in CSF, but the more accurate single-molecule array technology makes it possible to detect Nf in peripheral blood [13, 14].

Among the subunits of Nf, NfL is among the most promising biomarker candidates [15]. There is mounting evidence

that NfL is related to a series of neurodegenerative diseases [16]. However, the relationship between NfL and VaD is still dim. The purpose of this research is to detect the serum level of NfL and to further clarify whether NfL can be used as a potential biomarker for the prevention and treatment in VaD.

2. Patients and Methods

2.1. Patient Population. The current study is a prospective cross-sectional descriptive design. Totally, 96 patients with VaD and 80 normal controls who were admitted to Liaocheng People's Hospital from June 2018 to May 2020 were recruited. Diagnosis of VaD was confirmed by attending neurologist according to the National Institute for Neurological Disorders and Stroke (NINDS-AIREN) and Diagnostic and Statistical Manual of Mental Disorders (DSM-V) [17, 18]. Exclusion criteria were as follows: (1) suffering from other types of dementia; (2) suffering from mental illness; (3) suffering from acute cerebrovascular disease or infectious disease; (4) malignant tumor; (5) history of surgery or other severe trauma within 3 months; (6) heart, liver, or kidney insufficiency and other serious acute and chronic diseases. This research abided by the Declaration of Helsinki. We obtained written consent from all subjects and approved by the Ethics Committee of Liaocheng People's Hospital.

2.2. Clinical and Biochemical Characteristics. At admission, clinical and biochemical characteristics were collected: education years, smoking and alcohol habits, coronary heart disease (CHD), high blood pressure (HBP), systolic blood pressure (SBP), diastolic blood pressure (DBP), hyperlipidemia (HLP), total cholesterol (TC), triglycerides (TG), high-density lipoprotein cholesterol (HDL-C), low-density lipoprotein cholesterol (LDL-C), Diabetes Mellitus (DM), and fasting plasma glucose (FBG).

2.3. Cognitive Function Testing. Montreal cognitive assessment (MoCA) tool is a popular cognitive assessment tool having high sensitivity and specificity [19]. MoCA evaluation indicators include the following: alternating trail making, visuoconstructional skills, naming, memory, visuoconstructional skills attention, sentence repetition, verbal fluency, abstraction, delayed recall, and orientation. The MoCA evaluation takes about 10 minutes, and the total score is 30 points. One point is added to subjects who have received formal education for less than 12 years. A final total score of 26 and above is considered normal. The MoCA cognitive assessment is conducted under standard conditions by a professionally trained neurologist who is blind to the subjects' clinical baseline data.

2.4. Measurement of Serum NfL Levels. All subjects collected fasting serum samples within 24 hours of admission and stored them at -80°C . The serum levels of NfL were tested by the single-molecule array method (Simoa). The blood sample was placed at room temperature for 15 minutes and then centrifuged at 4°C for 15 minutes at a speed of $2000 \times g$ to obtain serum. The Simoa NF-light assay used commercial reagents (UmanDiagnostics, Umea, Sweden) on an

HD-1 platform (Neoline, Hangzhou, China) according to manufacturer's instructions. All samples were tested blindly, and the measurement was repeated [20].

2.5. Statistical Analysis. The concentration of NfL in serum showed a normal distribution. In this study, categorical variables are recorded by numbers (percentage, %), while continuous variables are recorded by mean \pm standard deviation (mean \pm SD). The *t*-test was applied for the comparison of continuous variables, and the chi-square test was applied for the comparison of categorical variables. Spearman's correlation analysis is used to assess the binary correlation. Multivariate regression analysis was applied to assess the predictive value of clinical and biochemical characteristics on the cognitive function in patients with VaD. The SPSS 22.0 statistical software (SPSS Inc., IL, USA) was used in the study, and a *p* value of 0.05 was considered significant.

3. Results

3.1. Clinical and Biochemical Characteristics. A total of 176 subjects including 96 VaD patients and 80 normal controls admitted to Liaocheng People's Hospital from June 2018 to May 2020 were enrolled. The clinical and biochemical characteristics of all subjects were presented in Table 1. No significant differences were found in age, gender, smoking and alcohol habits, history of chronic disease (CHD, HBP, HLP, and DM), SBP, DBP, TC, TG, HDL-C, LDL-C, and FBG between VaD and NC. However, significant differences were found in education years, MoCA scores, and serum NfL levels between the two groups (Figure 1).

3.2. Spearman's Correlation Analysis. The correlation between clinical and biochemical characteristics and MoCA score was assessed by Spearman's correlation analysis. The results of the correlation analysis are presented in Table 2. The results indicated that age ($r = -0.213$, $p = 0.040$) and the levels of serum NfL ($r = -0.395$, $p = 0.027$) were negatively correlated with MoCA scores in VaD patients, and the correlation was significant. The results also indicated that the education years in VaD is positively correlated with the MoCA score ($r = 0.238$, $p = 0.041$). However, in our current study, there is no significant correlation between cognitive decline and other clinical and biochemical characteristics of VaD patients ($p > 0.05$).

3.3. Multiple Regression Analysis. The results of multiple regression analysis of MoCA score and serum NfL level in VaD patients are presented in Table 3. The results showed that serum NfL level may serve as an independent predictive risk factor for the cognitive decline in patients with VaD. After adjusting for age, gender, years of education, SBP, DBP, TC, TG, HDL-C, LDL-C, FBG, and other clinical and biochemical characteristics, the serum NfL level still has important significance for the independent value of cognitive function in VaD ($\beta = 0.317$, $p = 0.021$).

TABLE 1: Clinical and biochemical characteristics of all the subjects.

Variables	NC	VaD	<i>p</i>
<i>N</i>	80	96	—
Age (years)	69.59 ± 5.31	69.27 ± 6.18	0.742
Gender (male/female)	49/31	60/36	0.865
Serum NfL (pg/mL)	8.49 ± 2.37	19.26 ± 4.71	<0.001
Education (years)	11.65 ± 3.04	10.53 ± 3.87	0.037
Smoking (<i>n</i> , %)	19 (23.75)	24 (25.00)	0.848
Alcohol (<i>n</i> , %)	27 (33.75)	30 (31.25)	0.724
CHD (<i>n</i> , %)	10 (12.50)	13 (13.54)	0.838
HBP (<i>n</i> , %)	24 (30.00)	29 (30.21)	0.976
SBP (mmHg)	134.46 ± 14.28	135.82 ± 13.59	0.519
DBP (mmHg)	87.62 ± 10.35	88.17 ± 11.63	0.743
HLP (<i>n</i> , %)	17 (21.25)	20 (20.83)	0.946
TC (mmol/L)	4.72 ± 0.93	4.89 ± 1.14	0.286
TG (mmol/L)	1.64 ± 0.31	1.69 ± 0.52	0.451
HDL-C (mmol/L)	1.26 ± 0.39	1.21 ± 0.28	0.325
LDL-C (mmol/L)	2.41 ± 0.67	2.59 ± 0.75	0.098
DM (<i>n</i> , %)	14 (17.50)	16 (16.67)	0.884
FBG (mmol/L)	6.59 ± 1.16	6.77 ± 1.38	0.356
MoCA (points)	28.12 ± 1.08	21.57 ± 3.40	<0.001

NC: normal controls; VaD: vascular dementia; NfL: neurofilament light chain; CHD: coronary heart disease; HBP: high blood pressure; SBP: systolic blood pressure; DBP: diastolic blood pressure; HLP: hyperlipidemia; TC: total cholesterol; TG: triglycerides; HDL-C: high-density lipoprotein cholesterol; LDL-C: low-density lipoprotein cholesterol; DM: Diabetes Mellitus; FBG: fasting plasma glucose; MoCA: Montreal cognitive assessment scale.

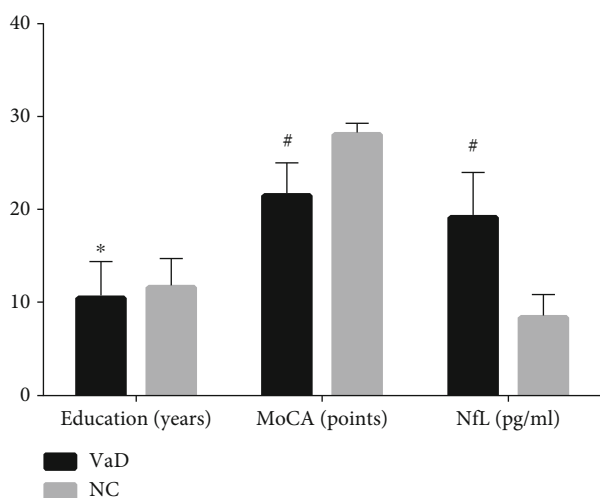


FIGURE 1: The differences in education years, MoCA scores, and serum NfL levels between VaD and NC. MoCA: Montreal cognitive assessment scale; NfL: neurofilament light chain; VaD: vascular dementia; NC: normal controls. Compared with NC group, **p* = 0.037, #*p* < 0.001.

TABLE 2: Correlation coefficients between MoCA scores and various parameters in VaD.

	MoCA (points)	
	<i>r</i>	<i>p</i>
Age (years)	-0.213	0.040
Gender	0.301	0.454
Education (years)	0.238	0.041
SBP (mmHg)	-0.372	0.245
DBP (mmHg)	-0.526	0.418
TG (mmol/L)	-0.377	0.183
TC (mmol/L)	-0.429	0.204
HDL-C (mmol/L)	0.284	0.312
LDL-C (mmol/L)	-0.267	0.059
FBG (mmol/L)	-0.482	0.656
Serum NfL (pg/mL)	-0.395	0.027

MoCA: Montreal cognitive assessment scale; VaD: vascular dementia; SBP: systolic blood pressure; DBP: diastolic blood pressure; TC: total cholesterol; TG: triglycerides; HDL-C: high-density lipoprotein cholesterol; LDL-C: low-density lipoprotein cholesterol; FBG: fasting plasma glucose; NfL: neurofilament light chain.

TABLE 3: Association between MoCA scores and various parameters in VaD.

	Regression coefficient	<i>p</i>	95% CI
Age (years)	0.138	0.184	0.725-1.203
Gender	0.263	0.196	0.788-1.194
Education (years)	0.214	0.086	0.672 - 1.145
SBP (mmHg)	0.386	0.437	0.783 - 1.092
DBP (mmHg)	0.379	0.322	0.561 - 1.236
TG (mmol/L)	0.272	0.195	0.826 - 1.215
TC (mmol/L)	0.305	0.618	0.487 - 1.309
HDL-C (mmol/L)	0.403	0.239	0.799 - 1.167
LDL-C (mmol/L)	0.260	0.193	0.915 - 1.128
FBG (mmol/L)	0.621	0.264	0.871 - 1.053
Serum NfL (pg/mL)	0.317	0.021	1.634 - 2.481

MoCA: Montreal cognitive assessment scale; VaD: vascular dementia; SBP: systolic blood pressure; DBP: diastolic blood pressure; TC: total cholesterol; TG: triglycerides; HDL-C: high-density lipoprotein cholesterol; LDL-C: low-density lipoprotein cholesterol; FBG: fasting plasma glucose; NfL: neurofilament light chain.

4. Discussion

The aim of the research was to study the relationship between cognitive function and serum NfL levels in VaD patients as well as normal controls. The results showed that the serum NfL level in VaD patients was significantly higher than that in the normal control group, while the MoCA score was lower. We also found that the MoCA score in VaD was significantly negatively correlated with serum NfL levels and age and positively correlated with years of education but had no significant correlation with other clinical and biochemical characteristics. This association is not affected by disturbing factors such as age, gender, years of education,

SBP, DBP, TC, TG, HDL-C, LDL-C, and FBG. To our knowledge, we have confirmed for the first time that serum NfL may serve as an independent risk factor for cognitive impairment in patients with VaD.

It has recently been discovered that NfL is related to a battery of neurological diseases. Johanna Gaiottino and his colleagues found that patients with AD, amyotrophic lateral sclerosis (ALS), and Guillain-Barré-syndrome (GBS) have higher levels of cerebrospinal fluid and serum NfL, and this change in NfL level is not accompanied by evidence of structural damage of central nervous system (CNS) [21]. Ching-Hua Lu's team further confirmed that serum NfL level was an easily accessible marker for prognostic of patients with ALS [22]. Interestingly, NfL mutations can cause severe early onset of Charcot-Marie-Tooth (CMT) disease [23]. In addition, elevated levels of NfL in cerebrospinal fluid or peripheral blood have also been reported in Parkinson's disease, relapsing-remitting multiple sclerosis, progressive supranuclear palsy, and brain metastases [24–28]. All the above studies suggested that NfL can be used as a biological target of certain nervous system disorders.

Emerging evidence indicates that NfL is involved in the pathological mechanism of cognitive declines [29]. A Chinese Taipei study showed that plasma NfL is a biomarker of cognitive decline in AD and Parkinson's disease (PD), and it is more specific for AD [24]. A 5-year longitudinal retrospective study in the United States showed that higher serum NfL levels are related to poor current and future clinical and cognitive performance [30]. In hereditary frontotemporal dementia, blood NfL can be used as a biomarker of disease progression, and the longitudinal measurement of NfL provides valuable information as a marker of treatment effect [31]. Not only in frontotemporal dementia, a Swedish study showed that plasma NfL is a noninvasive biomarker for AD [32]. Although the relationship between NfL and cognitive impairment has been widely reported, its mechanism is not completely clear.

Our research has some limitations. Firstly, the current study is a single-center study with a small sample size. Secondly, we did not monitor the serum NfL level longitudinally nor did we dynamically follow up the cognitive function and prognosis of patients. Thirdly, because the gold standard for diagnosis of VaD is biopsy, thus, our diagnosis for VaD may not be accurate enough, and VaD patients may also accompany by other types of cognitive impairment. However, our study confirmed for the first time the correlation between elevated serum NfL levels and cognitive decline, which has important clinical potential application value in VaD.

5. Conclusion

In conclusion, our study mainly found that the serum NfL levels of VaD patients were significantly elevated than that of the NC group. Our study reported for the first time that serum NfL plays an important role in the pathophysiology of the cognitive function of VaD patients. We expect the emergence of larger multicenter studies to confirm the association between serum NfL concentrations and cognitive function in patients with VaD. Elucidating the potential

pathological mechanism that NfL involved in the pathogenesis of VaD will have great applied value.

Data Availability

The data used to support the findings of this study are available from the corresponding author upon request.

Conflicts of Interest

The authors declare that they have no any conflict of interests.

Authors' Contributions

Weibin Ma and Jingjing Zhang are cofirst authors, and they contributed equally to this work.

Acknowledgments

All the authors are grateful to the Department of Neurology, Liaocheng People's Hospital.

References

- [1] J. Li, S. Li, Y. Song et al., "Association of serum FAM19A5 with cognitive impairment in vascular dementia," *Disease Markers*, vol. 2020, Article ID 8895900, 5 pages, 2020.
- [2] Q. Wang, W. Yang, J. Zhang, Y. Zhao, and Y. Xu, "TREM2 overexpression attenuates cognitive deficits in experimental models of vascular dementia," *Neural Plasticity*, vol. 2020, Article ID 8834275, 10 pages, 2020.
- [3] Y. Xu, Q. Wang, Z. Qu, J. Yang, X. Zhang, and Y. Zhao, "Protective effect of hyperbaric oxygen therapy on cognitive function in patients with vascular dementia," *Cell Transplantation*, vol. 28, no. 8, pp. 1071–1075, 2019.
- [4] Q. Wang, Y. Xu, C. Qi, A. Liu, and Y. Zhao, "Association study of serum soluble TREM2 with vascular dementia in Chinese Han population," *The International Journal of Neuroscience*, vol. 130, no. 7, pp. 708–712, 2020.
- [5] Y. Xu, Q. Wang, R. Cui, K. Lu, Y. Liu, and Y. Zhao, "Uric acid is associated with vascular dementia in Chinese population," *Brain and Behavior*, vol. 7, no. 2, article e00617, 2017.
- [6] J. O'Brien and A. Thomas, "Vascular dementia," *The Lancet*, vol. 386, no. 10004, pp. 1698–1706, 2015.
- [7] K. Shao, S. Shan, W. Ru, and C. Ma, "Association between serum NPTX2 and cognitive function in patients with vascular dementia," *Brain and Behavior*, vol. 10, article e01779, 2020.
- [8] Y. Xu, Q. Wang, Y. Liu, R. Cui, K. Lu, and Y. Zhao, "Association between *Helicobacter pylori* infection and carotid atherosclerosis in patients with vascular dementia," *Journal of the Neurological Sciences*, vol. 362, pp. 73–77, 2016.
- [9] B. A. Gordon, "Neurofilaments in disease: what do we know?," *Current Opinion in Neurobiology*, vol. 61, pp. 105–115, 2020.
- [10] R. Perrot, R. Berges, A. Bocquet, and J. Eyer, "Review of the multiple aspects of neurofilament functions, and their possible contribution to neurodegeneration," *Molecular Neurobiology*, vol. 38, no. 1, pp. 27–65, 2008.
- [11] M. Duerig, M. J. Konieczny, S. Tiedt et al., "Serum neurofilament light chain levels are related to small vessel disease burden," *Journal of Stroke*, vol. 20, no. 2, pp. 228–238, 2018.

- [12] S. Mariotto, E. Sechi, and S. Ferrari, "Serum neurofilament light chain studies in neurological disorders, hints for interpretation," *Journal of the Neurological Sciences*, vol. 416, p. 116986, 2020.
- [13] M. Khalil, C. E. Teunissen, M. Otto et al., "Neurofilaments as biomarkers in neurological disorders," *Nature Reviews Neurology*, vol. 14, no. 10, pp. 577–589, 2018.
- [14] C. Meregalli, G. Fumagalli, P. Alberti et al., "Neurofilament light chain: a specific serum biomarker of axonal damage severity in rat models of Chemotherapy-Induced Peripheral Neurotoxicity," *Archives of Toxicology*, vol. 94, no. 7, pp. 2517–2522, 2020.
- [15] F. Taghdiri, N. Multani, M. Ozzoude et al., "Neurofilament-light in former athletes: a potential biomarker of neurodegeneration and progression," *European Journal of Neurology*, vol. 27, no. 7, pp. 1170–1177, 2020.
- [16] Y. Lee, B. H. Lee, W. Yip, P. Chou, and B.-S. Yip, "Neurofilament proteins as prognostic biomarkers in neurological disorders," *Current Pharmaceutical Design*, vol. 25, pp. 4560–4569, 2019.
- [17] T. Erkinjuntti, "Clinical criteria for vascular dementia: the NINDS-AIREN criteria," *Dementia and Geriatric Cognitive Disorders*, vol. 5, pp. 189–192, 2004.
- [18] F. Edition, *Diagnostic and statistical manual of mental disorders*, Am Psychiatric Assoc, 2013.
- [19] Y. Xu, Q. Wang, Y. Liu, R. Cui, and Y. Zhao, "Is *Helicobacter pylori* infection a critical risk factor for vascular dementia?," *The International Journal of Neuroscience*, vol. 126, no. 10, pp. 899–903, 2016.
- [20] Q.-F. Li, Y. Dong, L. Yang et al., "Neurofilament light chain is a promising serum biomarker in spinocerebellar ataxia type 3," *Molecular Neurodegeneration*, vol. 14, pp. 1–8, 2019.
- [21] J. Gaiottino, N. Norgren, R. Dobson et al., "Increased neurofilament light chain blood levels in neurodegenerative neurological diseases," *PLoS One*, vol. 8, no. 9, article e75091, 2013.
- [22] C.-H. Lu, C. Macdonald-Wallis, E. Gray et al., "Neurofilament light chain: a prognostic biomarker in amyotrophic lateral sclerosis," *Neurology*, vol. 84, no. 22, pp. 2247–2257, 2015.
- [23] A. Jordanova, P. De Jonghe, C. Boerkoel et al., "Mutations in the neurofilament light chain gene (NEFL) cause early onset severe Charcot-Marie-Tooth disease," *Brain : A Journal of Neurology*, vol. 126, no. 3, pp. 590–597, 2003.
- [24] Y.-S. Lin, W.-J. Lee, S.-J. Wang, and J.-L. Fuh, "Levels of plasma neurofilament light chain and cognitive function in patients with Alzheimer or Parkinson disease," *Scientific Reports*, vol. 8, pp. 1–8, 2018.
- [25] J. Kuhle, G. Disanto, J. Lorscheider et al., "Fingolimod and CSF neurofilament light chain levels in relapsing-remitting multiple sclerosis," *Neurology*, vol. 84, no. 16, pp. 1639–1643, 2015.
- [26] J. C. Rojas, A. Karydas, J. Bang et al., "Plasma neurofilament light chain predicts progression in progressive supranuclear palsy," *Annals of Clinical and Translational Neurology*, vol. 3, no. 3, pp. 216–225, 2016.
- [27] N. D. Le, L. Muri, D. Grandgirard, J. Kuhle, D. Leppert, and S. L. Leib, "Evaluation of neurofilament light chain in the cerebrospinal fluid and blood as a biomarker for neuronal damage in experimental pneumococcal meningitis," *Journal of Neuroinflammation*, vol. 17, pp. 1–9, 2020.
- [28] A. Winther-Larsen, C. V. B. Hviid, P. Meldgaard, B. S. Sorensen, and B. Sandfeld-Paulsen, "Neurofilament light chain as a biomarker for brain metastases," *Cancers*, vol. 12, no. 10, p. 2852, 2020.
- [29] K. E. Osborn, O. A. Khan, H. A. Kresge et al., "Cerebrospinal fluid and plasma neurofilament light relate to abnormal cognition," *Alzheimer's & Dementia: Diagnosis, Assessment & Disease Monitoring*, vol. 11, no. 1, pp. 700–709, 2019.
- [30] D. Jakimovski, R. Zivadinov, M. Ramanathan et al., "Serum neurofilament light chain level associations with clinical and cognitive performance in multiple sclerosis: a longitudinal retrospective 5-year study," *Multiple Sclerosis Journal*, vol. 26, no. 13, pp. 1670–1681, 2020.
- [31] L. H. Meeter, E. G. Dopper, L. C. Jiskoot et al., "Neurofilament light chain: a biomarker for genetic frontotemporal dementia," *Annals of Clinical and Translational Neurology*, vol. 3, no. 8, pp. 623–636, 2016.
- [32] N. Mattsson, U. Andreasson, H. Zetterberg, and K. Blennow, "Association of plasma neurofilament light with neurodegeneration in patients with Alzheimer disease," *JAMA Neurology*, vol. 74, no. 5, pp. 557–566, 2017.

Research Article

Diagnostic and Prognostic Potentials of Long Noncoding RNA ELF3-AS1 in Glioma Patients

Jun-chi Mei,¹ Ge Yan,² and Si-qing Mei ¹

¹Department of Laboratory Medicine, The Renmin Hospital of Wuhan University, Wuhan, 410060 Hubei Province, China

²Department of Laboratory Medicine, The Maternal and Child Hospital of Hubei Province, Tongji Medical College, The Huazhong University of Science and Technology, Wuhan, 410060 Hubei Province, China

Correspondence should be addressed to Si-qing Mei; meisq66@yeah.net

Received 18 July 2020; Revised 30 August 2020; Accepted 2 September 2020; Published 18 September 2020

Academic Editor: Wen-Jun Tu

Copyright © 2020 Jun-chi Mei et al. This is an open access article distributed under the Creative Commons Attribution License, which permits unrestricted use, distribution, and reproduction in any medium, provided the original work is properly cited.

Objective. Accumulating evidence implies that long noncoding RNAs (lncRNAs) play a crucial role in predicting survival for glioma patients. However, the potential function of lncRNA ELF3-antisense RNA 1 (ELF3-AS1) in tumors remained largely unclear. The aim of this study was to explore the expression of lncRNA ELF3-antisense RNA 1 (ELF3-AS1) and evaluate its functions in glioma patients. **Patients and Methods.** ELF3-AS1 expressions were examined by RT-PCR in 182 pairs of glioma specimens and adjacent normal tissues. The receiver operating characteristic (ROC) curve was performed to estimate the diagnostic value of ELF3-AS1. The chi-square tests were used to examine the associations between ELF3-AS1 expression and the clinicopathological characters. The overall survival (OS) and disease-free survival (DFS) were analyzed by log-rank test, and survival curves were plotted according to Kaplan-Meier. The prognostic value of the ELF3-AS1 expression in glioma patients was further analyzed using univariate and multivariate Cox regression analyses. Loss-of-function assays were performed to determine the potential function of ELF3-AS1 on the proliferation and invasion of glioma cells. **Results.** The ELF3-AS1 expression level was significantly higher in glioma specimens compared with adjacent nontumor specimens ($p < 0.01$). A high expression of ELF3-AS1 was shown to be associated with the WHO grade ($p = 0.023$) and KPS score ($p = 0.012$). ROC assays revealed that high ELF3-AS1 expression had an AUC value of 0.8073 (95% CI: 0.7610 to 0.8535) for glioma. Using the Kaplan-Meier analysis, we found that patients with a high ELF3-AS1 expression had significantly poor OS ($p = 0.006$) and DFS ($p = 0.0002$). In a multivariate Cox model, we confirmed that ELF3-AS1 expression was an independent poor prognostic factor for glioma patients. The functional assay revealed that knockdown of ELF3-AS1 suppressed the proliferation and invasion of glioma cells. **Conclusions.** Our findings confirmed that ELF3-AS1 functions as an oncogene in glioma and indicated that ELF3-AS1 is not only an important prognostic marker but also a potential therapy target for glioma.

1. Introduction

Glioma is a common malignant primary brain tumor in adults and accounts for 35% of all central nervous system-related tumors as well as 85% of all primary malignant brain tumors^{1, 2}. The existing WHO classification divides glioma into grades I, II, III, and IV from a histological perspective³. An upward trend in morbidity and mortality for glioma was observed from 2005 to 2018 in China⁴. Although new biological therapies have made progression with regard to the therapeutic intervention, including chemotherapy, radiotherapy, glioma surgery, gene therapy, and immunotherapy, glioma

patients' overall survival (OS) is only 10-15 months after diagnosis⁵⁻⁷. On that account, it is necessary to develop new strategies for diagnosing and treating glioma, thereby reducing the recurrence as well as improving the OS.

Long noncoding RNAs (lncRNAs) are long RNA transcripts (>200 nucleotides) that do not possess protein-coding capabilities⁸. Different from short noncoding RNAs, lncRNAs exhibited an underestimated function role because of initially being identified as the transcriptional noise in the genome^{9, 10}. Growing studies have indicated that lncRNAs participate in various biological activities, like cell differentiation, apoptosis, and gene expression epigenetic

regulation, as well as RNA decay^{11, 12}. Recently, aberrant lncRNA expressions are frequently found in most human cancers and affect each of the six hallmarks of cancer, and an increasing number of studies focus on revealing the molecular mechanisms exhibited by lncRNAs during the above-mentioned pathological processes^{13, 14}. In addition, the development of high throughput sequencing promoted the detection technology of lncRNA, and according to the potential effects of lncRNAs acting as tumor promoters or suppressors, lncRNAs may serve as new diagnostic and prognostic biomarkers for various tumor patients, including glioma^{10, 15–18}.

lncRNA ELF3-antisense RNA 1 (ELF3-AS1) was a recently identified lncRNA whose effects have been reported in various tumors, like lung cancer, osteosarcoma, and bladder cancer^{19–21}. Interestingly, all previous studies have shown that the ELF3-AS1 expression was distinctly increased in various types of tumors. However, whether ELF3-AS1 also displayed a dysregulated expression in glioma and its biological significance have not been investigated.

2. Patients and Methods

2.1. Clinical Specimens. Between July 2012 and April 2015, 182 glioma samples together with paired adjacent noncancerous tissues were collected from glioma patients receiving surgical resection at our hospital. The five-year follow-up was completed specifically to all these patients, and their written informed consents were obtained. No patients had undergone previous treatments including radiation or chemotherapy. The inclusion criteria for the patient cohort included (i) having a distinctive pathological diagnosis of glioma; (ii) surgical resection, defined as the complete resection of all tumor nodules with the cut margin being free of tumors by histological examination; and (iii) having complete clinicopathological data. We obtained these samples during surgery and immediately froze them in liquid prior to use. Five-year follow-up was done through hospital medical records and telephone interviews. 172 glioma patients completed follow-up, and the rate of loss to follow-up was 5.4%. Table 1 lists the clinical features exhibited by all these patients. This study has obtained the approval of the Research Ethics Committee of the Renmin Hospital of Wuhan University (No. WN33171). Written informed consent was obtained from all the patients.

2.2. Cell Culture and Cell Transfection. The human glioma cell lines (U251, H4, SW1783, and LN229) and NHA cells were obtained from a cell bank at the Chinese Academy of Sciences (Shanghai, China) and grown in Dulbecco's modified Eagle's medium (DMEM; Hyclone, Haidian, Beijing, China) containing 10% fetal bovine serum (FBS; Gibco, Hangzhou, Zhejiang, China) and 100 μ g/ml streptomycin and penicillin. All cell lines were maintained at 37°C in a humidified atmosphere containing 5% CO₂.

2.3. RNA Extraction and Quantitative Real-Time PCR (qRT-PCR). The TRIzol reagent (Invitrogen, Suzhou, Jiangsu, China) was employed to extract the total RNA. A Prime-

TABLE 1: Association between ELF3-AS1 expression and different clinicopathological features of 182 human gliomas.

Parameter	No. of cases	ELF3-AS1 expression		<i>p</i> value
		High	Low	
Age				0.667
<50	102	49	53	
≥50	80	41	39	
Gender				0.356
Male	105	55	50	
Female	77	35	42	
WHO grade				0.023
I–II	116	50	66	
III–IV	66	40	26	
KPS score				0.012
<80	80	48	32	
≥80	102	42	60	
Extent of resection				0.380
<98%	105	49	56	
≥98%	77	41	36	
Tumor size				0.103
<5 cm	106	47	59	
≥5 cm	76	43	33	

Script 1st strand cDNA Synthesis Kit (TaKaRa Bio, Shenzhen, Guangdong, China) was applied to the synthesis of cDNA from total RNA relying on reverse transcription. The miScript SYBR Green PCR Kit (Qiagen, Haidian, Beijing, China) was applied to the ABI 7500 cycler (Applied Biosystems) for conducting the real-time PCR, based on the instruction of the manufacturer. The real-time PCR was conducted under the condition of 10 s at 94°C, 5 s at 94°C, 30 s of annealing at 52°C, and 15 s at 72°C followed by 40 cycles. The GenePharma company (Kunshan, Jiangsu, China) took charge of the design and synthesis of all these primers, as follows: ELF3-AS1, forward, 5'-GCAACGGCGTCTACCAC-3'; reverse, 5'-TAGCCCACGTCGTCTCACTATC-3'. GAPDH, forward, 5'-CGACTTATACATGGCCAAC-3'; reverse, 5'-TTCCGATCACTGGAATCAC-3'. GAPDH was used as an internal control. The relative level exhibited by gene expression was expressed relative to the GAPDH, and the 2^{- $\Delta\Delta$ Ct} methods were adopted to calculate the relative level.

2.4. CCK-8 Assays. Cell proliferation was determined using CCK-8 (Haidian, Beijing, China). Cells were seeded in 96-well plates at a density of 2 × 10³ cells. After culture for 0, 24, 48, and 72 h, 10 μ l CCK-8 reagent was added to each well and incubated at 37°C for another 1 h. Optical density (OD) values were measured at 450 nm.

2.5. Colony Formation Assays. The capability of anchorage-independent growth of H4 and LN229 cells was measured by the colony formation assays. 1 × 10³ cells were plated in 10 cm dish and incubated in a humidified atmosphere of 5% CO₂ incubator at 37°C for 10 days. For visualization,

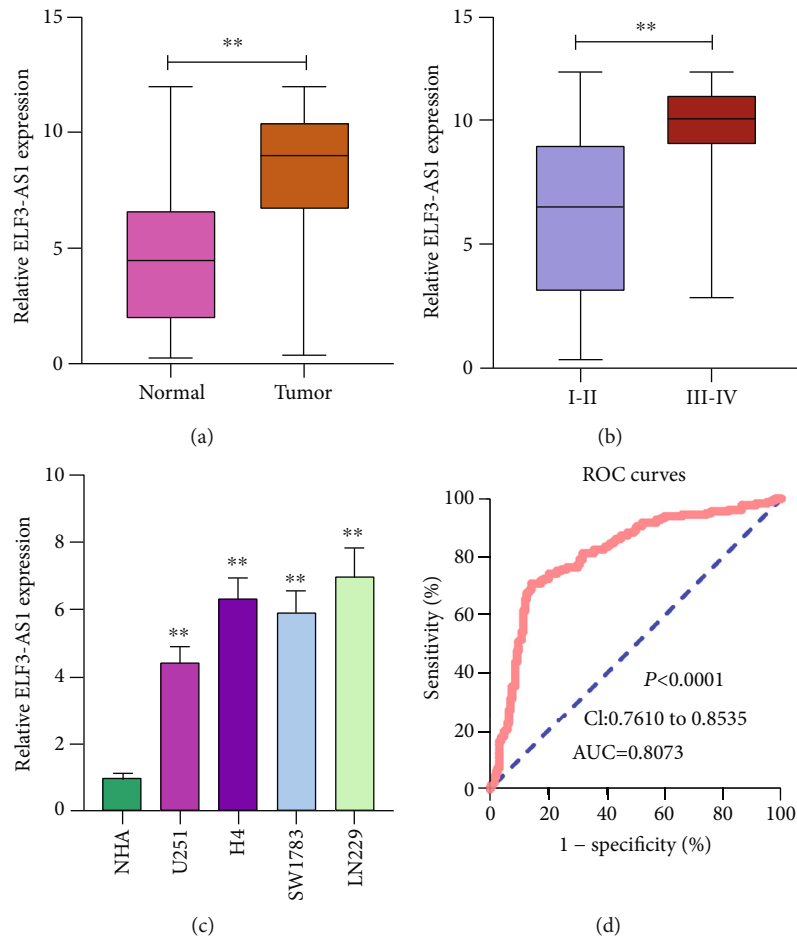


FIGURE 1: The expression of ELF3-AS1 and its diagnostic significance in glioma. (a) The expression levels of ELF3-AS1 in glioma tissues were significantly higher than those in corresponding noncancerous tissues. (b) RT-PCR for the determination of ELF3-AS1 expression in the glioma specimens with different stages. (c) qRT-PCR analysis of the expression of ELF3-AS1 in glioma cell lines and NHA cells. (d) ROC curve for diagnostic value of ELF3-AS1 in glioma. ** $p < 0.01$, * $p < 0.05$.

colonies were stained with 0.5% Crystal Violet (Sigma, Haidian, Beijing, China) in 50% methanol and 10% glacial acetic acid. The colonies with the diameters of >1 mm were counted.

2.6. Transwell Assays. Cells were transfected with 50 nM si-ELF3-AS1 or si-NC. Twenty-four hours postinfection, the infected cells were harvested and plated (1×10^5) in the top chamber of transwell assay inserts (Millipore, Pudong, Shanghai, China) with a Matrigel-coated membrane containing $8 \mu\text{m}$ pores. Inserts were then placed into the bottom chamber wells of a 24-well plate containing RPMI-1640 with 10% FBS as a chemoattractant. After 48 h of incubation, the remaining cells were removed from the top layer of the insert by scrubbing with a sterile cotton swab. Cells which passed through the filter were fixed and stained using 0.1% Crystal Violet. Numbers of invaded cells were counted in five randomly selected fields under a microscope.

2.7. Statistical Analysis. All data are represented as means \pm SD. SPSS 19.0 software (SPSS Inc., Chicago, IL, USA) was applied to the analysis. Student's *t*-test together with the chi-square test assisted in estimating the difference signifi-

cance between groups. The receiver operating characteristic (ROC) curves were aimed at discriminating glioma specimens from normal nontumor tissues. Kaplan-Meier methods together with a log-rank test assisted in determining the difference between patients in terms of the OS and DFS. Univariate and multivariate survival analyses adopted the Cox proportional hazard model. The values were considered to be statistically significant at $p < 0.05$.

3. Results

3.1. Expression Levels of ELF3-AS1 in Glioma. To determine whether ELF3-AS1 was abnormally expressed in glioma, qRT-PCR assisted in examining the ELF3-AS1 expression exhibited by 182 pairs of glioma tissues as well as the noncancerous tissues. Figure 1(a) demonstrates the obviously lower ELF3-AS1 expression in tumor tissues relative to noncancerous tissues ($p < 0.01$). In addition, we observed that the glioma specimens with advanced stages exhibited a higher level of ELF3-AS1 than those with early stages (Figure 1(b)). Moreover, we examined the levels of ELF3-AS1 in four glioma cell lines, finding that ELF3-AS1 expression levels were increased

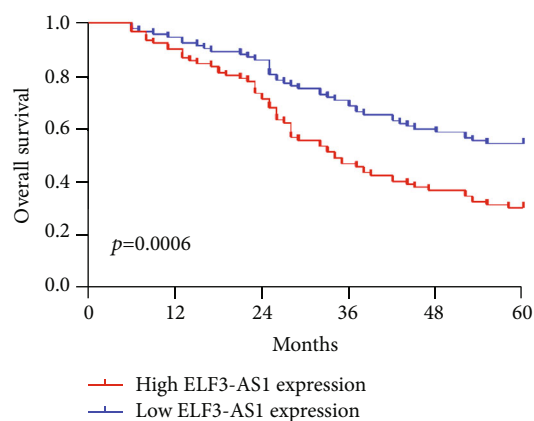


FIGURE 2: Kaplan-Meier curves estimating the 5-year overall survival rates according to the expression of ELF3-AS1 in patients with glioma.

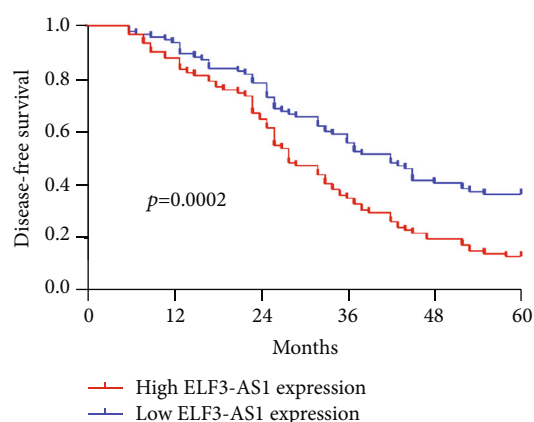


FIGURE 3: Kaplan-Meier curves estimating the 5-year disease-free survival rates according to the expression of ELF3-AS1 in patients with glioma.

in four glioma cell lines compared with NHA, particularly in H4 and LN229 cells (Figure 1(c), $p < 0.05$). Accordingly, H4 and LN229 cells were used in the subsequent experiments. Thus, our findings revealed ELF3-AS1 as a regulator in the progression of glioma.

3.2. The Diagnostic Significance of Overexpression of ELF3-AS1 in Glioma. Previous studies have revealed that several functional lncRNAs displayed a diagnostic value in glioma patients. Then, we performed ROC assays which showed that high ELF3-AS1 expression had an AUC value of 0.8073 (95% CI: 0.7610 to 0.8535) for glioma (Figure 1(d)). The sensitivity and specificity of ELF3-AS1 expressions for distinguishing glioma samples from normal samples were 67.23%/85.22%, indicating ELF3-AS1 as an early-diagnosis indicator for glioma patients.

3.3. Association between ELF3-AS1 Expression and the Clinicopathological Features of Glioma. For a better understanding of the clinical relevance of the ELF3-AS1 expression in glioma, we divided the 182 glioma patients into a group with a high expression ($n = 90$) and a group with a low

expression ($n = 92$), taking into account the median ELF3-AS1 expression level (5.232) in all glioma samples. Then, we performed a chi-square test and found that the high ELF3-AS1 expression affected the WHO grade ($p = 0.023$) and the KPS score ($p = 0.012$) (Table 1). However, there were no significant correlations of ELF3-AS1 expression with other clinical features.

3.4. Prognostic Values of ELF3-AS1 Expression as a Novel Biomarker in Glioma. Kaplan-Meier survival analysis assisted in confirming the association between the expression of ELF3-AS1 and 182 glioma patients' outcomes. Interestingly, we observed that patients who possessed a high ELF3-AS1 expression exhibited a weaker OS ($p = 0.0006$, Figure 2) and DFS ($p = 0.0002$, Figure 3) compared with those in the low ELF3-AS1 group. Moreover, univariate and multivariate assays were carried out to determine whether ELF3-AS1 was an independent factor for prognostic prediction in glioma patients. Importantly, our findings suggested that increased expression of ELF3-AS1 can be applied to independently predict the prognosis of patients regarding OS (HR = 2.673, 95% CI: 1.138-4.462, $p = 0.015$, Table 2) and DFS (HR = 2.762, 95% CI: 1.238-4.562, $p = 0.006$, Table 3).

3.5. The Effects of ELF3-AS1 Knockdown on the Proliferation and Invasion of Glioma Cells. To determine the function of ELF3-AS1 in the progression of glioma, the expression of ELF3-AS1 was suppressed using si-ELF3-AS1 in H4 and LN229 cells (Figure 4(a)). CCK-8 assays showed that ELF3-AS1 silencing significantly inhibited the proliferation ability of glioma cells compared with that of negative control transfection (Figures 4(b) and 4(c)). The colony formation assay showed that H4 and LN229 cells transfected with si-ELF3-AS1 formed significantly less colonies than those transfected with si-NC (Figure 4(d)). Moreover, we explored the possible influence of ELF3-AS1 on the metastasis ability of glioma cells using transwell assays, finding that the cell invasion was markedly suppressed in glioma cells transfected with si-ELF3-AS1 as compared with cells transfected with si-NC (Figure 4(e)). Overall, our findings suggested ELF3-AS1 as a tumor promoter in glioma cells.

4. Discussion

Glioma acts as a common malignant primary brain tumor, and the significant progress of related treatment in the past ten years fails to improve its weak prognosis^{22, 23}. The early screening and the prediction of clinical outcomes before various treatments may contribute to the optimization of therapeutic schedules for doctors, which then promoted the long-term survivals of glioma patients^{24, 25}. Up to date, in clinical practice, the sensitive biomarkers were limited due to the unclear molecular mechanisms involved in the progression of glioma. In recent years, more and more studies have highlighted the potential of lncRNAs used as novel biomarkers for tumor patients due to their frequent dysregulation in both specimens and blood in patients and important

TABLE 2: Univariate and multivariate Cox regression analyses of ELF3-AS1 for overall survival of glioma patients.

Variable	Univariate analysis			Multivariate analysis		
	RR	95% CI	<i>p</i> value	RR	95% CI	<i>p</i> value
Age	0.842	0.452-1.623	0.241	—	—	—
<50 vs. ≥50						
Gender	1.213	0.773-1.898	0.423	—	—	—
Male vs. female						
WHO grade	3.113	1.342-4.782	0.008	2.893	1.234-4.345	0.015
I-II vs. III-IV						
KPS score	3.225	1.423-5.113	0.005	3.014	1.223-4.783	0.009
<80 vs. ≥80						
Extent of resection	0.892	0.472-1.885	0.231	—	—	—
<98% vs. ≥98%						
Tumor size (cm)	1.448	0.783-2.218	0.149	—	—	—
<5 vs. ≥5						
ELF3-AS1 expression	2.952	1.342-4.832	0.009	2.673	1.138-4.462	0.015
High vs. low						

TABLE 3: Univariate and multivariate Cox regression analyses of ELF3-AS1 for disease-free survival of glioma patients.

Variable	Univariate analysis			Multivariate analysis		
	RR	95% CI	<i>p</i> value	RR	95% CI	<i>p</i> value
Age	1.332	0.672-1.989	0.223	—	—	—
<50 vs. ≥50						
Gender	1.556	0.732-2.114	0.145	—	—	—
Male vs. female						
WHO grade	3.183	1.327-4.672	0.014	2.985	1.182-4.328	0.019
I-II vs. III-IV						
KPS score	2.987	1.247-4.558	0.017	2.632	1.124-4.134	0.021
<80 vs. ≥80						
Extent of resection	1.561	0.767-2.137	0.137	—	—	—
<98% vs. ≥98%						
Tumor size (cm)	1.428	0.873-2.018	0.233	—	—	—
<5 vs. ≥5						
ELF3-AS1 expression	3.213	1.327-5.133	0.002	2.762	1.238-4.562	0.006
High vs. low						

effects in tumor progression^{26–29}. In this study, we identified a novel glioma-related lncRNA, ELF3-AS1.

In recent years, the dysregulation of the ELF3-AS1 expression and its biological function in several tumors have been reported. For instance, Zhang et al.²¹ found that high ELF3-AS1 expression in lung cancer specimens predicted a weak clinical prognosis of lung cancer patients. Functionally, ELF3-AS1 was shown to promote lung cancer cells with regard to migration and invasion via sponging miRNA-212. Yuan et al.²⁰ reported that ELF3-AS1, an overexpressed lncRNA in osteosarcoma, promoted the proliferation of osteosarcoma cells via increasing KLF12 potentially through methylation of miR-205. In bladder cancer, ELF3-AS1 was overexpressed and correlated with poor clinical outcome¹⁹.

Moreover, in vitro and in vivo assays revealed that ELF3-AS1 knockdown hindered the proliferation and metastasis via interaction with KLF8. As suggested by another study of Chu et al., ELF3-AS1 overexpression promoted the proliferation of oral squamous cell carcinoma cell³⁰. All the above findings suggested ELF3-AS1 as a tumor promotor. However, the expression and function of ELF3-AS1 in glioma have not been investigated.

Our study firstly proved the distinctly increased ELF3-AS1 in 182 glioma specimens compared to matched nontumor tissues, and increased ELF3-AS1 expression was associated with WHO grade and KPS score. Then, we explored the diagnostic value of a high ELF3-AS1 expression for glioma specimens, finding that a high ELF3-AS1 expression in the

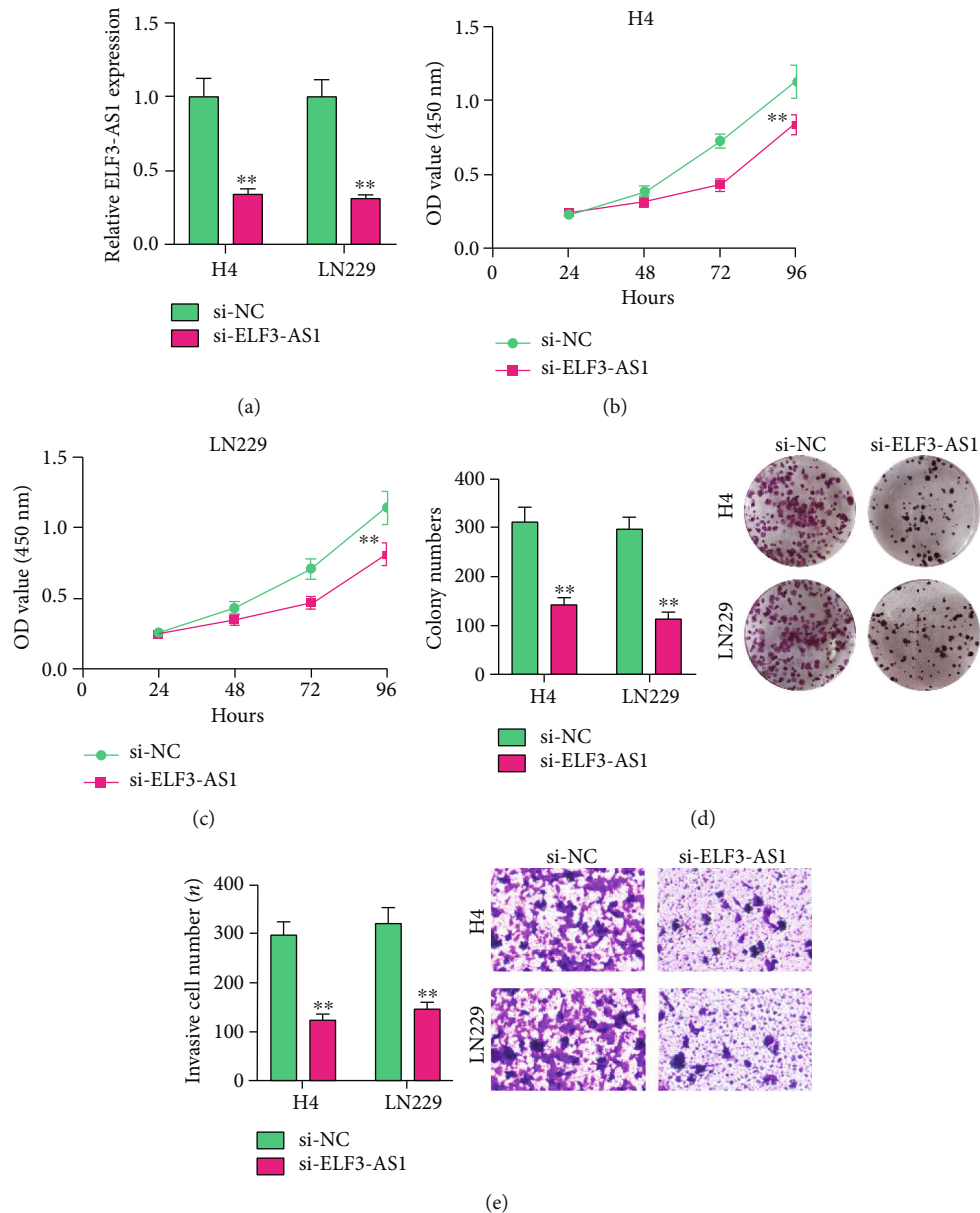


FIGURE 4: Effect of ELF3-AS1 on proliferation rate, colony formation ability, and invasion ability. (a) RT-PCR analysis of ELF3-AS1 knockdown efficiency in H4 and LN229 cells. (b, c) Cell proliferation was evaluated by CCK-8 assay in H4 and LN229 cells. (d) Colony-forming assays were performed to determine the growth of glioma cells. (e) Invasion ability was tested in Matrigel-coated transwell invasion chambers. ** $p < 0.01$, * $p < 0.05$.

tumor specimens enabled the discrimination of glioma patients from nontumor brain tissues with an AUC of 0.8073, indicating it as a possible diagnostic biomarker for glioma. Moreover, we performed Kaplan-Meier methods to explore the clinical significance of ELF3-AS1 expression in glioma patients, finding that patients with a high ELF3-AS1 expression have a shorter OS and DFS than those with a low ELF3-AS1 expression. More importantly, the results of univariate and multivariate analyses confirmed that increased ELF3-AS1 expression could serve as a significant and independent predictor of OS and DFS of glioma patients. To explore the potential function of ELF3-AS1 on the progress of glioma cells, we performed loss-of-function assays

and confirmed that knockdown of ELF3-AS1 suppressed the proliferation and invasion of glioma cells. The findings of the effects of ELF3-AS1 acting as a tumor promotor in glioma were consistent with previous findings in other types of tumors.

5. Conclusions

Our present study identified a novel glioma-related lncRNA, ELF3-AS1, which was associated with the progression of glioma. The findings revealed that ELF3-AS1 could be a new biomarker as well as a therapeutic target for effectively treating glioma.

Data Availability

The data used to support the findings of this study are available from the corresponding author upon request.

Conflicts of Interest

The authors declare that they have no conflicts of interest.

Authors' Contributions

Jun-chi Mei and Ge Yan contributed equally to this work.

Acknowledgments

This work was supported by the National Natural Science Foundation of China (No. 21775034).

References

- [1] R. L. Siegel, K. D. Miller, and A. Jemal, "Cancer statistics, 2018," *CA: A Cancer Journal for Clinicians*, vol. 68, no. 1, pp. 7–30, 2018.
- [2] P. D. Delgado-López, E. M. Corrales-García, J. Martino, E. Lastra-Aras, and M. T. Dueñas-Polo, "Diffuse low-grade glioma: a review on the new molecular classification, natural history and current management strategies," *Clinical and Translational Oncology*, vol. 19, no. 8, pp. 931–944, 2017.
- [3] Q. T. Ostrom, L. Bauchet, F. G. Davis et al., "The epidemiology of glioma in adults: a "state of the science" review," *Neuro-Oncology*, vol. 16, no. 7, pp. 896–913, 2014.
- [4] M. Yang, W. Guo, C. Yang et al., "Mobile phone use and glioma risk: a systematic review and meta-analysis," *PLoS One*, vol. 12, no. 5, article e0175136, 2017.
- [5] S. Gore, T. Chougule, J. Jagtap, J. Saini, and M. Ingalthalikar, "A review of radiomics and deep predictive modeling in glioma characterization," *Academic Radiology*, 2020.
- [6] A. Zottel, N. Šamec, A. V. Paska, and I. Jovčevska, "Coding of glioblastoma progression and therapy resistance through long noncoding RNAs," *Cancers*, vol. 12, no. 7, p. 1842, 2020.
- [7] C. Mecca, I. Giambanco, R. Donato, and C. Arcuri, "Targeting mTOR in glioblastoma: rationale and preclinical/clinical evidence," *Disease Markers*, vol. 2018, Article ID 9230479, 10 pages, 2018.
- [8] C. Achour and F. Aguilo, "Long non-coding RNA and polycomb: an intricate partnership in cancer biology," *Frontiers in bioscience*, vol. 23, no. 11, pp. 2106–2132, 2018.
- [9] Y. Fang and M. J. Fullwood, "Roles, functions, and mechanisms of long non-coding RNAs in cancer," *Genomics, Proteomics & Bioinformatics*, vol. 14, no. 1, pp. 42–54, 2016.
- [10] T. Gutschner and S. Diederichs, "The hallmarks of cancer: a long non-coding RNA point of view," *RNA Biology*, vol. 9, no. 6, pp. 703–719, 2014.
- [11] X. Zhang, W. Wang, W. Zhu et al., "Mechanisms and functions of long non-coding RNAs at multiple regulatory levels," *International journal of molecular sciences*, vol. 20, no. 22, p. 5573, 2019.
- [12] K. Muret, C. Désert, L. Lagoutte et al., "Long noncoding RNAs in lipid metabolism: literature review and conservation analysis across species," *BMC Genomics*, vol. 20, no. 1, p. 882, 2019.
- [13] T. R. Mercer and J. S. Mattick, "Structure and function of long noncoding RNAs in epigenetic regulation," *Biochimica et Biophysica Acta (BBA) - Molecular Cell Research*, vol. 20, no. 3, pp. 300–307, 2013.
- [14] Y. H. Li, Y. Q. Hu, S. C. Wang, Y. Li, and D. M. Chen, "lncRNA SNHG5: a new budding star in human cancers," *Gene*, vol. 749, article 144724, 2020.
- [15] N. Abu, K. W. Hon, S. Jeyaraman, and R. Jamal, "Long non-coding RNAs as biotargets in cisplatin-based drug resistance," *Future oncology*, vol. 14, no. 29, pp. 3085–3095, 2018.
- [16] A. Yamashita, Y. Shichino, and M. Yamamoto, "The long non-coding RNA world in yeasts," *Biochimica et Biophysica Acta*, vol. 1859, no. 1, pp. 147–154, 2016.
- [17] Y. Zhang, Y. Tao, and Q. Liao, "Long noncoding RNA: a cross-link in biological regulatory network," *Briefings in Bioinformatics*, vol. 19, no. 5, pp. 930–945, 2018.
- [18] J. Song, X. Chen, Q. Tian et al., "The value of lncRNA GHET1 as a prognostic factor for survival of Chinese cancer outcome: a meta-analysis," *Disease Markers*, vol. 2019, Article ID 5824190, 7 pages, 2019.
- [19] Y. Guo, D. Chen, X. Su, J. Chen, and Y. Li, "The lncRNA ELF3-AS1 promotes bladder cancer progression by interaction with Krüppel-like factor 8," *Biochemical and Biophysical Research Communications*, vol. 508, no. 3, pp. 762–768, 2019.
- [20] J. Yuan, J. Kang, and M. Yang, "Long non-coding RNA ELF3-antisense RNA 1 promotes osteosarcoma cell proliferation by upregulating Kruppel-like factor 12 potentially via methylation of the microRNA-205 gene," *Oncology Letters*, vol. 19, no. 3, pp. 2475–2480, 2020.
- [21] Z. Zhang, L. Nong, M.-L. Chen et al., "lncRNA ELF3-AS1 promotes nonsmall cell lung cancer cell invasion and migration by downregulating miR-212," *Cancer Biotherapy and Radiopharmaceuticals*, 2020.
- [22] R. Chen, M. Smith-Cohn, A. L. Cohen, and H. Colman, "Glioma subclassifications and their clinical significance," *Neurotherapeutics*, vol. 14, no. 2, pp. 284–297, 2017.
- [23] M. G. Filbin and D. Sturm, "Gliomas in children," *Seminars in Neurology*, vol. 38, no. 1, pp. 121–130, 2018.
- [24] L. Xiong, F. Wang, and X. X. Qi, "Advanced treatment in high-grade gliomas," *Journal of BUON*, vol. 24, no. 2, pp. 424–430, 2019.
- [25] H. Ohgaki and P. Kleihues, "Epidemiology and etiology of gliomas," *Acta Neuropathologica*, vol. 109, no. 1, pp. 93–108, 2005.
- [26] J. J. Chan and Y. Tay, "Noncoding RNA:RNA regulatory networks in cancer," *International journal of molecular sciences*, vol. 19, no. 5, p. 1310, 2018.
- [27] Y. Chi, D. Wang, J. Wang, W. Yu, and J. Yang, "Long Non-coding RNA in the pathogenesis of cancers," *Cells*, vol. 8, no. 9, p. 1015, 2019.
- [28] F. Momen-Heravi and S. Bala, "Emerging role of non-coding RNA in oral cancer," *Cellular Signalling*, vol. 42, pp. 134–143, 2018.
- [29] L. Bolha, M. Ravnik-Glavač, and D. Glavač, "Long noncoding RNAs as biomarkers in cancer," *Disease Makers*, vol. 2017, article 7243968, 14 pages, 2017.
- [30] H. Chu, Z. Li, Z. Gan, Z. Yang, Z. Wu, and M. Rong, "lncRNA ELF3-AS1 is involved in the regulation of oral squamous cell carcinoma cell proliferation by reprogramming glucose metabolism," *OncoTargets and Therapy*, vol. 12, pp. 6857–6863, 2019.

Review Article

Updating a Strategy for Histone Deacetylases and Its Inhibitors in the Potential Treatment of Cerebral Ischemic Stroke

Yuzhen Xu ¹, Qian Wang ², Jianxin Chen ³, Yihong Ma ⁴, and Xueyuan Liu ¹

¹Department of Neurology, Shanghai Tenth People's Hospital, Tongji University School of Medicine, No. 301 Middle Yanchang Road, Shanghai, China

²Department of Central Laboratory, Taian City Central Hospital, Shandong First Medical University & Shandong Academy of Medical Sciences, Taian, Shandong Province, China

³Department of Neurology, Jinan First People's Hospital, Shandong Traditional Chinese Medicine University, Jinan, Shandong Province, China

⁴Department of Neurology, Graduate School of Medical Sciences, Kumamoto University, Kumamoto, Japan

Correspondence should be addressed to Jianxin Chen; cjxneurology@sina.com, Yihong Ma; ma.ihon@kuh.kumamoto-u.ac.jp, and Xueyuan Liu; liuxy@tongji.edu.cn

Received 17 August 2020; Revised 25 August 2020; Accepted 26 August 2020; Published 7 September 2020

Academic Editor: Wen-Jun Tu

Copyright © 2020 Yuzhen Xu et al. This is an open access article distributed under the Creative Commons Attribution License, which permits unrestricted use, distribution, and reproduction in any medium, provided the original work is properly cited.

Background. Cerebral ischemic stroke is one of the severe diseases with a pathological condition that leads to nerve cell dysfunction with seldom available therapy options. Currently, there are few proven effective treatments available for improving cerebral ischemic stroke outcome. However, recently, there is increasing evidence that inhibition of histone deacetylase (HDAC) activity exerts a strong protective effect in in vivo and vitro models of ischemic stroke. **Review Summary.** HDAC is a posttranslational modification that is negatively regulated by histone acetyltransferase (HATS) and histone deacetylase. Based on function and DNA sequence similarity, histone deacetylases (HDACs) are organized into four different subclasses (I-IV). Modifications of histones play a crucial role in cerebral ischemic affair development after translation by modulating disrupted acetylation homeostasis. HDAC inhibitors (HDACi) mainly exert neuroprotective effects by enhancing histone and nonhistone acetylation levels and enhancing gene expression and protein modification functions. This article reviews HDAC and its inhibitors, hoping to find meaningful therapeutic targets. **Conclusions.** HDAC may be a new biological target for cerebral ischemic stroke. Future drug development targeting HDAC may make it a potentially effective anticerebral ischemic stroke drug.

1. Instruction

Cerebral ischemic stroke is a serious neurological disease that leads to morbidity, mortality, and severe long-term disability [1]. Because of its high basal metabolic rate, dependence on maintained ion gradients, and high concentrations of glutamate and aspartic acid, central nervous system neurons are particularly vulnerable to the direct effects of hypoglycemia and hypoxia [2–4]. The subsequent Na^{2+} influx and Ca^{2+} overload result in cytotoxic edema, acidosis, organelle, and necrotic cell death finally [5]. The endogenous neuronal repair occurred in the site of the penumbra, including neurogenesis and neovascularization, which appear days to weeks after an ischemic stroke [6]. It determines the final degree

of tissue regeneration and function recovery [7]. Ischemic stroke has a complex pathophysiological process involving excitotoxicity, oxidative stress, and inflammation [8]. Therefore, effective treatments should have a multitarget effect to achieve the purpose of reducing nerve damage and promoting tissue repair [9, 10].

Histone deacetylase (HDAC) is a significant enzyme that regulates intracellular protein acetylation. Abnormal HDAC activity is associated with many diseases. HDAC is an essential drug target, many of which have been developed into clinical drugs. Recently, preclinical studies have confirmed that HDAC and its inhibitor (HDACi) are potential drugs for the treatment of stroke [11]. HDAC and HDACi regulate a series of processes from cell survival to regeneration,

significantly reduce infarct area, and play a neuroprotective role in vivo and vitro [10]. Here, our review will discuss the role of histone deacetylases (HDACs) in cerebral ischemic stroke and update the potential therapeutic strategy of HDACi as emerging drugs in stroke treatment in recent times.

2. Overview of the HDACs and HDACi in Cerebral Ischemia

2.1. Overview of the HDACs. HDACs are conservative evolutionary enzymes involved in the epigenetic regulation of gene expression and protein functions [12]. To date, 18 potential HDACs have been identified in mammalian cells, and all of them are expressed in the adult brain [13]. Given that histone modification can regulate chromatin structure and gene expression in which abnormal alteration appearance in HDACs is associated with cerebral ischemic development, the mechanism of action between HDACs and cerebral infarction is summarized in Figure 1. Based on function and DNA sequence similarity, HDACs are organized into four different subclasses (I-IV) [14]: the zinc-dependent class I (HDAC 1, HDAC 2, HDAC 3, and HDAC 8), the zinc-independent class II (class IIa: HDAC 4, HDAC 5, HDAC 6, HDAC 7, and HDAC 9; class IIb (HDAC6), the NAD-dependent class III (sirtuins), and class IV (HDAC 10 and HDAC 11). The class I HDACs display an extensive presence in nuclei. In addition to nuclear localization, the expression of class I isoforms has also been observed in cytoplasmic domains. The class I HDACs are a large class of constitutive nuclear proteins, while class II HDACs, divided into classes IIa and IIb, mainly shuttle between the nucleus and cytoplasm. Class IV HDACs are generally composed of a member, HDAC11, and little is known about its role in ischemic stroke. Sirtuins have been discussed in a recent review, referred to as class III HDACs, which are structurally and enzymatically distinct NAD-dependent enzymes [15–18].

2.2. Overview of the HDACs. According to the HDAC classification, currently, the most common HDACi used in cerebral ischemic models are class I and class II inhibitors. Here, we summarized the related HDACi in cerebral ischemia. Class I is including MS-275 [19], Scriptaid [8], trichostatin A (TSA) [20], suberoylanilide hydroxamic acid (SAHA) [21, 22], valproic acid (VPA), sodium butyrate (SB) [23], and 4-phenylbutyric acid (4-PB) [24]. Besides that, nicotinamide is a nonspecific inhibitor of class III HDACs [25]. Here, we summarized the publication of HDAC and HDACi in recent years as a treatment strategy and probably mechanism in cerebral ischemia (Table 1).

3. HDACs in Cerebral Ischemia

3.1. Zinc-Dependent Class I. HDAC1 is the first mammalian protein identified to have histologically oriented deacetylase activity [26], which exerts an essential role in regulating the cell cycle and is necessary for the transcriptional suppression of cell cycle genes. The association between HDAC1 and the promoter region of specific genes is related to their transcrip-

tional suppression. The functional acquisition of HDAC1 provides adequate protection against DNA damage and neurotoxicity of cultured neurons, which is used as a model of ischemia in vivo [27]. The penumbra of HDAC2 in the rat cerebral cortex enhanced 4 or 24 hours after photothrombotic stroke (PTS). PTS increases the expression of HDAC1 and HDAC2 in the penumbra, which leads to the redistribution of HDAC1. However, the redistribution of HDAC2 from the nucleus to the cytoplasm is less than that of HDAC1 [28]. In transient middle cerebral artery occlusion (tMCAO) models of rats, the specificity protein family of transcription factor 3 (Sp3) together with HDAC1/HDAC2 complex could modulate the acetylation of *ncx1* brain promoter (*ncx1-br*), which may act as an innovative development strategy in stroke treatment intervention [29].

Furthermore, T-LAK-cell-originated protein kinase (TOPK) has a neuroprotective effect on cerebral ischemia-reperfusion injury by inhibiting HDAC1/HDAC2 activity, which may be related to the neuroprotective effect of TOPK on cerebral ischemia-reperfusion injury [30]. The expression of HDAC3 in the pathological process of diabetes and stroke can protect the brain from ischemia-reperfusion (I/R) injury by regulating oxidative stress, apoptosis, and autophagy in vivo and in vitro, and the mechanisms may be by the upregulated expressions of brain and muscle ARNT-Like 1 and AIM2 inflammatory bodies [31, 32]. Calpeptin pretreatment blocked the attenuation of the nuclear distribution of HDAC3 in vivo [33]. HDAC8 plays a protective role in the cytotoxicity of renal cell death [34], but its effect on cerebral ischemia was not obvious.

3.2. Class II HDACs. In ischemic stroke models, HDAC4 expression is reduced, while HDAC4 may reduce neuronal apoptosis by decreasing high-mobility group box 1 (hMGB1) protein expression and promote angiogenesis and nerve regeneration through the release of VEGF signal of hypoxia-inducible factor-1 [35–37]. HDAC4's interactive partners such as MEF2, ATF4, and NF- κ B may also mediate the roles of attenuation of neuronal apoptosis and promotion of angiogenesis and neurogenesis of ischemic stroke [38]. A recent study found that HDAC5 effectively inhibits the involvement of myocardial-associated transcription factor A (MRTF-A) in IR-induced apoptosis of cortical neurons [39]. In one study, miR-217 promotes the accumulation of HDAC5 in the nucleus and affects the cerebral ischemia-reperfusion injury via the miR-217/MEF2D/HDAC5 axis [40].

HDAC9 is expressed in the cerebral and systemic arteries. In rat cerebral ischemia/reperfusion injury, the brain injury can be alleviated by silencing the HDAC9 gene by lentivirus recombination in the brain with upregulated HDAC9. It is involved in hypoxia-glucose-induced dysfunction of cerebral microvascular endothelial cells, increased inflammatory response, apoptosis, endothelial cell permeability disorder, and decreased expression of tight junction protein [41]. HDAC9 deficiency and downregulation of phosphorylated I κ B α are related to the role of phosphorylated nuclear factor- κ B (NF- κ B) and mitogen-activated protein kinase (MAPKs), including regulating phosphorylated p38, phosphorylated extracellular signal-regulated kinase 1, ERK1/2,

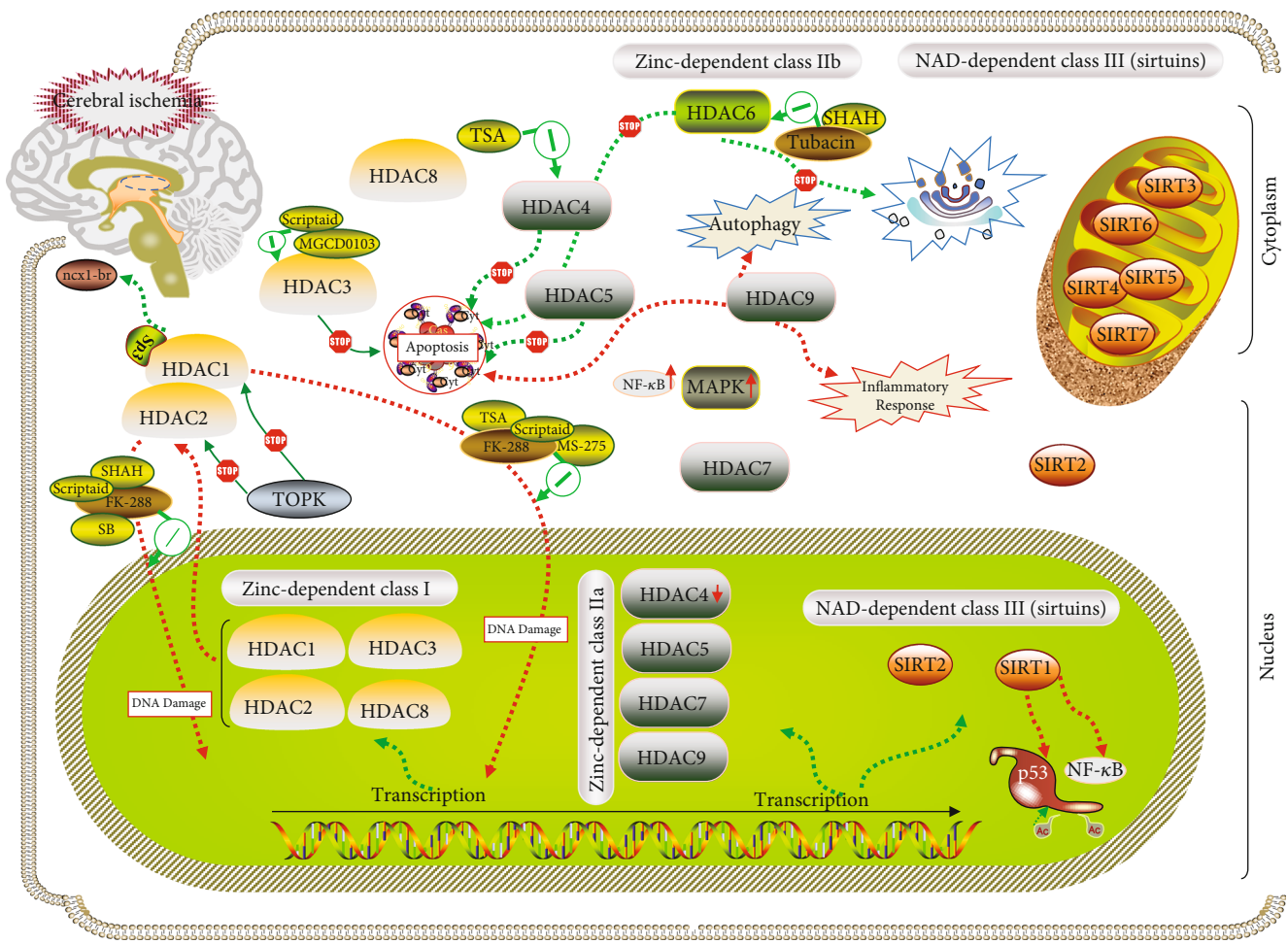


FIGURE 1: Overview of the probable mechanism between HDACs and their inhibitors. Due to the different distributions of HDACs in the cytoplasm and nuclei, the related mechanisms of cerebral ischemia show the different types. When cerebral infraction occurred, HDAC 1 and 2 in the nucleus were released into the cytoplasm that caused homeostasis of the cellular environment to be destroyed. It will continuously lead to the degradation of DNA. Meanwhile, HDAC 3, 4, 5, and 9 would participate in apoptosis, inflammation response, and Golgi apparatus dysfunction as well as autophagy, which is particularly apparent in HDAC9, respectively. Moreover, HDAC NAD⁺-dependent class III (SIRT1) could aggravate the ischemic injury p53 acetylation and NF-κB.

TABLE 1: Primary HDAC and HDAC inhibitors in cerebral ischemia.

HDAC classification	HDAC	HDAC inhibitors	Location
Zinc-dependent class I	HDAC 1	MS-275, FK-288, TSA, VPA, Scriptaid	NU
	HDAC 2	FK-288, SAHA, SB, Scriptaid	NU
	HDAC 3	MGCD0103, Scriptaid	NU/CM
	HDAC 8	/	NU/CM
Zinc-dependent class II (class IIa)	HDAC 4	TSA, 4-PBA	NU/CM
	HDAC 5	/	NU/CM
	HDAC 7	/	NU/CM
Zinc-dependent class II (class IIb)	HDAC 6	Tubacin, SAHA	CM
	HDAC 9	/	NU/CM
NAD ⁺ -dependent class III (sirtuins)	SIRT1	Sirtinol	NU
	SIRT2	AKG2	NU/CM
	SIRT3	/	Mitochondria

NU: nucleus; CM: cytoplasm.

and phosphorylated c-Jun n-terminal kinase, in promoting ischemic brain injury [42]. In addition, HDAC9 polymorphism can be used as a biomarker of susceptibility, severity, and short-term prognosis of atherosclerotic stroke [43]. However, Su et al. [44] indicate that variant rs2107595 of HDAC9 may have no association with higher ischemic stroke risks in southern Han Chinese.

HDAC6 can inhibit the survival and regeneration of neurons [18]. On the other hand, HDAC6 inhibits ODG reperfusion-induced tubulin deacetylation and caspase-3 activation and protects Golgi apparatus breakage and apoptosis induced by oxyglucose deprivation reperfusion (OGDR) [45]. Another research exhibits tripartite inhibition of HDAC6 that showed neuroprotection against various cellular insults [46]. Pharmacological or gene inhibition experiments on HDAC6 confirmed the block caused by stroke, indicating that the normal function of HDAC6 is necessary for the efficacy of rehabilitation treatment after stroke [47].

3.3. NAD-Dependent Class III (Sirtuins). Sirtuins are a group of histone deacetylase whose activity is dependent on and regulated by nicotinamide adenine dinucleotide (NAD⁺) [48]. In ischemic brain injury, the latest research shows that the decrease of SIRT1 activity may aggravate ischemic brain injury in permanent cerebral ischemia mice, whether by pharmacological or genetic methods [49]. This neuroprotective effect may be mediated by SIRT1 inhibition or deletion through p53 acetylation [50] and NF- κ B. Besides, the use of the SIRT1 activator can also reduce ischemic brain injury. SIRT3 has been reported to protect neurons from n-methyl-d-aspartate (NMDA) excitotoxicity, suggesting that SIRT3 may also play a beneficial role in cerebral ischemia. However, it is necessary further to illuminate the role of SIRT3 in cerebral ischemic injury [51].

3.4. HDACi in Cerebral Ischemia. In order to explore the usefulness of HDAC inhibitors, we discussed and summarized the mechanism and show the structural formula of the dominant HDAC inhibitors in vitro and in vivo, which is closely related to cerebral ischemia for brain protection (Figure 2).

3.5. HDACi Class I. MS-275 (entinostat), a class I histone deacetylase inhibitor (HDAC), modulates differentiation and prevents brain injury [52]. In stroke model MS-275, a neuroprotective effect had been demonstrated in vitro [53]. In ischemic pathology, p53 plays a role, which is regulated by class I HDA in processes of acetylation [54]. Sean P et al. had found that MS-275 is not responsible for modulating the activity of p53. Unlike affecting p53, the evidence showed the effect of mitochondria for protection in the cerebral ischemia model. TSA has been shown to have neuroprotective properties in neurons [55] through blocking p53 accumulation after DNA damage. Unlike MS-275, it had shown different mechanisms and manifestations in the role of brain protection. SHAH is an FDA-approved HDACi. Its has an anti-inflammatory effect and is carefully used for protection by early treatment of the cerebral ischemia mouse model, closely related to its effect of reducing microglial

activation and priming these activations toward an M2 phenotype [22].

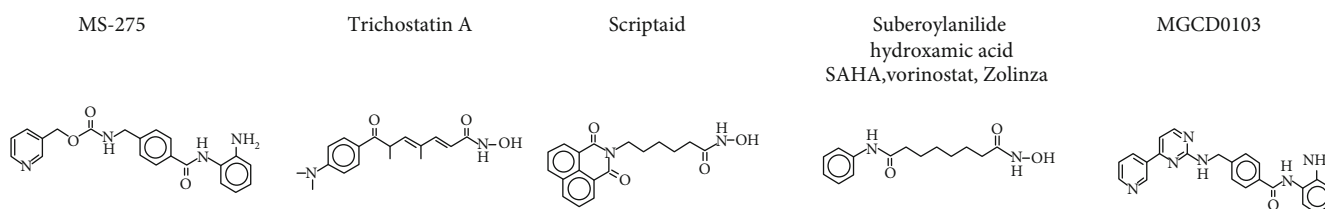
3.6. HDACi Class II. Compared with traditional HDAC inhibitor, Sirtinol, as a SIRT1-specific inhibitor and activator [56], significantly reversed the effect of resveratrol postconditioning on cerebral ischemia in a mouse model [57]. Otherwise, FK228 a kind of selective HDAC1/2 inhibitor could help restrain TOPK through the AKT pathway to attenuate the oxidative stress in the early stage of ischemic stroke. Besides that, in 2019, tubacin selectively inhibits HDAC6 activity which had been identified in transient occlusion of the middle cerebral artery by ameliorating endothelial dysfunction [58].

4. Summary and Perspective

Studies over the past few decades have shown that HDACs play an essential role in the development of cerebral ischemic stroke by reversibly regulating protein acetylation. As a histone acetylation remover and a key regulator of epigenetics, HDACs have been found to have abnormalities and dysfunctions in ischemic stroke, which provides a novel and attractive target to intervene. Also, HDAC has some anti-inflammatory effects and is involved in the mechanism of brain protection. As a target of an early inflammatory reaction, it acts on HDACi and plays a neuroprotective role. One of the inhibitors had been showing the protection against ischemic brain injury in the cerebral ischemia mouse model through increasing protein acetylation levels in the mouse brain. However, in human plasma, at the early stage of other diseases, such as chronic hepatitis B, HDAC activity abnormalities were found in patients with other diseases, and their levels were related to the severity of the disease [59]. However, the exact function of HDACs as a central medium for proliferation and regulation remains a mystery. At present, the biomarker of fresh blood has been applied and can be used as a clear indicator for cerebral ischemic prediction [60]. However, at present, no detailed research on HDAC is related to plasma, and CSF biomarkers had been explored in cerebral infarction.

Intriguingly, valproic acid, which is commonly prescribed as an anticonvulsant drug, was subsequently discovered to be an HDAC inhibitor [61]. In cellular and animal models, VPA has been shown to have neuroprotective properties at the therapeutic level. Valproic acid (VPA), a widely used antiepileptic mood stabilizer drug, has been shown to have neuroprotective effects against various injuries through a variety of signal pathways, such as blocking the increase in caspase-3 activity. VPA significantly upregulated the expression activity of ERK and Akt [62]. Recently, new research also found that VPA could inhibit the enzyme GSK3 for neuroprotective properties, which are related to the drug anti-inflammatory activity [63]. Like VPA, SB inhibits cell growth through cell cycle arrest, while stable transcriptional inhibition of cell cycle promotes the reduction of microglia and inhibition of other inflammatory markers in ischemic brain [55, 64]. 4-Phenylbutyrate (PBA) has the effect of anticerebral ischemia by inhibiting endoplasmic reticulum stress-

HDAC inhibitors I



HDAC inhibitors II

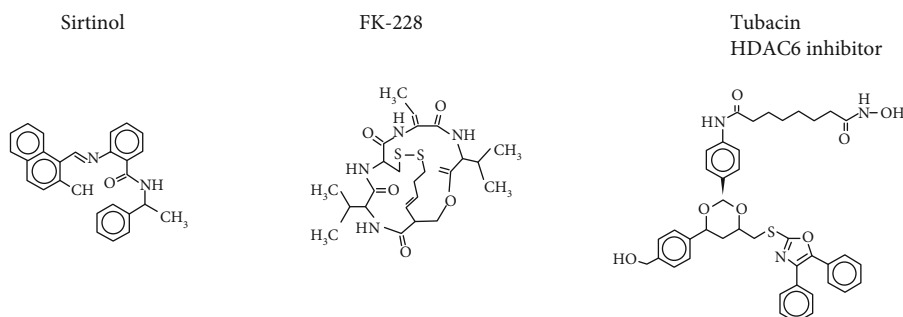


FIGURE 2: Primary structural formula of HDAC inhibitors in cerebral ischemia.

mediated apoptosis and inflammation [65]. The effect of these inhibitors may be related to the inhibition of HDAC, which leads to high acetylation of chromatin proteins and changes in gene expression. Besides that, TMP269 is a particular class IIA histone deacetylase inhibitor that has a protective role by upregulating the level of histone 2 acetylation in tMCAO mouse models, in the meantime, which upregulates the expression of tissue kallikrein [66]. Recently, one study has also indicated that SIRT2 inhibitor AGK2 can alleviate reperfusion injury of a myocardial ischemia model [67]. Because there are many common pathological mechanisms between myocardial and cerebral ischemia-reperfusion injuries, the inhibition of SIRT2 may also have a neuroprotective effect in cerebral ischemia [68]. Furthermore, tubastatin A (TubA) is a new type of HDAC6 inhibitor, which can improve the functional outcome, reduce cerebral infarction, and attenuate neuronal apoptosis in MCAO rats by downregulating fibroblast growth factor-21 (FGF-21) [69].

M344 is a kind of HDAC inhibitor, which led to a remarkable decrease in the phosphorylation of JNK and c-Jun, concomitant with a significant abrogation of apoptosis caused by potassium deprivation in cultured cerebellar granule neurons [70], but within the current scope of treatment for cerebral infarction, the function between HDAC and HDACi can play a minimal role. Although many protective effects have been achieved in animals, there are still many defects in clinical trials for therapy using them. In recent years, the use of HDACi alone is improbable to have a substantial impact in the clinic, and these promising drugs may lie in cognitive combination therapy in the future. A large number of reasonable, HDAC-based combinations are possible with the gradual elucidation of the multiple action mechanisms of these drugs and the emergence of new combinations. In the field of treatment, HDAC-based combination

therapy has made the fastest progress, including cytotoxic chemotherapy. More studies are needed to systematically analyze the role of a single HDAC in different types and stages of ischemic stroke. Further elucidation of the mechanism of action of HDACs and HDACi will provide a bright prospect for HDACi as one of the many tools to combat stroke.

Data Availability

The data used to support the findings of this study are available from the corresponding author upon reasonable request.

Conflicts of Interest

We declare that we have no financial and personal relationships with other people or organizations that can inappropriately influence our work; there is no professional or other personal interest of any nature or kind in any product, service, and a company that could be construed as influencing the position presented in, or the review of, the manuscript entitled.

Acknowledgments

The study was funded by grants from the National Natural Science Foundation of China (81771131) and the Major Projects of Science and Technology Commission of Shanghai Municipality (17411950100).

References

- [1] J. Krupinski, J. Kaluza, P. Kumar, S. Kumar, and J. M. Wang, "Role of angiogenesis in patients with cerebral ischemic stroke," *Stroke*, vol. 25, no. 9, pp. 1794–1798, 1994.

- [2] D. Mayor and M. Tymianski, "Neurotransmitters in the mediation of cerebral ischemic injury," *Neuropharmacology*, vol. 134, pp. 178–188, 2018.
- [3] Y. Xu, Q. Wang, D. Li et al., "Protective effect of lithium chloride against hypoglycemia-induced apoptosis in neuronal PC12 cell," *Neuroscience*, vol. 330, pp. 100–108, 2016.
- [4] Y. Xu, Q. Wang, Z. Wu et al., "The effect of lithium chloride on the attenuation of cognitive impairment in experimental hypoglycemic rats," *Brain Research Bulletin*, vol. 149, pp. 168–174, 2019.
- [5] G. J. Jeffs, B. P. Meloni, A. J. Bakker, and N. W. Knuckey, "The role of the Na⁺/Ca²⁺ exchanger (NCX) in neurons following ischaemia," *Journal of Clinical Neuroscience*, vol. 14, no. 6, pp. 507–514, 2007.
- [6] P. Ramos-Cabrer, F. Campos, T. Sobrino, and J. Castillo, "Targeting the ischemic penumbra," *Stroke*, vol. 42, 1, Supplement 1, pp. S7–11, 2010.
- [7] R. Liu, H. Yuan, F. Yuan, and S. H. Yang, "Neuroprotection targeting ischemic penumbra and beyond for the treatment of ischemic stroke," *Neurological Research*, vol. 34, no. 4, pp. 331–337, 2013.
- [8] Q. Meng, G. Yang, Y. Yang, F. Ding, and F. Hu, "Protective effects of histone deacetylase inhibition by Scriptaid on brain injury in neonatal rat models of cerebral ischemia and hypoxia," *International Journal of Clinical and Experimental Pathology*, vol. 13, no. 2, pp. 179–191, 2020.
- [9] S. Liu, S. R. Levine, and H. R. Winn, "Targeting ischemic penumbra: part I - from pathophysiology to therapeutic strategy," *Journal of Experimental Stroke and Translational Medicine*, vol. 3, no. 1, pp. 47–55, 2010.
- [10] L. Lv, Y. P. Tang, X. Han, X. Wang, and Q. Dong, "Therapeutic application of histone deacetylase inhibitors for stroke," *Central Nervous System Agents in Medicinal Chemistry*, vol. 11, no. 2, pp. 138–149, 2011.
- [11] E. Fessler, F. Chibane, Z. Wang, and D.-M. Chuang, "Potential roles of HDAC inhibitors in mitigating ischemia-induced brain damage and facilitating endogenous regeneration and recovery," *Current Pharmaceutical Design*, vol. 19, no. 28, pp. 5105–5120, 2013.
- [12] M. Haberland, R. L. Montgomery, and E. N. Olson, "The many roles of histone deacetylases in development and physiology: implications for disease and therapy," *Nature Reviews Genetics*, vol. 10, no. 1, pp. 32–42, 2009.
- [13] G. P. Delcuve, D. H. Khan, and J. R. Davie, "Roles of histone deacetylases in epigenetic regulation: emerging paradigms from studies with inhibitors," *Clinical Epigenetics*, vol. 4, no. 1, pp. 5–5, 2012.
- [14] M. Yoshida, N. Kudo, S. Kosono, and A. Ito, "Chemical and structural biology of protein lysine deacetylases," *Proceedings of the Japan Academy. Series B, Physical and Biological Sciences*, vol. 93, no. 5, pp. 297–321, 2017.
- [15] J.-S. Guan, S. J. Haggarty, E. Giacometti et al., "HDAC2 negatively regulates memory formation and synaptic plasticity," *Nature*, vol. 459, no. 7243, pp. 55–60, 2009.
- [16] O. H. Krämer, S. K. Knauer, G. Greiner et al., "A phosphorylation-acetylation switch regulates STAT1 signaling," *Genes & Development*, vol. 23, no. 2, pp. 223–235, 2009.
- [17] R. L. Montgomery, J. Hsieh, A. C. Barbosa, J. A. Richardson, and E. N. Olson, "Histone deacetylases 1 and 2 control the progression of neural precursors to neurons during brain development," *Proceedings of the National Academy of Sciences of the United States of America*, vol. 106, no. 19, pp. 7876–7881, 2009.
- [18] M. A. Riviaccio, C. Brochier, D. E. Willis et al., "HDAC6 is a target for protection and regeneration following injury in the nervous system," *Proceedings of the National Academy of Sciences*, vol. 106, no. 46, pp. 19599–19604, 2009.
- [19] S. P. Murphy, R. J. Lee, M. E. McClean et al., "MS-275, a class I histone deacetylase inhibitor, protects the p53-deficient mouse against ischemic injury," *Journal of Neurochemistry*, vol. 129, no. 3, pp. 509–515, 2014.
- [20] D. M. Vigushin, S. Ali, P. E. Pace et al., "Trichostatin A is a histone deacetylase inhibitor with potent antitumor activity against breast cancer in vivo," *Clinical Cancer Research*, vol. 7, no. 4, pp. 971–976, 2001.
- [21] S. H. Chen, H. M. Wu, B. Ossola et al., "Suberoylanilide hydroxamic acid, a histone deacetylase inhibitor, protects dopaminergic neurons from neurotoxin-induced damage," *British Journal of Pharmacology*, vol. 165, no. 2, pp. 494–505, 2012.
- [22] S. Li, X. Lu, Q. Shao et al., "Early histone deacetylase inhibition mitigates ischemia/reperfusion brain injury by reducing microglia activation and modulating their phenotype," *Frontiers in Neurology*, vol. 10, pp. 893–893, 2019.
- [23] M. J. Park and F. Sohrabji, "The histone deacetylase inhibitor, sodium butyrate, exhibits neuroprotective effects for ischemic stroke in middle-aged female rats," *Journal of Neuroinflammation*, vol. 13, no. 1, p. 300, 2016.
- [24] J. Kaufman, C. Gordon, R. Bergamaschi et al., "The effects of the histone deacetylase inhibitor 4-phenylbutyrate on gap junction conductance and permeability," *Frontiers in Pharmacology*, vol. 4, 2013.
- [25] X. Wang, X. Wei, Q. Pang, and F. Yi, "Histone deacetylases and their inhibitors: molecular mechanisms and therapeutic implications in diabetes mellitus," *Acta Pharmaceutica Sinica B*, vol. 2, no. 4, pp. 387–395, 2012.
- [26] J. Taunton, C. A. Hassig, and S. L. Schreiber, "A mammalian histone deacetylase related to the yeast transcriptional regulator Rpd3p," *Science*, vol. 272, no. 5260, pp. 408–411, 1996.
- [27] D. Kim, C. L. Frank, M. M. Dobbin et al., "Deregulation of HDAC1 by p25/Cdk5 in neurotoxicity," *Neuron*, vol. 60, no. 5, pp. 803–817, 2008.
- [28] S. V. Demyanenko, V. A. Dzreyan, M. A. Neginskaya, and A. B. Uzdensky, "Expression of histone deacetylases HDAC1 and HDAC2 and their role in apoptosis in the penumbra induced by photothrombotic stroke," *Molecular Neurobiology*, vol. 57, no. 1, pp. 226–238, 2020.
- [29] L. Formisano, N. Guida, V. Valsecchi et al., "Sp3/REST/HDAC1/HDAC2 complex represses and Sp1/HIF-1/p300 complex activates ncx1 gene transcription, in brain ischemia and in ischemic brain preconditioning, by epigenetic mechanism," *The Journal of Neuroscience*, vol. 35, no. 19, pp. 7332–7348, 2015.
- [30] Z. Han, H. Zhao, Z. Tao et al., "TOPK promotes microglia/macrophage polarization towards M2 phenotype via inhibition of HDAC1 and HDAC2 activity after transient cerebral ischemia," *Aging and Disease*, vol. 9, no. 2, pp. 235–248, 2018.
- [31] B. Zhao, Q. Yuan, J. B. Hou et al., "Inhibition of HDAC3 ameliorates cerebral ischemia reperfusion injury in diabetic mice in vivo and in vitro," *Journal Diabetes Research*, vol. 2019, article 8520856, 12 pages, 2019.
- [32] M. J. Zhang, Q. C. Zhao, M. X. Xia et al., "The HDAC3 inhibitor RGFP966 ameliorated ischemic brain damage by down-regulating the AIM2 inflammasome," *The FASEB Journal*, vol. 34, no. 1, pp. 648–662, 2020.

- [33] X. Yang, Q. Wu, L. Zhang, and L. Feng, "Inhibition of histone deacetylase 3 (HDAC3) mediates ischemic preconditioning and protects cortical neurons against ischemia in rats," *Frontiers in Molecular Neuroscience*, vol. 9, p. 131, 2016.
- [34] S.-D. Ha, O. Solomon, M. Akbari, A. Sener, and S. O. Kim, "Histone deacetylase 8 protects human proximal tubular epithelial cells from hypoxia-mimetic cobalt- and hypoxia/reoxygenation-induced mitochondrial fission and cytotoxicity," *Scientific Reports*, vol. 8, no. 1, article 11332, 2018.
- [35] Q. Kong, Y. Hao, X. Li, X. Wang, B. Ji, and Y. Wu, "HDAC4 in ischemic stroke: mechanisms and therapeutic potential," *Clinical Epigenetics*, vol. 10, no. 1, p. 117, 2018.
- [36] M. He, B. Zhang, X. Wei et al., "HDAC4/5-HMGB1 signalling mediated by NADPH oxidase activity contributes to cerebral ischaemia/reperfusion injury," *Journal of Cellular and Molecular Medicine*, vol. 17, no. 4, pp. 531–542, 2013.
- [37] D. Z. Qian, S. K. Kachhap, S. J. Collis et al., "Class II histone deacetylases are associated with VHL-independent regulation of hypoxia-inducible factor 1 α ," *Cancer Research*, vol. 66, no. 17, pp. 8814–8821, 2006.
- [38] S. Demyanenko, E. Berezhnaya, M. Neginskaya, S. Rodkin, V. Dzreyan, and M. Pitinova, "Class II histone deacetylases in the post-stroke recovery period—expression, cellular, and subcellular localization—promising targets for neuroprotection," *Journal of Cell Biochemistry*, vol. 120, no. 12, pp. 19590–19609, 2019.
- [39] N. Li, Q. Yuan, X. L. Cao et al., "Opposite effects of HDAC5 and p300 on MRTF-A-related neuronal apoptosis during ischemia/reperfusion injury in rats," *Cell Death & Disease*, vol. 8, no. 2, article e2624, 2017.
- [40] L. Shi, Z. Tian, Q. Fu et al., "miR-217-regulated MEF2D-HDAC5/ND6 signaling pathway participates in the oxidative stress and inflammatory response after cerebral ischemia," *Brain Research*, vol. 1739, article 146835, 2020.
- [41] W. Shi, X. Wei, Z. Wang et al., "HDAC9 exacerbates endothelial injury in cerebral ischaemia/reperfusion injury," *Journal of Cellular and Molecular Medicine*, vol. 20, no. 6, pp. 1139–1149, 2016.
- [42] S. Lu, H. Li, K. Li, and X. D. Fan, "HDAC9 promotes brain ischemic injury by provoking I κ B α /NF- κ B and MAPKs signaling pathways," *Biochemical and Biophysical Research Communications*, vol. 503, no. 3, pp. 1322–1329, 2018.
- [43] M. Wang, M. Gu, Z. Li et al., "HDAC9 polymorphisms predict susceptibility, severity, and short-term outcome of large artery atherosclerotic stroke in Chinese population," *Journal of Molecular Neuroscience*, vol. 67, no. 1, pp. 165–171, 2019.
- [44] L. Su, T. Shen, B. Liang et al., "Association of GWAS-supported loci rs2107595 in HDAC9 gene with ischemic stroke in southern Han Chinese," *Gene*, vol. 570, no. 2, pp. 282–287, 2015.
- [45] J. Zhang, J. Tan, Z. Hu, C. Chen, and L. Zeng, "HDAC6 inhibition protects against OGD-induced Golgi fragmentation and apoptosis," *Oxidative Medicine and Cellular Longevity*, vol. 2019, Article ID 6507537, 12 pages, 2019.
- [46] I. N. Gaisina, S. H. Lee, N. A. Kaidery et al., "Activation of Nrf2 and hypoxic adaptive response contribute to neuroprotection elicited by phenylhydroxamic acid selective HDAC6 inhibitors," *ACS Chemical Neuroscience*, vol. 9, no. 5, pp. 894–900, 2018.
- [47] J. R. Sheu, C. Y. Hsieh, T. Jayakumar et al., "HDAC6 dysfunction contributes to impaired maturation of adult neurogenesis in vivo: vital role on functional recovery after ischemic stroke," *Journal of Biomedical Science*, vol. 26, no. 1, p. 27, 2019.
- [48] J. M. Villalba, R. de Cabo, and F. J. Alcain, "A patent review of sirtuin activators: an update," *Expert Opinion on Therapeutic Patents*, vol. 22, no. 4, pp. 355–367, 2012.
- [49] M. Hernández-Jiménez, O. Hurtado, M. I. Cuartero et al., "Silent information regulator 1 protects the brain against cerebral ischemic damage," *Stroke*, vol. 44, no. 8, pp. 2333–2337, 2013.
- [50] Q. Zhang, S. X. Zeng, Y. Zhang et al., "A small molecule Inauhizin inhibits SIRT1 activity and suppresses tumour growth through activation of p53," *EMBO Molecular Medicine*, vol. 4, no. 4, pp. 298–312, 2012.
- [51] J. M. Lee, G. J. Zipfel, and D. W. Choi, "The changing landscape of ischaemic brain injury mechanisms," *Nature*, vol. 399, no. 6738, pp. A7–14, 1999.
- [52] Z.-Y. Zhang and H. J. Schluesener, "Oral administration of histone deacetylase inhibitor MS-275 ameliorates neuroinflammation and cerebral amyloidosis and improves behavior in a mouse model," *Journal of Neuropathology & Experimental Neurology*, vol. 72, no. 3, pp. 178–185, 2013.
- [53] S. Baltan, S. P. Murphy, C. A. Danilov, A. Bachleda, and R. S. Morrison, "Histone deacetylase inhibitors preserve white matter structure and function during ischemia by conserving ATP and reducing excitotoxicity," *The Journal of Neuroscience*, vol. 31, no. 11, pp. 3990–3999, 2011.
- [54] B. Wang, X. Zhu, Y. Kim et al., "Histone deacetylase inhibition activates transcription factor Nrf2 and protects against cerebral ischemic damage," *Free Radical Biology & Medicine*, vol. 52, no. 5, pp. 928–936, 2012.
- [55] H. J. Kim, M. Rowe, M. Ren, J. S. Hong, P. S. Chen, and D. M. Chuang, "Histone deacetylase inhibitors exhibit anti-inflammatory and neuroprotective effects in a rat permanent ischemic model of stroke: multiple mechanisms of action," *The Journal of Pharmacology and Experimental Therapeutics*, vol. 321, no. 3, pp. 892–901, 2007.
- [56] K. B. Koronowski and M. A. Perez-Pinzon, "Sirt1 in cerebral ischemia," *Brain circulation*, vol. 1, no. 1, pp. 69–78, 2015.
- [57] A. K. Grewal, N. Singh, and T. G. Singh, "Effects of resveratrol postconditioning on cerebral ischemia in mice: role of the sirtuin-1 pathway," *Canadian Journal of Physiology and Pharmacology*, vol. 97, no. 11, pp. 1094–1101, 2019.
- [58] J. Chen, J. Zhang, N. F. Shaik et al., "The histone deacetylase inhibitor tubacin mitigates endothelial dysfunction by up-regulating the expression of endothelial nitric oxide synthase," *The Journal of Biological Chemistry*, vol. 294, no. 51, pp. 19565–19576, 2019.
- [59] H. Zhang, X. Li, Q. Zhang et al., "Role of histone deacetylase expression levels and activity in the inflammatory responses of patients with chronic hepatitis B," *Molecular Medicine Reports*, vol. 15, no. 5, pp. 2744–2752, 2017.
- [60] W. J. Tu, X. Dong, S. J. Zhao, D. G. Yang, and H. Chen, "Prognostic value of plasma neuroendocrine biomarkers in patients with acute ischaemic stroke," *Journal of Neuroendocrinology*, vol. 25, no. 9, pp. 771–778, 2013.
- [61] M. Göttlicher, S. Minucci, P. Zhu et al., "Valproic acid defines a novel class of HDAC inhibitors inducing differentiation of transformed cells," *The EMBO Journal*, vol. 20, no. 24, pp. 6969–6978, 2001.
- [62] C. Zhang, J. Zhu, J. Zhang et al., "Neuroprotective and anti-apoptotic effects of valproic acid on adult rat cerebral cortex through ERK and Akt signaling pathway at acute phase of traumatic brain injury," *Brain Research*, vol. 1555, pp. 1–9, 2014.

- [63] M. R. Silva, A. O. Correia, G. C. A. dos Santos et al., “Neuroprotective effects of valproic acid on brain ischemia are related to its HDAC and GSK3 inhibitions,” *Pharmacology Biochemistry and Behavior*, vol. 167, pp. 17–28, 2018.
- [64] R. Patnala, T. V. Arumugam, N. Gupta, and S. T. Dheen, “HDAC inhibitor sodium butyrate-mediated epigenetic regulation enhances neuroprotective function of microglia during ischemic stroke,” *Molecular Neurobiology*, vol. 54, no. 8, pp. 6391–6411, 2017.
- [65] X. Qi, T. Hosoi, Y. Okuma, M. Kaneko, and Y. Nomura, “Sodium 4-phenylbutyrate protects against cerebral ischemic injury,” *Molecular Pharmacology*, vol. 66, no. 4, pp. 899–908, 2004.
- [66] L. Su, D. Liang, S.-Y. Kuang, Q. Dong, X. Han, and Z. Wang, “Neuroprotective mechanism of TMP269, a selective class IIA histone deacetylase inhibitor, after cerebral ischemia/reperfusion injury,” *Neural Regeneration Research*, vol. 15, no. 2, pp. 277–284, 2020.
- [67] N. Narayan, I. H. Lee, R. Borenstein et al., “The NAD-dependent deacetylase SIRT2 is required for programmed necrosis,” *Nature*, vol. 492, no. 7428, pp. 199–204, 2012.
- [68] S. H. Kim, H. F. Lu, and C. C. Alano, “Neuronal Sirt3 protects against excitotoxic injury in mouse cortical neuron culture,” *PLoS One*, vol. 6, no. 3, article e14731, 2011.
- [69] Z. Wang, Y. Leng, J. Wang et al., “Tubastatin A, an HDAC6 inhibitor, alleviates stroke-induced brain infarction and functional deficits: potential roles of α -tubulin acetylation and FGF-21 up-regulation,” *Scientific Reports*, vol. 6, no. 1, 2016.
- [70] L. Wu, S. Zeng, Y. Cao et al., “Inhibition of HDAC4 attenuated JNK/c-Jun-dependent neuronal apoptosis and early brain injury following subarachnoid hemorrhage by transcriptionally suppressing MKK7,” *Frontiers in Cellular Neuroscience*, vol. 13, pp. 468–468, 2019.

Research Article

Peripheral Blood Occludin Level as a Biomarker for Perioperative Cerebral Edema in Patients with Brain Tumors

Shuhai Shi,¹ Jingli Cheng,² Chunyang Zhang,² Tao Liang,³ Yunxin Zhang,¹ Yongxing Sun,³ Ying Zhao,¹ Weili Li,⁴ and Baoguo Wang³

¹Department of Critical Care Medicine, Sanbo Brain Hospital, Capital Medical University, Beijing 100093, China

²Department of Neurosurgery, First Affiliated Hospital of Baotou Medical College, Baotou 014010, Inner Mongolia Autonomous Region, China

³Department of Anesthesiology, Sanbo Brain Hospital, Capital Medical University, Beijing 100093, China

⁴Department of Neurology, Xuanwu Hospital, Capital Medical University, Beijing 100053, China

Correspondence should be addressed to Baoguo Wang; wbgshnk@163.com

Received 13 June 2020; Revised 2 July 2020; Accepted 31 July 2020; Published 20 August 2020

Academic Editor: Wen-Jun Tu

Copyright © 2020 Shuhai Shi et al. This is an open access article distributed under the Creative Commons Attribution License, which permits unrestricted use, distribution, and reproduction in any medium, provided the original work is properly cited.

Objective. Cerebral edema is a common complication of brain tumors in the perioperative period. However, there is currently no reliable and convenient method to evaluate the extent of brain edema. The objective is to explore the effectiveness of serum occludin on predicting the extent of perioperative brain edema and outcome in patients with brain tumors. **Methods.** This prospective study enrolled 55 patients with brain tumors and 24 healthy controls in Sanbo Brain Hospital from June 2019 through November 2019. Serum occludin levels were measured preoperatively and on postoperative day 1. Peritumoral edema was assessed preoperatively using MRI. Pericavity brain edema on postoperative day 1 was evaluated using CT. **Results.** Compared with healthy controls, the serum occludin level was higher in patients with brain tumors both preoperatively and postoperatively ($P < 0.001$). The serum occludin level correlated positively with the degree of brain edema preoperatively ($r = 0.78$, $P < 0.001$) and postoperatively ($r = 0.59$, $P < 0.001$). At an optimal cutoff of 3.015 ng/mL, the preoperative serum occludin level discriminated between mild and severe preoperative brain edema with a sensitivity of 90.48% and specificity of 84.62%. At an optimal cutoff value of 3.033 ng/mL, the postoperative serum occludin level distinguished between mild and severe postoperative brain edema with a sensitivity of 97.30% and specificity of 55.56%. **Conclusions.** The serum occludin level is associated with cerebral edema and could potentially be used as a biomarker for perioperative cerebral edema. This trial is registered with ChiCTR1900023742.

1. Introduction

Damage to the blood-brain barrier (BBB) in patients with brain tumors can cause cerebral edema or hemorrhage. Brain edema, as a major factor that governs clinical management, is responsible for clinical symptoms such as neurological deficit and intracranial hypertension. The severity of perioperative brain edema and the occurrence of postoperative hemorrhage in patients with brain tumors are directly related to prognosis and risk of death [1]. Computed tomography (CT) and magnetic resonance imaging (MRI) can be used

to indirectly evaluate the extent of brain edema and hemorrhage in patients with brain tumors. However, these imaging techniques are inconvenient and time-consuming and so cannot be used to screen for rapid deteriorations in the postoperative condition of a patient in the intensive care unit (ICU). Therefore, it is vital that a reliable biomarker be identified that reflects the degree of cerebral edema and risk of cerebral hemorrhage in the perioperative period, as this will facilitate the prevention of and/or timely intervention for cerebral edema or hemorrhage after surgery for craniocerebral tumors.

The expressions of several proteins in brain tissue, including N-cadherin, β -catenin, aquaporin-4, delta-like protein-4, matrix metalloproteinase- (MMP) 9, and vascular endothelial growth factor, are associated with the occurrence of peritumoral brain edema (PTBE) [2–5]. However, few studies have examined the relationships between serum proteins and PTBE.

Tight junction proteins such as claudin-5 and occludin are key structural components of the BBB [6, 7]. Occludin and claudin-5 form tight junction protein structures that seal the gap between the endothelial cells of the BBB and thus are responsible for maintaining the integrity of the BBB [8]. Since occludin expression alone does not result in tight junction formation [9], it is likely that claudin-5 forms the primary structure of the tight junction with occludin acting as an additional supporting structure [10]. This may make occludin vulnerable to release into the bloodstream following damage to the BBB. PTBE formation is widely accepted to be vasogenic brain edema due to the damage of BBB. There is some evidence that decreased expressions of occludin and claudin-5 in brain tissue are related to PTBE [11, 12], suggesting that brain edema can arise if occludin and claudin-5 are lost from the BBB. Our recent studies have confirmed that degraded tight junction protein fragments are released into the blood and that their levels in the blood are closely related to the degree of BBB damage after cerebral ischemia [13, 14]. This suggests that occludin could potentially be used as a biomarker to evaluate damage to the BBB. However, no previous investigations have reported whether occludin is degraded and released into the bloodstream because of damage to the BBB by a brain tumor or brain surgery.

It is widely recognized that patients with brain tumors can exhibit damage to their BBB both before and after surgery. Therefore, we hypothesized that the occludin level in peripheral blood might serve as a biomarker for cerebral edema due to BBB damage in patients with brain tumors. To the best of our knowledge, there are currently no studies describing the association between peripheral blood occludin levels and the extent of PTBE or postoperative pericavity edema in patients with brain tumors. Therefore, the aim of the present study was to investigate the relationships between the serum occludin level and the extent of PTBE before surgery and the extent of pericavity brain edema after surgery in patients with brain tumors.

2. Material and Methods

2.1. Study Design and Participants. This prospective study enrolled consecutive patients with brain tumors scheduled for surgery at the Department of Neurosurgery, Sanbo Brain Hospital, Capital Medical University, between June 1st, 2019, and November 1st, 2019. A control group of healthy people was also enrolled at the Physical Examination Center, Sanbo Brain Hospital, during the same period. The inclusion criteria for patients with brain tumors were as follows: (1) primary brain tumor confirmed by imaging investigations such as CT and MRI, (2) met the indications for surgical treatment and scheduled to undergo surgery, (3) aged 18–

80 years old, (4) had not received radiotherapy or chemotherapy before surgery, and (5) provided informed consent for inclusion in the study. The exclusion criteria were other diseases that might lead to the destruction of tight junction proteins between vascular endothelial cells, including (1) severe hepatorenal disease, (2) severe gastrointestinal system disease, (3) peripheral vascular disease, and (4) autoimmune disease. The healthy people included as a control group were randomly selected from persons undergoing routine physical examinations at Sanbo Brain Hospital. Patients with craniopharyngioma or hypophysoma were treated at a dose of 250 mg methylprednisolone, and the other brain tumor patients received 5 mL/kg 20% mannitol intravenously for 3 days after operation. The study was approved by the Ethics Committee of Sanbo Brain Hospital, and all patients provided informed written consent for inclusion in the study.

2.2. Measurement of Serum Occludin Levels. Peripheral venous blood samples (4 mL) were obtained from patients with brain tumors at admission (i.e., preoperatively) and approximately 24 hours (range, 20–28 hours) after surgery. Blood samples from healthy subjects were taken during their visit to the physical examination center. Serum (100 μ L) was separated from each blood sample, and the level of occludin in the serum was measured using a commercially available enzyme-linked immunosorbent assay (ELISA) kit for human samples (Occludin: USCN, Wuhan, China).

2.3. Measurement of PTBE before Surgery. PTBE was evaluated by 1.5T MRI (Achieva 1.5T, Philips, Amsterdam, Netherlands) before surgery (Figures 1(a) and 1(b)). The imaging sequences used in this study included axial T2-weighted sequences, fluid-attenuated inversion recovery (FLAIR) sequences, and axial and coronal T1-weighted spin-echo sequences before and after intravenous injection of the contrast agent (gadopentetate dimeglumine; 0.1 mg/kg body weight). All images were analyzed digitally using PACS workstations. Enhanced T1-weighted images were used to determine the tumor boundary, and these maps were then compared with the respective T2-weighted images or FLAIR sequences. The degree of PTBE was determined by measuring the vertical distance from the outer edge of the maximal edema zone to the tumor boundary. PTBE was graded according to the Steinhoff classification [15] as follows: 0, no edema; I, PTBE limited to 2 cm; II, PTBE limited to half the hemisphere; and III, PTBE extending to more than half the hemisphere. For the analysis, mild edema was defined as Steinhoff grade 0 or I, and severe edema was defined as Steinhoff grade II or III. Determination of the Steinhoff grade was made independently by two clinicians who were deputy directors of imaging and had more than 5 years of work experience, and any disagreements were resolved by discussion.

2.4. Measurement of Pericavity Edema after Surgery. Pericavity brain edema was evaluated by CT (Brilliance 64, Philips) at approximately 24 hours (range, 20–28 hours) after surgery (Figures 1(c) and 1(d)). The degree of pericavity edema was measured as the vertical distance from the outer edge of the maximal edema zone to the cavity boundary

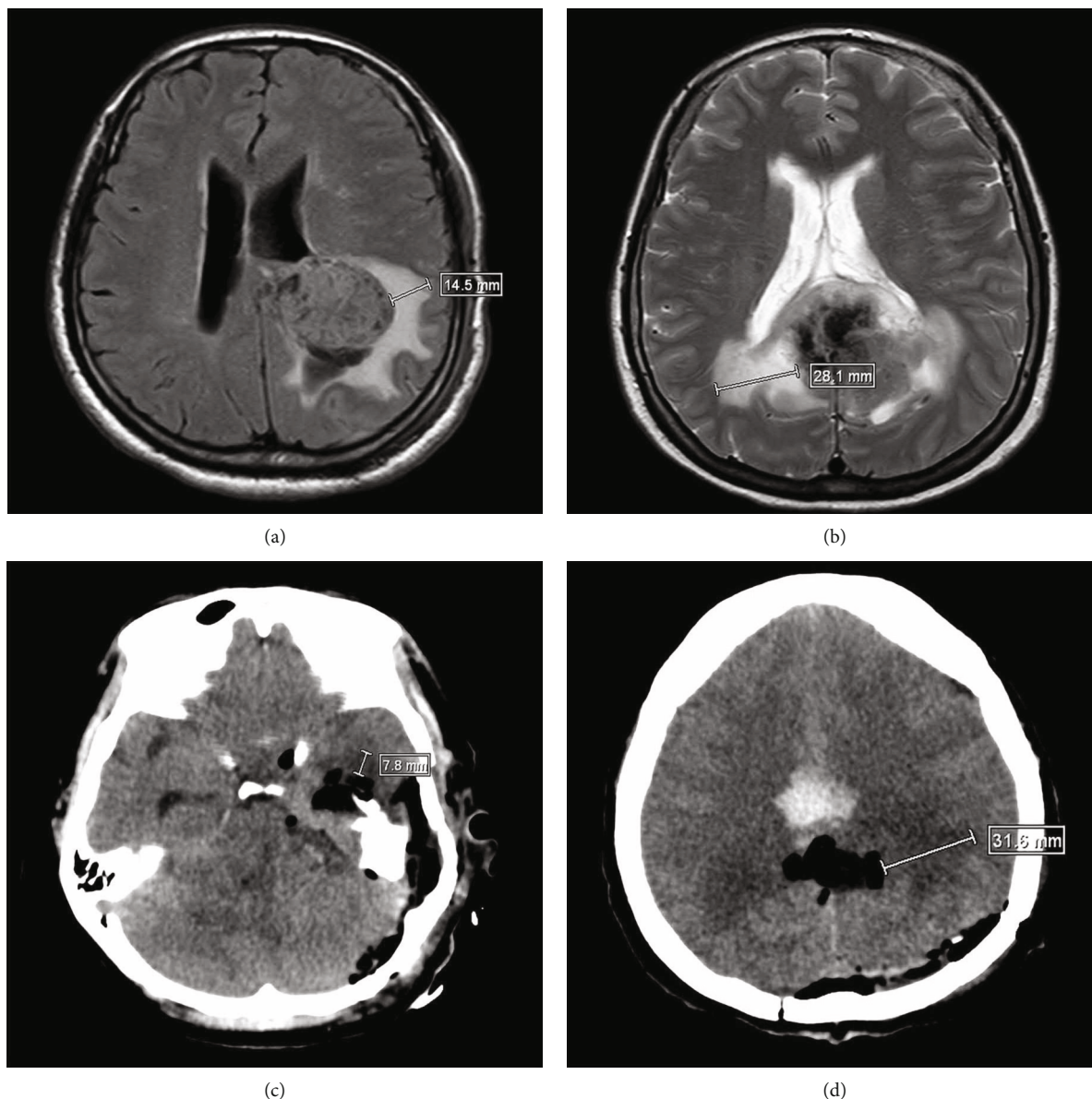


FIGURE 1: Evaluation of peritumoral brain edema (PTBE) and pericavity brain edema by magnetic resonance imaging (MRI) and computed tomography (CT), respectively. (a) MRI scan showing mild PTBE before surgery. (b) MRI scan showing severe PTBE before surgery. (c) CT scan showing mild brain edema around the cavity after surgery. (d) CT scan showing severe brain edema around the cavity after surgery.

after surgery. Evaluation of the degree of edema was the same as that for PTBE (*vide supra*).

2.5. Measurement of Neurological Function and Related Complications. To further analyze the relationships between the serum occludin level and the neurological function and related complications, the National Institutes of Health Stroke Scale (NIHSS) and Glasgow Coma Scale (GCS) were administered at admission and at around 24 hours (range, 20–28 hours) after surgery. Furthermore, information regarding the occurrence of intracranial hemorrhage was collected at approximately 24 hours (range, 20–28 hours) after surgery [16].

2.6. Statistical Analysis. The data were analyzed using SPSS 22.0 (IBM Corp., Armonk, NY, USA). All continuous data were confirmed to be normally distributed and so are presented as mean \pm standard deviation (SD). One-way analysis of variance was used to compare serum levels of occludin between groups. NIHSS and GCS scores were compared between groups using Student's *t*-test. Categorical data are presented as *n* (%) and were compared between groups using the chi-squared test or Fisher's exact test. The relationship between the extent of the brain edema (vertical distance from the outer edge of the maximal edema zone to the tumor/cavity boundary) and the serum occludin level was assessed by calculation of Pearson's correlation coefficient

TABLE 1: Baseline clinical characteristics of the study participants.

Characteristic	Patients with brain tumors ($n = 55$)	Healthy volunteers ($n = 24$)	P
Age (years)	47.42 ± 15.72	40.63 ± 14.42	0.074
Female	31 (56.4%)	13 (51.2%)	0.857
Tumor location			
Frontal lobe	15 (27.3%)	N/A	N/A
Temporal lobe	14 (25.5%)	N/A	N/A
Occipital lobe	6 (10.9%)	N/A	N/A
Parietal lobe	3 (5.5%)	N/A	N/A
Sella region	6 (10.9%)	N/A	N/A
Cerebellum	4 (7.3%)	N/A	N/A
Brain stem	5 (9.1%)	N/A	N/A
Basal ganglia	2 (3.6%)	N/A	N/A
Tumor pathology			
Glioma	22 (40.0%)	N/A	N/A
Meningioma	12 (21.8%)	N/A	N/A
Neurilemmoma	7 (12.7%)	N/A	N/A
Hypophysoma	4 (7.3%)	N/A	N/A
Hemangioma	4 (7.3%)	N/A	N/A
Germinoma	2 (3.6%)	N/A	N/A
Craniopharyngioma	2 (3.6%)	N/A	N/A
Chordoma	1 (1.8%)	N/A	N/A
Cholesteatoma	1 (1.8%)	N/A	N/A

Data are presented as mean ± standard deviation or n (%). N/A: not applicable.

(r). Receiver operating characteristic (ROC) curve analysis, with calculation of the area under the curve (AUC), was used to evaluate the ability of the serum occludin level to distinguish between mild and severe edema. The optical cutoff for the serum occludin level was established by calculation of the Youden index, and sensitivity and specificity values were determined. Statistical significance was defined as a two-tailed P value < 0.05.

3. Results

3.1. Baseline Clinical Characteristics of the Study Participants. A total of 55 patients with brain tumors and 24 healthy people were enrolled in this study. The group of patients with brain tumors and control group of healthy people exhibited no significant differences in mean age (47.42 ± 15.72 years vs. 40.63 ± 14.42 years) or gender (56.4% female vs. 51.2% female; Table 1). Additional clinical data for the patients with brain tumors are shown in Table 1.

3.2. Comparison of Serum Occludin Levels between Patients with Brain Tumors and Healthy Volunteers. There was no significant difference between the preoperative and postoperative serum occludin levels in patients with brain tumors. However, both the preoperative and postoperative serum occludin

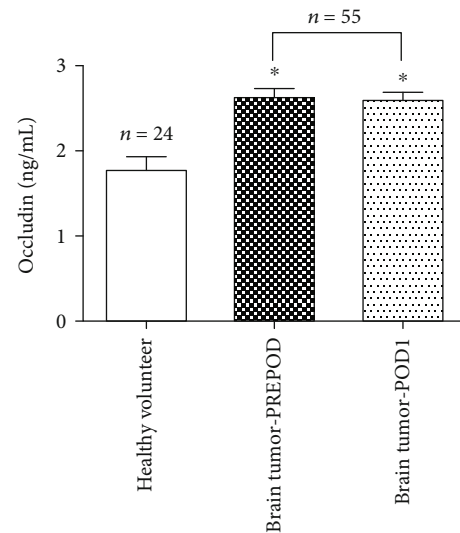


FIGURE 2: Comparison of serum occludin levels between patients with brain tumors and healthy volunteers. Compared with healthy volunteers ($n = 24$), serum occludin levels in patients with brain tumors ($n = 55$) were significantly higher both before surgery (Brain tumor-PREPOD) and 1 day after surgery (Brain tumor-POD1). Data are expressed as mean ± standard deviation. * $P < 0.05$ versus the healthy volunteer group.

levels in patients with brain tumors were significantly higher than the levels in healthy people (Figure 2). These results suggest that brain tumors may induce damage to the BBB, leading to the release of occludin into the bloodstream.

3.3. Analysis of the Relationship between the Preoperative Serum Occludin Level and the Extent of the Preoperative PTBE and Tumor Diameter. Pearson's correlation analysis revealed that the preoperative serum occludin level was significantly positively correlated with the extent of the preoperative PTBE as measured by the vertical distance from the outer edge of the maximal edema zone to the tumor boundary ($r = 0.78$, $P < 0.0001$; Figure 3(a)). Furthermore, the preoperative serum occludin level was also significantly correlated with the degree of preoperative PTBE as measured by the Steinhoff grade ($P < 0.05$ for all pairwise comparisons; Figure 3(b)). However, the preoperative serum occludin level was not significantly correlated with the diameter of the tumor ($r = 0.222$; $P = 0.103$; Figure 3(c)).

3.4. ROC Curve Analysis of the Ability of the Preoperative Serum Occludin Level to Predict the Severity of Preoperative PTBE. ROC curve analysis indicated that the preoperative serum occludin level showed excellent ability to distinguish between mild and severe PTBE, with an AUC value of 0.9002 (95% confidence interval, 0.8069–0.9934; $P < 0.0001$; Figure 3(d)). At an optimal cutoff value for the preoperative serum occludin level of 3.015 ng/mL, the sensitivity was 90.48% and the specificity was 84.62%. These results suggest that the preoperative serum occludin level could potentially be used to reflect the degree of PTBE before surgery.

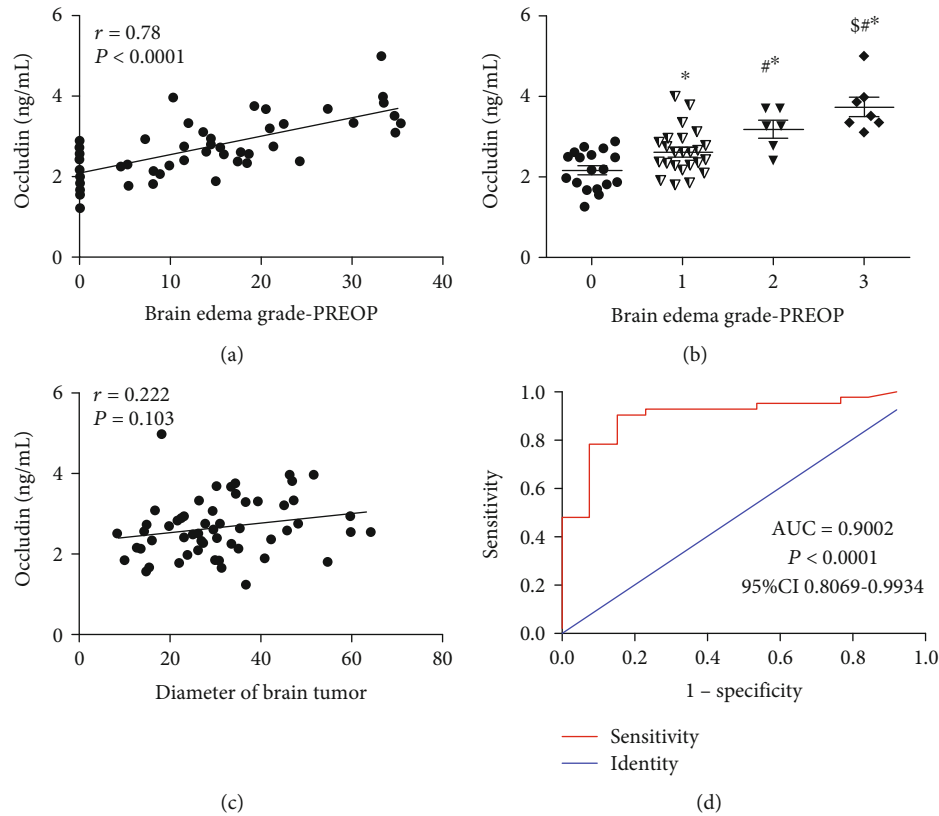


FIGURE 3: The relationship between the preoperative serum occludin level and the peritumoral brain edema (PTBE) before surgery. (a) Pearson's correlation analysis showing that the preoperative serum occludin level was significantly positively correlated with the extent of the preoperative PTBE as measured by the vertical distance from the outer edge of the maximal edema zone to the tumor boundary ($n = 55$). (b) Preoperative serum occludin levels for the various Steinhoff grades of PTBE. Data are presented as mean \pm standard deviation (grade 0, $n = 18$; grade I, $n = 24$; grade II, $n = 6$; and grade III, $n = 7$). * $P < 0.05$ vs. grade 0; $^{\#}P < 0.05$ vs. grade I; and $^{\$}P < 0.05$ versus grade II. (c) Pearson's correlation analysis showing that the preoperative serum occludin level was not significantly correlated with the tumor diameter. (d) Receiver operating characteristic curve for the ability of the serum occludin level to distinguish between mild and severe PTBE. AUC: area under the curve; CI: confidence interval.

3.5. *Analysis of the Relationship between the Postoperative Serum Occludin Level and the Extent of the Pericavity Edema and Tumor Diameter.* Pearson's correlation analysis indicated that the postoperative serum occludin level was significantly positively correlated with the extent of the postoperative pericavity edema as measured by the vertical distance from the outer edge of the maximal edema zone to the cavity boundary ($r = 0.590$, $P < 0.0001$; Figure 4(a)). Similarly, the postoperative serum occludin level was significantly related to the degree of the postoperative pericavity edema as measured by the Steinhoff grade ($P < 0.05$ for all pairwise comparisons; Figure 4(b)). The postoperative serum occludin level was not significantly correlated with the tumor diameter ($r = 0.104$, $P = 0.449$; Figure 4(c)).

3.6. *ROC Curve Analysis of the Ability of the Postoperative Serum Occludin Level to Predict the Severity of Postoperative Pericavity Edema.* ROC curve analysis demonstrated that the postoperative serum occludin level had good ability to discriminate between mild and severe pericavity edema, with an AUC value of 0.7763 (95% confidence interval, 0.6267–0.9258; $P < 0.0001$; Figure 4(d)). At an optimal cutoff value

for the postoperative serum occludin level of 3.033 ng/mL, the sensitivity was 97.30% and the specificity was 55.56%.

3.7. *Relationship between the Preoperative Serum Occludin Level and the Clinical Outcomes.* To examine whether the preoperative serum occludin level might be related to clinical outcomes, patients were divided into two groups according to the optimal cutoff value for the preoperative occludin level (3.015 ng/mL). Compared with patients with a preoperative serum occludin level < 3.015 ng/mL, those with an occludin level ≥ 3.015 ng/mL had a significantly higher NIHSS score at admission (3.60 ± 0.48 vs. 2.31 ± 0.42 ; $P < 0.001$; Figure 5(a)) and significantly higher incidence of severe PTBE at admission (65.3% vs. 15.2%; $P < 0.001$; Figure 5(b)) but similar GCS score at admission (14.47 ± 1.60 vs. 14.85 ± 0.70 ; $P = 0.219$; Figure 5(a)) and similar incidence of intracranial hemorrhage at 1 day after surgery (20.0% vs. 20.0%; $P = 1.000$; Figure 5(b)).

3.8. *Relationship between the Postoperative Serum Occludin Level and the Clinical Outcomes.* The relationship between the postoperative serum occludin level and the clinical outcomes was also assessed. Compared with patients with a

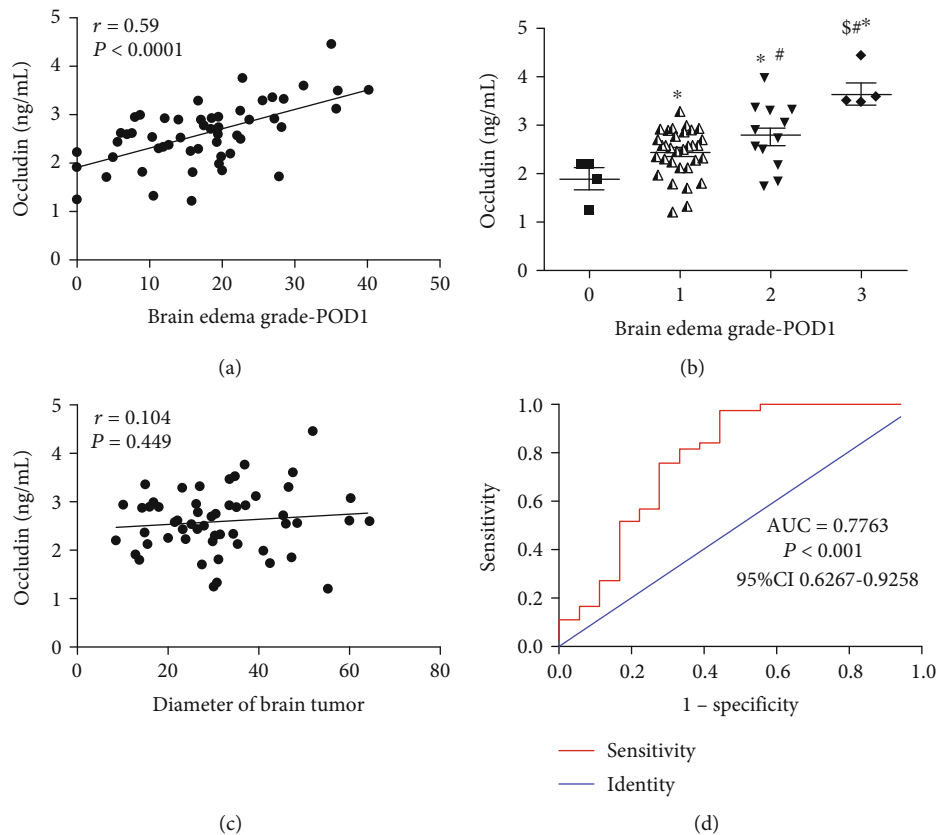


FIGURE 4: The relationship between the postoperative serum occludin level and the pericavity brain edema after surgery. (a) Pearson's correlation analysis indicating that the postoperative serum occludin level was significantly positively correlated with the extent of the postoperative pericavity edema as measured by the vertical distance from the outer edge of the maximal edema zone to the cavity boundary ($n = 55$). (b) Postoperative serum occludin levels for the various Steinhoff grades of pericavity edema. Data are presented as mean \pm standard deviation (grade 0, $n = 4$; grade I, $n = 33$; grade II, $n = 13$; and grade III, $n = 5$). * $P < 0.05$ vs. grade 0; # $P < 0.05$ vs. grade I; and \$ $P < 0.05$ versus grade II. (c) Pearson's correlation analysis indicating that the postoperative serum occludin level was not significantly correlated with the tumor diameter. (d) Receiver operating characteristic curve for the ability of the postoperative serum occludin level to distinguish between mild and severe pericavity edema. AUC: area under the curve; CI: confidence interval.

postoperative serum occludin level < 3.033 ng/mL (the optimal cutoff value), those with an occludin level ≥ 3.033 ng/mL had a significantly higher incidence of severe pericavity edema at 1 day after surgery (90.9% vs. 18.2%; $P < 0.001$) but a similar NIHSS score (6.82 ± 6.64 vs. 4.52 ± 6.66 ; $P = 0.306$), GCS score (13.55 ± 2.07 vs. 14.09 ± 1.09 ; $P = 0.407$), and incidence of intracranial hemorrhage (27.3% vs. 18.2%; $P = 0.800$) at 1 day after surgery (Figures 5(c) and 5(d)).

4. Discussion

The present report demonstrates that patients with brain tumors exhibit perioperative changes in the serum level of a protein that contributes to the structure and function of the BBB. Importantly, this study revealed a relationship between the serum level of occludin and the severity of brain edema in patients with brain tumors. Previous investigations have confirmed that peritumoral brain edema is vascular edema caused by damage to the BBB [17–19]. Occludin is an important component of tight junctions that constitute the BBB. Previous animal experiments have reported that cerebral ischemia results in the activation of MMP-2 and MMP-9 in

brain tissue, leading to the degradation of occludin and destruction of the BBB [20, 21]. In addition, a study of intracerebral hemorrhage has revealed that circulating tight junctions could be considered the potential biomarkers reflecting the integrity of the BBB in intracranial hemorrhage [22]. The present study found that the serum occludin level was increased in patients with brain tumors as compared with healthy controls, suggesting that tumor-induced damage to the BBB during the perioperative period may lead to the loss of occludin from the BBB. Furthermore, we demonstrated that the serum occludin level correlated well with the degree of brain edema and could be used to predict the severity of perioperative brain edema in patients with brain tumors.

We found that the serum level of occludin was significantly higher in patients with brain tumors, both before and after surgery, than in healthy people. These results suggest that damage to the BBB occurs in patients with brain tumors, leading to the release of degraded occludin fragments into the blood and thus an increase in the serum level of occludin. Notably, the patients included in this study had a broad range of tumor types located in different parts of the

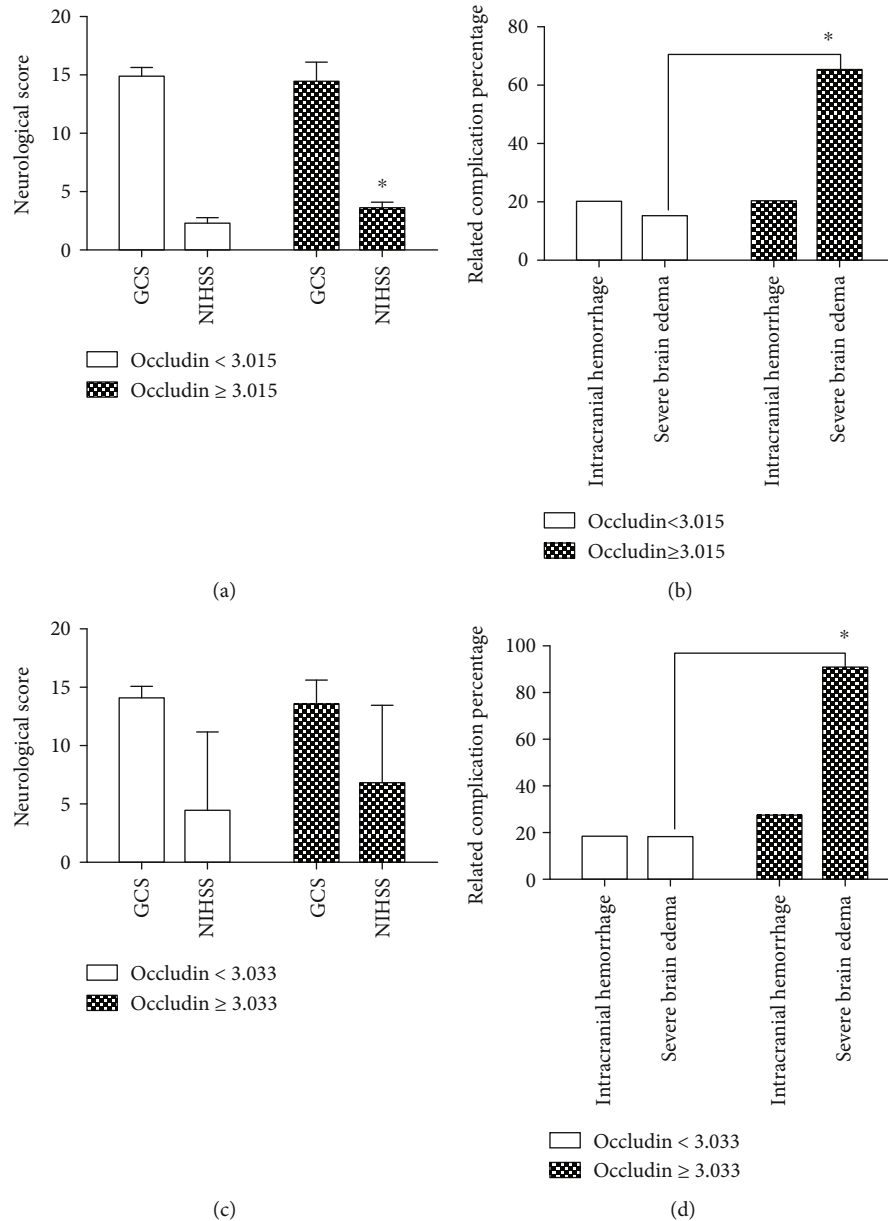


FIGURE 5: The relationship between the serum occludin level and the clinical outcomes in patients with brain tumors. (a) Comparison of National Institutes of Health Stroke Scale (NIHSS) and Glasgow Coma Scale (GCS) scores at admission between patients with a preoperative occludin level < 3.015 ng/mL ($n = 40$) and those with a preoperative occludin level ≥ 3.015 ng/mL ($n = 15$). (b) Comparison of the incidences of preoperative severe brain edema and intracranial hemorrhage between patients with a preoperative occludin level < 3.015 ng/mL ($n = 40$) and those with a preoperative occludin level ≥ 3.015 ng/mL ($n = 15$). (c) Comparison of NIHSS and GCS scores at 1 day after surgery between patients with a postoperative occludin level < 3.033 ng/mL ($n = 44$) and those with a postoperative occludin level ≥ 3.033 ng/mL ($n = 11$). (d) Comparison of the incidences of postoperative severe brain edema and intracranial hemorrhage between patients with a postoperative occludin level < 3.033 ng/mL ($n = 44$) and those with a postoperative occludin level ≥ 3.033 ng/mL ($n = 11$).

brain, suggesting that damage to the BBB and degradation/-release of occludin may be a common consequence of many different types of brain tumors, irrespective of the mechanism by which the BBB is damaged. Therefore, our study has identified a novel circulating biomarker that may be beneficial for the detection or/and monitoring of BBB damage during the perioperative period in patients with brain tumors. Of course, future studies will need to establish whether the performance of the serum occludin level as a

clinical biomarker varies between different pathological types of tumor.

Interestingly, we found a positive correlation between the peritumoral or pericavity brain edema and the level of serum occludin, with a higher occludin level associated with more severe brain edema. Notably, the serum occludin level was related only to the degree of brain edema and not to the size of the tumor. Vascular brain edema is a well-recognized feature of BBB damage, which likely leads to the release of

degraded occludin. Previous studies have shown that peritumoral brain edema is associated with a low content of occludin in the tumor [23, 24], but it has not been clarified whether the low content of occludin in the BBB of brain tumors is mainly due to degradation or low expression of occludin. Our observation of an elevated level of serum occludin suggests that a low content of occludin within a tumor may, at least in part, be due to the degradation of occludin rather than downregulated expression. There is also some evidence that matrix metalloproteinases (MMPs) are considered to be the key to mediate the opening of the blood-brain barrier [25] and highly expressed in brain tumors which can be activated by the upregulation of the beta-catenin pathway [26]. They may play an important role in the destruction of the blood-brain barrier. Further studies are needed to clarify the mechanisms underlying BBB damage and alterations in brain tumor levels of occludin.

Depending on the type of the brain tumor, the development of brain edema can involve a variety of factors including glioma cells, vascular endothelial cells, neuroglial cells, microglial cells [27, 28], and cyclooxygenase-2 [29]. Our study found that the serum occludin level correlated well with the grade of brain edema, suggesting that damage to occludin in the BBB may be a common molecular mechanism underlying the development of brain edema in patients with brain tumors. Some studies of glioma have shown that MMP expression or activation is related to the downregulation of occludin in the BBB, which leads to destruction of the BBB [30, 31]. It is possible that MMP activation may be a major mechanism by which degradation of occludin and damage to the BBB occur in patients with brain tumors. However, further research is needed to clarify the relevant molecular mechanisms in humans.

This study utilized ROC curve analysis to evaluate the ability of the preoperative and postoperative serum occludin levels to distinguish between mild and severe edema. The preoperative and postoperative serum occludin levels showed excellent (AUC value of 0.9002) and good (AUC value of 0.7763) discriminatory ability, respectively. At an optimal cutoff value of 3.015 ng/mL, the preoperative serum occludin level discriminated between mild and severe preoperative brain edema with a high sensitivity (90.48%) and specificity (84.62%). At an optimal cutoff value of 3.033 ng/mL, the postoperative serum occludin level also distinguished between mild and severe postoperative brain edema with a high sensitivity (97.30%), although the specificity was somewhat lower (55.56%). Taken together, the findings of the ROC curve analysis suggest that the serum occludin level has the potential to be a novel biomarker for perioperative brain edema in patients with brain tumors.

Brain edema may be an important factor affecting the neurological function of patients with brain tumors. This study found that patients with a high serum occludin level before surgery also had a higher preoperative NIHSS score, which may be related to more severe damage to the BBB. However, although the group of patients with elevated serum occludin levels after surgery had more severe brain edema, their postoperative NIHSS score did not differ from that for patients with lower occludin levels. This apparent discrep-

ancy may be due to the neurological functions of these patients being more affected by other surgery-related factors. We also found no difference in the incidence of postoperative cerebral hemorrhage between patients with high and low preoperative or postoperative levels of occludin. This latter finding suggests that postoperative acute cerebral hemorrhage may be primarily related to surgical factors (such as damage to microvessels or incomplete hemostasis) rather than BBB injury.

This study has some limitations. First, the sample size was not large, and an extensive range of tumor pathological types was included. Further large-scale clinical studies are needed to validate our results and perform subgroup analyses based on different brain tumor types. Second, we did not perform long-term follow-up to evaluate the prognosis of the patients and explore whether outcomes were related to the serum occludin level.

5. Conclusion

The perioperative serum occludin level is associated with the severity of peritumoral/pericavity edema in patients with brain tumors. The serum occludin level could potentially be used as a biomarker for perioperative cerebral edema in patients with brain tumors. Further large-scale clinical studies are needed to validate our results and perform subgroup analyses based on different brain tumor types.

Data Availability

The results of our study supporting the findings are included within this paper. In order to protect patient privacy, the personal data supporting the findings of this study are restricted by the Ethics Committee of Sanbo Brain Hospital, Capital Medical University. Data are available to researchers who meet the criteria for access to confidential data from the corresponding author.

Conflicts of Interest

The authors declare that there are no conflicts of interest regarding the publication of this article.

Acknowledgments

This work was supported by the National Key Basic Research Program (2013CB531900).

References

- [1] K. D. Kochanek, J. Xu, S. L. Murphy, A. M. Minino, and H. C. Kung, "Deaths: final data for 2009," *National Vital Statistics Reports*, vol. 60, no. 3, pp. 1–116, 2011.
- [2] R. Rutkowski, R. Chrzanowski, M. Trwoga et al., "Expression of N-cadherin and β -catenin in human meningioma in correlation with peritumoral edema," *International Journal of Neuroscience*, vol. 128, no. 9, pp. 805–810, 2018.
- [3] M. Gawlitza, E. Fiedler, S. Schob, K. T. Hoffmann, and A. Surov, "Peritumoral brain edema in meningiomas depends on aquaporin-4 expression and not on tumor grade, tumor

- volume, cell count, or Ki-67 labeling index,” *Molecular Imaging and Biology*, vol. 19, no. 2, pp. 298–304, 2017.
- [4] J. Reszec, A. Hermanowicz, R. Rutkowski, G. Turek, Z. Mariak, and L. Chyczewski, “Expression of MMP-9 and VEGF in meningiomas and their correlation with peritumoral brain edema,” *BioMed Research International*, vol. 2015, Article ID 646853, 8 pages, 2015.
 - [5] X. X. Qiu, C. H. Wang, Z. X. Lin et al., “Correlation of high delta-like ligand 4 expression with peritumoral brain edema and its prediction of poor prognosis in patients with primary high-grade gliomas,” *Journal of Neurosurgery*, vol. 123, no. 6, pp. 1578–1585, 2015.
 - [6] B. T. Hawkins and T. P. Davis, “The blood-brain barrier/neurovascular unit in health and disease,” *Pharmacological Reviews*, vol. 57, no. 2, pp. 173–185, 2005.
 - [7] Y. Yang, J. F. Thompson, S. Taheri et al., “Early inhibition of MMP activity in ischemic rat brain promotes expression of tight junction proteins and angiogenesis during recovery,” *Journal of Cerebral Blood Flow and Metabolism*, vol. 33, no. 7, pp. 1104–1114, 2013.
 - [8] E. E. Benarroch, “Blood-brain barrier: recent developments and clinical correlations,” *Neurology*, vol. 78, no. 16, pp. 1268–1276, 2012.
 - [9] M. Yamamoto, S. H. Ramirez, S. Sato et al., “Phosphorylation of claudin-5 and occludin by rho kinase in brain endothelial cells,” *American Journal of Pathology*, vol. 172, no. 2, pp. 521–533, 2008.
 - [10] Y. Persidsky, S. H. Ramirez, J. Haorah, and G. D. Kanmogne, “Blood-brain barrier: structural components and function under physiologic and pathologic conditions,” *Journal of Neuroimmune Pharmacology*, vol. 1, no. 3, pp. 223–236, 2006.
 - [11] M. C. Papadopoulos, S. Saadoun, D. K. Binder, G. T. Manley, S. Krishna, and A. S. Verkman, “Molecular mechanisms of brain tumor edema,” *Neuroscience*, vol. 129, no. 4, pp. 1011–1020, 2004.
 - [12] W. Wang, W. L. Dentler, and R. T. Borchardt, “VEGF increases BMEC monolayer permeability by affecting occludin expression and tight junction assembly,” *American Journal of Physiology. Heart and Circulatory Physiology*, vol. 280, no. 1, pp. H434–H440, 2001.
 - [13] R. Pan, K. Yu, T. Weatherwax, H. Zheng, W. Liu, and K. J. Liu, “Blood occludin level as a potential biomarker for early blood brain barrier damage following ischemic stroke,” *Scientific Reports*, vol. 7, no. 1, p. 40331, 2017.
 - [14] S. Shi, Z. Qi, Q. Ma et al., “Normobaric hyperoxia reduces blood occludin fragments in rats and patients with acute ischemic stroke,” *Stroke*, vol. 48, no. 10, pp. 2848–2854, 2017.
 - [15] S. Jung, K. S. Moon, S. T. Kim et al., “Increased expression of intracystic matrix metalloproteinases in brain tumors: relationship to the pathogenesis of brain tumor-associated cysts and peritumoral edema,” *Journal of Clinical Neuroscience*, vol. 14, no. 12, pp. 1192–1198, 2007.
 - [16] Y. Hu, R. Meng, X. Zhang et al., “Serum neuron specific enolase may be a marker to predict the severity and outcome of cerebral venous thrombosis,” *Journal of Neurology*, vol. 265, no. 1, pp. 46–51, 2018.
 - [17] Y. Doi, M. Kanagawa, Y. Maya et al., “Evaluation of trans-1-amino-3-18F-fluorocyclobutanecarboxylic acid accumulation in low-grade glioma in chemically induced rat models: PET and autoradiography compared with morphological images and histopathological findings,” *Nuclear Medicine and Biology*, vol. 42, no. 8, pp. 664–672, 2015.
 - [18] L. G. Dubois, L. Campanati, C. Righy et al., “Gliomas and the vascular fragility of the blood brain barrier,” *Frontiers in Cellular Neuroscience*, vol. 8, p. 418, 2014.
 - [19] E. Harford-Wright, K. M. Lewis, M. N. Ghabriel, and R. Vink, “Treatment with the NK1 antagonist emend reduces blood brain barrier dysfunction and edema formation in an experimental model of brain tumors,” *PLoS One*, vol. 9, no. 5, article e97002, 2014.
 - [20] J. Liu, X. Jin, K. J. Liu, and W. Liu, “Matrix metalloproteinase-2-mediated occludin degradation and caveolin-1-mediated claudin-5 redistribution contribute to blood-brain barrier damage in early ischemic stroke stage,” *Journal of Neuroscience*, vol. 32, no. 9, pp. 3044–3057, 2012.
 - [21] W. Liu, J. Hendren, X. J. Qin, J. Shen, and K. J. Liu, “Normobaric hyperoxia attenuates early blood-brain barrier disruption by inhibiting MMP-9-mediated occludin degradation in focal cerebral ischemia,” *Journal of Neurochemistry*, vol. 108, no. 3, pp. 811–820, 2009.
 - [22] X. Jiao, P. He, Y. Li et al., “The role of circulating tight junction proteins in evaluating blood brain barrier disruption following intracranial hemorrhage,” *Disease Markers*, vol. 2015, Article ID 860120, 12 pages, 2015.
 - [23] M. W. Park, C. H. Kim, J. H. Cheong, K. H. Bak, J. M. Kim, and S. J. Oh, “Occludin expression in brain tumors and its relevance to peritumoral edema and survival,” *Cancer Research and Treatment*, vol. 38, no. 3, pp. 139–143, 2006.
 - [24] R. Murayi and P. Chittiboana, “Glucocorticoids in the management of peritumoral brain edema: a review of molecular mechanisms,” *Child’s Nervous System*, vol. 32, no. 12, pp. 2293–2302, 2016.
 - [25] M. Castellazzi, T. Bellini, A. Trentini et al., “Serum gelatinases levels in multiple sclerosis patients during 21 months of natalizumab therapy,” *Disease Markers*, vol. 2016, Article ID 8434209, 7 pages, 2016.
 - [26] C. Martelli, R. Serra, I. Inserra et al., “Investigating the protein signature of adamantinomatous craniopharyngioma pediatric brain tumor tissue: towards the comprehension of its aggressive behavior,” *Disease Markers*, vol. 2019, Article ID 3609789, 18 pages, 2019.
 - [27] D. C. Davies, “Blood-brain barrier breakdown in septic encephalopathy and brain tumours,” *Journal of Anatomy*, vol. 200, no. 6, pp. 639–646, 2002.
 - [28] D. Brandsma, L. Stalpers, W. Taal, P. Sminia, and M. J. van den Bent, “Clinical features, mechanisms, and management of pseudoprogression in malignant gliomas,” *The Lancet Oncology*, vol. 9, no. 5, pp. 453–461, 2008.
 - [29] B. Badie, J. M. Schartner, A. R. Hagar et al., “Microglia cyclooxygenase-2 activity in experimental gliomas: possible role in cerebral edema formation,” *Clinical Cancer Research*, vol. 9, no. 2, pp. 872–877, 2003.
 - [30] X. Liu, P. Su, S. Meng et al., “Role of matrix metalloproteinase-2/9 (MMP2/9) in lead-induced changes in an in vitro blood-brain barrier model,” *International Journal of Biological Sciences*, vol. 13, no. 11, pp. 1351–1360, 2017.
 - [31] H. Cai, Y. Xue, Z. Li et al., “Roundabout4 suppresses glioma-induced endothelial cell proliferation, migration and tube formation in vitro by inhibiting VEGF2-mediated PI3K/AKT and FAK signaling pathways,” *Cellular Physiology and Biochemistry*, vol. 35, no. 5, pp. 1689–1705, 2015.

Research Article

Association of Serum FAM19A5 with Cognitive Impairment in Vascular Dementia

Juan Li,¹ Shoulin Li,² Yihong Song,¹ Wei Zhou,² Xiaohao Zhu,² Suo Xu,² Yihong Ma,³ and Chunlin Zhu¹ 

¹Department of Neurology, The First People's Hospital of Lianyungang/ Department of Neurology, The First Affiliated Hospital of Kangda College of Nanjing Medical University, Lianyungang, Jiangsu Province 222000, China

²Department of Emergency Medicine, The First People's Hospital of Lianyungang/ Department of Neurology, The First Affiliated Hospital of Kangda College of Nanjing Medical University, Lianyungang, Jiangsu Province 222000, China

³Department of Neurology, Graduate School of Medical Sciences, Kumamoto University, Kumamoto 860-8556, Japan

Correspondence should be addressed to Chunlin Zhu; zhuchunlin_njmu@163.com

Received 10 June 2020; Revised 15 July 2020; Accepted 20 July 2020; Published 3 August 2020

Academic Editor: Wen-Jun Tu

Copyright © 2020 Juan Li et al. This is an open access article distributed under the Creative Commons Attribution License, which permits unrestricted use, distribution, and reproduction in any medium, provided the original work is properly cited.

Objective. Family with sequence similarity 19 member A5 (FAM19A5), a novel chemokine-like peptide, is a secreted protein mainly expressed in the brain. FAM19A5 was recently found to be involved in a variety of neurological diseases; however, its correlation with vascular dementia (VaD) remains unclear. The aim of the study is to explore the association between serum FAM19A5 and cognitive impairment in subjects with VaD. **Method.** 136 VaD subjects and 81 normal controls were recruited in the study. Their demographic and clinical baseline data were collected on admission. All subjects received Mini-Mental State Examination (MMSE) evaluation, which was used to test their cognitive functions. A sandwich enzyme-linked immunosorbent assay (ELISA) was applied to detect the serum levels of FAM19A5. **Results.** No significant differences were found between the two groups regarding the demographic and clinical baseline data ($p > 0.05$). The serum FAM19A5 levels were significantly higher compared to normal controls ($p < 0.001$). The Spearman correlation analysis indicated that serum FAM19A5 levels and MMSE scores have a significant negative correlation in VaD patients ($r = -0.414, < 0.001$). Further multiple regression analysis indicated that serum FAM19A5 levels were independent risk predictors for cognitive functions in VaD ($\beta = 0.419, p = 0.031$). **Conclusion.** The serum FAM19A5 level of VaD patients is significantly increased, which may serve as a biomarker to predict cognitive function of VaD.

1. Introduction

Vascular dementia (VaD) is defined as a syndrome with different degrees of cognitive function and memory loss, which may range from mild deficits to severe dementia attributed to impaired blood flow to the brain [1, 2]. VaD is the second commonest subtype of dementia after Alzheimer's disease (AD) and has gained more and more attention in recent years [3, 4]. There are no less than 50 million people suffering from dementia globally; this number is predicted to have a three-fold increase by 2050 [5, 6]. Growing with age, the risk of VaD almost doubled every 3–5 years [7]. With the increase in human life expectancy and the advent of aging, VaD has emerged as one of the leading health problems in society [8]. Though much progress has been made over the past

years, the pathogenesis underlying VaD is still not fully understood, and there are also no effective drugs or other licensed treatments for VaD.

The family with sequence similarity 19 (FAM19A5), first discovered in 2004, was also named TAF5. FAM19A5 and a member of the CC-chemokine family (MIP-1 α) were predicted to be distant relatives. Thus, FAM19A5 has recently been described as a novel chemokine-like peptide [9]. As a secretory protein, FAM19A5 is mainly expressed in some specific regions of the brain and adipose tissues with very low expression in other peripheral organs [10]. The FAM19A genes encode more than 100 amino acid proteins at fixed positions characterized by conserved cysteine residues, which are postulated to function as brain-specific chemokines to regulating immune and nervous cells [11].

Though the FAM19A5 protein has been considered to be related to a variety of neurological diseases, little data about its functions in VaD is available. Therefore, the purpose of our study was to explore the relationship between serum FAM19A5 levels and the cognitive function of VaD patients. If the relationship between FAM19A5 and VaD is confirmed, it will have important scientific and clinical implications.

2. Materials and Methods

2.1. Subjects. Eventually, 136 VaD subjects and 81 normal controls were recruited from the Department of Neurology, The First People's Hospital of Lianyungang/Department of Neurology, The First Affiliated Hospital of Kangda College of Nanjing Medical University. The diagnosis of VaD was on the basis of DSM-V and NINDS-AIREN (National Institute for Neurological Disorders and Stroke, NINDS-AIREN) by attending physician of neurology [12, 13]. Exclusion criteria for recruitment in the study were as follows: [1] subjects suffering from acute cerebral infarction or cerebral embolism; [2] subjects with mental disorders or other types of dementia such as AD; [3] subject with autoimmune disease or infectious disease; [4] subjects with brain trauma or alcohol and drug abuse; and [5] subject has a history of cancer or other serious organic diseases. All the subjects' demographic and clinical baseline information including age, gender, education levels, blood pressure, body mass index (BMI), blood glucose, and lipid index were collected and recorded. The research was authorized by the Ethics Committee of The First People's Hospital of Lianyungang/The First Affiliated Hospital of Kangda College of Nanjing Medical University. The procedures of our study were performed according to the Helsinki declaration. The written approval consents were signed before the study.

2.2. Measurement of Serum FAM19A5 Levels. All subjects were fasted for more than 8 hours, and blood samples were collected via the cubital vein the morning after admission. All blood samples were centrifuged at 1200g for 15 minutes and subjected to the determination of serum FAM19A5 levels. Serum FAM19A5 levels of all subjects were tested by a sandwich enzyme-linked immunosorbent assay (ELISA) kits (ProteinTech Group, Wuhan, China) as described previously [14, 15]. The other biochemical parameters were tested using an automatic blood cell analyzer (Hitachi, Tokyo, Japan).

2.3. Cognitive Function Testing. Mini-Mental State Examination (MMSE) is a widely used cognitive evaluation tool in the world with 100% sensitivity and 71.4 specificity [16, 17]. The highest score on the MMSE scale is 30, mainly evaluating orientation, writing, registration, visual construction, recording, and other items related to cognitive function. Cognitive impairment is defined as a score of less than 24 by the investigators, who were blinded to the subjects' baseline clinical characteristics [18].

2.4. Data Analysis. Quantitative variables were expressed as mean \pm SD or percentage. The independent two-sample *t* test was used to compare the differences between continuous var-

TABLE 1: Baseline characteristics and serum FAM19A5 levels.

	VaD (<i>n</i> = 136)	NC (<i>n</i> = 81)	<i>p</i>
Age, years	69.8 \pm 7.1	70.5 \pm 6.9	0.479
Male, <i>n</i> (%)	77 (56.7)	47 (58.0)	0.761
Education, years	7.2 \pm 1.9	7.4 \pm 2.2	0.481
BMI, kg/m [2]	24.8 \pm 1.7	24.6 \pm 1.5	0.383
SBP, mmHg	145.2 \pm 10.4	143.9 \pm 9.6	0.361
DBP, mmHg	93.3 \pm 7.2	92.8 \pm 7.5	0.627
FBG, mmol/L	6.38 \pm 0.72	6.41 \pm 0.81	0.777
HbA1c, mmol/L	6.36 \pm 0.70	6.38 \pm 0.77	0.845
TC, mmol/L	4.47 \pm 0.65	4.52 \pm 0.62	0.578
HDL-C, mmol/L	1.28 \pm 0.16	1.25 \pm 0.13	0.154
LDL-C, mmol/L	2.73 \pm 0.21	2.69 \pm 0.26	0.216
TG, mmol/L	1.64 \pm 0.20	1.61 \pm 0.24	0.323
FAM19A5, pg/mL	186.3 \pm 17.9	103.2 \pm 11.6	<0.001
MMSE	21.8 \pm 2.1	27.0 \pm 0.9	<0.001

VaD: vascular dementia; NC: normal controls; SBP: systolic blood pressure; DBP: diastolic blood pressure; BMI: body mass index; FBG: fasting blood glucose; HbA1c: hemoglobin A1c; TC: total cholesterol; HDL-C: high-density lipoprotein cholesterol; LDL-C: low-density lipoprotein cholesterol; TG: triglycerides; FAM19A5: family with sequence similarity 19 member A5; MMSE: Mini-Mental State Examination.

iables conforming to normal distribution. The chi-square test was used for categorical variables. The Spearman correlation analysis was used to analyze the relationship between demographic and clinical characteristics and the cognitive function of VaD patients. Multivariate linear regression analysis determined the predictive value of demographic and clinical characteristics for the cognitive function of VaD patients. A two-tailed *p* < 0.05 was considered statistically significant. The SPSS 23.0 statistical software (SPSS Inc., IL, USA) was used to analyze the data.

3. Results

3.1. Demographic and Clinical Baseline Characteristics. A total of 196 patients presented to the Neurology department at the Lianyungang First People's Hospital for VaD between March 2017 and March 2020. 136 of them and 81 normal controls were found to fulfill the criteria for further analysis. The demographic and clinical baseline data of VaD subjects and normal controls are shown in Table 1. The two groups did not have significant difference in age, gender, educational, SBP, DBP, BMI, FBG, HbA1c, TC, HDL-C, LDL-C, or TG (*p* > 0.05). As shown in Figure 1, there was a significant difference between serum FAM19A5 levels and MMSE scores (*p* < 0.001).

3.2. Spearman's Correlation Analysis. Spearman's correlation analysis identified the correlation between demographic and clinical characteristics and MMSE scores, and the results are shown in Table 2. Spearman's correlation analysis showed that the levels of serum FAM19A5 were negatively correlated with MMSE scores in VaD patients, and the correlation was

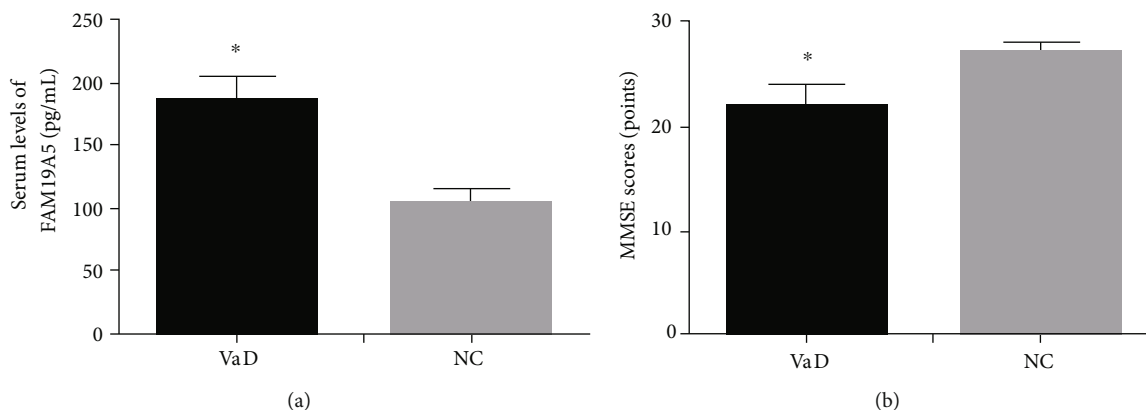


FIGURE 1: Serum levels of FAM19A5 and MMSE scores in VaD and NC. (a) Serum levels of FAM19A5. (b) MMSE scores. Compared with NC, $*p < 0.001$. VaD: vascular dementia; NC: normal controls.

TABLE 2: Spearman's correlation analysis of MMSE scores and various parameters in VaD patients.

	MMSE	Scores
	r	p
FAM19A5, pg/mL	-0.424	<0.001

VaD: vascular dementia; FAM19A5: family with sequence similarity 19 member A5; MMSE: Mini-Mental State Examination.

significantly ($r = -0.424$, $p < 0.05$). However, there was no significant correlation in our current study among serum FAM19A5 levels and demographic and statistical characteristics of VaD patients such as age, gender, educational, SBP, DBP, BMI, FBG, HbA1c, TC, HDL-C, LDL-C, and TG ($p > 0.05$).

3.3. Multiple Regression Analysis. The results of multiple linear regression analysis among demographic and clinical baseline characteristics, MMSE scores, and serum FAM19A5 levels of VaD subjects are shown in Table 3. The results of multiple linear regression analysis demonstrated that serum FAM19A5 level is an independent predictive risk marker for cognitive function in VaD patients. After adjusting for demographic and clinical baseline characteristics such as age, gender, educational, SBP, DBP, BMI, FBG, HbA1c, TC, HDL-C, LDL-C, and TG, the independent value of serum FAM19A5 level for VaD patients' cognitive function is still significant ($\beta = 0.419$, $p = 0.031$).

4. Discussion

This study is investigating the association between cognitive functions and FAM19A5 levels in patient and control groups. We found that patients with VaD had higher serum FAM19A5 levels and lower MMSE scores than normal controls. We also found that in VaD patients, serum levels of FAM19A5 were significantly negatively correlated with MMSE scores. Serum FAM19A5 levels were found to be related to cognitive functions in VaD, whereas other demographic and statistical characteristics were not related to cognitive functions in VaD. This association was independent of the interference factors of age, gender, educational, SBP,

TABLE 3: Regression analyses between MMSE and characteristics of VaD patients.

	Standardized	Coefficients	95% CI for B	
	β	p	Lower bound	Upper bound
FAM19A5	0.419	0.031	1.239	1.708

MMSE: Mini-Mental State Examination; VaD: vascular dementia; FAM19A5: family with sequence similarity 19 member A5.

DBP, BMI, FBG, HbA1c, TC, HDL-C, LDL-C, and TG. As far as we know, we demonstrated for the first time that serum FAM19A5 level was an independent risk factor for cognitive impairment in VaD patients.

FAM19A5 is one of the five highly homologous family members of family with sequence similarity 19 (FAM19A) [19]. The secreted proteins discovered by a new database search strategy are mainly expressed in the adipose tissue and central nervous system [20]. According to reports, FAM19A5 is mainly expressed in the hippocampus, hypothalamic paranucleus, and suprabranial nucleus in rats, while in mice, the main expression site is in the hippocampus [21, 22]. Kong and his team first proved that FAM19A5 is a secreted protein, and the 43 amino acids starting at the N-terminus are its main signal peptides [11]. Although FAM19A5 has been discovered for more than ten years, its function has not been fully elucidated.

Recently, FAM19A5 has been found to be associated with a variety of diseases and disorders. Han and his colleagues explore the significance of a novel chemokine-like peptide (FAM19A5), which was associated with the presence of depressive symptoms and might be a biomarker of neuroinflammation and neurodegeneration for major depressive disorder [23]. In addition, researchers from Korea University confirmed that serum FAM19A5 may be a novel biomarker for cardiovascular metabolic diseases, which was significantly correlated to various human metabolic and vascular risk factors [9]. Proteomics research demonstrates that FAM19A5 has a potential to serve as a novel biomarker for differentiating cholangiocarcinoma from benign biliary tract diseases [24]. In parallel, a Chinese study showed that FAM19A5 had significant effects on gastric cancer progression and

may serve as a potential therapeutic target for gastric cancer [25]. However, the correlation between FAM19A5 and VaD has not been reported so far.

Emerging evidence has indicated that FAM19A family is involved in the pathological mechanism of cognition. FAM19A2 knockout mice exhibited decline in short-term and long-term memory via novel object recognition test and decline in spatial learning and memory via the Morris water maze (MWM) test [26, 27]. However, FAM19A1 knockout mice only exhibited reduced anxiety and sensitivity to pain, and spatial learning and exploration are preserved [28, 29]. Interestingly, recent studies have shown that FAM19A5 is involved in the development of the nervous system. A Korean study shows FAM19A5 plays a vital role at an early stage of nervous system development, and its functions are critical to the generation of stem cells in the adult brain such as neural stem cells and oligodendrocyte precursor cells [22]. Not only in animal experiments, the correlation between FAM19A5 and neurodevelopment in clinical studies has also been found [30, 31]. More recent research shows that selective overexpression of FAM19A5 in the mouse hippocampus can alleviate chronic stress-related spatial learning and memory impairment [32]. All the above studies indicate that the FAM19A family including FAM19A5 plays an important role in cognition. However, the level of FAM19A5 in different neurological diseases is fluctuating. The mechanism by which FAM19A5 participates in cognitive impairment is complex and needs further elucidation.

The current study has some limitations. First of all, this study has a relatively small sample size. Secondly, the subjects are all Chinese, and the results may not apply to other ethnic groups. Thirdly, we did not investigate the FAM19A5 levels in other types of dementias such as Alzheimer's dementia and hydrocephalus with normal intracranial pressure. Thus, the correlation between serum FAM19A5 levels and cognitive impairment may not be unique to VaD. At last, we just did a cross-sectional study of serum FAM19A5 levels and did not follow up longitudinally. However, the advantage of our study is that this is the first report of the association between FAM19A5 levels and cognitive impairment in VaD.

5. Conclusions

In short, the main findings of our research are that VaD subjects have a significantly lower serum level of FAM19A5 compared to normal controls. Our study revealed that serum FAM19A5 plays an important role for the first time in the regulation of cognitive impairment in VaD. We look forward to a larger multicenter study in the future to further confirm the correlation between serum FAM19A5 levels and cognitive functions in VaD subjects. Clarifying the underlying pathological mechanisms of FAM19A5 involved in the onset of VaD will have important clinical significance.

Data Availability

The data used to support the findings of this study are available from the corresponding author upon request.

Conflicts of Interest

The authors declare that they have no any conflict of interests.

Authors' Contributions

Juan Li and Shoulin Li contributed equally to this work.

Acknowledgments

All the authors are grateful to the Department of Neurology, The First People's Hospital of Lianyungang/Department of Neurology, The First Affiliated Hospital of Kangda College of Nanjing Medical University, for invaluable assistance.

References

- [1] J. T. O'Brien and A. Thomas, "Vascular dementia," *Lancet*, vol. 386, no. 10004, pp. 1698–1706, 2015.
- [2] Q. Wang, Y. Xu, C. Qi, A. Liu, and Y. Zhao, "Association study of serum soluble TREM2 with vascular dementia in Chinese Han population," *The International Journal of Neuroscience*, vol. 130, no. 7, pp. 708–712, 2020.
- [3] Y. Xu, Q. Wang, Y. Liu, R. Cui, K. Lu, and Y. Zhao, "Association between Helicobacter pylori infection and carotid atherosclerosis in patients with vascular dementia," *Journal of the Neurological Sciences*, vol. 362, pp. 73–77, 2016.
- [4] Q. Wang, W. Yang, J. Zhang, Y. Zhao, and Y. Xu, "TREM2 overexpression attenuates cognitive deficits in experimental models of vascular dementia," *Neural Plasticity*, vol. 2020, Article ID 8834275, 10 pages, 2020.
- [5] L. Jia, M. Quan, Y. Fu et al., "Dementia in China: epidemiology, clinical management, and research advances," *The Lancet Neurology*, vol. 19, no. 1, pp. 81–92, 2020.
- [6] G. Zuliani, A. Passaro, C. Bosi et al., "Testing a Combination of Markers of Systemic Redox Status as a Possible Tool for the Diagnosis of Late Onset Alzheimer's Disease," *Disease Markers*, vol. 2018, Article ID 2576026, 9 pages, 2018.
- [7] Y. Xu, Q. Wang, R. Cui, K. Lu, Y. Liu, and Y. Zhao, "Uric acid is associated with vascular dementia in Chinese population," *Brain and behavior*, vol. 7, no. 2, article e00617, 2017.
- [8] Y. Xu, Q. Wang, Y. Liu, R. Cui, and Y. Zhao, "Is Helicobacter pylori infection a critical risk factor for vascular dementia?," *The International Journal of Neuroscience*, vol. 126, no. 10, pp. 899–903, 2015.
- [9] Y. B. Lee, H. J. Hwang, J. A. Kim et al., "Association of serum FAM19A5 with metabolic and vascular risk factors in human subjects with or without type 2 diabetes," *Diabetes & Vascular Disease Research*, vol. 16, no. 6, pp. 530–538, 2019.
- [10] M. Y. Park, H. S. Kim, M. Lee et al., "FAM19A5, a brain-specific chemokine, inhibits RANKL-induced osteoclast formation through formyl peptide receptor 2," *Scientific Reports*, vol. 7, no. 1, p. 15575, 2017.
- [11] Y. Wang, D. Chen, Y. Zhang et al., "Novel adipokine, FAM19A5, inhibits neointima formation after injury through sphingosine-1-phosphate receptor 2," *Circulation*, vol. 138, no. 1, pp. 48–63, 2018.
- [12] G. C. Roman, T. K. Tatemichi, T. Erkinjuntti et al., "Vascular dementia: diagnostic criteria for research studies. Report of

- the NINDS-AIREN International Workshop,” *Neurology*, vol. 43, no. 2, pp. 250–260, 1993.
- [13] P. S. Sachdev, D. Blacker, D. G. Blazer et al., “Classifying neurocognitive disorders: the DSM-5 approach,” *Neurology*, vol. 10, no. 11, pp. 634–642, 2014.
- [14] Y. Xu, Q. Wang, Z. Wu et al., “The effect of lithium chloride on the attenuation of cognitive impairment in experimental hypoglycemic rats,” *Brain Research Bulletin*, vol. 149, pp. 168–174, 2019.
- [15] P. H. Wu, Y. T. Lin, C. S. Chen et al., “Associations of bone turnover markers with cognitive function in patients undergoing hemodialysis,” *Disease Markers*, vol. 2020, Article ID 8641749, 10 pages, 2020.
- [16] Y. Xu, Q. Wang, Z. Qu, J. Yang, X. Zhang, and Y. Zhao, “Protective effect of hyperbaric oxygen therapy on cognitive function in patients with vascular dementia,” *Cell Transplantation*, vol. 28, no. 8, pp. 1071–1075, 2019.
- [17] R. Cassani, M. Estarellas, R. San-Martin, F. J. Fraga, and T. H. Falk, “Systematic Review on Resting-State EEG for Alzheimer’s Disease Diagnosis and Progression Assessment,” *Disease Markers*, vol. 2018, Article ID 5174815, 26 pages, 2018.
- [18] J. Zhang, L. Tang, J. Hu, Y. Wang, and Y. Xu, “Uric acid is associated with cognitive impairment in the elderly patients receiving maintenance hemodialysis—a two-center study,” *Brain and behavior*, vol. 10, no. 3, article e01542, 2020.
- [19] D. Kang, H. R. Kim, K. K. Kim et al., “Brain-specific chemokine FAM19A5 induces hypothalamic inflammation,” *Biochemical and Biophysical Research Communications*, vol. 523, no. 4, pp. 829–834, 2020.
- [20] Y. T. Tang, P. Emtage, W. D. Funk et al., “Tafa: a novel secreted family with conserved cysteine residues and restricted expression in the brain,” *Genomics*, vol. 83, no. 4, pp. 727–734, 2004.
- [21] S. J. Paulsen, M. T. Christensen, N. Vrang, and L. K. Larsen, “The putative neuropeptide Tafa5 is expressed in the hypothalamic paraventricular nucleus and is regulated by dehydration,” *Brain Research*, vol. 1199, pp. 1–9, 2008.
- [22] A. Shahapal, E. B. Cho, H. J. Yong et al., “FAM19A5 expression during embryogenesis and in the adult traumatic brain of FAM19A5-LacZ knock-in mice,” *Frontiers in Neuroscience*, vol. 13, p. 917, 2019.
- [23] K. M. Han, W. S. Tae, A. Kim et al., “Serum FAM19A5 levels: a novel biomarker for neuroinflammation and neurodegeneration in major depressive disorder,” *Brain, behavior, and immunity*, vol. 87, pp. 852–859, 2020.
- [24] T. Janvilisri, K. Leelawat, S. Roytrakul, A. Paemane, and R. Tohtong, “Novel serum biomarkers to differentiate cholangiocarcinoma from benign biliary tract diseases using a proteomic approach,” *Disease Markers*, vol. 2015, Article ID 105358, 11 pages, 2015.
- [25] Z. Hu, G. Niu, J. Ren et al., “Tafa5 promotes proliferation and migration in gastric cancer,” *Molecular Medicine Reports*, vol. 20, no. 5, pp. 4477–4488, 2019.
- [26] X. Wang, C. Shen, X. Chen et al., “Tafa-2 plays an essential role in neuronal survival and neurobiological function in mice,” *Acta Biochimica et Biophysica Sinica*, vol. 50, no. 10, pp. 984–995, 2018.
- [27] J. Okada, E. Yamada, T. Saito et al., “Analysis of FAM19A2/Tafa-2 function,” *Physiology & Behavior*, vol. 208, p. 112581, 2019.
- [28] X. Lei, L. Liu, C. E. Terrillion et al., “FAM19A1, a brain-enriched and metabolically responsive neurokinin, regulates food intake patterns and mouse behaviors,” *FASEB Journal : Official Publication of the Federation of American Societies for Experimental Biology*, vol. 33, no. 12, pp. 14734–14747, 2019.
- [29] H. J. Yong, N. Ha, E. B. Cho et al., “The unique expression profile of FAM19A1 in the mouse brain and its association with hyperactivity, long-term memory and fear acquisition,” *Scientific Reports*, vol. 10, no. 1, p. 3969, 2020.
- [30] A. A. Kashevarova, E. O. Belyaeva, A. M. Nikonov et al., “Compound phenotype in a girl with r(22), concomitant microdeletion 22q13.32-q13.33 and mosaic monosomy 22,” *Molecular Cytogenetics*, vol. 11, no. 1, 2018.
- [31] C. Inan, N. C. Sayin, H. Gurkan et al., “Schizencephaly accompanied by occipital encephalocele and deletion of chromosome 22q13.32: a case report,” *Fetal and Pediatric Pathology*, vol. 38, no. 6, pp. 496–502, 2019.
- [32] S. Huang, C. Zheng, G. Xie et al., “FAM19A5/Tafa5, a novel neurokinin, plays a crucial role in depressive-like and spatial memory-related behaviors in mice,” *Molecular Psychiatry*, 2020.